ENCLOSURE 5 TO
NRC-99-0084

FERMI 2

NRC DOCKET NO. 50-341
OPERATING LICENSE NPF-43

LICENSING REPORT FOR FERMI 2 SPENT FUEL POOL RACK INSTALLATION

Holtec Report HI-992154, Revision 6
Non-Proprietary Version

HOLTEC INTERNATIONAL

Holtec Center, 555 Lincoln Drive West, Marlton, NJ 08053
Telephone (856) 797-0900
Fax (856) 797-0909

LICENSING REPORT

for

SPENT FUEL RACK INSTALLATION

at

FERMI Unit 2

Holtec Report HI-992154 (Non-Proprietary Version)
Report Category: A

Prepared for Detroit Edison Co.
Purchase Order No. 317788
Holtec Project 80964

HOLTEC INTERNATIONAL

Holtec Center, 555 Lincoln Drive West, Marlton, NJ 08053
Telephone (609) 797- 0900
Fax (609) 797 - 0909

QA AND ADMINISTRATIVE INFORMATION LOG

(To Be Filled In By the Principal Author of the Document and Placed After the Title Page)

Document No: **HI-992154**	CATEGORY: ☐ **Generic** ☒ **Project Specific**

Holtec Project No: **80964**

In accordance with the Holtec Quality Assurance Manual, and associated Holtec Quality Procedures (HQPs), this document is categorized as a :

☐ **Calculation Package * (Per HQP 3.2)**

☒ **Technical Report (Per HQP 3.2) (Such as a Licensing report)**

☐ **Design Criterion Document (Per HQP 3.4)**

☐ **Design Specification (Per HQP 3.4)**

☐ **Other (Specify):** _____

The formatting of the contents of this document is in accordance with the instructions of HQP 3.2 or 3.4 except as noted below:

_____

_____

_____

This document is labelled :

☒ **Nonproprietary** ☐ **Holtec Proprietary** ☐ **Privileged Intellectual Property (PIP)**

Documents labelled Privileged Intellectual Property contains extremely valuable intellectual/commercial property of Holtec International. They can not be released to external organizations or entites without explicit approval of a company corporate officer. The recipient of Holtec's proprietary or Privileged Intellectual Property (PIP) document bears full and undivided responsibility to safeguard it against loss or duplication.

* Revisions to the calculation Packages may be made by adding supplements to the document and replacing the "Table of Contents", the "Review and Certification" page and the "Revision Log".

REVIEW AND CERTIFICATION LOG FOR MULTIPLE AUTHOR DOCUMENTS†

REPORT NUMBER: HI-992154 PROJECT NUMBER: 80964 REPORT TYPE: Licensing

No.	Document Portion††	REVISION No. 5		REVISION No. 6		REVISION No.	
		Author & Date	Reviewer & Date	Author & Date	Reviewer & Date	Author & Date	Reviewer & Date
1.	Sec 5	Pankaj Chaudhary PCC 11/1/99	Scott H. Pellet SHP 11-1-99	Pankaj Chaudhary PCC 11/4/99	Scott H. Pellet SHP 11-4-99		
2.							
3.							
4.							
5.							
6.							
7.							
8.							
P.M. (OR DESIGNEE) & DATE		Pankaj Chaudhary PCC 11/1/99		Pankaj Chaudhary PCC 11/4/99			
QA APPROVAL AND DATE		S. Shah S.S. 11/1/99		S. Shah S.S. 11/4/99			

† The associated Design Verification Checklist must be filled out by the author and the reviewer(s), and saved in the company qualify file *before* this log is signed off. Per HQP 3.2, up to two reviewers may be needed for work product which is new or novel for the company.

†† Chapter or section number.

Notes: A revision of this document will be ordered by the Project Manager if any of its contents is materially affected during evolution of the project. The determination as to the need for revision will be made by the Project Manager with oral input from the Project Team. Signatures and printed names are required in the review block.

THE REVISION CONTROL OF THIS DOCUMENT IS BY A "SUMMARY OF REVISIONS LOG" PLACED BEFORE THE TEXT OF THE REPORT. Form: CL3.2.5

REVIEW AND CERTIFICATION LOG FOR MULTIPLE AUTHOR DOCUMENTS†

REPORT NUMBER: HI-992154 PROJECT NUMBER: 80964 REPORT TYPE: Licensing

No.	Document Portion††	REVISION No. 2		REVISION No.		REVISION No.	
		Author & Date	Reviewer & Date	Author & Date	Reviewer & Date	Author & Date	Reviewer & Date
1.	Sec 1	Pankaj Chaudhary PKC 11/1/99	Scott H. Pellet SHP 11-1-99				
2.	Sec 2	Pankaj Chaudhary PKC 11/1/99	Scott H. Pellet SHP 11-1-99				
3.	Sec 3	Pankaj Chaudhary PKC 11/1/99	Scott H. Pellet SHP 11-1-99				
4.	Sec 4	Pankaj Chaudhary PKC 11/1/99	Scott H. Pellet SHP 11-1-99				
5.	Sec 5	—	—				
6.	Sec 6	Pankaj Chaudhary PKC 11/1/99	Scott H. Pellet SHP 11-1-99				
7.	Sec 7	Pankaj Chaudhary PKC 11/1/99	Scott H. Pellet SHP 11-1-99				
8.	Sec 8	Pankaj Chaudhary PKC 11/1/99	Scott H. Pellet SHP 11-1-99				
P.M. (OR DESIGNEE) & DATE		Pankaj Chaudhary PKC 11/1/99					
QA APPROVAL AND DATE		S. S. 11/1/99					

† The associated Design Verification Checklist must be filled out by the author and the reviewer(s), and saved in the company qualify file *before* this log is signed off. Per HQP 3.2, up to two reviewers may be needed for work product which is new or novel for the company.

†† Chapter or section number.

Notes: A revision of this document will be ordered by the Project Manager if any of its contents is materially affected during evolution of the project. The determination as to the need for revision will be made by the Project Manager with oral input from the Project Team. Signatures and printed names are required in the review block.

THE REVISION CONTROL OF THIS DOCUMENT IS BY A "SUMMARY OF REVISIONS LOG" PLACED BEFORE THE TEXT OF THE REPORT. Form: CL3.2.5

REVIEW AND CERTIFICATION LOG FOR MULTIPLE AUTHOR DOCUMENTS†

REPORT NUMBER: HI-992154 PROJECT NUMBER: 80964 REPORT TYPE: Licensing

No.	Document Portion††	REVISION No. 2		REVISION No. _____		REVISION No. _____	
		Author & Date	Reviewer & Date	Author & Date	Reviewer & Date	Author & Date	Reviewer & Date
1.	Sec 9	Pankaj Chandhay Rice 11/1/99	Scott H. Pellet SHP 11-1-99				
2.	Sec 10	Pankaj Chandhay Rice 11/1/99	Scott H. Pellet SHP 11-1-99				
3.	Sec 11	Pankaj Chandhay Rice 11/1/99	Scott H. Pellet SHP 11-1-99				
4.							
5.							
6.							
7.							
8.							
P.M. (OR DESIGNEE) & DATE		Pankaj Chandhay Rice 11/1/99					
QA APPROVAL AND DATE		S.S 11/1/99					

† The associated Design Verification Checklist must be filled out by the author and the reviewer(s), and saved in the company qualify file *before* this log is signed off. Per HQP 3.2, up to two reviewers may be needed for work product which is new or novel for the company.

†† Chapter or section number.

Notes: A revision of this document will be ordered by the Project Manager if any of its contents is materially affected during evolution of the project. The determination as to the need for revision will be made by the Project Manager with oral input from the Project Team. Signatures and printed names are required in the review block.

THE REVISION CONTROL OF THIS DOCUMENT IS BY A "SUMMARY OF REVISIONS LOG" PLACED BEFORE THE TEXT OF THE REPORT. Form: CL3.2.5

REVIEW AND CERTIFICATION LOG FOR MULTIPLE AUTHOR DOCUMENTS†

REPORT NUMBER: H1 992154 PROJECT NUMBER: 80964 REPORT TYPE: LICENSING

No.	Document Portion††	REVISION No. 0		REVISION No. 1		REVISION No. 2	
		Author & Date	Reviewer & Date	Author & Date	Reviewer & Date	Author & Date	Reviewer & Date
1.	See 1	Scott H. Pellet SHP 7-21-99	E Rosenbaum E Rosenbaum 7/21/99	Pankaj Chaudhary PKC 9/24/99	Scott H. Pellet SHP 9-24-99	N/A	
2.	See 2	Scott H. Pellet SHP 7-21-99	E Rosenbaum E Rosenbaum 7/21/99	Pankaj Chaudhary PKC 9/24/99	Scott H. Pellet SHP 9-24-99	N/A	
3.	See 3	Scott H. Pellet SHP 7-21-99	Pankaj Chaudhary PKC 7/22/99	Pankaj Chaudhary PKC 9/24/99	Scott H. Pellet SHP 9-24-99	N/A	
4.	See 4	Pankaj Chaudhary For Stan Turner per letter 7/22/99	Steven Anton S. ANTON 7/23/99	Pankaj Chaudhary For Stan Turner per letter 9/27/99	Steven Anton S. ANTON 9-27-99	N/A	
5.	See 5	E Rosenbaum E Rosenbaum 7/21/99	D. MITRA-MAJUMDAR 7/21/99.	E Rosenbaum E Rosenbaum 9/30/99	Indrasen Ramphal (IR) 9/30/99	E Rosenbaum E Rosenbaum 10/1/99	Pankaj Chaudhary PKC 10/1/99
6.	See 6	E.J. JANINA 7-22-99	Pankaj Chaudhary PKC 7/22/99	E.J. JANINA 9-27-99	Pankaj Chaudhary PKC 9/27/99	N/A	
7.	See 7	John Shin JZ. 07/21/99	7.23.99	John Shin JZ 09/27/99	Pankaj Chaudhary PKC 9/27/99	N/A	
8.	See 8	Ruben Todorovski LT 7-20-99	A S 7/22/99	Ruben Todorovski LT 09-27-99	Scott H. Pellet SHP 9-27-99	N/A	
P.M. (OR DESIGNEE) & DATE		Pankaj Chaudhary PKC 7/26/99		Pankaj Chaudhary PKC 9/30/99		Pankaj Chaudhary PKC 10/1/99	
QA APPROVAL AND DATE		S-S 7/26/99		M PHIPPS 9/27/99		M PHIPPS 10/1/99	

† The associated Design Verification Checklist must be filled out by the author and the reviewer(s), and saved in the company qualify file *before* this log is signed off. Per HQP 3.2, up to two reviewers may be needed for work product which is new or novel for the company.

†† Chapter or section number.

Notes: A revision of this document will be ordered by the Project Manager if any of its contents is materially affected during evolution of the project. The determination as to the need for revision will be made by the Project Manager with oral input from the Project Team. Signatures and printed names are required in the review block.

THE REVISION CONTROL OF THIS DOCUMENT IS BY A "SUMMARY OF REVISIONS LOG" PLACED BEFORE THE TEXT OF THE REPORT. Form: CL3.2.5

REVIEW AND CERTIFICATION LOG FOR MULTIPLE AUTHOR DOCUMENTS†

REPORT NUMBER: HI 992154 PROJECT NUMBER: 80964 REPORT TYPE: LICENSING

No.	Document Portion††	REVISION No. 0		REVISION No. 1		REVISION No. 2	
		Author & Date	Reviewer & Date	Author & Date	Reviewer & Date	Author & Date	Reviewer & Date
1.	Sec 9	Scott H. Pellet SHP 7-16-99	E. R. Burch ERB 7/22/99	Pankaj Chandhary for S. Turner per telecon 9/21/99	Scott H. Pellet SHP 9-24-99	N/A	
2.	Sec 10	Scott H. Pellet SHP 7-21-99	Om Chopra 7-22-99	— This section has been removed. Sec 11 and sec 12 have been renumbered to sec 10 & sec 11. PCC 9/28/99		N/A	
3.	Sec 11	Scott H. Pellet SHP 7-21-99	E. R. Burch ERB 7/22/99	Pankaj Chandhary PCC 9/27/99	Scott H. Pellet SHP 9-24-99	N/A	
4.	Sec 12	Scott H. Pellet SHP 7-21-99	Om Chopra 7-22-99	Pankaj Chandhary PCC 9/27/99	Scott H. Pellet SHP 9-24-99	N/A	
5.							
6.							
7.							
8.							
P.M. (OR DESIGNEE) & DATE		Pankaj Chandhary PCC 7/26/99		Pankaj Chandhary PCC 9/30/99		Pankaj Chandhary PCC 10/1/99	
QA APPROVAL AND DATE		S. Shah 7/26/99		M. Phippen 9/24/99		M. Phippen 10/4/99	

† The associated Design Verification Checklist must be filled out by the author and the reviewer(s), and saved in the company qualify file *before* this log is signed off. Per HQP 3.2, up to two reviewers may be needed for work product which is new or novel for the company.

†† Chapter or section number.

Notes: A revision of this document will be ordered by the Project Manager if any of its contents is materially affected during evolution of the project. The determination as to the need for revision will be made by the Project Manager with oral input from the Project Team. Signatures and printed names are required in the review block.

THE REVISION CONTROL OF THIS DOCUMENT IS BY A "SUMMARY OF REVISIONS LOG" PLACED BEFORE THE TEXT OF THE REPORT. Form: CL3.2.5

REVIEW AND CERTIFICATION LOG FOR MULTIPLE AUTHOR DOCUMENTS†

REPORT NUMBER: HI-912354 PROJECT NUMBER: 80964 REPORT TYPE: Licensing

No.	Document Portion††	REVISION No. 3		REVISION No. 4		REVISION No.	
		Author & Date	Reviewer & Date	Author & Date	Reviewer & Date	Author & Date	Reviewer & Date
1.							
2.		N/A					
3.							
4.							
5.	Sec 5	E Rosenbaum ER 10/6/99	Pankaj Chaudhary PCC 10/6/99	10/11/99	E Rosenbaum ER 10/11/99		
6.							
7.		N/A					
8.							
P.M. (OR DESIGNEE) & DATE		Pankaj Chaudhary PCC 10/6/99		Pankaj Chaudhary PCC 10/11/99			
QA APPROVAL AND DATE		M PHIPPS 10/6/99		M PHIPPS 10/11/99			

† The associated Design Verification Checklist must be filled out by the author and the reviewer(s), and saved in the company qualify file *before* this log is signed off. Per HQP 3.2, up to two reviewers may be needed for work product which is new or novel for the company.

†† Chapter or section number.

Notes: A revision of this document will be ordered by the Project Manager if any of its contents is materially affected during evolution of the project. The determination as to the need for revision will be made by the Project Manager with oral input from the Project Team. Signatures and printed names are required in the review block.

THE REVISION CONTROL OF THIS DOCUMENT IS BY A "SUMMARY OF REVISIONS LOG" PLACED BEFORE THE TEXT OF THE REPORT. Form: CL3.2.5

SUMMARY OF REVISIONS

Revision 0: Initial issue.

Revision 1: This revision incorporates DECO's comments dated Sep. 13 and Sep. 16 of 1999. As per DECO's request, Chapter 10 (Boral Surveillance Program) has been removed from this report and chapters 11 and 12 have been renumbered accordingly.

Revision 2: Client's comments were incorporated in Chapter 5.0 of this report.

Revision 3: A typographical error associated with the energy balance equation on page 5-8 of this report was corrected.

Revision 4: Chapter 5.0 was revised to incorporate changes following a change in the RHR Cooling Water Temperature from 85 degrees to 89 degrees in the supporting Thermal hydraulic analyses.

Revision 5: All chapters were revised to incorporate client's comments and internal review comments. Two rounds of Client's comments were received from Mr. Hari Arora of Detroit Edison dated 10/22/99 and 10/29/99. These were mostly editorial comments. Specifically, typographical errors on page 5-21, 6-28, 6-57, 8-13, 8-14 were corrected in this revision. The incorporation of these comments did not affect the conclusion of the report. Also, the DFC calculation results were revised in chapter 5.0 due to the change in the supporting design calculation i.e. Bulk Pool Temperature Analysis.

Revision 6: Editorial changes were made to pages 5-2, 5-3, 5-5 and 5-10 of Chapter 5.0.

TABLE OF CONTENTS

Figures

Figures (continued)

1.0 IMPERATIVE FOR WET STORAGE EXPANSION AND REPORT OUTLINE

1.1 Background

Enrico Fermi Unit 2 (Fermi 2) is a single unit BWR reactor installation located in a rural area approximately thirty miles southwest of the city of Detroit, Michigan. Fermi 2 has been in commercial operation since 1988. Additional historical data on Fermi 2 is provided in Table 1.1.1. Fermi 2 is owned and operated by the Detroit Edison Company (DECo).

The wet storage facility at Fermi 2 consists of a 34 feet by 40 feet rectangular spent fuel pool with an integral cask laydown area. Figure 1.1.1 shows the existing storage arrangement in the Fermi 2 pool that, at the present time, is the sole repository for the discharged spent nuclear fuel. The pool contains 2,383 useable storage cells (out of a total of 2,385 cells installed) in fourteen existing J. Oat high-density rack (HDR) modules and four GE low density rack (LDR) modules. An additional defective fuel rack containing 35 oversize cylindrical cells (to store control rods, defective fuel canisters, control rod guide tubes, etc.) is also installed in the north end of the pool.

The existing HDR storage modules, although of the high-density genre, are laid out in a decidedly low-density manner. [redacted]

[redacted] In summary, from a physical space standpoint, the Fermi 2 pool is capable of storing a much larger number of fuel bundles than is available from its present storage arrangement.

This licensing report presents a multi-campaign plan to remove all existing racks from the Fermi 2 pool and rerack with Holtec high density rack (HDR) modules utilizing Boral™, which has gained near universal acceptance as the preferred neutron absorber over the past fifty years. Several plants, notably Callaway, Wolf Creek, Byron 1 and 2, and Braidwood 1 and 2, have recently implemented a similar plan (to rerack with Boral™ racks).

DECo has selected Holtec International of Marlton, New Jersey, to engineer and fabricate the new high-density racks, assist DECo in the operating license amendment request effort, and perform all site construction services to produce the required capacity increases. Holtec International has provided high density racks and performed practically all fuel storage capacity expansions in the U.S. and a great majority of them overseas within the past ten years [Table 1.1.2].

The primary reason for the capacity expansion proposed in this licensing report is the projected loss of "full-core-discharge" (FCD) capability in the Fermi 2 pool. The Fermi 2 reactor core holds 764 fuel bundles. Based on current spent fuel inventory and the projected refueling outage discharges shown in Table 5.3.1, Fermi 2 will lose FCD capability after new fuel receipt for cycle 9, around June 2001. At that time Fermi 2 will have a fuel inventory (new and spent) of 1744 assemblies. With the current storage capacity of 2383 cells there would not be enough empty cells to store the full core of 764 assemblies.

To rectify the looming spent fuel storage deficit, DECo performed an in-depth evaluation of available options in 1994 which led the company to select a three-step wet storage capacity expansion program for the Fermi 2 spent fuel pool as the safest and most economical option. A summary of the cost/benefit analysis of all candidate options carried out by DECo is provided in Chapter 11 of this document. As we describe in the next section, the three-phase Fermi 2 implementation is similar to multi-campaign capacity increases implemented by Duane Arnold in 1993 and Nine Mile Point Unit 1 in 1998.

1.2 Multi-Campaign Storage Capacity Expansion

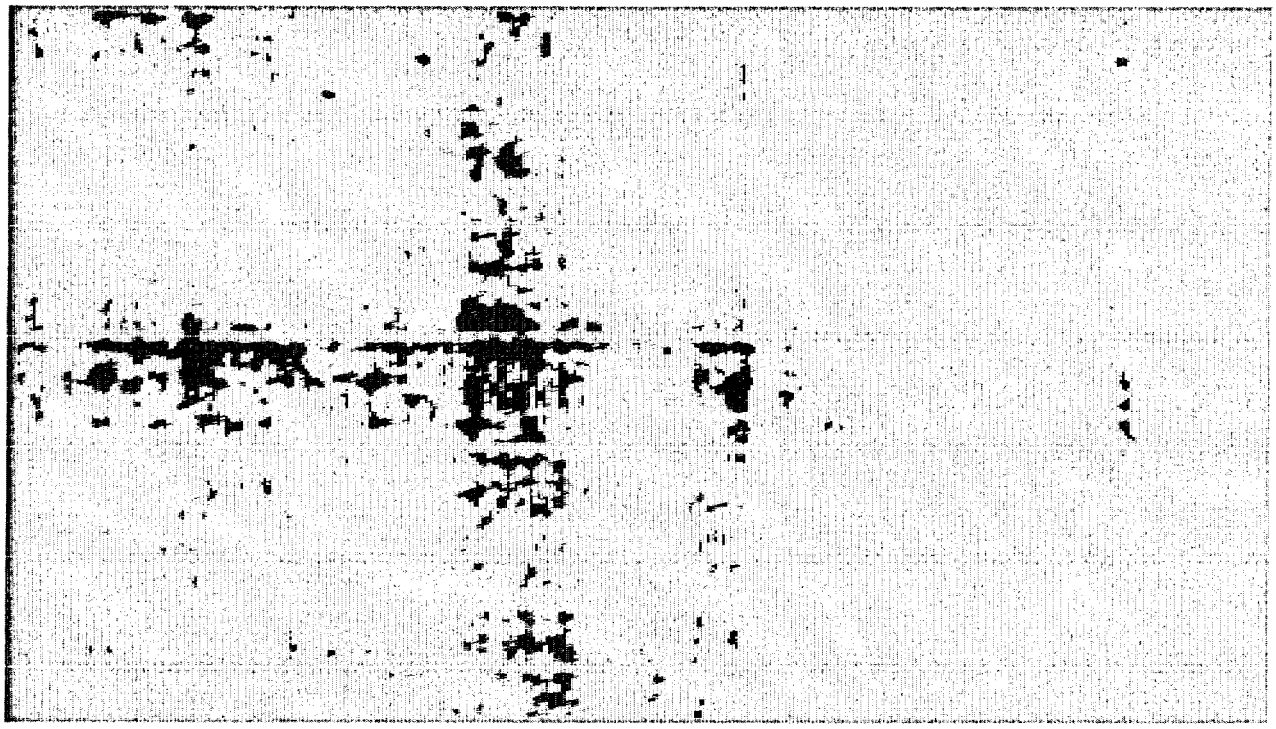

The successive gains in storage capacity upon execution of the three campaigns are summarized in Table 1.2.1. With the increased installed capacities, Table 1.2.1 shows that the loss of FCD date for Fermi 2 is deferred further in the future after each rerack campaign. Upon conclusion of the final rerack campaign, the Fermi 2 pool will not run out of full-core discharge capacity until ca. 2015 at the end of cycle 17.

1.3 Report Content Outline

Chapter 2 of this licensing document provides a summary of the principal design criteria applicable to the proposed capacity expansion. The new Holtec high density racks, like the existing Fermi 2 high density rack modules, are free-standing and self-supporting. The new racks, as well as the existing racks, are designed to the stress limits of, and analyzed in

accordance with, Section III, Division 1, Subsection NF of the ASME Boiler and Pressure Vessel (B&PV) Code, albeit to different Code years and addenda.

The principal construction materials for the new and existing high density racks are austenitic steel sheet and plate stock. Both the existing and new high density racks utilize the ^{10}B isotope for reactivity control. Despite the anatomical similarity between the new and existing fuel racks, it is necessary that confirmatory analyses on the existing racks be performed wherever the addition of the new racks is expected to alter the margin of safety. Accordingly, Chapter 3 of this report provides an abstract of the design and material information for the new Holtec high density racks.

The criticality safety analysis requires that the neutron multiplication factor for the stored fuel array be bounded by the k_{eff} limit of 0.95 under assumptions of 95% probability and 95% confidence. The criticality safety analysis provided in Chapter 4 establishes the requirements on the Boral™ panel length and the ^{10}B areal density for the new Holtec high density racks. The new Holtec high density racks are designed to a k_{inf} in the Standard Cold Core Geometry (SCCG) of 1.33, as discussed in Chapter 4 of this report. However, in order to include additional criticality margin for the new racks and maintain consistency with the existing Technical Specifications, storage will be limited to fuel with a maximum k_{inf} in the standard cold core geometry (SCCG) of 1.31.

The thermal-hydraulic considerations warrant that fuel cladding does not fail due to excessive thermal stress and that the steady-state pool bulk temperature remains within the prescribed structural, operational, and regulatory limits. The thermal-hydraulic analyses carried out in support of this storage expansion effort are described in Chapter 5.

Demonstrations of seismic and structural adequacy are presented in Chapter 6. The analysis shows that the primary stresses in the rack module structure remain below the ASME B&PV Code (Subsection NF) [1.4.1] allowables. Chapter 6 also contains results of analyses performed to demonstrate that the racks provide adequate robustness against fatigue failure resulting from multiple seismic events. The structural qualification also provides conclusive evidence that the

subcriticality of the stored fuel is maintained under all postulated accident scenarios in the Updated Final Safety Analysis Reports (UFSAR) for Fermi 2. The structural consequences of these postulated accidents are presented and evaluated in Chapter 7 of this report.

Chapter 8 provides a general description of the fuel pool structure, the results of the structural evaluation of the reinforced concrete spent fuel pool, and an assessment of the integrity of the pool liner.

The radiological considerations are documented in Chapter 9. An outline of the construction services for Campaign I is presented in Chapter 10 to provide a summary of the defense-in-depth measures contemplated for implementation in the Fermi 2 project to realize ALARA and absolute personnel safety. Chapter 10 also contains a summary of heavy load handling considerations germane to the construction effort associated with the capacity expansion proposed by this licensing application.

Finally, Chapter 11 presents a cost/benefit and environmental assessment to establish the prudence of DECo's decision to proceed with the rerack project.

All computer programs utilized to perform the analyses documented in this licensing report are benchmarked and verified in accordance with Holtec International's Quality Assurance procedures. These programs have been utilized by Holtec International in numerous rerack applications over the past decade. All analyses and evaluations conform to the guidelines of the OT position paper [1.4.2] and subsequent clarification of the Staff's position through SERs on peer operating license amendment applications.

The analyses presented herein clearly demonstrate that the rack module arrays possess wide margins of safety in respect to all considerations of safety specified in the USNRC OT position paper, namely nuclear subcriticality, thermal-hydraulic safety, seismic and structural adequacy, radiological compliance, and mechanical integrity.

1.4 References for Chapter 1

[1.4.1] ASME Boiler and Pressure Vessel Code, Section III, Subsection NF and Appendices (1995).

[1.4.2] USNRC Letter to All Power Reactor Licensees transmitting the "OT Position for Review and Acceptance of Spent Fuel Storage and Handling Applications," April 14, 1978, and Addendum dated January 18, 1979.

TABLE 1.1.1 FERMI 2 PLANT DATA	
Docket Number	50-341
Reactor Supplier	General Electric
Turbine Generator Supplier	English Electric/General Electric
Announced	August 1968
Applied to NRC	April 1969
Construction Permit	September 1972
Initial Startup	June 1985
Began Commercial Operation	January 1988
Operating License Expiration Date	March 2025
MW(e)	1150
MW(t)	3430
Containment	Mark I
Reactor	BWR 4
Number of Assemblies in Reactor Core	764

TABLE 1.1.2

HOLTEC RACK INSTALLATION / RERACKING PROJECTS

Plant	Utility	Docket No.	Reactor / Fuel Type	Mfg. Year
Hope Creek	Public Service Electric & Gas	50-354/355	BWR	1989
Millstone Unit 1	Northeast Utilities	50-245	BWR	1989
Three Mile Island I	GPU Nuclear	50-289	PWR	1990
James A. FitzPatrick	NY Power Authority	50-333	BWR	1990
Hope Creek	Public Service Electric & Gas Company	50-354	BWR	1991
Harris Pool 'B' †	Carolina Power & Light	50-401	BWR	1991
Kuosheng 1,2	Taiwan Power Company (Taiwan)	--	BWR	1991
Laguna Verde 1,2	Comision Federal de Electricidad (Mexico)	--	BWR	1991
Sequoyah	Tennessee Valley Authority	50-327	PWR	1992
Donald C. Cook	American Electric Power	50-315/316	PWR	1992
LaSalle 1	Commonwealth Edison	50-373	BWR	1992
Beaver Valley Unit 1	Duquesne Light Company	50-334	PWR	1993
Fort Calhoun	Omaha Public Power District	50-285	PWR	1993
Zion 1 & 2	Commonwealth Edison	50-295/304	PWR	1993
Duane Arnold	Iowa Electric Light & Power	50-331	BWR	1993
Duane Arnold Energy Center	Iowa Electric Power Company	50-331	BWR	1994
Limerick Units 1,2	PECO Energy	50-352/50-353	BWR	1994

TABLE 1.1.2

HOLTEC RACK INSTALLATION / RERACKING PROJECTS

Plant	Utility	Docket No.	Reactor / Fuel Type	Mfg. Year
Ulchin Unit 2	Korea Electric Power Company (Korea)	--	PWR	1996
Kori-4	Korea Electric Power Company (Korea)	--	PWR	1996
Yonggwang 1,2	Korea Electric Power Company (Korea)	--	PWR	1996
Harris Pool 'B' †	Carolina Power & Light Company	50-401	BWR	1996
Sizewell B	Nuclear Electric, plc (United Kingdom)	--	PWR	1997
Angra 1	Furnas Centrais-Electricas SA (Brazil)	--	PWR	1997
Waterford 3	Entergy Operations	50-382	PWR	1997
Harris Pool 'B' †	Carolina Power & Light Company	50-401	BWR	1998
Callaway	Union Electric	50-483	PWR	1998
James A. FitzPatrick	NY Power Authority	50-333	BWR	1998
Wolf Creek	Wolf Creek Operating Corporation	50-482	PWR	1999
Chin Shan	Taiwan Power Company (Taiwan)	--	BWR	1999
Davis Besse	First Energy	50-346	PWR	1999
Harris Pool 'C'	Carolina Power & Light Company	50-401	BWR	1999

† Fabricated racks for storage of spent fuel transhipped from Brunswick.

TABLE 1.2.1

RACK AND STORAGE CAPACITY SUMMARY

Existing Rack Layout		
Rack Description	Size	Total Cells
E1 through E10	13x13	169x10 = 1690
E11	9x12	108
E12 through E14	13x13	169x3 = 507
E15	5x7	35
GE Racks	2x10	20x4 = 80
Current Storage Cell Total		2383 †
Campaign I		

† Value excludes rack E15 and two additional existing cells, which are used for Boraflex In-surveillance program.
* Holtec Rack A to be installed as needed to maintain full-core-discharge capability.

TABLE 1.2.1 (CONT'D)

RACK AND STORAGE CAPACITY SUMMARY

Campaign II

† Value excludes two existing cells, which are used for Boraflex In-Service surveillance program.

TABLE 1.2.1 (CONT'D)

RACK AND STORAGE CAPACITY SUMMARY

Campaign III

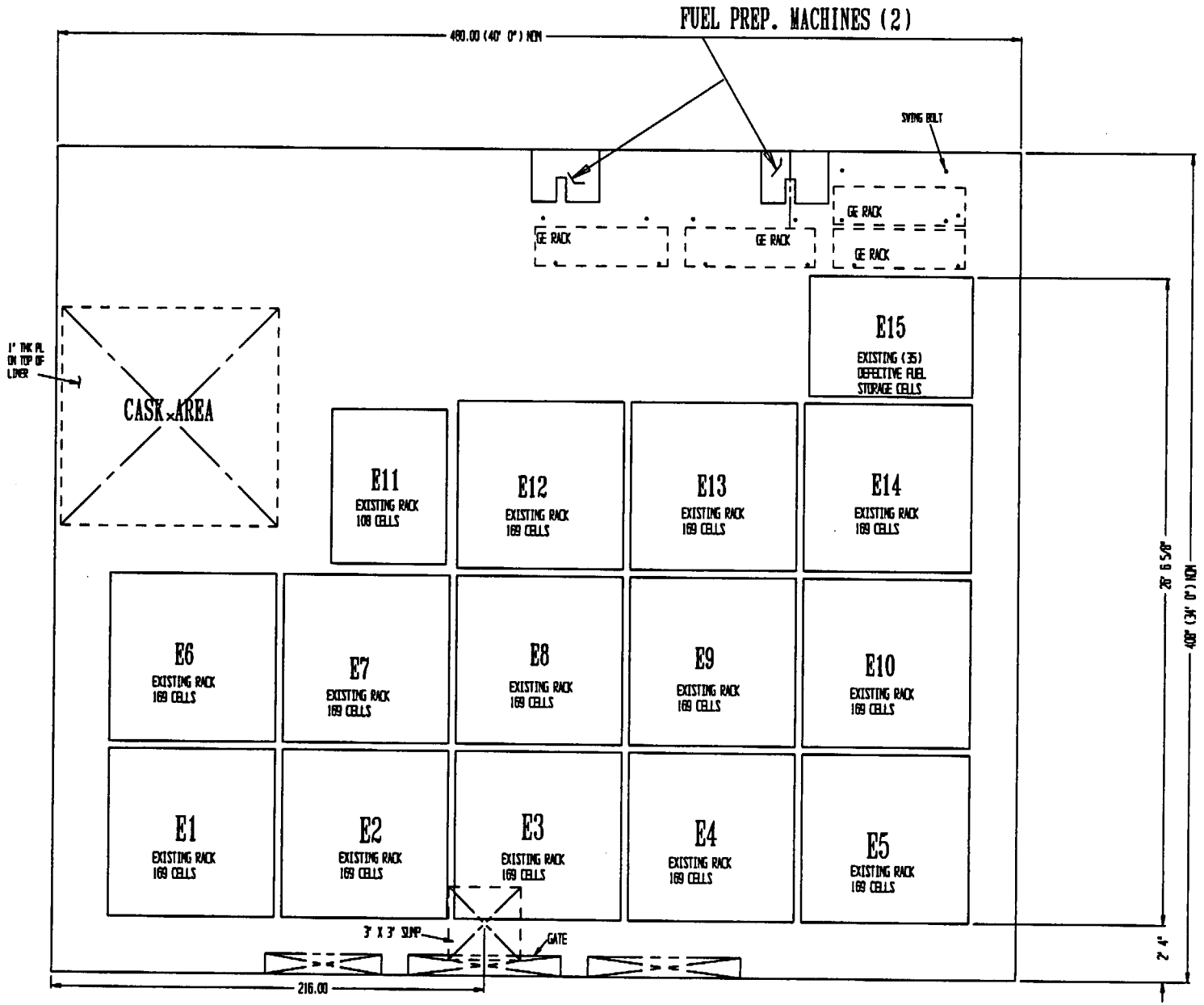

FIGURE 1.1.1; EXISTING RACK LAYOUT

HI-992154

Proprietary information removed.

FIGURE 1.2.1; CAMPAIGN I RACK LAYOUT

Proprietary information removed.

FIGURE 1.2.2; CAMPAIGN II RACK LAYOUT

Proprietary information removed.

FIGURE 1.2.3; CAMPAIGN III RACK LAYOUT

2.0 PRINCIPAL DESIGN CRITERIA AND GOVERNING CODES

In this chapter, a synopsis of the principal design criteria applicable to the design of the Holtec high density racks for the Enrico Fermi 2 Plant is presented. For convenience, the entire range of codes, industry standards, publications, and plant-specific documents utilized or consulted in the preparation of this licensing report is also provided. In general, the information provided in this chapter serves as the common reference material for the safety analyses documented in Chapters 4 through 9 herein.

2.1 Summary of Principal Design Criteria

The key design criteria for the new Fermi 2 spent fuel racks are set forth in the USNRC memorandum entitled "OT Position for Review and Acceptance of Spent Fuel Storage and Handling Applications," April 14, 1978 as modified by amendment dated January 18, 1979. The individual chapters of this report address the specific design bases that are described in the above-mentioned "OT Position Paper." A brief summary of the design basis requirements for the Fermi 2 racks is provided below.

a. Disposition: All new rack modules are required to be free-standing.

b. Kinematic Stability: All free-standing modules must be kinematically stable (against overturning) when subjected to a seismic event. Factors of safety of 1.5 and 1.1 are required for OBE and SSE conditions, respectively.

c. Structural Compliance: All primary stresses in the rack modules must satisfy the limits postulated in Section III, Subsection NF of the 1995 ASME Boiler and Pressure Vessel Code. Also, the cumulative damage factor for fatigue life must be less than 1.0 when the rack is subjected to 1 SSE and 20 OBE events. The fatigue assessment of the fuel rack follows the applicable guidelines in Subsection NB, Paragraph NB-3222.4.

d. Thermal-Hydraulic Compliance: The spatial average bulk pool temperature is required to remain under 150°F following a normal refueling. For a full core off-load, it is required to demonstrate that bulk pool boiling does not occur, with single active failure.

In addition to the limitations on the bulk pool temperature, the local water temperature in the Fermi 2 pool must remain below the boiling temperature coincident with local hydraulic pressure condition under normal refueling scenarios.

e. Criticality Compliance: The maximum calculated reactivity of the storage rack must be such that the true k_{eff} shall be less than 0.95 with a 95% probability at a 95% confidence level for normal and accident conditions.

f. Radiological Compliance: The capacity expansion campaign in the Fermi 2 pool must not lead to violation of the off-site dose limits, or adversely affect the area dose environment as set forth in the plant UFSAR. The radiological implications of the installation of the new racks also need to be ascertained and deemed to be acceptable.

g. Pool Structure: The ability of the reinforced concrete structure to satisfy the load combinations set forth in the plant UFSAR must be demonstrated.

h. Liner Integrity: The integrity of the liner under cyclic in-plane loading during a seismic event must be demonstrated.

i. Bearing Pads: The bearing pads must be sufficiently thick such that the pressure on the concrete underlying the liner continues to satisfy the ACI-349 limits during and after a design basis seismic event.

j. Accident Events: In the event of a load drop (e.g., uncontrolled lowering of a fuel assembly), it is necessary to demonstrate that the subcriticality of the rack structure is not compromised.

k. Construction Events: The field construction services required to be carried out for executing the reracking must be demonstrated to be within the "state of proven art."

The foregoing design basis requirements are further articulated in Chapters 4 through 9 of this licensing report.

2.2 Applicable Codes and Standards

The fabrication of the rack modules is performed under a strict quality assurance system suitable for 10CFR50 Appendix B manufacturing.

The following codes, standards and practices are used as applicable for the design, construction, and assembly of the Fermi 2 fuel storage racks. Additional specific references related to detailed analyses are given in each section.

a. Design Codes

(1) AISC Manual of Steel Construction, 8th Edition, 1980.

(2) ANSI N210-1976, "Design Requirements for Light Water Reactor Spent Fuel Storage Facilities at Nuclear Power Stations" (contains guidelines for fuel rack design).

(3) American Society of Mechanical Engineers (ASME), Boiler and Pressure Vessel Code Section III (Subsections NB and NF), 1995 Edition; ASME Section V, 1995 edition; ASME Section VIII, 1995 Edition; ASME Section IX, 1995 Edition; and ASME Section XI, 1995 Edition.

(4) ASNT-TC-1A, American Society for Nondestructive Testing (Recommended Practice for Personnel Qualifications), June 1980.

(5) American Concrete Institute Building Code Requirements for Reinforced Concrete (ACI 318-63) and (ACI 318-71, 77, 83).

(6) Code Requirements for Nuclear Safety Related Concrete Structures, ACI 349-85/ACI 349R-85 and ACI 349.1R-80.

(7) ASME NQA-1-1989, Quality Assurance Program Requirements for Nuclear Facilities.

(8) ASME NQA-2-1989, Quality Assurance Requirements for Nuclear Facility Applications.

(9) ASME Y14.5M-1994, Dimensioning and Tolerancing (revision and redesignation of ANSI Y14.5M-1982)

(10) ACI Detailing Manual, 1980.

b. Material Codes - Standards of ASTM

(1) E165-95, Liquid Penetrant Examination.

(2) A240/A240M-97a, Standard Specification for Heat-Resisting Chromium and Chromium-Nickel Stainless Steel Plate, Sheet, and Strip for Pressure Vessels.

(3) A262-93a, Detecting Susceptibility to Intergranular Attack in Austenitic Stainless Steel.

(4) A276-97, Stainless Steel Bars and Shapes.

(5) A479/A479M-97a, Stainless Steel Bars and Shapes for Use in Boilers and Other Pressure Vessels.

(6) A564/A564M-95, Hot-Rolled and Cold-Finished Age-Hardening Stainless Steel Bars and Shapes.

(7) C750-89, Nuclear-Grade Boron Carbide Powder.

(8) A380-96, Cleaning, Descaling, and Passivation of Stainless Steel Parts, Equipment, and Systems.

(9) C992-89, Boron-Based Neutron Absorbing Material Systems for Use in Nuclear Spent Fuel Storage Racks.

(10) E3-95, Preparation of Metallographic Specimens.

(11) E190-92, Guided Bend Test for Ductility of Welds.

(12) American Society of Mechanical Engineers (ASME), Boiler and Pressure Vessel Code, Section II-Parts A and C, 1995 Edition.

(13) NCA3800 - Metallic Material Manufacturer's and Material Supplier's Quality System Program.

c. Welding Codes: ASME Boiler and Pressure Vessel Code, Section IX - Welding and Brazing Qualifications, 1995 Edition.

d. Quality Assurance, Cleanliness, Packaging, Shipping, Receiving, Storage, and Handling Requirements

(1) ANSI N45.2.1-1980, Cleaning of Fluid Systems and Associated Components During Construction Phase of Nuclear Power Plants.

(2) ANSI N45.2.2-1972, Packaging, Shipping, Receiving, Storage and Handling of Items for Nuclear Power Plants (During the Construction Phase).

(3) ANSI N45.2.6-1978, Qualifications of Inspection, Examination, and Testing Personnel for Nuclear Power Plants (Regulatory Guide 1.58).

(4) ANSI N45.2.8-1975, Supplementary Quality Assurance Requirements for Installation, Inspection and Testing of Mechanical Equipment and Systems for the Construction Phase of Nuclear Plants.

(5) ANSI N45.2.11-1974, Quality Assurance Requirements for the Design of Nuclear Power Plants.

(6) ANSI N45.2.12-1977, Requirements for Auditing of Quality Assurance Programs for Nuclear Power Plants.

(7) ANSI N45.2.13-1976, Quality Assurance Requirements for Control of Procurement of Equipment Materials and Services for Nuclear Power Plants (Regulatory Guide 1.123).

(8) ANSI N45.2.15-18, Hoisting, Rigging, and Transporting of Items for Nuclear Power Plants.

(9) ANSI N45.2.23-1978, Qualification of Quality Assurance Program Audit Personnel for Nuclear Power Plants (Regulatory Guide 1.146).

(10) ASME Boiler and Pressure Vessel, Section V, Nondestructive Examination, 1995 Edition.

(11) ANSI N16.9-1975, Validation of Calculation Methods for Nuclear Criticality Safety.

e. Governing NRC Design Documents

(1) "OT Position for Review and Acceptance of Spent Fuel Storage and Handling Applications," dated April 14, 1978, and the modifications to this document of January 18, 1979.

(2) NUREG 0612, "Control of Heavy Loads at Nuclear Power Plants", USNRC, Washington, D.C., July 1980.

(3) NUREG-0800, Radiological Consequences of Fuel Handling Accidents.

f. Other ANSI Standards (not listed in the preceding)

(1) ANSI/ANS 8.1 (N16.1), Nuclear Criticality Safety in Operations with Fissionable Materials Outside Reactors.

(2) ANSI/ANS 8.17-1984 (R1997), Criteria for the Handling, Storage, and Transportation of LWR Fuel Outside Reactors.

(3) ANSI N45.2-1971, Quality Assurance Program Requirements for Nuclear Facilities.

(4) ANSI N45.2.10-1973, Quality Assurance Terms and Definitions.

(5) ANSI/ANS 57.2 (N210), Requirements for Light Water Reactor Spent Fuel Storage Facilities.

(6) ANSI N14.6-1993, Radioactive Materials - Special Lifting Devices for Shipping Containers Weighing 10,000 pounds (4,500 kg) or More.

(7) ASME N626.3-1993, Qualification and Duties of Specialized Professional Engineers.

(8) ANSI 8.21, Use of Fixed Neutron Absorbers in Nuclear Facilities Outside Reactor (supplemented by 4.1e (2) as applicable).

g. Code of Federal Regulations

(1) 10CFR20, Standards for Protection Against Radiation, 1997 Edition.

(2) 10CFR21, Reporting of Defects and Non-compliance, 1997 Edition.

(3) 10CFR50 Appendix A, General Design Criteria for Nuclear Power Plants, 1997 Edition.

(4) 10CFR50 Appendix B, Quality Assurance Criteria for Nuclear Power Plants and Fuel Reprocessing Plants, 1997 Edition.

(5) 10CFR61, Licensing Requirements for Land Disposal of Radioactive Material, 1997 Edition.

(6) 10CFR71, Packaging and Transportation of Radioactive Material, 1997 Edition.

(7) 10CFR100, Reactor Site Criteria

(8) 49CFR, Subchapter C-Hazardous Materials Regulations, Parts 171-178

h. Regulatory Guides

(1) RG 1.13 – Rev. 1, Spent Fuel Storage Facility Design Basis (Revision 2 Proposed).

(2) RG 1.25 – Rev. 0, Assumptions Used for Evaluating the Potential Radiological Consequences of a Fuel Handling Accident in the Fuel Handling and Storage Facility of Boiling and Pressurized Water Reactors.

(3) RG 1.28 – Rev. 3 (ANSI N45.2), Quality Assurance Program Requirements .

(4) RG 1.29, Seismic Design Classification (Rev. 3).

(5) RG 1.31 – Rev. 3, Control of Ferrite Content in Stainless Steel Weld Material.

(6) RG 1.38 – Rev. 2 (ANSI N45.2.2), Quality Assurance Requirements for Packaging, Shipping, Receiving, Storage and Handling of Items for Water-Cooled Nuclear Power Plants.

(7) RG 1.44 – Rev. 0, Control of the Use of Sensitized Stainless Steel.

(8) RG 1.58 – Rev. 1 (ANSI N45.2.6), Qualification of Nuclear Power Plant Inspection, Examination, and Testing Personnel.

(9) RG 1.61, Damping Values for Seismic Design of Nuclear Power Plants, Rev. 0, 1973.

(10) RG 1.64 – Rev. 2 (ANSI N45.2.11), Quality Assurance Requirements for the Design of Nuclear Power Plants.

(11) RG 1.71 – Rev. 0, Welder Qualifications for Areas of Limited Accessibility.

(12) RG 1.74 (ANSI N45.2.10), Quality Assurance Terms and Definitions, February 1974.

(13) RG 1.85, Materials Code Case Acceptability - ASME Section 3, Div. 1.

(14) RG 1.88 – Rev. 2 (ANSI N45.2.9), Collection, Storage and Maintenance of Nuclear Power Plant Quality Assurance Records.

(15) RG 1.92, Combining Modal Responses and Spatial Components in Seismic Response Analysis.

(16) RG 1.122, Development of Floor Design Response Spectra for Seismic Design of Floor-Supported Equipment or Components.

(17) RG 1.123 – Rev. 1 (ANSI N45.2.13), Quality Assurance Requirements for Control of Procurement of Items and Services for Nuclear Power Plants.

(18) RG 1.124 – Rev. 1, Service Limits and Loading Combinations for Class 1 Linear-Type Component Supports, Revision 1, 1978.

(19) RG 3.4, Nuclear Criticality Safety in Operations with Fissionable Materials at Fuels and Materials Facilities.

(20) RG 3.41 – Rev. 1, Validation of Calculational Methods for Nuclear Criticality Safety, Revision 1, 1977.

(21) RG 8.38, Control of Access to High and Very High Radiation Areas in Nuclear Power Plants, June 1993.

(22) RG 8.8, Information Relative to Ensuring that Occupational Radiation Exposure at Nuclear Power Plants will be as Low as Reasonably Achievable (ALARA).

(22) DG-8006, "Control of Access to High and Very High Radiation Areas in Nuclear Power Plants."

(24) IE Information Notice 83-29 - Fuel Binding Caused by Fuel Rack Deformation.

i. Branch Technical Position

(1) CPB 9.1-1, Criticality in Fuel Storage Facilities.

(2) ASB 9-2, Residual Decay Energy for Light-Water Reactors for Long-Term Cooling.

j. Standard Review Plan

(1) SRP 3.2.1, Seismic Classification.

(2) SRP 3.2.2, System Quality Group Classification.

(3) SRP 3.7.1, Seismic Design Parameters.

(4) SRP 3.7.2, Seismic System Analysis.

(5) SRP 3.7.3, Seismic Subsystem Analysis.

(6) SRP 3.8.4, Other Seismic Category I Structures (including Appendix D), Technical Position on Spent Fuel Rack.

(7) SRP 3.8.5, Foundations for Seismic Category I Structures, Revision 1, 1981.

(8) SRP 9.1.2, Spent Fuel Storage, Revision 3, 1981.

(9) SRP 9.1.3, Spent Fuel Pool Cooling and Cleanup System.

(10) SRP 9.1.4, Light Load Handling System.

(11) SRP 9.1.5, Heavy Load Handling System.

(12) SRP 15.7.4, Radiological Consequences of Fuel Handling Accidents.

k. AWS Standards

(1) AWS D1.1-94, Standard for Steel - Structural Welding Code.

(2) AWS D1.3-98, Structure Welding Code - Sheet Steel.

(3) AWS D9.1-90, Sheet Metal Welding Code.

(4) AWS A2.4-98, Symbols for Welding, Brazing, and Nondestructive Examination.

(5) AWS A3.0-94, Standard Welding Terms and Definitions.

(6) AWS A5.12/A5.12M-98, Tungsten and Tungsten Alloy Electrodes for Arc Welding and Cutting.

(7) AWS QC1-96, AWS Certification of Welding Inspectors.

l. Other

(1) EPRI: "A Methodology for Assessment of Nuclear Power Plant Seismic Margin (Rev. 1), EPRI NP-6041-SL.

(2) Fermi 2 UFSAR, SER, and plant Technical Specifications.

(3) NCIG-01, Rev. 2, Visual Weld Acceptance Criteria for Structural Welding at Nuclear Power Plants.

(4) Fermi 2 Chemical Control Program.

(5) "Critical Experiments Supporting Close Proximity Water Storage of Power Reactor Fuel," BAW-1484-7, July 1979.

3.0 RACK DESIGN AND MODULE LAYOUT

The object of this section is to provide a self-contained description of the new Holtec high density rack module construction and to enable an independent appraisal of the adequacy of design.

3.1 New Holtec High Density Rack Modules

The new Holtec high density spent fuel racks for Fermi 2 follow the proven design concept of non-flux trap honeycomb prismatic construction developed by Holtec International in the mid-1980s and utilized to add storage capacity in over forty spent fuel pools over the past ten years. In the following, a self-contained summary of the rack module design features is provided, with special emphasis on the design characteristics which are significant to the structural, criticality, and thermal-hydraulic performance of the racks.

A pictorial view of a rectangular cross-section non-flux trap module is shown Figure 3.1.1. As can be readily deduced from this figure, the non-flux trap module is essentially a cellular prismatic structure. The following design features are central to the functional performance of Fermi-2 racks (and other racks of non-flux trap genré designed by Holtec International for BWR pools).

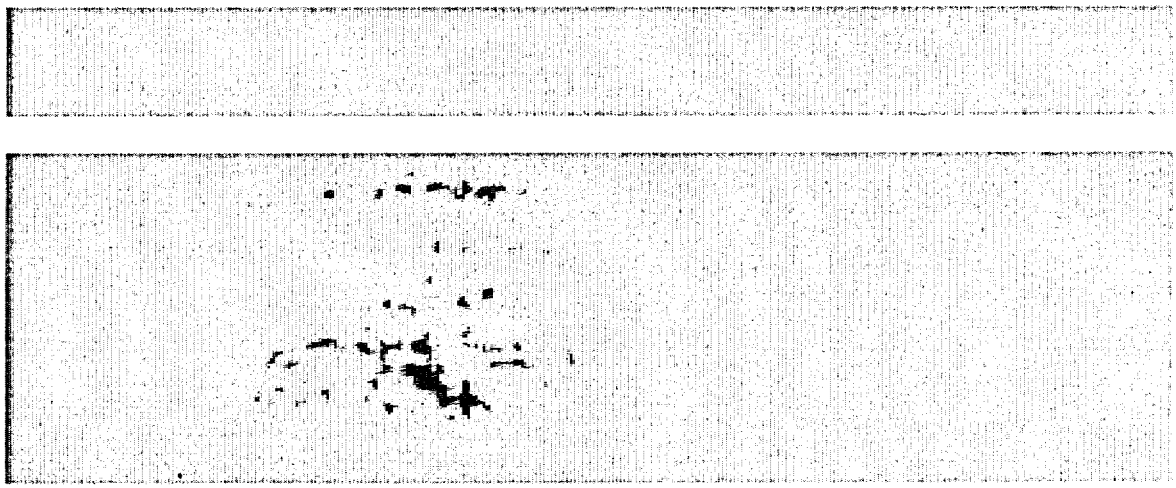

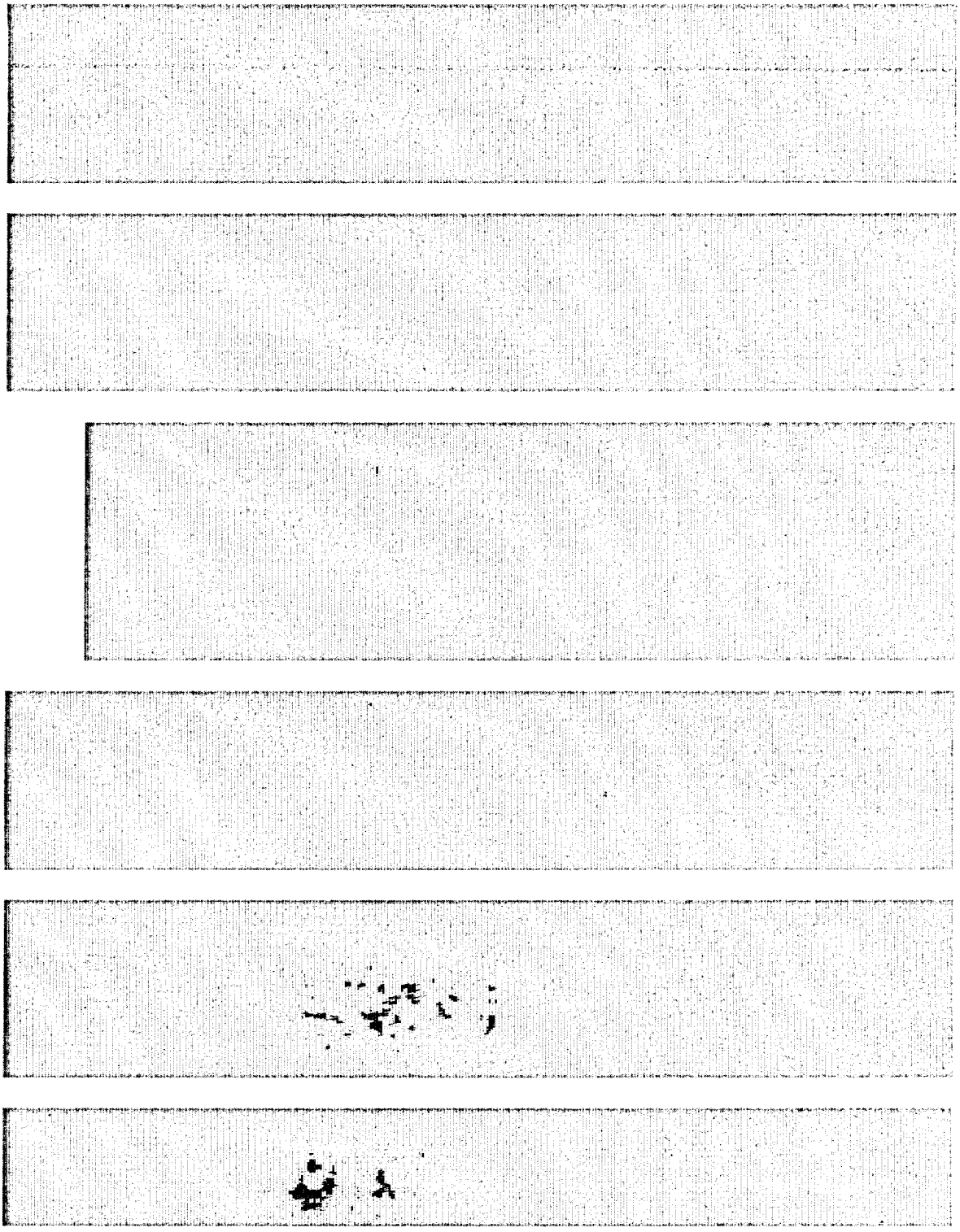

Table 3.1.1 provides key design data on the Holtec modules engineered for Enrico Fermi Unit 2.

3.2 Material Considerations

3.2.1 Structural Materials

The following structural materials are utilized in the fabrication of the new spent fuel racks:

a. ASME SA240-304L for all sheet metal stock

b. Baseplate: ASME SA240-304L

c. Internally threaded support legs: ASME SA240-304L

d. Externally threaded support spindle: ASME SA564-630 precipitation hardened stainless steel (heat treated to 1100°F)

e. Bearing pads: ASME SA240-304

f. Weld material - per the following ASME specification:

3.2.2 Neutron Absorber Materials

In addition to the structural and non-structural stainless material, the racks employ Boral, a patented product of AAR Manufacturing, as the neutron absorber material. A brief description of Boral and its pool experience list follows.

Boral is a thermal neutron poison material composed of boron carbide and 1100 alloy aluminum. Boron carbide is a compound having a high boron content in a physically stable and chemically inert form. The 1100 alloy aluminum is a lightweight metal with high tensile strength, which is protected from corrosion by a highly resistant oxide film. The two materials, boron carbide and aluminum, are chemically compatible and ideally suited for long-term use in the radiative, thermal, and chemical environment of a nuclear reactor or a spent fuel pool.

Boral's use in spent fuel pools as the neutron absorbing material can be attributed to its proven performance (over 150 pool years of experience) and the following unique characteristics:

a. The content and placement of boron carbide provides a very high removal cross-section for thermal neutrons.

b. Boron carbide, in the form of fine particles, is homogeneously dispersed throughout the central layer of the Boral panels.

c. The boron carbide and aluminum materials in Boral do not degrade as a result of long-term exposure to radiation.

d. The neutron absorbing central layer of Boral is clad with permanently bonded surfaces of aluminum.

e. Boral is stable, strong, durable, and corrosion resistant.

Holtec International's QA program ensures that Boral is manufactured by AAR Manufacturing under the control and surveillance of a Quality Assurance/Quality Control Program that conforms to the requirements of 10CFR50 Appendix B, "Quality Assurance Criteria for Nuclear Power Plants."

As indicated in Tables 3.2.1 and 3.2.2, Boral has been licensed by the USNRC for use in numerous PWR and BWR spent fuel storage racks and has been extensively used in nuclear installations worldwide.

Boral Material Characteristics

Aluminum: Aluminum is a silvery-white, ductile metallic element that is the most abundant in the earth's crust. The 1100 alloy aluminum is used extensively in heat exchangers, pressure and storage tanks, chemical equipment, reflectors and sheet metal work.

It has high resistance to corrosion in industrial and marine atmospheres. Aluminum has an atomic number of 13, an atomic weight of 26.98, a specific gravity of 2.69, and a valence of 3. The physical, mechanical, and chemical properties of the 1100 alloy aluminum are listed in Tables 3.2.3 and 3.2.4.

The excellent corrosion resistance of the 1100 alloy aluminum is provided by the protective oxide film that develops on its surface from exposure to the atmosphere or water. This film prevents the loss of metal from general corrosion or pitting corrosion.

Boron Carbide: The boron carbide contained in Boral is a fine granulated powder that conforms to ASTM C-750-80 nuclear grade Type III. The material conforms to the chemical composition and properties listed in Table 3.2.5.

3.2.3 Compatibility with Coolant

All materials used in the construction of the Holtec racks have an established history of in-pool usage. Their physical, chemical, and radiological compatibility with the pool environment is an established fact. As noted in Tables 3.2.1 and 3.2.2 and References [3.2.1] and [3.2.2], Boral has been successfully used in fuel pools and is suitable for use in this application. Austenitic stainless steel (304L) is perhaps the most widely used stainless alloy in nuclear power plants.

3.3 Fabrication and Quality Assurance Considerations

The governing quality assurance requirements for fabrication of the spent fuel racks are enunciated in 10CFR50 Appendix B. The quality assurance program for design of the Fermi 2 racks are described in Holtec's Nuclear Quality Assurance Manual, which has been reviewed and approved by the Detroit Edison Company. This program is designed to provide a flexible, but highly controlled system for the design, analysis and licensing of customized components in accordance with various codes, specifications, and regulatory requirements.

The manufacturing of the racks will be carried out by Holtec's designated manufacturer, U.S. Tool & Die, Inc. (UST&D). The Quality Assurance System enforced on the manufacturer's shop floor shall provide for all controls necessary to fulfill all quality assurance requirements with sufficient simplicity to make it functional on a day-to-day basis. UST&D has manufactured high-density racks for over sixty nuclear plants around the world. Holtec audits UST&D on a periodic basis to ensure that its Quality Assurance Program meets the requirements of 10CFR50 Appendix B. UST&D has also been audited by the industry group NUPIC and the QA branch of NMSS with satisfactory results and Fermi 2 quality assurance has scheduled audits during important portions of the rack fabrication. UST&D holds ASME nuclear Class 1, 2, and 3 stamps

(N-Stamp) since the mid-1960s. Practically the entire manufacturing output of UST&D has been destined for use in nuclear plants.

The Quality Assurance System that will be used by Holtec to install the racks is also controlled by the Holtec Nuclear Quality Assurance Manual and by any site-specific requirements.

3.4 Module Layout

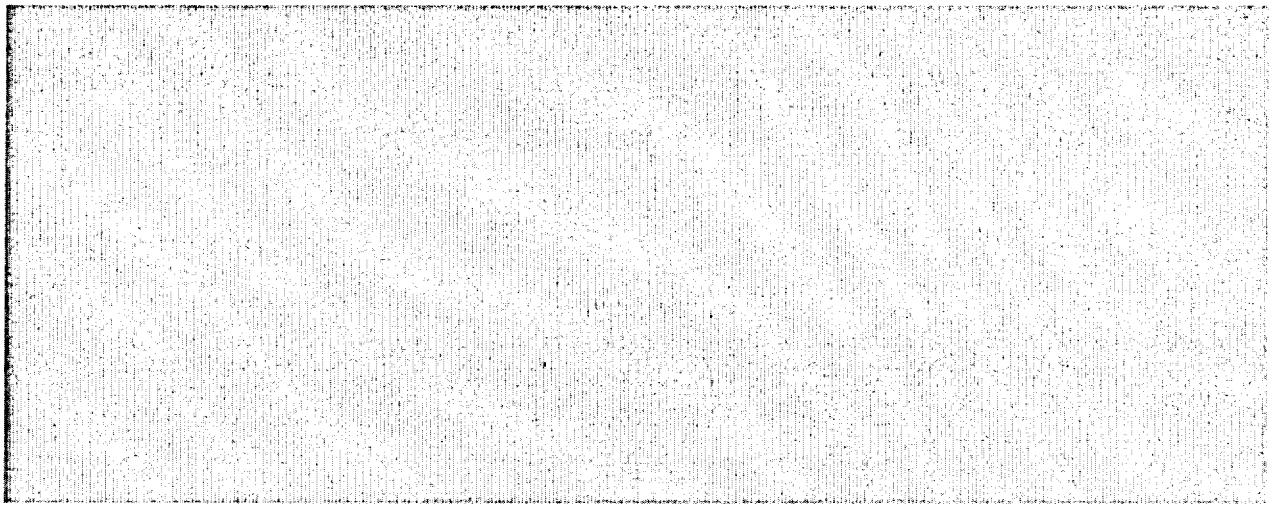

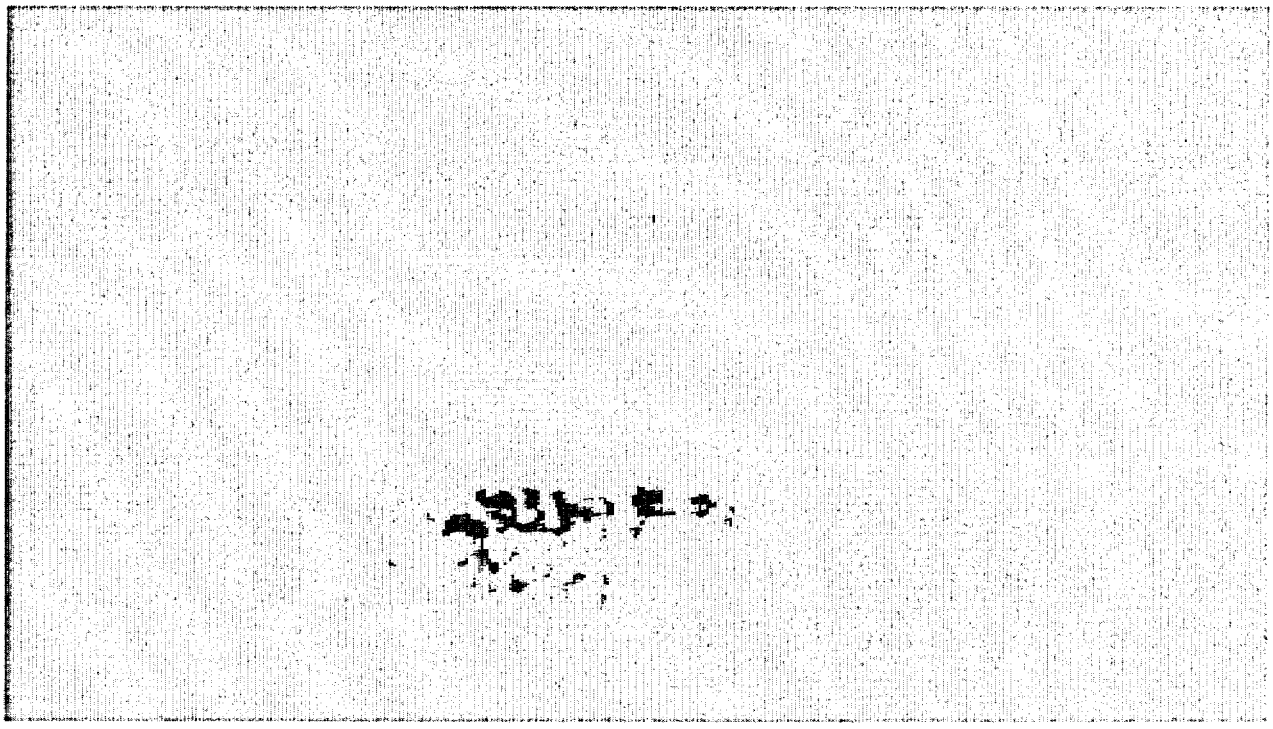

Furthermore, new Holtec high density racks B from Campaign I and G from Campaign II are also designed to support a specially engineered overhead platform referred to as "Holtec Overhead Platform" which permits storage of miscellaneous objects [redacted] without interferring with the normal function of the module as an assemblage of spent fuel storage cavities. The structural and thermal-hydraulic qualification of these racks includes the appropriate consideration of the overhead platform.

The Fermi 2 pool, upon completion of Campaign III (final campaign) will feature only Boral-equipped racks, with the layout shown in Figure 1.2.3. Because of the maximized capacity (and, therefore, maximum fuel inventory) corresponding to this campaign, [redacted] This final Campaign includes the so-called "cask pit rack" which, [redacted] The cask pit rack is identical in its anatomical details to the new Holtec high density racks in the spent fuel pool and such, all analyses (seismic, thermal-hydraulic and criticality) have been carried out for the cask pit rack in an identical manner to the fuel pool racks.

The geometric and weight data on all new modules is provided in Table 3.4.1.

3.5 References for Section 3

[3.2.1] "Spent Fuel Storage Module Corrosion Report," Brooks & Perkins Report 554, June 1, 1977.

[3.2.2] "Boral Neutron Absorbing/Shielding Material - Product Performance Report," Brooks & Perkins Report 624, July 20, 1982.

Table 3.1.1 KEY DESIGN DATA FOR NEW FERMI-2 MODULES	
Cell wall thickness (nom.), inch	0.75
Cell height (nom.), inch	175
Cell I.D. (nom.), inch	6.035
^{10}B areal loading in Boral (min.), g/cm^2	0.020
Boral panel thickness, inch	0.075
External Sheathing thickness, inch	0.075
Internal Sheathing thickness, inch	0.035
Height of bottom of baseplate above liner (nom.), inch	7.5
Layout pitch (nom.), inch	6.23
Number of support pedestals (min.)	4

Table 3.2.1

BORAL EXPERIENCE LIST - PWR PLANTS

Plant	Utility	Docket No.	Mfg. Year
Maine Yankee	Maine Yankee Atomic Power	50-309	1977
Donald C. Cook	Indiana & Michigan Electric	50-315/316	1979
Sequoyah 1,2	Tennessee Valley Authority	50-327/328	1979
Salem 1,2	Public Service Electric & Gas	50-272/311	1980
Zion 1,2	Commonwealth Edison Co.	50-295/304	1980
Bellefonte 1, 2	Tennessee Valley Authority	50-438/439	1981
Yankee Rowe	Yankee Atomic Power	50-29	1964/1983
Indian Point 3	NY Power Authority	50-286	1987
Byron 1,2	Commonwealth Edison Co.	50-454/455	1988
Braidwood 1,2	Commonwealth Edison Co.	50-456/457	1988
Yankee Rowe	Yankee Atomic Power	50-29	1988
Three Mile Island I	GPU Nuclear	50-289	1990
Sequoyah (rerack)	Tennessee Valley Authority	50-327	1992
Donald C. Cook (rerack)	American Electric Power	50-315/316	1992
Beaver Valley Unit 1	Duquesne Light Company	50-334	1993
Fort Calhoun	Omaha Public Power District	50-285	1993
Zion 1 & 2 (rerack)	Commonwealth Edison Co.	50-295/304	1993
Salem Units 1 & 2 (rerack)	Public Gas and Electric Company	50-272/311	1995
Haddam Neck	Connecticut Yankee Atomic Power Company	50-213	1996
Waterford Unit 3	Entergy Operations, Inc.	50-382	1997
Callaway	Union Electric Company	50-483	1997
Gosgen	Kernkraftwerk Gosgen-Daniken AG (Switzerland)	—	1984
Koeberg 1,2	ESCOM (South Africa)	—	1985

Table 3.2.1 (continued)

BORAL EXPERIENCE LIST – PWR PLANTS

Plant	Utility	Docket No.	Mfg. Year
Beznau 1,2	Nordostschweizerische Kraftwerke AG (Switzerland)	—	1985
12 Various Plants	Electricite de France (France)	—	1986
Ulchin Unit 1	Korea Electric Power Company (Korea)	—	1995
Ulchin Unit 2	Korea Electric Power Company (Korea)	—	1996
Kori-4	Korea Electric Power Company (Korea)	—	1996
Yonggwang 1,2	Korea Electric Power Company (Korea)	—	1996
Sizewell B	Nuclear Electric, plc (United Kingdom)	—	1997
Angra 1	Furnas Centrais-Electricas SA (Brazil)	—	1997
Wolf Creek	Wolf Creek Nuclear Operating Corp.	50-482	1999

Table 3.2.2

BORAL EXPERIENCE LIST - BWR PLANTS

Plant	Utility	Docket No.	Mfg. Year
Cooper	Nebraska Public Power	50-298	1979
J.A. FitzPatrick	NY Power Authority	50-333	1978
Duane Arnold	Iowa Electric Light & Power	50-331	1979
Browns Ferry 1,2,3	Tennessee Valley Authority	50-259/260/296	1980
Brunswick 1,2	Carolina Power & Light	50-324/325	1981
Clinton	Illinois Power	50-461/462	1981
Dresden 2,3	Commonwealth Edison Company	50-237/249	1981
E.I. Hatch 1,2	Georgia Power	50-321/366	1981
Hope Creek	Public Service Electric & Gas	50-354/355	1985
Humboldt Bay	Pacific Gas & Electric Company	50-133	1985
LaCrosse	Dairyland Power	50-409	1976
Limerick 1,2	Philadelphia Electric Company	50-352/353	1980
Monticello	Northern States Power	50-263	1978
Peachbottom 2,3	Philadelphia Electric	50-277/278	1980
Perry 1,2	Cleveland Electric Illuminating	50-440/441	1979
Pilgrim	Boston Edison Company	50-293	1978
Susquehanna 1,2	Pennsylvania Power & Light	50-387,388	1979
Vermont Yankee	Vermont Yankee Atomic Power	50-271	1978/1986
Hope Creek	Public Service Electric & Gas	50-354/355	1989
Harris Pool B †	Carolina Power & Light	50-401	1991
Duane Arnold	Iowa Electric Light & Power	50-331	1993
Pilgrim	Boston Edison Company	50-293	1993
LaSalle 1	Commonwealth Edison Company	50-373	1992
Millstone Unit 1	Northeast Utilities	50-245	1989

† Fabricated racks for storage of spent fuel transshipped from Brunswick.

Table 3.2.2 (continued)

BORAL EXPERIENCE LIST – BWR PLANTS

Plant	Utility	Docket No.	Mfg. Year
James A. FitzPatrick	NY Power Authority	50-333	1990
Hope Creek	Public Service Electric & Gas Company	50-354	1991
Duane Arnold Energy Center	Iowa Electric Power Company	50-331	1994
Limerick Units 1,2	PECO Energy	50-352/50-353	1994
Harris Pool B †	Carolina Power & Light Company	50-401	1996
Nine Mile Point Unit 1	Niagara Mohawk Power Corporation	50-220	1997
J.A. FitzPatrick (racks added)	NY Power Authority	50-333	1997
Chinshan 1,2	Taiwan Power Company (Taiwan)	—	1986
Kuosheng 1,2	Taiwan Power Company (Taiwan)	—	1991
Laguna Verde 1,2	Comision Federal de Electricidad (Mexico)	—	1991

† Fabricated racks for storage of spent fuel transshipped from Brunswick.

Table 3.2.3

1100 ALLOY ALUMINUM PHYSICAL CHARACTERISTICS

Density	0.098 lb/in^3 2.713 g/cm^3
Melting Range	1190°F - 1215°F 643°C - 657°C
Thermal Conductivity (77°F)	128 BTU/hr/ft^2/°F/ft 0.53 cal/sec/cm^2/°C/cm
Coefficient of Thermal Expansion (68°F - 212°F)	13.1 x 10^{-6} in/in-°F 23.6 x 10^{-6} cm/cm-°C
Specific Heat (221°F)	0.22 BTU/lb/°F 0.23 cal/g/°C
Modulus of Elasticity	10 x 10^6 psi
Tensile Strength (75°F)	13,000 psi (annealed) 18,000 psi (as rolled)
Yield Strength (75°F)	5,000 psi (annealed) 17,000 psi (as rolled)
Elongation (75°F)	35-45% (annealed) 9-20% (as rolled)
Hardness (Brinell)	23 (annealed) 32 (as rolled)
Annealing Temperature	650°F 343°C

Table 3.2.4

CHEMICAL COMPOSITION - ALUMINUM
(1100 ALLOY)

Aluminum	99.00% min.
Silicone and Iron	1.00% max.
Copper	0.05-0.20% max.
Manganese	0.05% max.
Zinc	0.10% max.
Other	0.15% max.

Table 3.2.5

CHEMICAL COMPOSITION AND PHYSICAL PROPERTIES
OF BORON CARBIDE

CHEMICAL COMPOSITION (WEIGHT PERCENT)	
Total boron	70.0 min.
B^{10} isotopic content in natural boron	18.0
Boric oxide†	3.0 max.
Iron†	2.0 max.
Total boron plus total carbon	94.0 min.
PHYSICAL PROPERTIES	
Chemical formula	B_4C
Boron content (weight percent)	78.28%
Carbon content (weight percent)	21.72%
Crystal structure	rhombohedral
Density	0.0907 lb/in^3 2.51 g/cm^3
Melting Point	4442°F 2450°C
Boiling Point	6332°F 3500°C

† Impurity that forms due to the chemical manufacturing process.

TABLE 3.4.1

RACK GEOMETRIC AND WEIGHT DATA

Rack Description	Size	Total Cells	Module Envelope Dimensions (inches)	Weight (Max.) (lbs)
Campaign I				
Campaign II				
Campaign III				

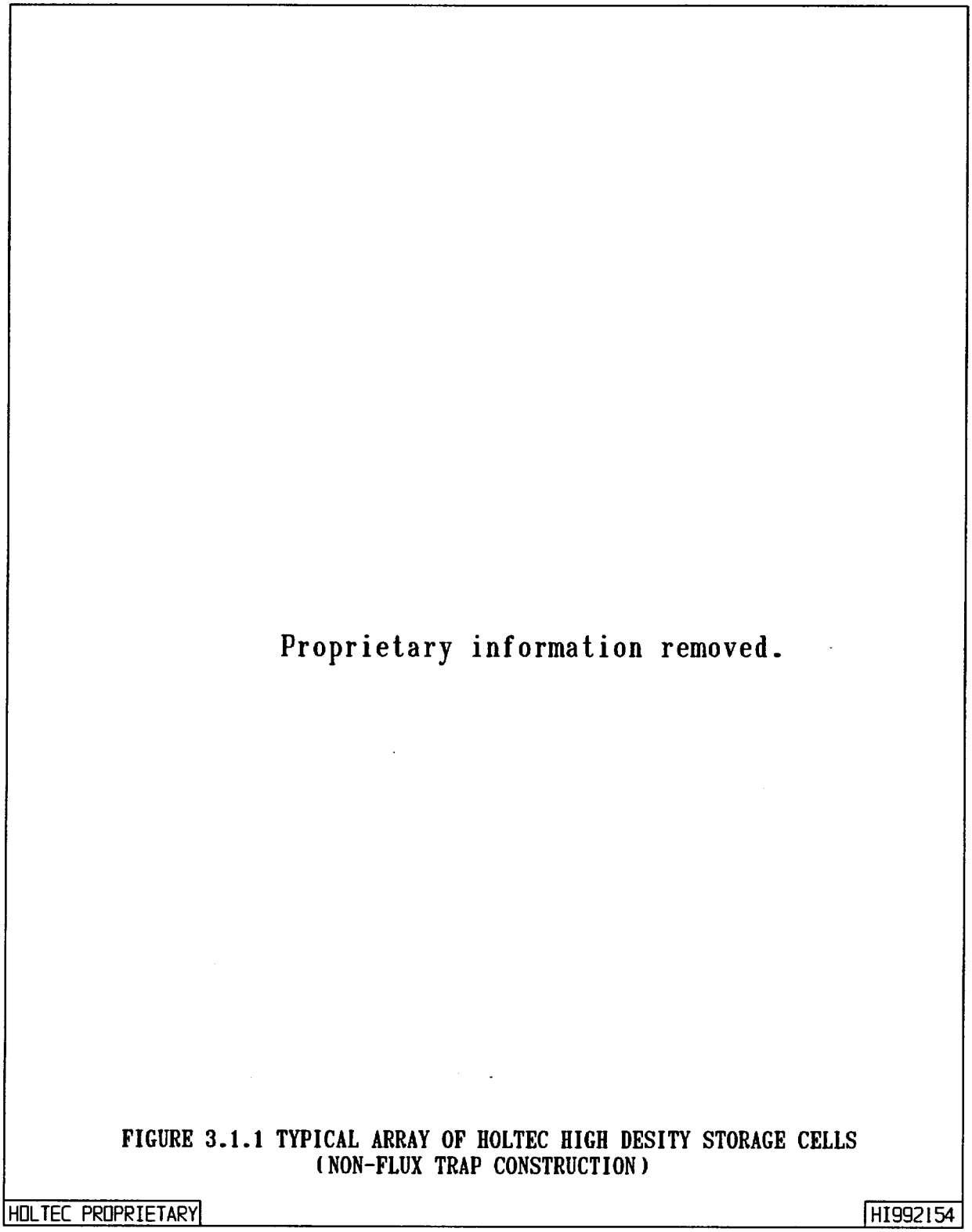

FIGURE 3.1.1 TYPICAL ARRAY OF HOLTEC HIGH DESITY STORAGE CELLS (NON-FLUX TRAP CONSTRUCTION)

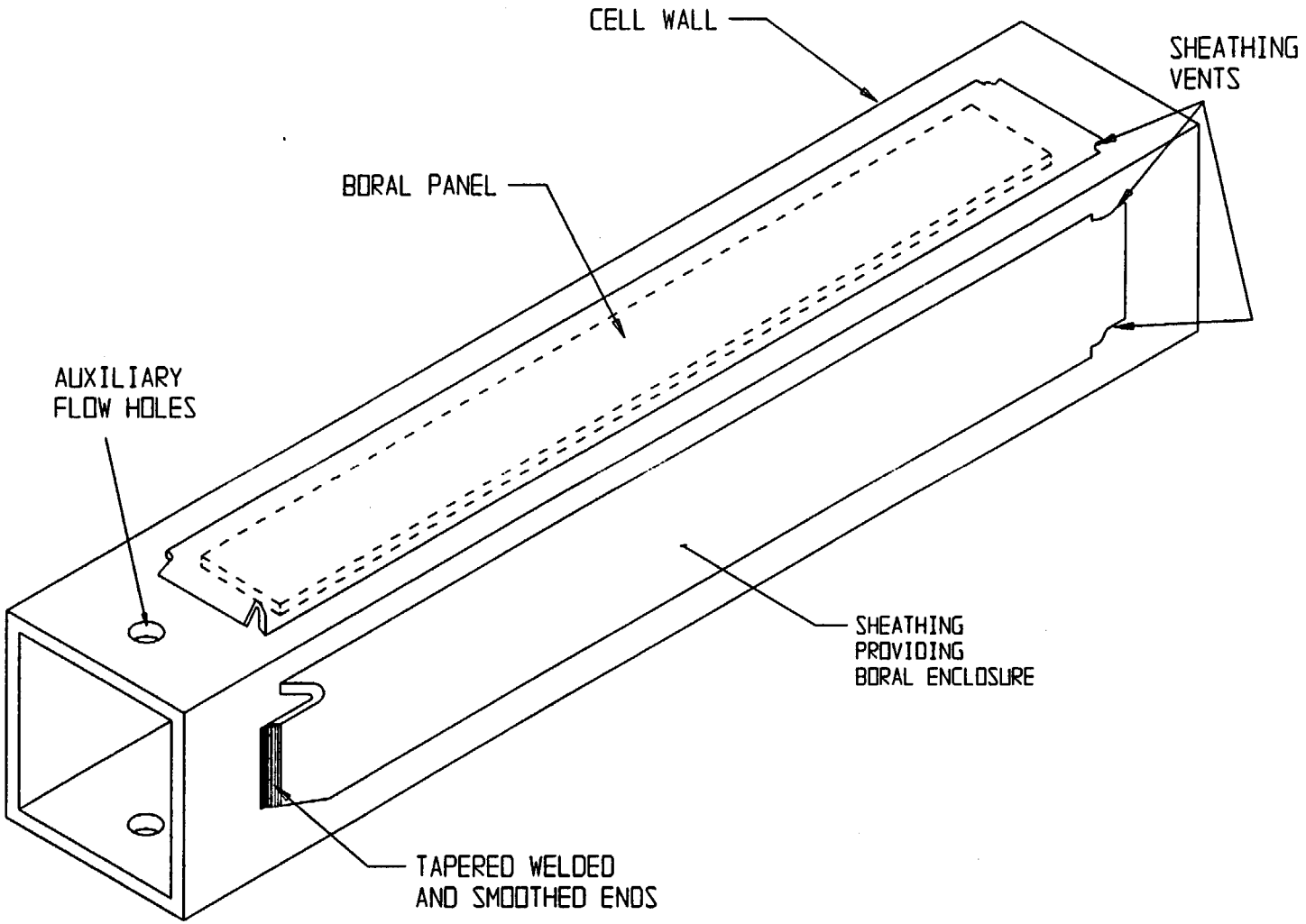

FIGURE 3.1.2; COMPOSITE BOX ASSEMBLY

HI-992154

\PROJECTS\980964\HI992154\3_2_2

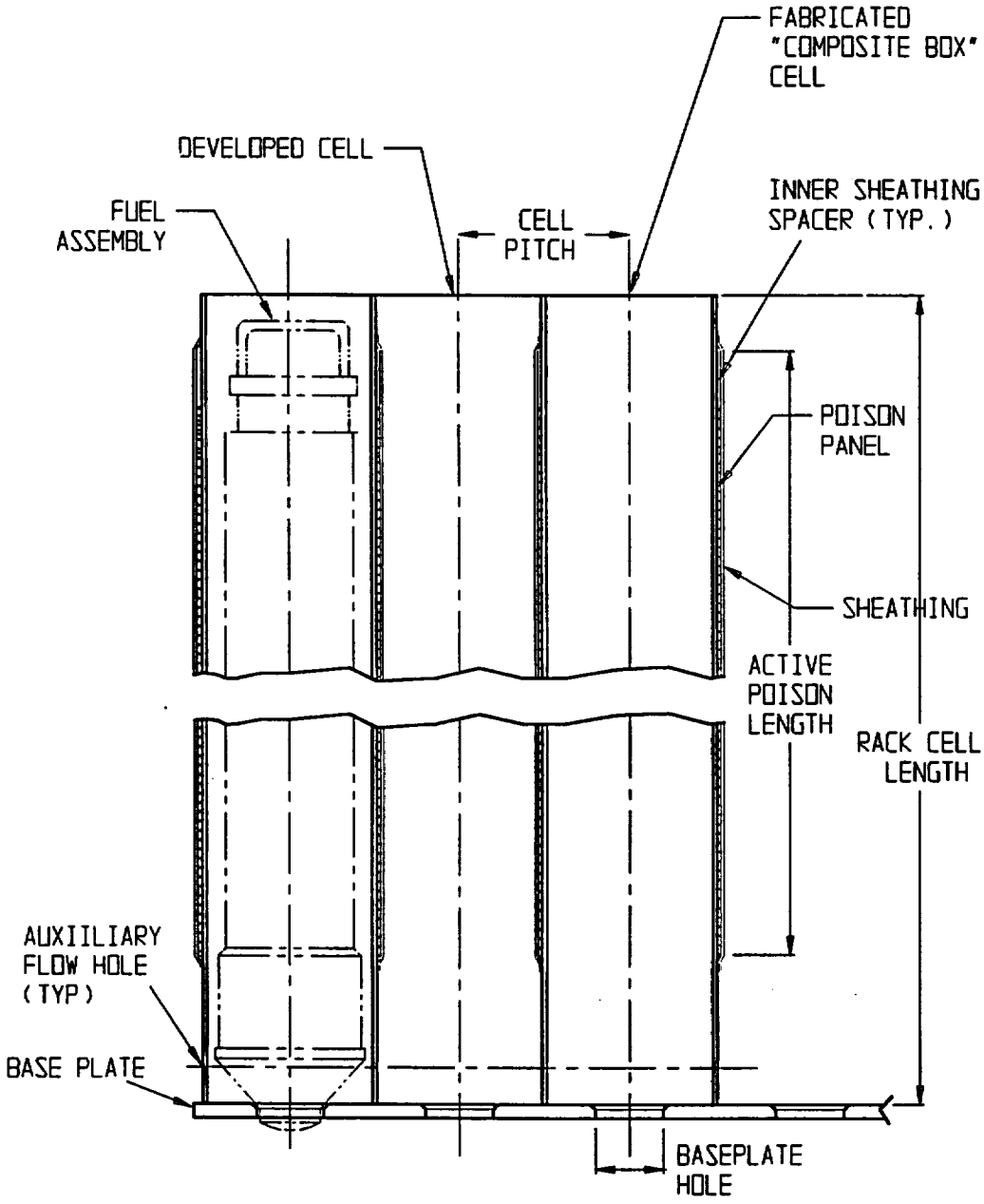

FIGURE 3.1.3
ELEVATION VIEW OF A TYPICAL BWR STORAGE RACK MODULE

HI-992154

\PROJECTS\980964\HI992154\3_2_3

4.0 CRITICALITY SAFETY EVALUATION

4.1 Introduction

4.1.1 Purpose

The Holtec high-density spent fuel storage racks for the Fermi 2 Nuclear Power Plant are designed to assure that the neutron multiplication factor (k_{eff}) is equal to or less than 0.95 with the racks fully loaded with fuel of the highest anticipated reactivity and the pool flooded with unborated water at a temperature corresponding to the highest reactivity. The maximum calculated reactivity includes a margin for uncertainty in reactivity calculations and in mechanical tolerances, statistically combined, giving assurance that the true k_{eff} will be equal to or less than 0.95 with a 95% probability at a 95% confidence level. Reactivity effects of abnormal and accident conditions have also been evaluated to assure that under credible abnormal and accident conditions, the reactivity will be maintained less than or equal to 0.95. The purpose of the present analysis is to confirm the acceptability of the rack design for the designated fuel assembly designs.

The fuel used as the design basis for the racks is a GE-12 (10x10) assembly with a (uniform) initial enrichment up to 5.0% U-235. All fuel assembly types to be stored in the high-density racks were explicitly analyzed to demonstrate their acceptability for storage.

Applicable codes, standards, and regulations, or pertinent sections thereof, include the following:

- *Code of Federal Regulations*, Title 10, Part 50, Appendix A, General Design Criterion 62, "Prevention of Criticality in Fuel Storage and Handling".
- USNRC Standard Review Plan, NUREG-0800, Section 9.1.2, Spent Fuel Storage, Rev. 3, July 1981.
- USNRC letter of April 14, 1978 to all Power Reactor Licensees - OT Position for Review and Acceptance of Spent Fuel Storage and Handling Applications, including modification letter dated January 18, 1979.

- USNRC Regulatory Guide 1.13, Spent Fuel Storage Facility Design Basis, Rev. 2 (proposed), December 1981.
- ANSI-8.17-1984, Criticality Safety Criteria for the Handling, Storage and Transportation of LWR Fuel Outside Reactors.
- L. Kopp, "Guidance On The Regulatory Requirements For Criticality Analysis Of Fuel Storage At Light-Water Reactor Power Plants", USNRC Internal Memorandum, L. Kopp to Timothy Collins, August 19, 1998.

4.1.2 Design Criteria and Assumptions

To assure the true reactivity will always be less than the calculated reactivity, the following conservative design criteria and assumptions were made.

- The racks were assumed to contain the most reactive fuel authorized to be stored in the facility without any control rods or any uncontained burnable poison.
- Moderator is pure, unborated water at a temperature within the design basis range corresponding to the highest reactivity.
- Criticality safety analyses are based upon the infinite multiplication factor (k_{inf}), i.e., lattice of storage racks is assumed infinite in all directions. No credit is taken for axial or radial neutron leakage, except in the assessment of certain abnormal/accident conditions where neutron leakage is inherent.
- Neutron absorption in minor structural members is neglected, i.e., spacer grids are replaced by water.

For the Fermi 2 spent fuel pool, the new fuel racks will be installed in three campaigns. At the completion of the first campaign, there will be three types of storage racks in the pool – (1) the new storage racks with Boral poison plates, (2) the existing racks with Boraflex poison panels , and (3) earlier model unpoisoned racks with large spacing. For the new racks, Boral panels on exterior surfaces of the storage modules prevent neutronic interaction with either of the two earlier rack types. The water gap between modules provide further isolation. Thus, there are no restrictions on storage in the new racks imposed by the other two types of racks in the same pool.

4.2 Summary and Conclusions

The fuel assembly used as the principal design basis for the racks is a standard GE 10x10 array (GE-12) of BWR fuel rods containing UO_2 clad in Zircaloy, and using uniform initial enrichments up to 5.0 wt% U-235. Explicit analyses of all other fuel assembly types were performed to confirm their acceptability for storage in the high-density racks. The effects of calculational and manufacturing tolerances were evaluated and added in determining the maximum k_{inf} in the storage rack. In BWR fuel, there is a wide variety of designs, including enrichment distribution and gadolinia loading, which often vary in the axial direction. Three different criteria, which bound fuel acceptability, for safe storage are defined as follows.

1. A maximum enrichment of 3.3% U-235, independent of burnup or the gadolinia normally used in BWR fuel or burnup.

2. A maximum nominal enrichment of 5.0 wt% U-235, with a maximum planar k_{inf} in the standard cold core geometry (SCCG) of 1.33, where the SCCG is defined as the multiplication factor (k_∞) for an infinite array of fuel assemblies on a 6-inch lattice spacing, at 20°C without voids or control rods.

3. A maximum nominal enrichment of 5.0 wt% U-235 with a minimum of 3.9 wt% Gd_2O_3 in at least 6 fuel rods.

These criteria are discussed more fully in subsequent paragraphs of this report. Any one of the three criteria is sufficient to determine the acceptability of fuel for safe storage in the spent fuel racks. These criteria should be applied to the axial (planar) region of highest reactivity. Each planar region should be separately evaluated to assure that the planar region of highest reactivity is assessed.

The basic calculations supporting the criticality safety of the Fermi 2 fuel storage racks are summarized in Tables 4.2.1a, 4.2.1b, and 4.2.1c. Abnormal and accident conditions were also evaluated. None of the abnormal or accident conditions that have been identified as credible will result in exceeding the limiting reactivity (k_{eff} of 0.95). The effects on reactivity of credible abnormal and accident conditions are summarized in Table 4.2.2. The double contingency principle endorsed in the USNRC letter of April 1978 specifies that it shall require at least two unlikely independent

and concurrent events to produce a criticality accident. This principle precludes consideration of the simultaneous occurrence of multiple accident conditions. Other hypothetical events were considered and no credible occurrences or configurations have been identified that might have any adverse effect on the storage rack criticality safety.

4.3 Input Parameters

4.3.1 Fuel Assembly Specifications

The design basis fuel assembly is a standard GE 10x10 array (GE-12) of BWR fuel rods containing UO_2 clad in Zircaloy. The ABB SVEA-96 fuel showed a slightly higher reactivity than the GE-12 fuel at 3.3% U-235 enrichment, but for practical purposes, the two fuel designs have comparable reactivities. For spent fuel, the GE-12 fuel exhibits the higher reactivity under comparable conditions. The GE-12 fuel assemblies (and the GE-11 fuel listed below) have some part-length rods resulting in a higher reactivity in the upper (partly-rodded) region. The designation "T" following the fuel designation, e.g. GE-12 (T) or GE-11 (T) refers to the upper, partly-rodded region.

Other designs were also evaluated, as listed below.

1. A GE-6 design 8x8 assembly with 62 fuel rods and 2 water rods,
2. A GE-8B design 8x8 assembly with 60 fuel rods and 4 water rods,
3. A GE-9B design 8x8 assembly with 60 fuel rods and 1 large water rod,
4. A GE-11 design 9x9 assembly with 74 fuel rods and 2 large water rods,
5. A ABB design SVEA-96 assembly, with a 10x10 rod array and a single large water rod and four smaller water rods.

The GE-11 and the GE-12 fuel designs have part-length fuel rods, resulting in a planar region of higher reactivity above the part-length rods. For conservatism, this region was used for the design basis calculations for the GE-11 and GE-12 assemblies. Design parameters for the six types of fuel assemblies considered in this evaluation are summarized in Table 4.3.1

4.3.2 Storage Rack Cell Specifications

The high-density storage rack cells consists of an egg-crate structure, a cell of which is illustrated in Figure 4.3.1, with fixed neutron absorber material (Boral) of [ ] boron-10 areal density positioned between the fuel assembly storage cells in a [ ] channel. This arrangement provides a nominal center-to-center lattice spacing of 6.23[ ] Manufacturing tolerances used in evaluating uncertainties in reactivity are indicated in Table 4.3.2. The 0.075-inches stainless-steel box that defines the fuel assembly storage cell has a nominal inside dimension of 6.035 inches. This allows adequate clearance for inserting/removing the fuel assemblies, with or without the Zircaloy flow channel. The Boral panels are [ ] long [ ] wide, and [ ] thick. Boral panels are not needed or used on the exterior walls of modules facing non-fueled regions, i.e., the pool walls. Similarly, Boral panels are used on only one exterior surface of the modules that face each other across the small water gap between the modules.

4.4 Analytical Methodology

4.4.1 Computer Codes and Benchmarking

In the fuel rack evaluation, criticality analyses of the high-density spent fuel storage racks were performed with the CASMO4 code [4.7.1], a two-dimensional multi-group transport theory code. Independent verification calculations were made with the KENO5a code [4.7.2] using the 238-group SCALE* cross-section library with the NITAWL subroutine for U-238 resonance shielding effects (Nordheim integral treatment), and with the MCNP code [4.7.3] (a continuous energy Monte Carlo code developed by the Los Alamos National Laboratory). KENO5a has been endorsed by the USNRC [4.7.4].

Benchmark calculations are presented in Appendix 4A and indicate a bias of 0.0009 ± 0.0011 for MCNP4a and 0.0030 ± 0.0012 for NITAWL-KENO5a, when applying the one sided k-factor for

---

* SCALE is an acronym for Standardized Computer Analysis for Licensing Evaluation, a computer code system developed by the Oak Ridge Laboratory for the USNRC.

95% probability at the 95% confidence level (95%/95% level). In the geometric model used in the calculations, each fuel rod and its cladding were explicitly described and reflecting boundary conditions (zero neutron current) were used in the axial direction and at the equivalent centerline of the Boral and steel plate between storage cells. These boundary conditions have the effect of conservatively creating an infinite array of storage cells in all directions.

The CASMO4 computer code was used as the primary method of analysis as well as a means of evaluating small reactivity increments associated with manufacturing tolerances. Burnup calculations were also performed with CASMO4, using the restart option to describe spent fuel in the storage cell. KENO5a was used to assess the reactivity consequences of eccentric fuel positioning, and abnormal locations of fuel assemblies.

4.4.2 CASMO4 Validation

The CASMO4 calculations were validated (benchmarked) against KENO5a and MCNP for the specific fuel assemblies and geometries involved. Comparison calculations are listed in Table 4.4.1 for fuel of 3.3% enrichment. (KENO5a and MCNP results are bias corrected and listed at the 95%/95% level)*. These data confirm the validity of the CASMO4 calculations, and suggest that they are conservative.

4.4.3 Gadolinia Effects and Burnup

Gadolinia (Gd_2O_3) is used in all BWR fuel designs as a means of augmenting reactivity control in core operations. Gadolinium has a higher cross-section than U-235 and the reactivity of an assembly increases with burnup, reaching a maximum at some point in burnup where the Gadolinium is virtually depleted. For fuel of 5.0% average enrichment, Figure 4.4.1 illustrates the reactivity variation with burnup for several illustrative Gadolinia loadings with GE-12 fuel of 5.0% enrichment, evaluated in the spent fuel storage racks (without bias or uncertainties). Some of these example fuel assemblies would be acceptable for storage and some would not. Also shown in Figure 4.4.1 is the calculation without any Gd_2O_3.

* K-factor for one-sided tolerance at 95%/ 95% from NBS Handbook 91 [4.7.5] is 1.70.

These cases also include calculation of the k_{inf} in the SCCG. Associated with each of the fuel assemblies in Figure 4.4.1 are values of the k_{inf} in the standard cold core geometry. Figure 4.4.2 is a correlation of the k_{inf} in the SCCG to the corresponding peak values of k_{inf} in the storage rack. Figure 4.4.2 also shows the correlation curve calculated without any Gadolinia. This latter curve correlates well with the cases calculated with gadolinia and illustrates that assemblies with a maximum k_{inf} of 1.33 in the SCCG will be acceptable for storage in the racks. (Note the values in the figure do not include uncertainties; see Table 4.2.1b for the maximum k_{inf} values with uncertainties.)

Figure 4.4.3 shows similar correlations for all of the fuel types considered (calculated without gadolinia) and confirms that the GE-12 assembly type at 5.0% enrichment bounds all other fuel types considered at a k_{inf} (SCCG) of 1.33. However, in order to include additional criticality margin for the new racks and maintain consistency with the existing Technical Specifications, storage will be limited to fuel with a maximum k_{inf} in the standard cold core geometry (SCCG) of 1.31.

The data in Figure 4.4.1, which corresponds to the design basis assembly, may also be correlated with Gd_2O_3 loading as illustrated in Figure 4.4.4. These data may be used to define the minimum acceptable (initial) Gd_2O_3 loading for 6 or 8 Gd_2O_3 rod configurations.

4.5 Criticality Analyses and Tolerance Variations

4.5.1 Nominal Design Case

4.5.1.1 Enrichment Limit Criterion

Calculations were made for the various fuel types considered conservatively assuming an average uniform enrichment of 3.3% U-235 without any gadolinia. The maximum reactivity values, including all calculational and manufacturing uncertainties, are listed in Table 4.2.1a. These calculations confirm that 3.3% enrichment for all fuel types is acceptable for storage in the racks. The criteria of a maximum enrichment of 3.3% is therefore acceptable, without any consideration of the Gadolinia normally present in the fuel, burnup, or the SCCG k_{inf}.

4.5.1.2 Maximum k_{inf} in the Standard Cold Core Geometry

It is conventional practice for the fuel vendor, in developing a specific assembly design, to provide values for k_{inf} in the SCCG for each planar (axial) region of significantly different composition or arrangements. These k_{inf} values are provided at 0% void (core inlet), 40% void (core average), and 70% void (exit condition). The 40% core average is the most meaningful since the 0% and 70% void calculations are applicable only to the ends of the assemblies (small volume and high leakage). The initial design Gd_2O_3 loading enters into the fuel vendor's calculations of the burnup at which the peak reactivity occurs. At this burnup, the gadolinium is essentially depleted. Consequently, calculations of the reactivity in the storage rack do not need to include gadolinium, but only the average enrichment. Calculations are provided herein illustrating this fact and correlating the k_{inf} in the storage rack to the vendor-supplied k_{inf} in the SCCG. Figure 4.4.2 illustrates the variation in reactivity of the storage rack with values of the k_{inf} in the SCCG. The acceptance criterion for safe storage of spent fuel is that the vendor-supplied k_{inf} in the SCCG must be equal to or less than 1.33 for the planar region of highest reactivity. Thus, the k_{inf} values in the storage rack are interpolated for a k_{inf} in the SCCG of 1.33.

The maximum k_{inf} values in the racks for the limiting k_{inf} in the core, including all calculational and manufacturing uncertainties, are listed in Table 4.2.1b. The maximum k_{inf} values include a conservative allowance of 0.01 Δk for possible differences between fuel vendor calculations of the SCCG k_{inf} and those reported here. These calculations confirm that, for fuel of 5.0% enrichment or less, the criteria of a maximum k_{inf} of 1.33 in the SCCG will assure compliance with the regulatory guidelines (k_{eff} limit of 0.95).

4.5.1.3 Criteria for Minimum Gadolinia Loading

Gadolinia (Gd_2O_3) is normally used in BWR fuel to augment reactivity control during in-core operation. A very wide variety of Gd_2O_3 loadings are commonly used – often differing in axial (planar) regions. Furthermore, the Gd_2O_3 loadings for fuel of 5% average enrichment have not yet been developed. However, it is possible to develop and define criteria for the minimum Gd_2O_3

loadings required to assure that the peak reactivity over burnup is always less than the regulatory limit.

Results of the analysis of a series of cases with various Gd_2O_3 loadings were described earlier (Section 4.4.3) and summarized in Figures 4.4.1 and 4.4.4, for fuel of 5% initial average enrichment. Figure 4.4.4 shows the effect of Gd_2O_3 concentration for 6 and 8 Gd_2O_3 rods per assembly. The upper curve for 6 Gd_2O_3 rods per assembly may be interpolated for a reference k_{inf} of 0.9200, to obtain a bounding criteria of 3.9% Gd_2O_3 in each rod (see Table 4.2.1c). The 6-rod case bounds cases of 8 or more Gd_2O_3 rods per assembly. At enrichments less than 5%, the peak reactivity will be even lower, and the criteria of 3.9% Gd_2O_3 in at least 6 rods will be even more conservative. Thus, the criterion on a minimum Gadolinia loading (including tolerance on Gd_2O_3 content), evaluated at the axial planar region of the highest reactivity, will assure safe storage of all fuel assemblies and conformance with the NRC guidelines.

For enrichments less than 3.3%, the maximum k_{inf} in the rack is less than 0.95 (including uncertainties and allowances) regardless of gadolinia content or the k_{inf} in the SCCG, and thus, these two criteria need not be considered

4.5.2 Uncertainties Due to Manufacturing Tolerances

4.5.2.1 Rack Manufacturing Tolerances

The GE-12 assembly was used for the evaluation of incremental reactivity changes due to manufacturing tolerances. The reactivity effects associated with manufacturing tolerances are listed in Table 4.3.2 and discussed below. Values at 14 MWD/kgU burnup (the approximate burnup for a k_{inf} of 1.33 in the SCCG) were used, although the reactivity uncertainties are nearly insensitive to burnup.

4.5.2.2 Boron Loading Variation

The Boral absorber panels used in the storage cells are nominally [redacted], with a B-10 areal density of [redacted]. The manufacturing tolerance limit is [redacted] in B-10 content, including both thickness and composition tolerances. This assures that the minimum boron-10 areal density will not be less than [redacted] in any panel. Differential CASMO4 calculations were performed for the incremental reactivity uncertainty due to Boron loading variations. The results are shown in Table 4.3.2.

4.5.2.3 Boral Width Tolerance Variation

The reference storage cell design uses a Boral panel width of [redacted]. The tolerance on the Boral width is [redacted]. Since the analysis used the minimum Boral panel width, no tolerance uncertainty is necessary.

4.5.2.4 Lattice Spacing Variation

The design storage cell lattice spacing is 6.23 inches. Decreasing the lattice spacing increases the reactivity. The manufacturing tolerance is [redacted] and the corresponding uncertainty in reactivity is listed in Table 4.3.2.

4.5.2.5 Stainless Steel Thickness Tolerances

The nominal thickness of the stainless steel box is 0.075 inches with [redacted] for the steel sheath. The maximum positive reactivity effects of the expected stainless steel thickness tolerance were calculated with CASMO4, and are listed in Table 4.3.2.

4.5.2.6 Zircaloy Flow Channel

Elimination of the Zircaloy flow channel results in a small decrease in reactivity. More significant is a positive reactivity effect resulting from potential bulging of the Zircaloy channel, which moves the channel wall outward replacing water near the Boral absorber. For the maximum expected

bulging (based on estimates provided by GE) and conservatively assumed to be uniform throughout all assemblies, an incremental reactivity of + 0.0053 Δk could result (determined by differential CASMO4 calculations). Although the bulging penalty would not be expected to occur uniformly everywhere, the maximum penalty was conservatively treated as an additive factor, rather than being statistically combined with other uncertainties. [ ] With unburned fuel of 3.3% enrichment, channel bulging will not yet have developed. As burnup progresses, the reduction in reactivity due to depletion would more than compensate for any reactivity increase as bulging slowly develops. Because of the way the SVEA-96 assembly is designed, channel bulging would not occur, and thus, the reactivity penalty is not applicable to the SVEA-96 assembly.

4.5.3 Fuel Tolerances (Enrichment, Density, and Depletion Uncertainties)

CASMO4 calculations of the sensitivity to small changes in fuel enrichment and UO_2 density gave uncertainties listed in Table 4.3.2. The enrichment tolerance was assumed to be 0.05 wt% U-235, evaluated at 3.3% enrichment, and becomes smaller for higher enrichments. Calculations were also made to determine the sensitivity to the tolerance in UO_2 fuel density (± 0.20 g/cc). These calculations are summarized in Table 4.3.2, based on an assumed maximum density of 10.72 g/cc* stack density. Lower fuel densities would result in lower values of reactivity.

Since critical experiment data with spent fuel is not available for determining the uncertainty in depletion calculations, an allowance for uncertainty in reactivity was assigned based upon other considerations. In the Fermi racks, the reactivity decrement (from fresh to the burnup at which the peak occurs) in the absence of gadolinium is 0.0966 Δk. It is assumed that the uncertainty in depletion calculations is less than 5% of the total reactivity decrement, as shown in Tables 4.2.1b, and 4.2.1c.

* Calculations actually run with a UO_2 density of 10.77, which is conservative.

4.6 Abnormal and Accident Conditions

4.6.1 Temperature and Water Density Effects

The moderator temperature coefficient of reactivity is negative. Using the minimum temperature of 4°C (maximum possible water density) therefore assures that the true reactivity will always be lower than the calculated value regardless of the temperature. Temperature effects on reactivity have been calculated and the results are shown in Table 4.6.1. Introducing voids in the water in the storage cells (to simulate boiling) decreased reactivity, as shown in the table. Boiling at the submerged depth of the racks would occur at approximately 120°C. The only significance of these calculations is to confirm that the temperature and void coefficients of reactivity are negative and the reference temperature of 4°C is conservative.

4.6.2 Abnormal Location of a Fuel Assembly

It is hypothetically possible to suspend a fuel assembly of the highest allowable reactivity outside and adjacent to the fuel rack, although such an accident condition is highly unlikely. The exterior walls of the rack modules facing the outside (where such an accident condition might be conceivable) is a region of high neutron leakage. For comparison to the reference k_{inf}, calculations were performed for this condition with and without an extraneous fuel assembly present. The calculations were performed with the GE-12 (T) fuel assembly at 3.3% enrichment and Boral panels were not included on the exterior rack wall. With neutron leakage included, the k_{eff} with an extraneous fuel assembly of the maximum reactivity, located outside and adjacent to the fuel rack, is less than the reference KENO k_{inf}. Thus it is concluded that the abnormal location of a fuel assembly will have a negligible reactivity effect.

4.6.3 Eccentric Fuel Assembly Positioning

The fuel assembly is normally located in the center of the storage rack cell with bottom fittings and spacers that mechanically restrict lateral movement of the fuel assemblies. Nevertheless, calculations were performed with the fuel assembly moved into the corner of the storage rack cell (four-assembly cluster at closest approach) to investigate the effect on reactivity. An enrichment of 3.3% was used. These calculations resulted in a small negative reactivity effect. Thus, the nominal case, with the fuel assembly positioned in the center of the storage cell, yields the higher reactivity. KENO5a was used for these calculations.

4.6.4 Zircaloy Fuel Channel Distortion

Consequences of bulging of the Zircaloy fuel channel are treated as a mechanical deviation in Section 4.5.2.6, where a small reactivity increase is shown. Bowing of the zirconium channel (including fuel rods) results in a local negative reactivity effect analogous to that of eccentric positioning the fuel assembly toward one side of the storage cell. Thus, any bowing that might occur will result in a reduction in reactivity.

4.6.5 Dropped Fuel Assembly

For a drop on top of the rack, the fuel assembly will come to rest horizontally on top of the rack with a minimum separation distance from the active fuel region of more than the 12 inches, which is sufficient to preclude neutron coupling (i.e., an effectively infinite separation). Maximum expected deformation under seismic or accident conditions will not reduce the minimum spacing to less than 12 inches. It is conceivable that a dropped assembly might penetrate a storage cell in a vertical position, impacting and causing local deformation of the base plate. Analysis indicates that the maximum local deformation is [redacted], with smaller deformations in the immediately adjacent cells. Conservative calculations, using a bounding deviation of [redacted] of exposed fuel in all cells everywhere, showed that the k_{eff} of the rack was less than the reference k_{inf} and therefore there would be no significant increase in the design basis reactivity. Consequently, fuel assembly drop accidents

will not result in a significant increase in reactivity and are within the expected statistical variation of KENO5a calculations.

4.6.6 Fuel Rack Lateral Movement

Boral panels are installed in the rack wall along one side of the water gap between adjacent racks. With this configuration, the maximum reactivity of the storage rack is not dependent upon the water-gap spacing between modules. Thus, misalignment of the racks or seismically induced movement will not affect the reactivity of the rack. The reactivity effects of abnormal and accident conditions are summarized in Table 4.2.2.

4.7 References for Chapter 4

[4.7.1] A. Ahlin and M. Edenius, "CASMO - A Fast Transport Theory Depletion Code for LWR Analysis," ANS Transactions, Vol. 26, p. 604, 1977.

M. Edenius, et al., "CASMO4, A Fuel Assembly Burnup Program, Users Manual", Studsvik Report SOA/95/1, Studsvik Report (proprietary).

[4.7.2] N.M. Greene, et al., "NITAWL-II: Scale System Module for Performing Resonance Shielding and Working Library Production", in SCALE: A Modular Code System for Performing Standardized Computer Analyses for Licensing Evaluation, NUREG/CR-0200, Rev. 4, January 1990.

L.M. Petrie and N.F. Landers, "KENO5a - An Improved Monte Carlo Criticality Program with Supergrouping:, in SCALE: A Modular Code System for Performing Standardized Computer Analyses for Licensing Evaluation, NUREG/CR-0200, Rev. 4, January 1990.

[4.7.3] J.F. Briesmeister, Ed., "MCNP- A General Purpose Monte Carlo N-Particle Transport Code, Version 4A", Los Alamos National Laboratory, LA-12625-M (1993).

[4.7.4] L.I. Kopp, "Guidance on the Regulatory Requirements for Criticality Analysis of Fuel Storage at Light Water Reactor Plants", USNRC memorandum, Kopp to Collins, August 1998.

[4.7.5] M.G. Natrella, Experimental Statistics, National Bureau of Standards, Handbook 91, August 1963.

Table 4.2.1a

SUMMARY OF CRITICALITY SAFETY ANALYSES

For Fuel of 3.3% Enrichment

Temperature assumed for analysis	4°C
Fuel Enrichment (average)	3.3%
Gd_2O_3 loading %	N/A
Reference CASMO4 k_{inf}	
GE-12 Fuel (T)	0.9218
GE-6 Fuel	0.9193
GE-8B Fuel	0.9189
GE-9B Fuel	0.9181
GE-11 Fuel (T)	0.9204
SVEA-96 Fuel	0.9232
Uncertainties	
Removal of flow channel	negative
Eccentric assembly location	negative
Tolerances (Table 4.3.2)	±0.0073
Uncertainty in Depletion calculations	N/A
Effect of Channel Bulge	N/A
Maximum Reactivity	
GE-12 Fuel (T)	0.9218 ± 0.0073 = 0.9291
GE-6 Fuel	0.9193 ± 0.0073 = 0.9266
GE-8B Fuel	0.9189 ± 0.0073 = 0.9262
GE-9B Fuel	0.9181 ± 0.0073 = 0.9254
GE-11 Fuel (T)	0.9204 ± 0.0073 = 0.9277
SVEA-96 Fuel	0.9232 ± 0.0073 = 0.9305

Table 4.2.1b
SUMMARY OF CRITICALITY SAFETY ANALYSES
For Limiting k_{inf} in the SCCG

Temperature assumed for analysis	4°C
Initial Fuel Enrichment (average)	5.0
Maximum k_{inf} in SCCG	1.33
Reference CASMO4 k_{inf}	
GE-12 Fuel (T)	0.9241
GE-6 Fuel	0.9167
GE-8B Fuel	0.9181
GE-9B Fuel	0.9182
GE-11 Fuel (T)	0.9235
SVEA-96 Fuel	0.9205
Uncertainties	
Removal of flow channel	negative
Eccentric assembly location	negative
Tolerances (Table 4.3.2)	± 0.0073
Uncertainty in Depletion calculations	± 0.0048
Statistical Combination*	± 0.0087
Effect of Channel Bulge	+ 0.0053**
Comparison to Vendor Calculations	+ 0.0100
Maximum Reactivity	
GE-12 Fuel (T)	0.9394 ± 0.0087 = 0.9481
GE-6 Fuel	0.9320 ± 0.0087 = 0.9407
GE-8B Fuel	0.9334 ± 0.0087 = 0.9421
GE-9B Fuel	0.9335 ± 0.0087 = 0.9422
GE-11 Fuel (T)	0.9388 ± 0.0087 = 0.9475
SVEA-96 Fuel	0.9305 ± 0.0087 = 0.9392**

* Square root of sum of squares of all independent tolerance effects
** Channel bulging not applicable to SVEA fuel

Table 4.2.1c
SUMMARY OF CRITICALITY SAFETY ANALYSES
For Minimum Gd_2O_3

Temperature assumed for analysis	4°C
Initial Fuel Enrichment (average)	5.0%
Gd_2O_3 loading %	6 rods with 3.9% Gd_2O_3
Reference CASMO4 k_{inf} GE-12 Fuel (T)	0.9200
Uncertainties	
Removal of flow channel	negative
Eccentric assembly location	negative
Tolerances (Table 4.3.2)	± 0.0073
Uncertainty in Depletion calculations	± 0.0048
Statistical Combination*	± 0.0087
Effect of Channel Bulge	+ 0.0053
Maximum Reactivity GE-12 Fuel (T)	0.9253 ± 0.0087 = 0.9340 (Peak)

* Square root of sum of squares of all independent tolerance effects

Table 4.2.2

REACTIVITY EFFECTS OF ABNORMAL AND ACCIDENT CONDITIONS

Accident/Abnormal Condition	Reactivity Effect
Temperature increase	Negative (Table 4.6.1)
Void (boiling)	Negative (Table 4.6.1)
Eccentric Fuel Assembly Positioning	Negative
Zircaloy Fuel Channel Distortion	Negative
Assembly dropped on top of rack	Negligible
Abnormal Location of a fuel assembly	Negligible
Seismic Movement	Negligible

Table 4.3.1

FUEL ASSEMBLY DESIGN SPECIFICATIONS

FUEL ROD DATA	GE-6	GE-8B	GE-9B
Cladding outside diameter, in.	0.483	0.483	0.483
Cladding inside diameter, in.	0.419	0.419	0.419
Cladding material	Zr-2	Zr-2	Zr-2
Pellet diameter, in.	0.410	0.411	0.411
Enrichment (design basis)	5%	5%	5%
UO_2 density (stack), % of theoretical	95.5-96.5%	95.5-96.5%	95.5-96.5%
WATER ROD DATA			
Number of water rods	2	4	1
Inside diameter, inch	0.531	0.531, 0.433	1.260
Outside diameter	0.591	0.591, 0.483	1.340
Material	Zr-2	Zr-2	Zr-2
FUEL ASSEMBLY DATA			
Fuel rod array	8x8	8x8	8x8
Number of fuel rods	62	60	60
Fuel rod pitch, inch	0.64	0.64	0.64
Fuel channel, material	Zr-2	Zr-2	Zr-2
Inside dimension, inch	5.278	5.278	5.278
Outside dimension, inch	100 mil	100 mil	80 mil

(Continues on following page)

Table 4.3.1 (continued)

FUEL ASSEMBLY DESIGN SPECIFICATIONS

FUEL ROD DATA	GE-11	GE-12	ABB SVEA-96
Cladding outside diameter, in.	0.440	0.404	0.3787
Cladding inside diameter, in.	0.384	0.352	0.3291
Cladding material	Zr-2	Zr-2	Zr-2
Pellet diameter, in.	0.376	0.345	0.3224
Enrichment (design basis)	5%	5%	5%
UO_2 density (stack), % of theoretical	95.5-96.5%	95.5-96.5%	95.5-96.5%
WATER ROD DATA			
Number of water rods	2	2	5
Inside diameter, inch	0.920	0.920	4 small
Outside diameter	0.980	0.980	1 large
Material	Zr-2	Zr-2	Zr-2
FUEL ASSEMBLY DATA			
Fuel rod array	9x9	10x10	10x10
Number of fuel rods	66/74*	78/92†	96
Fuel rod pitch, inch	0.566	0.510	0.488
Fuel channel, material	Zr-2	Zr-2	Zr-2
Inside dimension, inch	5.278	5.278	5.126
Outside dimension, inch	100/65 mil**	100/65 mil**	5.457

* The GE-11 (9x9) assembly contains 66 full-length rods and 8 part-length rods

† Thr GE-12 assembly contains 78 full length-rods and 14 part-length rods.

** Actual fuel channel is 50 or 65 mil thick with 100 mil on corners. Conservative average of 80 mil is used.

Table 4.3.2

REACTIVITY UNCERTAINTIES DUE TO
MANUFACTURING TOLERANCES

Quantity	Nominal Value	Tolerance	Δk_{inf}
B-10 Loading	[redacted]	[redacted]	±0.0043
Lattice spacing	[redacted]	[redacted]	±0.0031
SS thickness	[redacted]	[redacted]	±0.0011
Fuel enrichment	@ 3.3% U-235	±0.05% U-235	±0.0039*
Fuel density	10.52 g/cm^3	±0.20 g/cm^3	±0.0029
Statistical combination **of tolerance uncertainties			±0.0073

Note: uncertainty in depletion calculations (Section 4.5.3) is included in Table 4.2.1.

* Effect of enrichment tolerance is significantly smaller at higher enrichments
** Square root of sum of squares of all independent tolerance effects.

Table 4.4.1
COMPARISON OF CALCULATIONAL METHODS
@ 3.3% ENRICHMENT

	CASMO4	KENO5a	MCNP
GE 12 Fuel			
Calculated k_{inf}	0.9189	0.9142 ± 0.0003	0.9161 ± 0.0004
Corrected* k_{inf}		0.9172 ± 0.0013	0.9169 ± 0.0013
GE 12 Fuel (T)			
Calculated k_{inf}	0.9218	0.9171 ± 0.0003	0.9191 ± 0.0004
Corrected* k_{inf}		0.9201 ± 0.0013	0.9200 ± 0.0013
GE-6 8x8			
Calculated k_{inf}	0.9193	0.9114 ± 0.0003	0.9156 ± 0.0003
Corrected* k_{inf}		0.9144 ± 0.0013	0.9165 ± 0.0012
GE-8B 8x8			
Calculated k_{inf}	0.9189	0.9104 ± 0.0003	0.9145 ± 0.0004
Corrected* k_{inf}		0.9134 ± 0.0013	0.9154 ± 0.0013
GE-9B 9x9			
Calculated k_{inf}	0.9181	0.9121 ± 0.0003	0.9144 ± 0.0003
Corrected* k_{inf}		0.9151 ± 0.0013	0.9153 ± 0.0012
GE-11			
Calculated k_{inf}	0.9183	0.9121 ± 0.0003	0.9163 ± 0.0004
Corrected* k_{inf}		0.9151 ± 0.0013	0.9172 ± 0.0013
GE-11 (T)			
Calculated k_{inf}	0.9204	0.9141 ± 0.0003	0.9177 ± 0.0004
Corrected* k_{inf}		0.9171 ± 0.0013	0.9186 ± 0.0013
ABB SVEA-96			
Calculated k_{inf}	0.9232	0.9202 ± 0.0003	0.9233 ± 0.0004
Corrected* k_{inf}		0.9232 ± 0.0013	0.9242 ± 0.0013

* Includes Monte Carlo statistics and uncertainty in bias, at 95% probability, 95% confidence level (one-sided), where the k-factor is 1.70.

Table 4.6.1

EFFECT OF TEMPERATURE AND VOID ON CALCULATED REACTIVITY OF STORAGE RACK

Case	Incremental Reactivity Change, Δk	
	GE-12 Partly-Rodded	GE-12 Fully-Rodded
4°C (39°F)	Reference	Reference
20°C (68°F)	-0.0020	-0.0017
50°C (122°F)	-0.0072	-0.0068
110°C (230°F)	-0.0188	-0.0180
120°C (248°F)	-0.0203	-0.0193
120°C + 20% void	-0.0399	-0.0400

PROPRIETARY

Proprietary information removed.

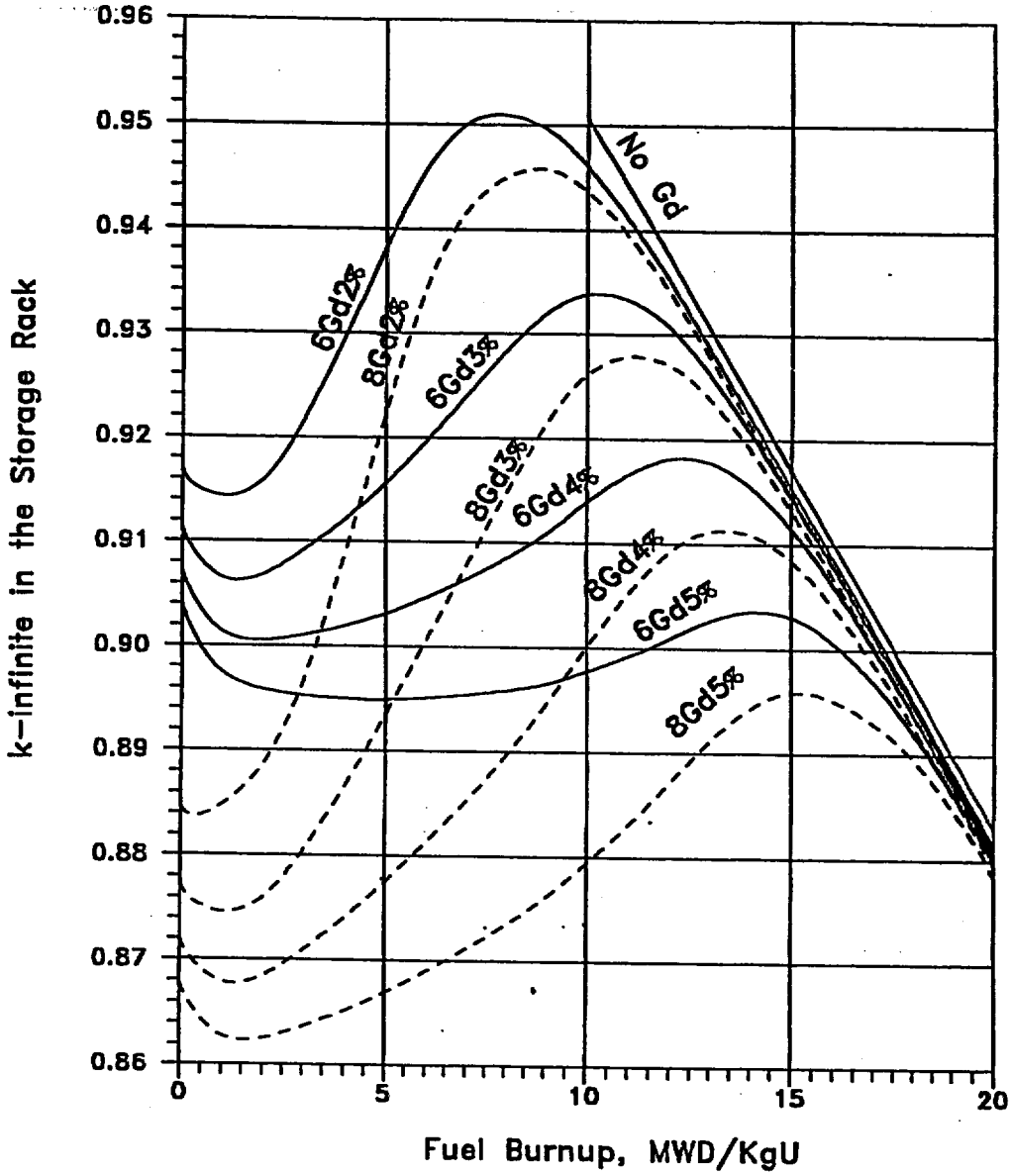

Fig. 4.4.1 k-inf in the Storage Rack at Various Fuel Burnups and Gadolinia Loadings

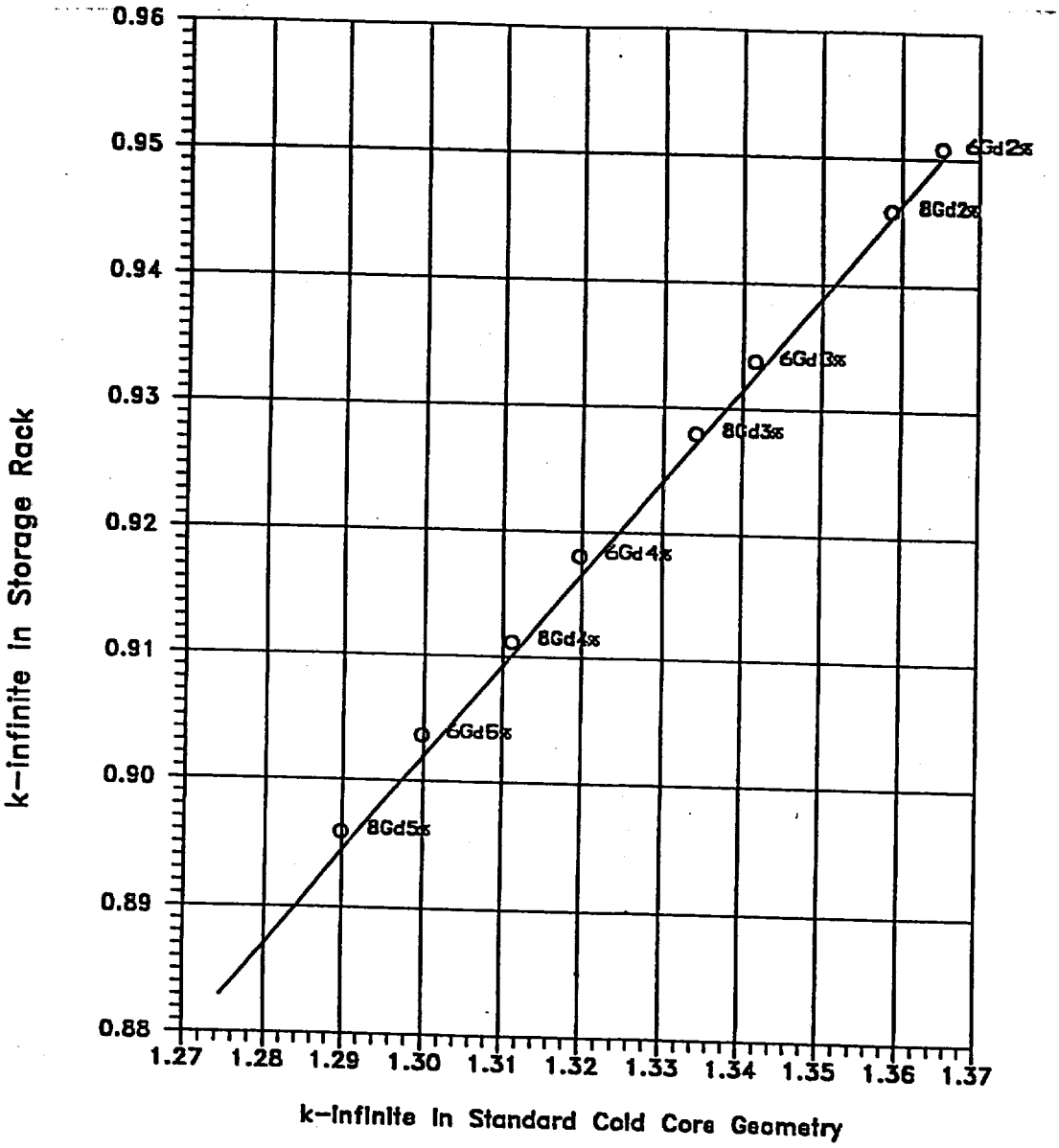

Fig. 4.4.2 Correlation of k-infinite in the Storage Rack and the k-infinite in the SCCG

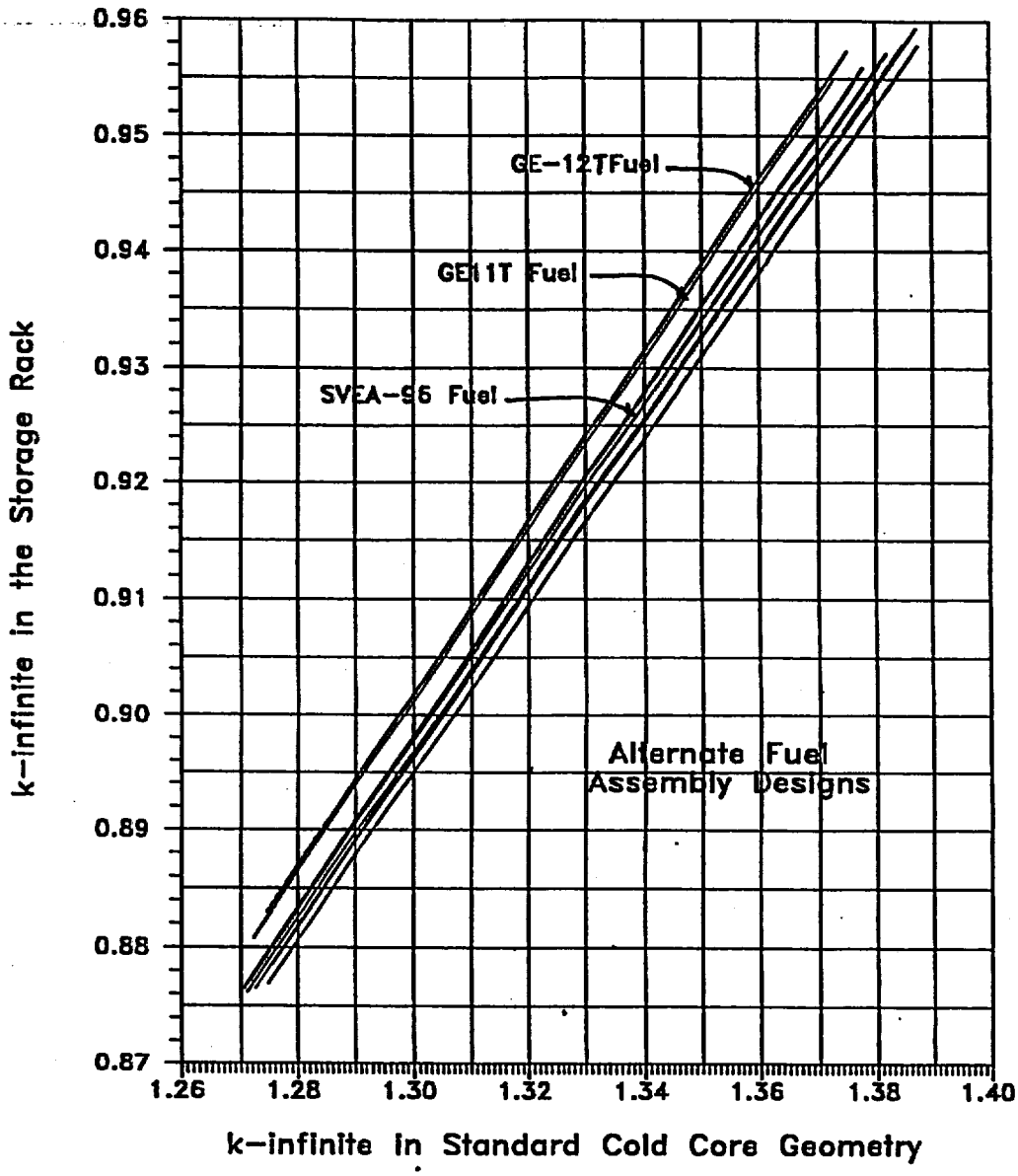

Fig. 4.4.3 Correlation of k-infinite in the SCCG and k-inf in the Storage Rack for Fuel of Various Designs

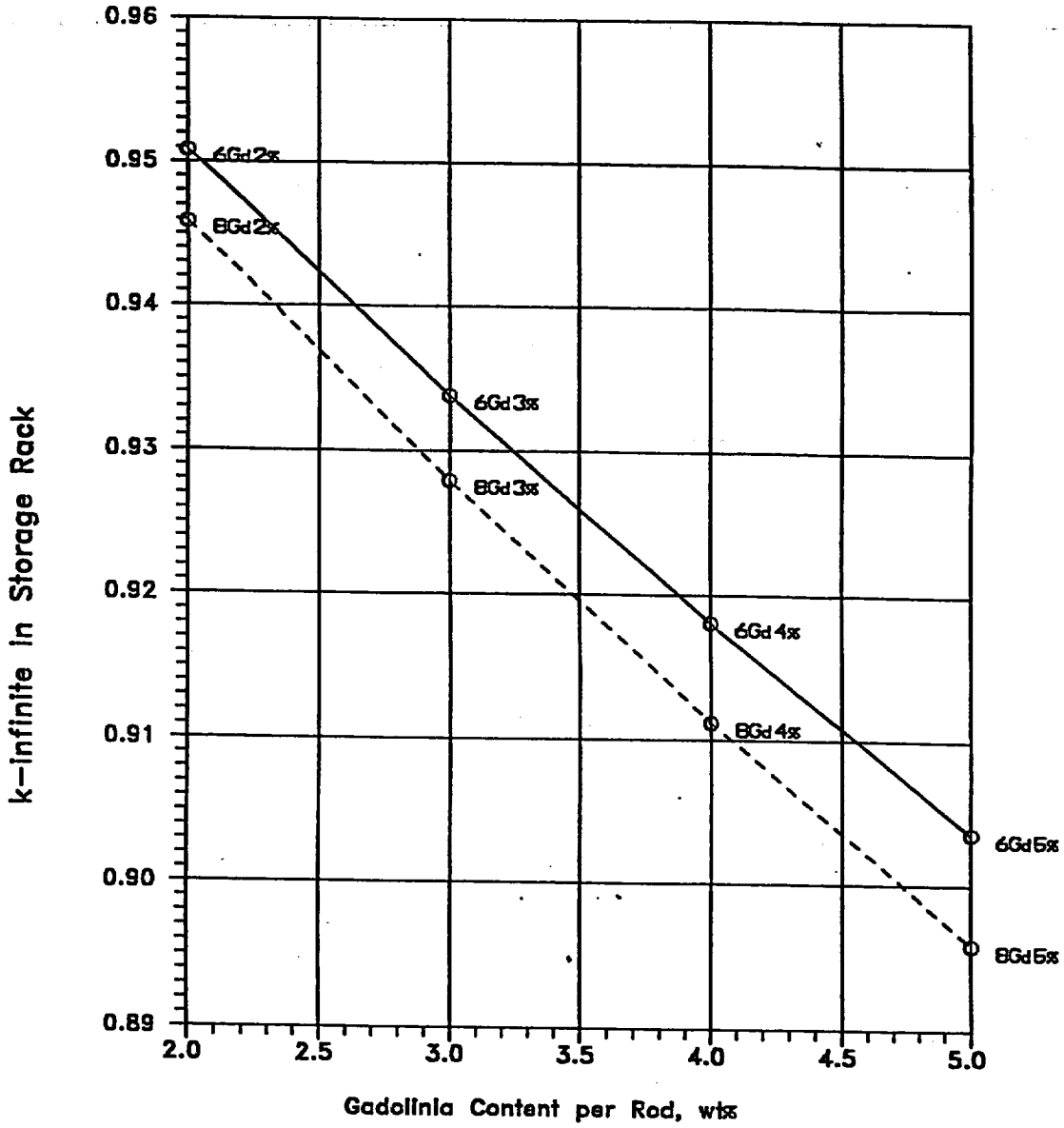

Fig. 4.4.4 Gadolinia Concentration Required for 6 and 8 Rod Patterns

APPENDIX 4A: BENCHMARK CALCULATIONS

4A.1 INTRODUCTION AND SUMMARY

Benchmark calculations have been made on selected critical experiments, chosen, in so far as possible, to bound the range of variables in the rack designs. Two independent methods of analysis were used, differing in cross section libraries and in the treatment of the cross sections. MCNP4a [4A.1] is a continuous energy Monte Carlo code and KENO5a [4A.2] uses group-dependent cross sections. For the KENO5a analyses reported here, the 238-group library was chosen, processed through the NITAWL-II [4A.2] program to create a working library and to account for resonance self-shielding in uranium-238 (Nordheim integral treatment). The 238 group library was chosen to avoid or minimize the errors† (trends) that have been reported (e.g., [4A.3 through 4A.5]) for calculations with collapsed cross section sets.

In rack designs, the three most significant parameters affecting criticality are (1) the fuel enrichment, (2) the ^{10}B loading in the neutron absorber, and (3) the lattice spacing (or water-gap thickness if a flux-trap design is used). Other parameters, within the normal range of rack and fuel designs, have a smaller effect, but are also included in the analyses.

Table 4A.1 summarizes results of the benchmark calculations for all cases selected and analyzed, as referenced in the table. The effect of the major variables are discussed in subsequent sections below. It is important to note that there is obviously considerable overlap in parameters since it is not possible to vary a single parameter and maintain criticality; some other parameter or parameters must be concurrently varied to maintain criticality.

One possible way of representing the data is through a spectrum index that incorporates all of the variations in parameters. KENO5a computes and prints the "energy of the average lethargy causing fission" (EALF). In MCNP4a, by utilizing the tally option with the identical 238-group energy structure as in KENO5a, the number of fissions in each group may be collected and the EALF determined (post-processing).

---

† Small but observable trends (errors) have been reported for calculations with the 27-group and 44-group collapsed libraries. These errors are probably due to the use of a single collapsing spectrum when the spectrum should be different for the various cases analyzed, as evidenced by the spectrum indices.

Figures 4A.1 and 4A.2 show the calculated k_{eff} for the benchmark critical experiments as a function of the EALF for MCNP4a and KENO5a, respectively (UO_2 fuel only). The scatter in the data (even for comparatively minor variation in critical parameters) represents experimental error† in performing the critical experiments within each laboratory, as well as between the various testing laboratories. The B&W critical experiments show a larger experimental error than the PNL criticals. This would be expected since the B&W criticals encompass a greater range of critical parameters than the PNL criticals.

Linear regression analysis of the data in Figures 4A.1 and 4A.2 show that there are no trends, as evidenced by very low values of the correlation coefficient (0.13 for MCNP4a and 0.21 for KENO5a). The total bias (systematic error, or mean of the deviation from a k_{eff} of exactly 1.000) for the two methods of analysis are shown in the table below.

Calculational Bias of MCNP4a and KENO5a	
MCNP4a	0.0009 ± 0.0011
KENO5a	0.0030 ± 0.0012

The bias and standard error of the bias were derived directly from the calculated k_{eff} values in Table 4A.1 using the following equations††, with the standard error multiplied by the one-sided K-factor for 95% probability at the 95% confidence level from NBS Handbook 91 [4A.18] (for the number of cases analyzed, the K-factor is ~2.05 or slightly more than 2).

$$\bar{k} = \frac{1}{n} \sum_{i}^{n} k_i \qquad (4A.1)$$

† A classical example of experimental error is the corrected enrichment in the PNL experiments, first as an addendum to the initial report and, secondly, by revised values in subsequent reports for the same fuel rods.

†† These equations may be found in any standard text on statistics, for example, reference [4A.6] (or the MCNP4a manual) and is the same methodology used in MCNP4a and in KENO5a.

$$\sigma^2_{\bar{k}} = \frac{\sum_{i=1}^{n} k_i^2 - (\sum_{i=1}^{n} k_i)^2 / n}{n\,(n-1)} \qquad (4A.2)$$

$$Bias = (1 - \bar{k}) \pm K\,\sigma_{\bar{k}} \qquad (4A.3)$$

where k_i are the calculated reactivities of n critical experiments; $\sigma_{\bar{k}}$ is the unbiased estimator of the standard deviation of the mean (also called the standard error of the bias (mean)); K is the one-sided multiplier for 95% probability at the 95% confidence level (NBS Handbook 91 [4A.18]).

Formula 4.A.3 is based on the methodology of the National Bureau of Standards (now NIST) and is used to calculate the values presented on page 4.A-2. The first portion of the equation, (1- $\bar{k}$), is the actual bias which is added to the MCNP4a and KENO5a results. The second term, $K\sigma_{\bar{k}}$, is the uncertainty or standard error associated with the bias. The K values used were obtained from the National Bureau of Standards Handbook 91 and are for one-sided statistical tolerance limits for 95% probability at the 95% confidence level. The actual K values for the 56 critical experiments evaluated with MCNP4a and the 53 critical experiments evaluated with KENO5a are 2.04 and 2.05, respectively.

The bias values are used to evaluate the maximum k_{eff} values for the rack designs. KENO5a has a slightly larger systematic error than MCNP4a, but both result in greater precision than published data [4A.3 through 4A.5] would indicate for collapsed cross section sets in KENO5a (SCALE) calculations.

4A.2 Effect of Enrichment

The benchmark critical experiments include those with enrichments ranging from 2.46 w/o to 5.74 w/o and therefore span the enrichment range for rack designs. Figures 4A.3 and 4A.4 show the calculated k_{eff} values (Table 4A.1) as a function of the fuel enrichment reported for the critical experiments. Linear regression analyses for these data confirms that there are no trends, as indicated by low values of the correlation coefficients (0.03 for MCNP4a and 0.38 for KENO5a). Thus, there are no corrections to the bias for the various enrichments.

As further confirmation of the absence of any trends with enrichment, a typical configuration was calculated with both MCNP4a and KENO5a for various enrichments. The cross-comparison of calculations with codes of comparable sophistication is suggested in Reg. Guide 3.41. Results of this comparison, shown in Table 4A.2 and Figure 4A.5, confirm no significant difference in the calculated values of k_{eff} for the two independent codes as evidenced by the 45° slope of the curve. Since it is very unlikely that two independent methods of analysis would be subject to the same error, this comparison is considered confirmation of the absence of an enrichment effect (trend) in the bias.

4A.3 Effect of ^{10}B Loading

Several laboratories have performed critical experiments with a variety of thin absorber panels similar to the Boral panels in the rack designs. Of these critical experiments, those performed by B&W are the most representative of the rack designs. PNL has also made some measurements with absorber plates, but, with one exception (a flux-trap experiment), the reactivity worth of the absorbers in the PNL tests is very low and any significant errors that might exist in the treatment of strong thin absorbers could not be revealed.

Table 4A.3 lists the subset of experiments using thin neutron absorbers (from Table 4A.1) and shows the reactivity worth (Δk) of the absorber.†

No trends with reactivity worth of the absorber are evident, although based on the calculations shown in Table 4A.3, some of the B&W critical experiments seem to have unusually large experimental errors. B&W made an effort to report some of their experimental errors. Other laboratories did not evaluate their experimental errors.

To further confirm the absence of a significant trend with ^{10}B concentration in the absorber, a cross-comparison was made with MCNP4a and KENO5a (as suggested in Reg. Guide 3.41). Results are shown in Figure 4A.6 and Table 4A.4 for a typical geometry. These data substantiate the absence of any error (trend) in either of the two codes for the conditions analyzed (data points fall on a 45° line, within an expected 95% probability limit).

† The reactivity worth of the absorber panels was determined by repeating the calculation with the absorber analytically removed and calculating the incremental (Δk) change in reactivity due to the absorber.

4A.4 Miscellaneous and Minor Parameters

4A.4.1 Reflector Material and Spacings

PNL has performed a number of critical experiments with thick steel and lead reflectors.† Analysis of these critical experiments are listed in Table 4A.5 (subset of data in Table 4A.1). There appears to be a small tendency toward overprediction of k_{eff} at the lower spacing, although there are an insufficient number of data points in each series to allow a quantitative determination of any trends. The tendency toward overprediction at close spacing means that the rack calculations may be slightly more conservative than otherwise.

4A.4.2 Fuel Pellet Diameter and Lattice Pitch

The critical experiments selected for analysis cover a range of fuel pellet diameters from 0.311 to 0.444 inches, and lattice spacings from 0.476 to 1.00 inches. In the rack designs, the fuel pellet diameters range from 0.303 to 0.3805 inches O.D. (0.496 to 0.580 inch lattice spacing) for PWR fuel and from 0.3224 to 0.494 inches O.D. (0.488 to 0.740 inch lattice spacing) for BWR fuel. Thus, the critical experiments analyzed provide a reasonable representation of power reactor fuel. Based on the data in Table 4A.1, there does not appear to be any observable trend with either fuel pellet diameter or lattice pitch, at least over the range of the critical experiments applicable to rack designs.

4A.4.3 Soluble Boron Concentration Effects

Various soluble boron concentrations were used in the B&W series of critical experiments and in one PNL experiment, with boron concentrations ranging up to 2550 ppm. Results of MCNP4a (and one KENO5a) calculations are shown in Table 4A.6. Analyses of the very high boron concentration experiments (> 1300 ppm) show a tendency to slightly overpredict reactivity for the three experiments exceeding 1300 ppm. In turn, this would suggest that the evaluation of the racks with higher soluble boron concentrations could be slightly conservative.

---

† Parallel experiments with a depleted uranium reflector were also performed but not included in the present analysis since they are not pertinent to the Holtec rack design.

4A.5 MOX Fuel

The number of critical experiments with PuO_2 bearing fuel (MOX) is more limited than for UO_2 fuel. However, a number of MOX critical experiments have been analyzed and the results are shown in Table 4A.7. Results of these analyses are generally above a k_{eff} of 1.00, indicating that when Pu is present, both MCNP4a and KENO5a overpredict the reactivity. This may indicate that calculation for MOX fuel will be expected to be conservative, especially with MCNP4a. It may be noted that for the larger lattice spacings, the KENO5a calculated reactivities are below 1.00, suggesting that a small trend may exist with KENO5a. It is also possible that the overprediction in k_{eff} for both codes may be due to a small inadequacy in the determination of the Pu-241 decay and Am-241 growth. This possibility is supported by the consistency in calculated k_{eff} over a wide range of the spectral index (energy of the average lethargy causing fission).

4A.6 References

[4A.1] J.F. Briesmeister, Ed., "MCNP4a - A General Monte Carlo N-Particle Transport Code, Version 4A; Los Alamos National Laboratory, LA-12625-M (1993).

[4A.2] SCALE 4.3, "A Modular Code System for Performing Standardized Computer Analyses for Licensing Evaluation", NUREG-0200 (ORNL-NUREG-CSD-2/U2/R5, Revision 5, Oak Ridge National Laboratory, September 1995.

[4A.3] M.D. DeHart and S.M. Bowman, "Validation of the SCALE Broad Structure 44-G Group ENDF/B-Y Cross-Section Library for Use in Criticality Safety Analyses", NUREG/CR-6102 (ORNL/TM-12460) Oak Ridge National Laboratory, September 1994.

[4A.4] W.C. Jordan et al., "Validation of KENOV.a", CSD/TM-238, Martin Marietta Energy Systems, Inc., Oak Ridge National Laboratory, December 1986.

[4A.5] O.W. Hermann et al., "Validation of the Scale System for PWR Spent Fuel Isotopic Composition Analysis", ORNL-TM-12667, Oak Ridge National Laboratory, undated.

[4A.6] R.J. Larsen and M.L. Marx, An Introduction to Mathematical Statistics and its Applications, Prentice-Hall, 1986.

[4A.7] M.N. Baldwin et al., Critical Experiments Supporting Close Proximity Water Storage of Power Reactor Fuel, BAW-1484-7, Babcock and Wilcox Company, July 1979.

[4A.8] G.S. Hoovier et al., Critical Experiments Supporting Underwater Storage of Tightly Packed Configurations of Spent Fuel Pins, BAW-1645-4, Babcock & Wilcox Company, November 1991.

[4A.9] L.W. Newman et al., Urania Gadolinia: Nuclear Model Development and Critical Experiment Benchmark, BAW-1810, Babcock and Wilcox Company, April 1984.

[4A.10] J.C. Manaranche et al., "Dissolution and Storage Experimental Program with 4.75 w/o Enriched Uranium-Oxide Rods," Trans. Am. Nucl. Soc. 33: 362-364 (1979).

[4A.11] S.R. Bierman and E.D. Clayton, Criticality Experiments with Subcritical Clusters of 2.35 w/o and 4.31 w/o ^{235}U Enriched UO_2 Rods in Water with Steel Reflecting Walls, PNL-3602, Battelle Pacific Northwest Laboratory, April 1981.

[4A.12] S.R. Bierman et al., Criticality Experiments with Subcritical Clusters of 2.35 w/o and 4.31 w/o ^{235}U Enriched UO_2 Rods in Water with Uranium or Lead Reflecting Walls, PNL-3926, Battelle Pacific Northwest Laboratory, December, 1981.

[4A.13] S.R. Bierman et al., Critical Separation Between Subcritical Clusters of 4.31 w/o ^{235}U Enriched UO_2 Rods in Water with Fixed Neutron Poisons, PNL-2615, Battelle Pacific Northwest Laboratory, October 1977.

[4A.14] S.R. Bierman, Criticality Experiments with Neutron Flux Traps Containing Voids, PNL-7167, Battelle Pacific Northwest Laboratory, April 1990.

[4A.15] B.M. Durst et al., Critical Experiments with 4.31 wt % ^{235}U Enriched UO_2 Rods in Highly Borated Water Lattices, PNL-4267, Battelle Pacific Northwest Laboratory, August 1982.

[4A.16] S.R. Bierman, Criticality Experiments with Fast Test Reactor Fuel Pins in Organic Moderator, PNL-5803, Battelle Pacific Northwest Laboratory, December 1981.

[4A.17] E.G. Taylor et al., Saxton Plutonium Program Critical Experiments for the Saxton Partial Plutonium Core, WCAP-3385-54, Westinghouse Electric Corp., Atomic Power Division, December 1965.

[4A.18] M.G. Natrella, Experimental Statistics, National Bureau of Standards, Handbook 91, August 1963.

Table 4A.1

Summary of Criticality Benchmark Calculations

	Reference	Identification	Enrich.	Calculated k_{eff}		EALF † (eV)	
				MCNP4a	KENO5a	MCNP4a	KENO5a
1	B&W-1484 (4A.7)	Core I	2.46	0.9964 ± 0.0010	0.9898± 0.0006	0.1759	0.1753
2	B&W-1484 (4A.7)	Core II	2.46	1.0008 ± 0.0011	1.0015 ± 0.0005	0.2553	0.2446
3	B&W-1484 (4A.7)	Core III	2.46	1.0010 ± 0.0012	1.0005 ± 0.0005	0.1999	0.1939
4	B&W-1484 (4A.7)	Core IX	2.46	0.9956 ± 0.0012	0.9901 ± 0.0006	0.1422	0.1426
5	B&W-1484 (4A.7)	Core X	2.46	0.9980 ± 0.0014	0.9922 ± 0.0006	0.1513	0.1499
6	B&W-1484 (4A.7)	Core XI	2.46	0.9978 ± 0.0012	1.0005 ± 0.0005	0.2031	0.1947
7	B&W-1484 (4A.7)	Core XII	2.46	0.9988 ± 0.0011	0.9978 ± 0.0006	0.1718	0.1662
8	B&W-1484 (4A.7)	Core XIII	2.46	1.0020 ± 0.0010	0.9952 ± 0.0006	0.1988	0.1965
9	B&W-1484 (4A.7)	Core XIV	2.46	0.9953 ± 0.0011	0.9928 ± 0.0006	0.2022	0.1986
10	B&W-1484 (4A.7)	Core XV ††	2.46	0.9910 ± 0.0011	0.9909 ± 0.0006	0.2092	0.2014
11	B&W-1484 (4A.7)	Core XVI ††	2.46	0.9935 ± 0.0010	0.9889 ± 0.0006	0.1757	0.1713
12	B&W-1484 (4A.7)	Core XVII	2.46	0.9962 ± 0.0012	0.9942 ± 0.0005	0.2083	0.2021
13	B&W-1484 (4A.7)	Core XVIII	2.46	1.0036 ± 0.0012	0.9931 ± 0.0006	0.1705	0.1708

Table 4A.1

Summary of Criticality Benchmark Calculations

	Reference	Identification	Enrich.	Calculated k_{eff}		EALF† (eV)	
				MCNP4a	KENO5a	MCNP4a	KENO5a
14	B&W-1484 (4A.7)	Core XIX	2.46	0.9961 ± 0.0012	0.9971 ± 0.0005	0.2103	0.2011
15	B&W-1484 (4A.7)	Core XX	2.46	1.0008 ± 0.0011	0.9932 ± 0.0006	0.1724	0.1701
16	B&W-1484 (4A.7)	Core XXI	2.46	0.9994 ± 0.0010	0.9918 ± 0.0006	0.1544	0.1536
17	B&W-1645 (4A.8)	S-type Fuel, w/886 ppm B	2.46	0.9970 ± 0.0010	0.9924 ± 0.0006	1.4475	1.4680
18	B&W-1645 (4A.8)	S-type Fuel, w/746 ppm B	2.46	0.9990 ± 0.0010	0.9913 ± 0.0006	1.5463	1.5660
19	B&W-1645 (4A.8)	SO-type Fuel, w/1156 ppm B	2.46	0.9972 ± 0.0009	0.9949 ± 0.0005	0.4241	0.4331
20	B&W-1810 (4A.9)	Case 1 1337 ppm B	2.46	1.0023 ± 0.0010	NC	0.1531	NC
21	B&W-1810 (4A.9)	Case 12 1899 ppm B	2.46/4.02	1.0060 ± 0.0009	NC	0.4493	NC
22	French (4A.10)	Water Moderator 0 gap	4.75	0.9966 ± 0.0013	NC	0.2172	NC
23	French (4A.10)	Water Moderator 2.5 cm gap	4.75	0.9952 ± 0.0012	NC	0.1778	NC
24	French (4A.10)	Water Moderator 5 cm gap	4.75	0.9943 ± 0.0010	NC	0.1677	NC
25	French (4A.10)	Water Moderator 10 cm gap	4.75	0.9979 ± 0.0010	NC	0.1736	NC
26	PNL-3602 (4A.11)	Steel Reflector, 0 separation	2.35	NC	1.0004 ± 0.0006	NC	0.1018

Table 4A.1

Summary of Criticality Benchmark Calculations

	Reference	Identification	Enrich.	Calculated k_{eff}		EALF † (eV)	
				MCNP4a	KENO5a	MCNP4a	KENO5a
27	PNL-3602 (4A.11)	Steel Reflector, 1.321 cm sepn.	2.35	0.9980 ± 0.0009	0.9992 ± 0.0006	0.1000	0.0909
28	PNL-3602 (4A.11)	Steel Reflector, 2.616 cm sepn	2.35	0.9968 ± 0.0009	0.9964 ± 0.0006	0.0981	0.0975
29	PNL-3602 (4A.11)	Steel Reflector, 3.912 cm sepn.	2.35	0.9974 ± 0.0010	0.9980 ± 0.0006	0.0976	0.0970
30	PNL-3602 (4A.11)	Steel Reflector, infinite sepn.	2.35	0.9962 ± 0.0008	0.9939 ± 0.0006	0.0973	0.0968
31	PNL-3602 (4A.11)	Steel Reflector, 0 cm sepn.	4.306	NC	1.0003 ± 0.0007	NC	0.3282
32	PNL-3602 (4A.11)	Steel Reflector, 1.321 cm sepn.	4.306	0.9997 ± 0.0010	1.0012 ± 0.0007	0.3016	0.3039
33	PNL-3602 (4A.11)	Steel Reflector, 2.616 cm sepn.	4.306	0.9994 ± 0.0012	0.9974 ± 0.0007	0.2911	0.2927
34	PNL-3602 (4A.11)	Steel Reflector, 5.405 cm sepn.	4.306	0.9969 ± 0.0011	0.9951 ± 0.0007	0.2828	0.2860
35	PNL-3602 (4A.11)	Steel Reflector, Infinite sepn. ††	4.306	0.9910 ± 0.0020	0.9947 ± 0.0007	0.2851	0.2864
36	PNL-3602 (4A.11)	Steel Reflector, with Boral Sheets	4.306	0.9941 ± 0.0011	0.9970 ± 0.0007	0.3135	0.3150
37	PNL-3926 (4A.12)	Lead Reflector, 0 cm sepn.	4.306	NC	1.0003 ± 0.0007	NC	0.3159
38	PNL-3926 (4A.12)	Lead Reflector, 0.55 cm sepn.	4.306	1.0025 ± 0.0011	0.9997 ± 0.0007	0.3030	0.3044
39	PNL-3926 (4A.12)	Lead Reflector, 1.956 cm sepn.	4.306	1.0000 ± 0.0012	0.9985 ± 0.0007	0.2883	0.2930

Table 4A.1

Summary of Criticality Benchmark Calculations

	Reference	Identification	Enrich.	Calculated k_{eff}		EALF † (eV)	
				MCNP4a	KENO5a	MCNP4a	KENO5a
40	PNL-3926 (4A.12)	Lead Reflector, 5.405 cm sepn.	4.306	0.9971 ± 0.0012	0.9946 ± 0.0007	0.2831	0.2854
41	PNL-2615 (4A.13)	Experiment 004/032 - no absorber	4.306	0.9925 ± 0.0012	0.9950 ± 0.0007	0.1155	0.1159
42	PNL-2615 (4A.13)	Experiment 030 - Zr plates	4.306	NC	0.9971 ± 0.0007	NC	0.1154
43	PNL-2615 (4A.13)	Experiment 013 - Steel plates	4.306	NC	0.9965 ± 0.0007	NC	0.1164
44	PNL-2615 (4A.13)	Experiment 014 - Steel plates	4.306	NC	0.9972 ± 0.0007	NC	0.1164
45	PNL-2615 (4A.13)	Exp. 009 1.05% Boron-Steel plates	4.306	0.9982 ± 0.0010	0.9981 ± 0.0007	0.1172	0.1162
46	PNL-2615 (4A.13)	Exp. 012 1.62% Boron-Steel plates	4.306	0.9996 ± 0.0012	0.9982 ± 0.0007	0.1161	0.1173
47	PNL-2615 (4A.13)	Exp. 031 - Boral plates	4.306	0.9994 ± 0.0012	0.9969 ± 0.0007	0.1165	0.1171
48	PNL-7167 (4A.14)	Experiment 214R - with flux trap	4.306	0.9991 ± 0.0011	0.9956 ± 0.0007	0.3722	0.3812
49	PNL-7167 (4A.14)	Experiment 214V3 - with flux trap	4.306	0.9969 ± 0.0011	0.9963 ± 0.0007	0.3742	0.3826
50	PNL-4267 (4A.15)	Case 173 - 0 ppm B	4.306	0.9974 ± 0.0012	NC	0.2893	NC
51	PNL-4267 (4A.15)	Case 177 - 2550 ppm B	4.306	1.0057 ± 0.0010	NC	0.5509	NC
52	PNL-5803 (4A.16)	MOX Fuel - Type 3.2 Exp. 21	20% Pu	1.0041 ± 0.0011	1.0046 ± 0.0006	0.9171	0.8868

Table 4A.1

Summary of Criticality Benchmark Calculations

	Reference	Identification	Enrich.	Calculated k_{eff}		EALF† (eV)	
				MCNP4a	KENO5a	MCNP4a	KENO5a
53	PNL-5803 (4A.16)	MOX Fuel - Type 3.2 Exp. 43	20% Pu	1.0058 ± 0.0012	1.0036 ± 0.0006	0.2968	0.2944
54	PNL-5803 (4A.16)	MOX Fuel - Type 3.2 Exp. 13	20% Pu	1.0083 ± 0.0011	0.9989 ± 0.0006	0.1665	0.1706
55	PNL-5803 (4A.16)	MOX Fuel - Type 3.2 Exp. 32	20% Pu	1.0079 ± 0.0011	0.9966 ± 0.0006	0.1139	0.1165
56	WCAP-3385 (4A.17)	Saxton Case 52 PuO2 0.52" pitch	6.6% Pu	0.9996 ± 0.0011	1.0005 ± 0.0006	0.8665	0.8417
57	WCAP-3385 (4A.17)	Saxton Case 52 U 0.52" pitch	5.74	1.0000 ± 0.0010	0.9956 ± 0.0007	0.4476	0.4580
58	WCAP-3385 (4A.17)	Saxton Case 56 PuO2 0.56" pitch	6.6% Pu	1.0036 ± 0.0011	1.0047 ± 0.0006	0.5289	0.5197
59	WCAP-3385 (4A.17)	Saxton Case 56 borated PuO2	6.6% Pu	1.0008 ± 0.0010	NC	0.6389	NC
60	WCAP-3385 (4A.17)	Saxton Case 56 U 0.56" pitch	5.74	0.9994 ± 0.0011	0.9967 ± 0.0007	0.2923	0.2954
61	WCAP-3385 (4A.17)	Saxton Case 79 PuO2 0.79" pitch	6.6% Pu	1.0063 ± 0.0011	1.0133 ± 0.0006	0.1520	0.1555
62	WCAP-3385 (4A.17)	Saxton Case 79 U 0.79" pitch	5.74	1.0039 ± 0.0011	1.0008 ± 0.0006	0.1036	0.1047

Notes: NC stands for not calculated.

† EALF is the energy of the average lethargy causing fission.

†† These experimental results appear to be statistical outliers ($>3\sigma$) suggesting the possibility of unusually large experimental error. Although they could justifiably be excluded, for conservatism, they were retained in determining the calculational basis.

Table 4A.2

COMPARISON OF MCNP4a AND KENO5a CALCULATED REACTIVITIES† FOR VARIOUS ENRICHMENTS

Enrichment	Calculated $k_{eff} \pm 1\sigma$	
	MCNP4a	KENO5a
3.0	0.8465 ± 0.0011	0.8478 ± 0.0004
3.5	0.8820 ± 0.0011	0.8841 ± 0.0004
3.75	0.9019 ± 0.0011	0.8987 ± 0.0004
4.0	0.9132 ± 0.0010	0.9140 ± 0.0004
4.2	0.9276 ± 0.0011	0.9237 ± 0.0004
4.5	0.9400 ± 0.0011	0.9388 ± 0.0004

† Based on the GE 8x8R fuel assembly.

Table 4A.3

MCNP4a CALCULATED REACTIVITIES FOR
CRITICAL EXPERIMENTS WITH NEUTRON ABSORBERS

Ref.	Experiment		Δk Worth of Absorber	MCNP4a Calculated k_{eff}	EALF † (eV)
4A.13	PNL-2615	Boral Sheet	0.0139	0.9994±0.0012	0.1165
4A.7	B&W-1484	Core XX	0.0165	1.0008±0.0011	0.1724
4A.13	PNL-2615	1.62% Boron-steel	0.0165	0.9996±0.0012	0.1161
4A.7	B&W-1484	Core XIX	0.0202	0.9961±0.0012	0.2103
4A.7	B&W-1484	Core XXI	0.0243	0.9994±0.0010	0.1544
4A.7	B&W-1484	Core XVII	0.0519	0.9962±0.0012	0.2083
4A.11	PNL-3602	Boral Sheet	0.0708	0.9941±0.0011	0.3135
4A.7	B&W-1484	Core XV	0.0786	0.9910±0.0011	0.2092
4A.7	B&W-1484	Core XVI	0.0845	0.9935±0.0010	0.1757
4A.7	B&W-1484	Core XIV	0.1575	0.9953±0.0011	0.2022
4A.7	B&W-1484	Core XIII	0.1738	1.0020±0.0011	0.1988
4A.14	PNL-7167	Expt 214R flux trap	0.1931	0.9991±0.0011	0.3722

†EALF is the energy of the average lethargy causing fission.

Table 4A.4

COMPARISON OF MCNP4a AND KENO5a
CALCULATED REACTIVITIES† FOR VARIOUS ^{10}B LOADINGS

^{10}B, g/cm^2	Calculated $k_{eff} \pm 1\sigma$	
	MCNP4a	KENO5a
0.005	1.0381 ± 0.0012	1.0340 ± 0.0004
0.010	0.9960 ± 0.0010	0.9941 ± 0.0004
0.015	0.9727 ± 0.0009	0.9713 ± 0.0004
0.020	0.9541 ± 0.0012	0.9560 ± 0.0004
0.025	0.9433 ± 0.0011	0.9428 ± 0.0004
0.03	0.9325 ± 0.0011	0.9338 ± 0.0004
0.035	0.9234 ± 0.0011	0.9251 ± 0.0004
0.04	0.9173 ± 0.0011	0.9179 ± 0.0004

† Based on a 4.5% enriched GE 8x8R fuel assembly.

Table 4A.5

CALCULATIONS FOR CRITICAL EXPERIMENTS WITH THICK LEAD AND STEEL REFLECTORS†

Ref.	Case	E, wt%	Separation, cm	MCNP4a k_{eff}	KENO5a k_{eff}
4A.11	Steel Reflector	2.35	1.321	0.9980±0.0009	0.9992±0.0006
		2.35	2.616	0.9968±0.0009	0.9964±0.0006
		2.35	3.912	0.9974±0.0010	0.9980±0.0006
		2.35	∞	0.9962±0.0008	0.9939±0.0006
4A.11	Steel Reflector	4.306	1.321	0.9997±0.0010	1.0012±0.0007
		4.306	2.616	0.9994±0.0012	0.9974±0.0007
		4.306	3.405	0.9969±0.0011	0.9951±0.0007
		4.306	∞	0.9910±0.0020	0.9947±0.0007
4A.12	Lead Reflector	4.306	0.55	1.0025±0.0011	0.9997±0.0007
		4.306	1.956	1.0000±0.0012	0.9985±0.0007
		4.306	5.405	0.9971±0.0012	0.9946±0.0007

† Arranged in order of increasing reflector-fuel spacing.

Table 4A.6

CALCULATIONS FOR CRITICAL EXPERIMENTS WITH VARIOUS SOLUBLE BORON CONCENTRATIONS

Reference	Experiment	Boron Concentration, ppm	Calculated k_{eff}	
			MCNP4a	KENO5a
4A.15	PNL-4267	0	0.9974 ± 0.0012	-
4A.8	B&W-1645	886	0.9970 ± 0.0010	0.9924 ± 0.0006
4A.9	B&W-1810	1337	1.0023 ± 0.0010	-
4A.9	B&W-1810	1899	1.0060 ± 0.0009	-
4A.15	PNL-4267	2550	1.0057 ± 0.0010	-

Table 4A.7

CALCULATIONS FOR CRITICAL EXPERIMENTS WITH MOX FUEL

Reference	Case†	MCNP4a		KENO5a	
		k_{eff}	EALF††	k_{eff}	EALF††
PNL-5803 [4A.16]	MOX Fuel - Exp. No. 21	1.0041±0.0011	0.9171	1.0046±0.0006	0.8868
	MOX Fuel - Exp. No. 43	1.0058±0.0012	0.2968	1.0036±0.0006	0.2944
	MOX Fuel - Exp. No. 13	1.0083±0.0011	0.1665	0.9989±0.0006	0.1706
	MOX Fuel - Exp. No. 32	1.0079±0.0011	0.1139	0.9966±0.0006	0.1165
WCAP-3385-54 [4A.17]	Saxton @ 0.52" pitch	0.9996±0.0011	0.8665	1.0005±0.0006	0.8417
	Saxton @ 0.56" pitch	1.0036±0.0011	0.5289	1.0047±0.0006	0.5197
	Saxton @ 0.56" pitch borated	1.0008±0.0010	0.6389	NC	NC
	Saxton @ 0.79" pitch	1.0063±0.0011	0.1520	1.0133±0.0006	0.1555

Note: NC stands for not calculated

† Arranged in order of increasing lattice spacing.

†† EALF is the energy of the average lethargy causing fission.

5.0 THERMAL-HYDRAULIC CONSIDERATIONS

5.1 Introduction

This document requests an operating license amendment to expand the storage capacity of the spent fuel storage pool (SFP) at Fermi 2, a revision of the maximum normal SFP bulk temperature from 125°F to 150°F, and a reduction in the minimum time-to-boil values associated with various postulated plant conditions and discharge scenarios. The effects of this increase in bulk temperature on the rack and pool structures are addressed in Sections 6.0 and 8.0. As will be shown in this section, the reduction in time-to-boil still allows sufficient time to provide makeup water to the SFP. As discussed in Section 1.0, this capacity expansion would be achieved by replacing some or all of the existing spent fuel storage racks (SFSRs) with new Holtec high density SFSRs in a series of campaigns. This section provides a summary of the analyses performed to demonstrate the compliance of the SFP and its attendant cooling systems with the provisions of Section III of the USNRC "OT Position Paper for Review and Acceptance of Spent Fuel Storage and Handling Applications," (April 14, 1978). Similar methods of thermal-hydraulic analysis have been used in the licensing evaluations for other SFP capacity expansion projects.

Although the capacity expansion would occur over a series of campaigns, with the storage capacity increasing after each campaign, the bounding configuration for a thermal-hydraulic standpoint is the final, maximized configuration. The final configuration would result in the largest number of stored assemblies and would, therefore, have the highest SFP decay heat load and the lowest net SFP thermal capacity. All analyses discussed in this section are performed for the final configuration, and thereby bound all intermediate configurations.

The thermal-hydraulic qualification analyses for the modified rack array may be broken down into the following categories:

i. Evaluation of the maximum bulk temperatures for the design-basis discharge scenarios, to establish that maximum bulk temperature limits are not exceeded.

The bulk temperature is limited to 150°F for all conditions where forced cooling is available.

ii. Evaluation of loss-of-forced cooling scenarios, to establish minimum times to perform corrective actions and maximum makeup water requirements.

iii. Determination of the maximum temperature difference between the pool local temperature and the SFP bulk temperature, at the instant when the bulk temperature reaches its maximum value, to establish that localized boiling in the SFSRs is not possible.

iv. Evaluation of the maximum temperature difference between the fuel rod cladding temperature and the local SFP water temperature, to establish that nucleate boiling is not possible while SFP forced cooling is operating.

With respect to the maximum bulk temperature limit of 150°F proscribed in category i, above, Fermi 2 is increasing the maximum normal SFP bulk temperature to 150°F from the previous value of 125°F. During normal SFP operation, the maximum normal bulk temperatures are based on the Fuel Pool Cooling and Cleanup System with the SFP gates installed.

The following sections present plant system descriptions, analysis methodologies and assumptions, a synopsis of the input data employed and summaries of the calculated results.

5.2 Cooling Systems Description

The Fuel Pool Cooling and Cleanup System (FPCCS) at Fermi 2 cools the SFP by transferring decay heat through heat exchangers to the reactor building closed cooling water system (RBCCWS). The FPCCS is composed of two trains, each containing one fuel pool cooling pump and one heat exchanger. The FPCCS pumps are horizontal, centrifugal units with a rated capacity of 550 gpm. The FPCCS heat exchangers are shell and tube units with the following design performance per unit:

Heat Transferred:	4.56×10^6 Btu/hr
Shell Side Water Flow Rate:	800 gpm
Shell Side Water Inlet Temperature:	95°F
Tube Side Water Flow Rate:	550 gpm
Tube Side Water Inlet Temperature:	125°F

The cold shell side flow is supplied from the RBCCWS and the tube side water is from the SFP. The above performance data are for a single operating train. The heat transferred would be doubled to 9.12×10^6 Btu/hr if both trains are operating.

Under specific plant and system conditions, backup cooling is provided to the SFP by the RHR System. In this configuration, supplemental cooling is provided to the SFP by means of a permanently piped crosstie to the RHR System. In this mode of operation, one RHR pump and the corresponding RHR division heat exchanger will provide the means to cool the SFP.

For the designed piping configuration, the RHR pump will deliver approximately 3500 gpm. The RHR heat exchangers are shell and tube units with the following design performance in fuel pool cooling assist mode:

Heat Transferred:	30.72×10^6 Btu/hr
Tube Side Water Flow Rate:	9000 gpm
Tube Side Water Inlet Temperature:	89 °F
Inlet Terminal Temperature Difference:	36 °F

The cold tube side flow is supplied from the RHR Service Water (RHRSW) System and the shell side water is from the SFP.

To ensure the availability of backup cooling via the RHR System, the crosstie piping and the necessary FPCCS is Seismic Category I. Coolant can be added to the SFP from the normal makeup source from the condensate storage tanks (up to 100 gpm) or from the Fire Protection System (up to 500 gpm) easily within a one hour period. The above means of makeup water to the SFP exceed the maximum calculated boiloff rate of 90.77 gpm. Should it become necessary,

due to plant conditions or outages of the above systems, other means of SFP makeup are available to the operators including the RHR system (up to 3500 gpm) and the RHRSW system cross-tie (up to 2000 gpm) to the RHR system from the Ultimate Heat Sink. Under the most limiting decay heat load contained within the SFP, the multiple sources of makeup to the SFP can be made available prior to exceeding the calculated time-to-boil of 4.20 hours, preventing a loss of SFP water inventory.

5.3 Discharge/Cooling Alignment Scenarios

Three discharge scenarios are postulated. These scenarios are:

Scenario	Discharge Type	Number of Assemblies Discharged
1	Normal Partial Core	260
2	Normal Full Core	764
3	Emergency Full Core	764

A partial core discharge is comprised of 260 assemblies discharged into an SFP that already contains 4016 previously discharged assemblies. This analyzed stored fuel inventory (4276) conservatively corresponds to a condition that results in a loss of full core reserve in the SFP. The minimum decay time of the previously discharged fuel assemblies for this scenario is 18 months.

A normal full core discharge is comprised of 764 assemblies discharged into an SFP that already contains 4016 previously discharged assemblies. This analyzed fuel inventory (4780) conservatively exceeds the maximum possible inventory of 4608 assemblies. The 764 discharged assemblies are separated into two distinct groups: 260 assemblies with a burnup of 50,000 MWD/MTU and 504 assemblies with a burnup of 33,333 MWD/MTU. The minimum decay time of the previously discharged fuel assemblies for this scenario is 18 months.

An emergency full core discharge is comprised of 764 assemblies discharged into an SFP that already contains 4016 previously discharged assemblies. This analyzed fuel inventory (4780) conservatively exceeds the maximum possible inventory of 4608 assemblies. The 764 discharged assemblies are separated into two distinct groups: 260 assemblies with a burnup of 50,000 MWD/MTU and 504 assemblies with a burnup of 33,333 MWD/MTU. The minimum decay time of the previously discharged fuel assemblies for this scenario is 12 months. Table 5.3.1 presents the historic and projected discharge schedule used for these analyses.

As described in Fermi 2 operating procedures, two trains of the FPCCS provide cooling for the SFP until the bulk temperature exceeds 125°F. Once the 125°F point is reached, one division of the RHR System is aligned to cool the SFP. This provides a satisfactory margin of safety to maintain the bulk pool temperature below 150°F as the decay heat load is rising in the pool. To be consistent with the operating procedure, all three of the scenarios described above considered supplemental RHR cooling when the bulk temperature exceeded 125°F. In all scenarios, the cooling water that removes heat from the FPCCS and RHR heat exchangers is assumed to be at its design temperature and design basis flow rate.

An evaluation was performed to determine the SFP bulk temperatures at the end of an outage (i.e., plant restart) with only two trains of the FPCCS operating. This evaluation provides the decay heat load and corresponding time after shutdown when supplemental RHR cooling may be removed from the SFP. Subsequent to confirmation that the SFP decay heat load has fallen below 15.83 MBtu/hr, supplemental cooling is no longer required to be provided to the SFP by the Residual Heat Removal (RHR) system.

5.4 Maximum Pool Bulk Temperatures

In this section, we present the methodology for calculating the maximum pool bulk temperatures for the scenarios presented in the preceding section.

The following conservatism are applied in the maximum pool bulk temperature calculations:

- As previously discussed in this section, all analyses are performed for the SFP configuration after the final campaign. This configuration has the largest number of fuel storage locations and, correspondingly, the highest decay heat load and lowest SFP thermal capacity.

- The decay heat load is based in a discharge schedule with bounding parameters (i.e., maximum irradiation time and batch size) for all projected discharges.

- The decay heat calculations are performed for a fuel inventory that exceeds the maximum possible pool storage capacity.

- The thermal capacity of the SFP is based on the net SFP water volume only. The considerable energy storage capability of the fuel racks, fuel assemblies, and pool structure is neglected.

- The cooling effects of evaporation heat losses and all other passive heat removal mechanisms (i.e., conduction through walls and slab) are neglected.

- Design temperatures are used for the coolant water flow inlet to the FPCCS and RHR System heat exchangers.

- The calculated temperature effectiveness values for the cooling systems heat exchangers are reduced by 5%, to account for up to 5% tube plugging.

- The once-burned fuel assemblies for full-core discharge scenarios are conservatively assumed as twice-burned, thereby increasing their decay heat generation rate.

The transient thermal response of the SFP and the attendant cooling systems is governed by a first-order, ordinary differential equation. The governing differential equation can be written by utilizing conservation of energy as:

$$C\frac{dT}{d\tau} = Q(\tau) - Q_{HX}(T) - Q_{EV}(T)$$

where:

C = SFP thermal capacity, Btu/°F
T = SFP bulk temperature, °F
τ = Time after reactor shutdown, hr
$Q(\tau)$ = Time varying decay heat generation rate, Btu/hr
$Q_{HX}(T)$ = Temperature dependent FPCCS or RHR System heat rejection rate, Btu/hr
$Q_{EV}(T)$ = Temperature dependent evaporative heat loss, Btu/hr

$Q_{HX}(T)$ is a function of the bulk pool temperature and the coolant water flow rate and temperature, and can be written in terms of the temperature effectiveness (p) as follows:

$$Q_{HX}(T) = W_t C_t p(T - t_i)$$

where:

W_t = Coolant water flow rate, lb/hr
C_t = Coolant water specific heat capacity, Btu/(lb-°F)
p = FPCCS or RHR heat exchanger temperature effectiveness
T = SFP bulk water temperature, °F
t_i = Coolant water inlet temperature, °F

The temperature effectiveness, a measure of the heat transfer efficiency of the FPCCS or RHR heat exchangers, is defined as:

$$p = \frac{t_o - t_i}{T - t_i}$$

where t_o is the coolant outlet temperature (°F) and all other terms are as defined above.

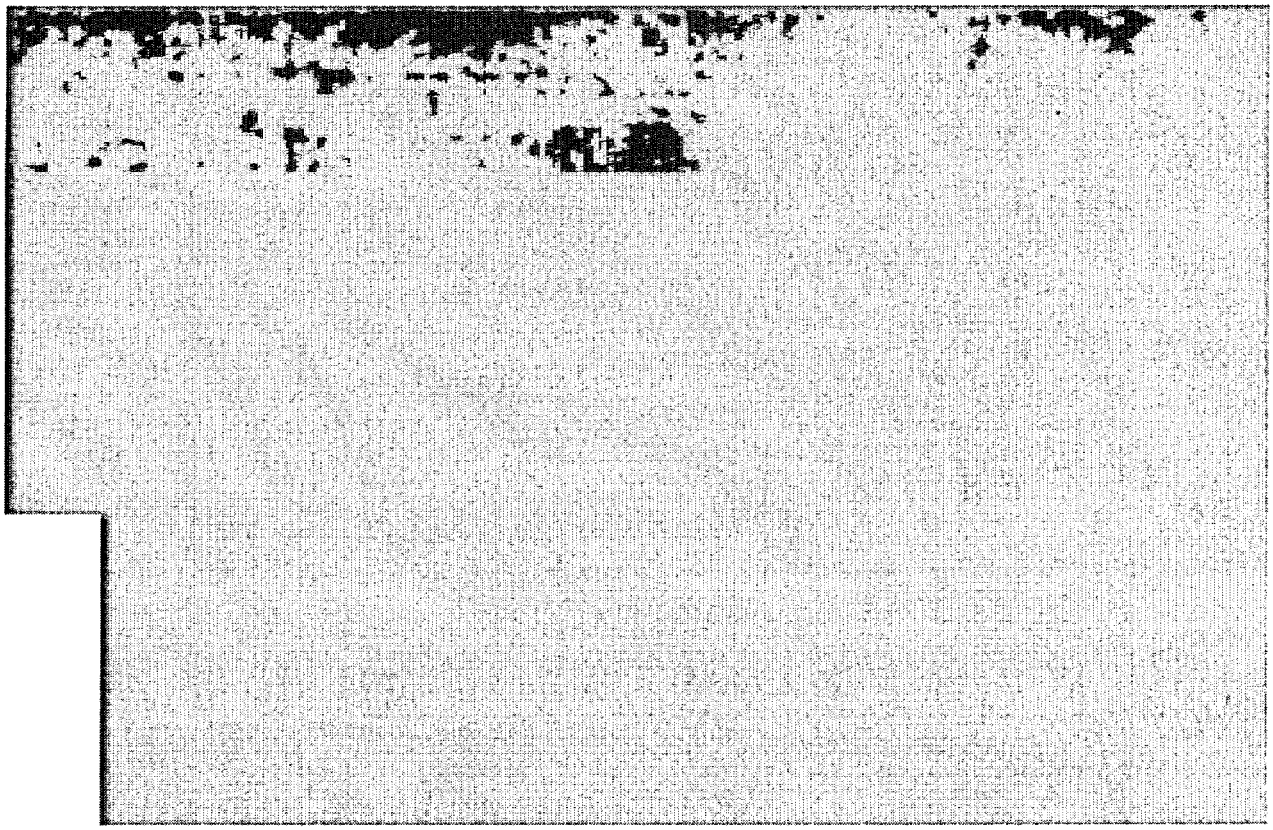

The differential equation that defines the transient thermal response of the pool is solved numerically. The decay heat load from previously discharged fuel assemblies is calculated using Holtec's QA validated DECAY program [5.4.3]. This program incorporates the USNRC Branch Technical Position ASB 9-2 methodology [5.4.4] to perform the decay heat calculations. The transient decay heat loads and pool bulk temperatures are calculated using Holtec's QA validated ONEPOOL program [5.4.5], which also incorporates the ASB 9-2 methodology. The maximum SFP bulk temperature is extracted from the results of the transient evaluations. The major input values for this analysis are summarized in Table 5.4.1.

5.5 Minimum Time-to-Boil and Maximum Boiloff Rate

In this section, we present the methodology for calculating the minimum time-to-boil and corresponding maximum boiloff rate for the scenarios presented in Section 5.3.

The following conservatism are applied in the time-to-boil and boiloff rate calculations:

- The loss of forced cooling is assumed to occur coincident with the SFP peak decay heat generation. Maximizing the initial decay heat generation rate will conservatively minimize the calculated time-to-boil.
- The thermal capacity of the SFP is based on the net SFP water volume only. The considerable energy storage capability of the fuel racks, fuel assemblies, and pool structure is neglected.
- The cooling effects of evaporation heat losses and all other passive heat removal mechanisms (i.e., conduction through walls and slab) are neglected.
- The makeup water supplied to maintain the SFP water level is assumed to be at the coincident SFP bulk temperature. This conservatively neglects the difference in enthalpy between the SFP water and the cooler makeup water, thus reducing the time-to-boil.

The governing energy balance equation for this condition, subject to these conservative assumptions, can be written as:

$$C\frac{dT}{d\tau} = Q(\tau + \tau_0) - Q_{EV}(T)$$

where τ is the time after cooling is lost (hr), τ_0 is the time between reactor shutdown and loss of cooling (hr) and all other terms are the same as defined in Section 5.4.

This differential equation is solved using a numerical solution technique to obtain the bulk pool temperature as a function of time. The SFP decay heat loads for these analyses are extracted from the results of the ONEPOOL transient evaluations. The major input values for these analyses are summarized in Table 5.5.1.

5.6 Maximum SFP Local Water Temperature

In this section, a summary of the methodology for evaluating the maximum SFP local water temperature is presented. A single conservative evaluation for a bounding condition is performed. The result of this single evaluation is a bounding maximum local water temperature.

In order to determine an upper bound on the maximum local water temperature, a series of conservative assumptions are made. The most important of these assumptions are:

- The walls and floor of the SFP are all modeled as adiabatic surfaces, thereby neglecting conduction heat loss through these items.
- Heat losses by thermal radiation and natural convection from the hot SFP surface to the reactor building walls are neglected.
- The rack-to-wall downcomer gaps are modeled as 2 inches wide. The actual rack-to-wall gaps are larger.
- The bottom plenum gap used in the model is approximately 50% of the actual gap.
- No downcomer flow is assumed to exist between the rack modules.
- The hydraulic resistance of every SFSR cell is determined based on the most hydraulically limiting fuel assembly type, the GE-12 10×10.

- The hydraulic resistance of every SFSR cell is determined based on the most restrictive water inlet geometry of the cells over rack support pedestals.

- The hydraulic resistance of every SFSR cell includes the effects of blockage due to an assumed dropped fuel assembly lying horizontally on top of the SFSRs. This condition bounds the effects of overhead platforms, which add little extra flow resistance as a result of the large (~16") spacing between the cell exit and the platform. The blockage due to a dropped assembly also bounds that of a vertically blocked gate, because the width of a channeled assembly is larger than the gate thickness.

- The hydraulic resistance parameters for the rack cells, permeability and inertial resistance, are worsened by 15% and 25%, respectively.

- With a full core discharged into the SFP racks and placed approximately equidistant from the coolant water inlet and outlet, the remaining cells in the spent fuel pool are postulated to be occupied with previously discharged fuel.

- All fuel storage locations are assigned a hydraulic resistance that corresponds to pedestal cells. These cells have a reduced water entrance area, caused by the pedestal blocking the baseplate hole, and a correspondingly increased hydraulic resistance.

- The in-pool sparger piping is modeled as truncated above the elevation of the racks. Sparger truncation is planned for the 2nd campaign of the proposed rerack to avoid interference with the new racks. Because the truncated-sparger condition eliminates the forced feed of cooled water to the racks bottom plenum, the modeled sparger condition is the most conservative.

- In the evaluation of local water temperatures in dual-purpose rack cells containing loaded damaged fuel containers, only two of the cell baseplate holes are credited. This conservatively neglects the two additional baseplate holes and the eight cell side holes, thereby yielding greater than 100% redundancy in these cells.

5.6.1 Local Temperature Evaluation Methodology

As part of the capacity expansion, the inlet piping that returns cooled pool water from the FPCCS and RHR System will be truncated above the level of the SFSRs. It is not apparent from heuristic reasoning alone that the cooled water delivered to the SFP would not bypass the hot fuel and exit through the outlet piping. To demonstrate adequate cooling of hot fuel in the SFP, it is therefore necessary to rigorously quantify the velocity field in the pool created by the interaction of buoyancy driven and forced water flows. A Computational Fluid Dynamics (CFD) analysis for this demonstration is required. The objective of this study is to demonstrate that the thermal-

hydraulic criterion of ensuring local subcooled conditions in the pool is met for all postulated fuel discharge/cooling alignment scenarios. The local thermal-hydraulic analysis is performed such that partial cell blockage and slight fuel assembly variations are bounded. An outline of the CFD approach is described in the following.

There are several significant geometric and thermal-hydraulic features of the Fermi 2 SFP which need to be considered for a rigorous CFD analysis. From a fluid flow modeling standpoint, there are two regions to be considered. One region is the SFP bulk region where the classical Navier-Stokes equations [5.6.1] are solved, with turbulence effects included. The other region is the SFSRs containing heat generating fuel assemblies, located near the bottom of the SFP. In this region, water flow is directed vertically upwards due to buoyancy forces through relatively small flow channels formed by the hydraulically most resistive GE-12 10×10 fuel assemblies in each SFSR cell. This situation is modeled as a porous solid region, where fluid flow is governed by Darcy's Law as:

$$\frac{\partial P}{\partial X_i} = -\frac{\mu}{K(i)} V_i - C \rho |V| \frac{V_i}{2}$$

where $\partial P/\partial Xi$ is the pressure gradient, K(i), V_i and C are the corresponding permeability, velocity and inertial resistance parameters and μ is the fluid viscosity. The permeability and inertial resistance parameters for the rack cells loaded with GE-12 10×10 fuel assemblies are determined based on friction factor correlations for the laminar flow conditions typically encountered due to the low buoyancy induced velocities and the small size of the flow channels.

The Fermi 2 pool geometry required an adequate portrayal of large scale and small scale features, spatially distributed heat sources in the spent fuel racks and water inlet/outlet piping. Relatively cooler bulk pool water normally flows down between the fuel rack outline and pool wall liner clearance known as the downcomer. Near the bottom of the racks the flow turns from a vertical to horizontal direction into the bottom plenum, supplying cooling water to the rack cells. Heated water issuing out of the top of the racks mixes with the SFP bulk water. An adequate modeling of these features on the CFD program involves meshing the large scale bulk pool region and small

scale downcomer and bottom plenum regions with sufficient number of computational cells to capture both the global and local features of the flow field.

The distributed heat sources in the spent fuel pool racks are modeled by identifying distinct heat generation zones considering full-core discharge, bounding peak effects, and the presence of background decay heat from previous discharges. Three heat generating zones are modeled. The first consists of background fuel from previous discharges, the remaining two zones consist of fuel from a bounding full-core-discharge scenario. The two full core discharge zones are differentiated by one zone with higher than average decay heat generation and the other with less than average decay heat generation. This is a conservative model, since all of the fuel with higher than average decay heat is placed in a contiguous area. A uniformly distributed heat generation rate was applied throughout each distinct zone.

The CFD analysis was performed on the commercially available FLUENT [5.6.4] computational fluids program, which has been benchmarked under Holtec's QA program. The FLUENT code enables buoyancy flow and turbulence effects to be included in the CFD analysis. Turbulence effects are modeled by relating time-varying Reynolds' Stresses to the mean bulk flow quantities with the standard k-ε turbulence model.

The governing differential equation (in modified form for turbulent flows with buoyancy effects included) is written as:

$$\frac{\partial \rho_o u_i}{\partial t} + \frac{\partial \rho_o u_i u_j}{\partial X_i} = \frac{\partial}{\partial X_j}\left[\mu\left(\frac{\partial u_i}{\partial X_j} + \frac{\partial u_j}{\partial X_i}\right)\right] - \frac{\partial P}{\partial X_i} - (\rho - \rho_o)g_i + \frac{\partial \rho_o \langle u_i' u_j' \rangle}{\partial X_j}$$

where u_i are the three time-averaged velocity components, $\rho \langle u'_i u'_j \rangle$ are time-averaged Reynolds stresses derived from the turbulence induced fluctuating velocity components u'_i, P is the static pressure head, ρ_o is the fluid density at temperature T_o, μ is the fluid viscosity, g_i are the components of gravitational acceleration and X_j are the Cartesian coordinate directions.

The Reynolds stress tensor is expressed in terms of the mean flow quantities by defining a turbulent viscosity μ_t and a turbulent velocity scale $k^{1/2}$ as shown below [5.6.2]:

$$\rho\left\langle u'_i u'_j \right\rangle = \frac{2}{3}\rho \times \left(k^{1/2}\right)^2 \times \delta_{ij} - \mu_t\left[\frac{\partial u_i}{\partial X_j} + \frac{\partial u_j}{\partial X_i}\right]$$

The procedure to obtain the turbulent viscosity and velocity length scales involves a solution of two additional transport equations for kinetic energy (k) and rate of energy dissipation (ε). This methodology is known as the k-ε model for turbulent flows as described by Launder and Spalding [5.6.3].

Some of the major input values for this analysis are summarized in Table 5.6.1. An isometric view of the assembled CFD model for the Fermi 2 SFP is presented in Figure 5.6.1. Figures 5.6.2 and 5.6.3 present converged temperature contours and velocity vectors, respectively, in a vertical slice through the hot fuel region.

5.6.2 Damaged Fuel Container Evaluation Methodology

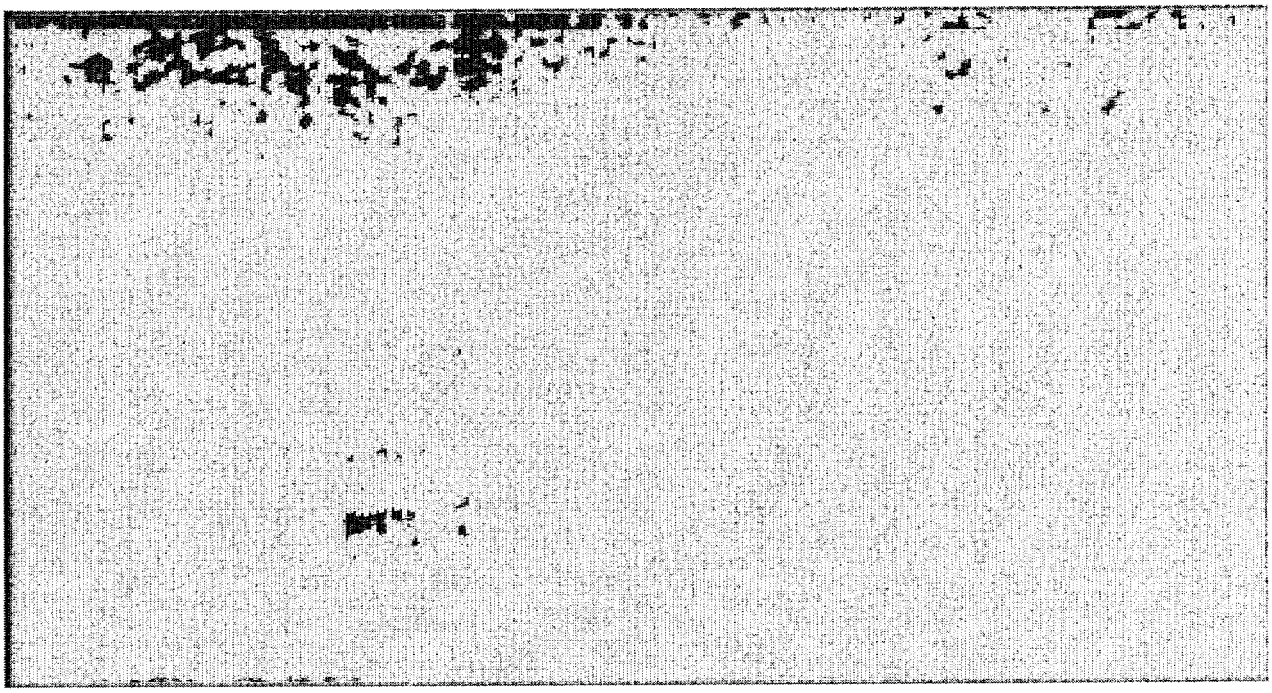

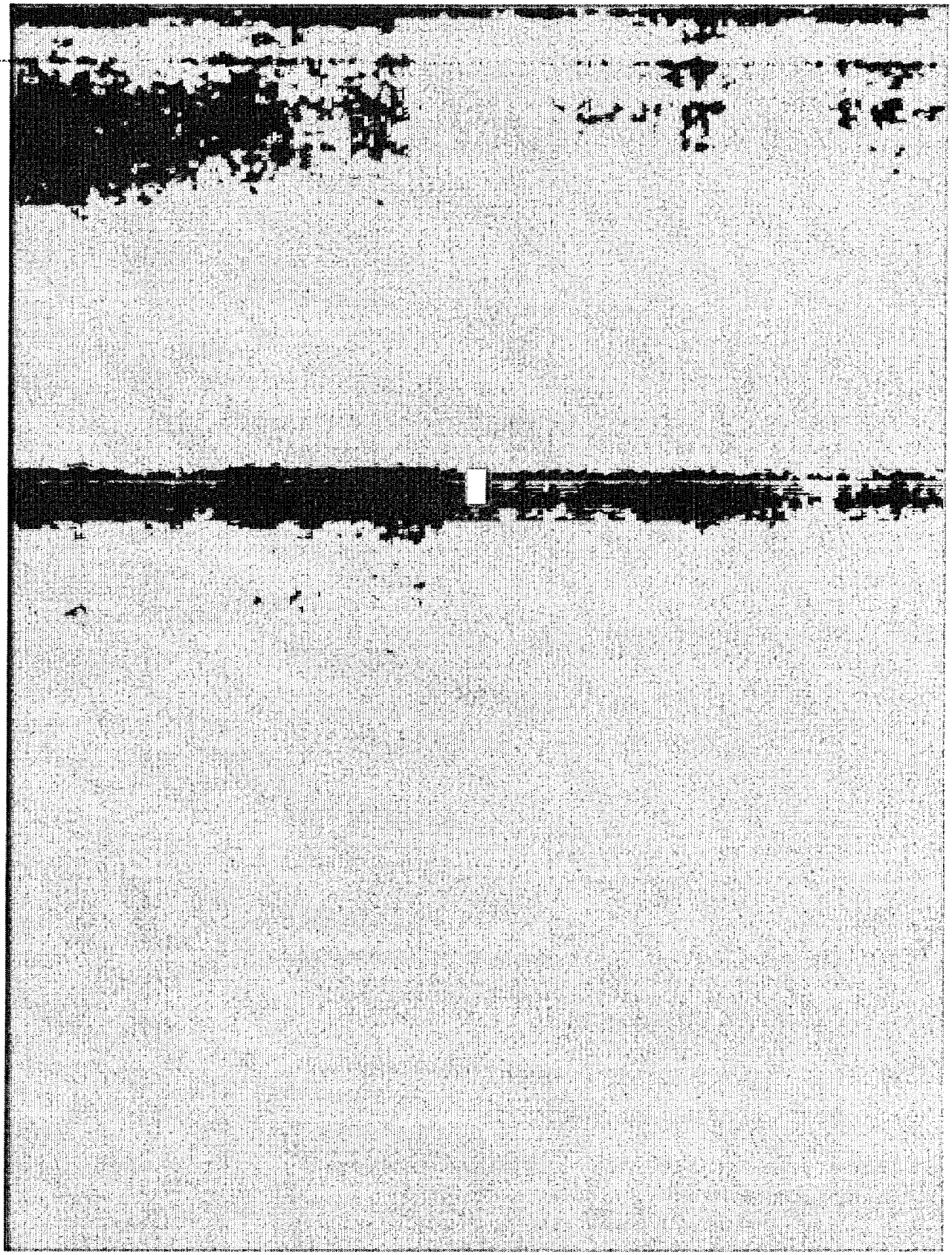

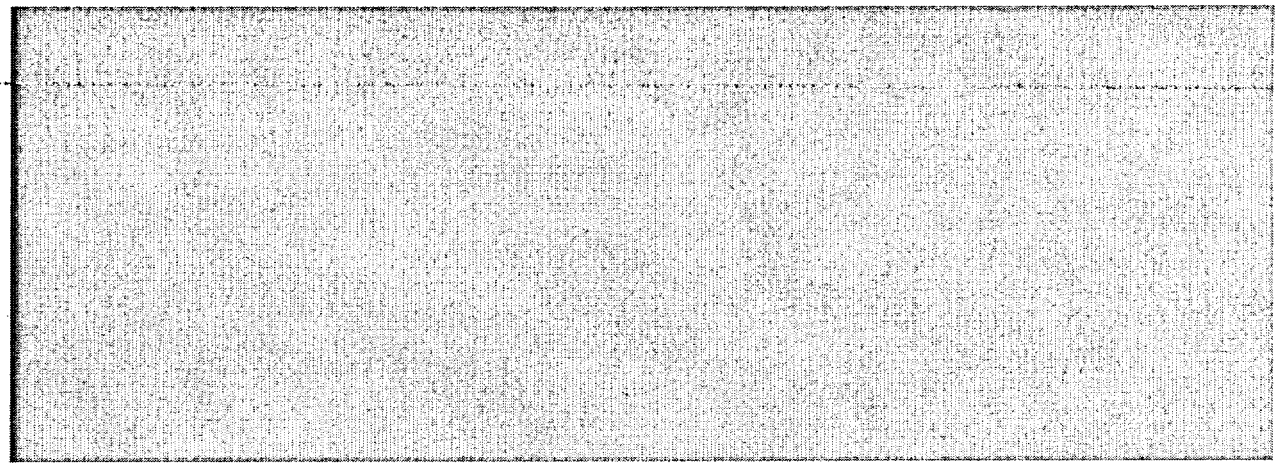

5.7 Fuel Rod Cladding Temperature

In this section, the method to calculate the temperature of the fuel rod cladding is presented. Similar to the local water temperature calculation methodology presented in the preceding section, this evaluation is performed for a single, bounding scenario. The maximum fuel cladding superheat above the local water temperature is calculated.

A fuel rod can produce F_z times the average heat emission rate over a small length, where F_z is the axial peaking factor. The axial heat distribution in a rod is generally a maximum in the central region, and tapers off at its two extremities. Thus, peak cladding heat flux over an infinitesimal rod section is given by the equation:

$$q_c = \frac{q\ F_z}{A_c}$$

where q is the hottest assembly average power and A_c is the total cladding external heat transfer area in the active fuel length region. The axial peaking factor is given in Table 5.6.1.

As described previously, the maximum SFP local water temperature was computed for a bounding condition. Within each fuel assembly sub-channel, water is continuously heated by the cladding as it moves axially upwards under laminar flow conditions. Rohsenow and Hartnett

[5.7.1] report a Nusselt-number for laminar flow heat transfer in a heated channel. The film temperature driving force (ΔT_f) at the peak cladding flux location is calculated as follows:

$$\Delta T_f = \frac{q_c}{h_f}$$

$$h_f \frac{D_h}{Kw} = Nu$$

where h_f is the waterside film heat transfer coefficient, D_h is sub-channel hydraulic diameter, Kw is water thermal conductivity and Nu is the Nusselt number for laminar flow heat transfer.

In order to introduce some additional conservatism in the analysis, we assume that the fuel cladding has a crud deposit resistance R_c (equal to 0.005 ft^2-hr-°F/Btu) which covers the entire surface. Thus, including the temperature drop across the crud resistance, the cladding to water local temperature difference (ΔT_c) is given by the equation $\Delta T_c = \Delta T_f + R_c \times q_c$.

5.8 Results

This section contains results from the analyses performed for the postulated discharge scenario.

5.8.1 Maximum Pool Bulk Temperatures

For the discharge/cooling scenarios described in Section 5.3, the maximum calculated pool bulk temperatures are summarized in Table 5.8.1. Per the Fermi 2 licensing basis, the maximum allowable SFP bulk temperature is 150°F for all scenarios. The results presented in Table 5.8.1 demonstrate that all calculated bulk temperatures remain below the 150°F allowable limit. Given the conservatisms incorporated into the calculations, actual pool bulk temperatures will be lower than these calculated values.

5.8.2 Minimum Time-to-Boil and Maximum Boiloff Rate

For the discharge/cooling described in Section 5.3, the calculated times-to-boil and maximum boiloff rates are summarized in Table 5.8.2. These results show that, in the extremely unlikely event of a complete failure of both the FPCCS and RHR System, there would be at least 4.20 hours available for corrective actions. The maximum water boiloff rate is less than 91 gpm. This is less than the minimum available makeup capacity of 100 gpm available from the condensate storage tanks, and additional sources of makeup are also available.

5.8.3 Local Water and Fuel Cladding Temperatures

Consistent with our approach to make conservative assessments of temperature, the local water temperature calculations are performed for an SFP with decay heat generation equal to the maximum calculated decay heat load. Thus, the local water temperature evaluation is a calculation of the temperature increment over the theoretical spatially uniform value due to local hot spots (due to the presence of a highly heat emissive fuel bundle).

The CFD study has analyzed a single bounding local thermal-hydraulic scenario. In this scenario, a bounding full-core discharge is considered in which the 764 assemblies are located in the pool, equidistant from the water inlet and outlet, while the balance of the rack cells are postulated to be occupied by fuel from old discharges.

In this analysis, the peak local temperature is conservatively calculated to be 169 °F. For the hottest cell location in the SFP, the peak fuel cladding superheat is determined from the CFD model results. The maximum temperature difference between the fuel cladding and the local water (ΔT_c) is calculated to be 28.12°F. Adding this calculated cladding superheat to the calculated maximum local water temperature yields a conservatively bounding 197.12°F peak cladding temperature. The maximum local water temperature is substantially lower than the 238° F local boiling temperature at the top of the SFSRs and nucleate boiling does not occur anywhere within the Fermi 2 SFP.

To determine the local water temperature in a dual-purpose rack cell containing a DFC, the Fermi 2 design-basis DFC heat generation rate of 68,000 Btu/hr was used. It is noted that the analysis performed is intended to confirm that the surface temperature of the DFC is well below the local saturation temperature. The existing DFC design basis is not being changed in this amendment request and as such the DFC internal thermal hydraulic condition was not separately evaluated. At a SFP bulk water temperature equal to the design-basis maximum value of 150°F, the maximum temperature of the water in the dual-purpose rack cell is calculated as 158°F. As noted in Subsection 5.6, this assumed only two of the five baseplate holes were available for flow, thereby providing greater than 100% redundancy for cooling in these racks. The maximum DFC surface temperature is also determined in this analysis and is determined to be 212°F, considerably less than the local saturation temperature of 238°F. Therefore, no vapor bubbles will be formed in the dual-purpose rack cells or on the DFC exterior surfaces when placed into the new dual-purpose rack cells. It is significant to note that the maximum calculated bulk water temperature (see Table 5.8.1) is substantially less than the 150°F used in the DFC analysis, so actual margins will be larger than calculated.

5.9 References for Chapter 5

[5.4.1] "Heat Loss to the Ambient from Spent Fuel Pools: Correlation of Theory with Experiment", Holtec Report HI-90477, Rev. 0, April 3, 1990.

[5.4.2] "An Improved Correlation for Evaporation from Spent Fuel Pools", Holtec Report HI-971664, Rev. 0.

[5.4.3] "QA Documentation - DECAY," Holtec Report HI-92830, Revision 1.

[5.4.4] USNRC Auxiliary Systems Branch (ASB) Technical Position 9-2, "Residual Decay Energy for Light Water Reactors for Long Term Cooling," Revision 2, July 1981.

[5.4.5] "QA Documentation - ONEPOOL," Holtec Report HI-92831, Revision 1.

[5.6.1] Batchelor, G.K., "An Introduction to Fluid Dynamics", Cambridge University Press, 1967.

[5.6.2] Hinze, J.O., "Turbulence", McGraw Hill Publishing Co., New York, NY, 1975.

[5.6.3] Launder, B.E., and Spalding, D.B., "Lectures in Mathematical Models of Turbulence", Academic Press, London, 1972.

[5.6.4] "Validation of FLUENT/UNS Version 4.2.8", Holtec Report HI-982089, Revision 0.

[5.7.1] Rohsenow, N.M., and Hartnett, J.P., "Handbook of Heat Transfer", McGraw Hill Book Company, New York, 1973.

TABLE 5.3.1

HISTORIC AND PROJECTED FUEL DISCHARGE SCHEDULE

End-of-Cycle Number	Date of Discharge	Discharge Batch Size	Cumulative Inventory
1	09/1989	220	220
2	03/1991	228	448
3	09/1992	224	672
4	12/1993	228	900
5	07/1996	176	1076
6	09/1998	220	1296
7	03/2000	224	1520
8	09/2001	224	1744
9	03/2003	224	1968
10	09/2004	224	2192
11	03/2006	224	2416
12	09/2007	200	2616
13	03/2009	200	2816
14	09/2010	200	3016
15	03/2012	200	3216
16	09/2013	200	3416
17	03/2015	200	3616
18	09/2016	200	3816
19	03/2018	200	4016
20	09/2019*	764	4780

* Note: In the planned full core discharge scenario, the full core offload occurs one 18-month cycle after the preceding refueling discharge. As EOC-19 is in March 2018, the subsequent emergency full core offload would therefore occur in September 2019. In the emergency full core discharge scenario, the full core offload occurs one year after the preceding refueling discharge. As EOC-19 is in March 2018, the subsequent emergency full core offload would therefore occur in March 2019.

TABLE 5.4.1 DATA FOR POOL BULK TEMPERATURE EVALUATION	
Reactor Thermal Power	3,430 MWt
Reactor Core Size	764 assemblies
FPCCS HX Coolant Flow Rate	800 gpm
FPCCS HX Coolant Temperature	95°F
RHR HX Coolant Flow Rate	9000 gpm
RHR HX Coolant Temperature	89°F
Minimum In-Core Hold Time	60 hours
Spent Fuel Pool Length (N-S)	408 inches
Spent Fuel Pool Length (E-W)	480 inches
Minimum Pool Water Depth	37.25 feet
FPCCS HX Design Conditions Coolant Inlet Temperature SFP Water Inlet Temperature Coolant Flow Rate Heat Removal Rate	 95°F 125°F 800 gpm 4.56×10^6 Btu/hr
RHR HX Design Conditions Coolant Inlet Temperature SFP Water Inlet Temperature Coolant Flow Rate Heat Removal Rate	 89°F 125°F 9000 gpm 30.72×10^6 Btu/hr
Bounding Fuel Assembly Weight	680 pounds
Ratio of the burnup of the 260 hottest assemblies to the burnup of the remainder 504 assemblies in a full core discharge	1.5

TABLE 5.5.1 DATA FOR TIME-TO-BOIL EVALUATION	
Spent Fuel Pool Length (N-S)	408 inches
Spent Fuel Pool Length (E-W)	480 inches
Minimum Pool Water Depth	37.25 feet
Total Fuel Rack Weight	483,420 lb
Bounding Fuel Assembly Weight	680 pounds
Pool Net Water Volume	42,030 ft^3

TABLE 5.6.1 DATA FOR LOCAL TEMPERATURE EVALUATION	
Bounding Maximum Assembly Weight	680 pounds
Axial Peaking Factor	1.69
Number of Fuel Assemblies	4780
Cooled SFP Water Flow Rate through RHR Heat Exchanger	3500 gpm
Hydraulically Limiting Fuel Assembly	GE-12 10×10
Fuel Rod Outer Diameter	0.404 inches
Active Fuel Length	146 inches
Number of Rods per Assembly*	100 rods
Rack Cell Inner Dimension	6.035 inches
Rack Cell Length	175 inches
Bottom Plenum Height	7.5 inches

* Note: Fuel assembly is modeled as a square array with all locations containing fuel rods.

TABLE 5.8.1

RESULTS OF BULK TEMPERATURE TRANSIENT EVALUATION

Scenario	Maximum Bulk Temperature (°F)	Coincident Decay Heat Load (Btu/hr)	Time After Reactor Shutdown (hrs)
1	125.43	12.20×10^6	72
2	140.55	41.84×10^6	160
3	141.08	42.37×10^6	159

TABLE 5.8.2

RESULTS OF MINIMUM TIME-TO-BOIL AND MAXIMUM BOILOFF RATE EVALUATION

Scenario	Minimum Time-to-Boil (hrs)	Maximum Boiloff Rate (gpm)
1	11.67	44.27
2	4.27	89.82
3	4.20	90.77

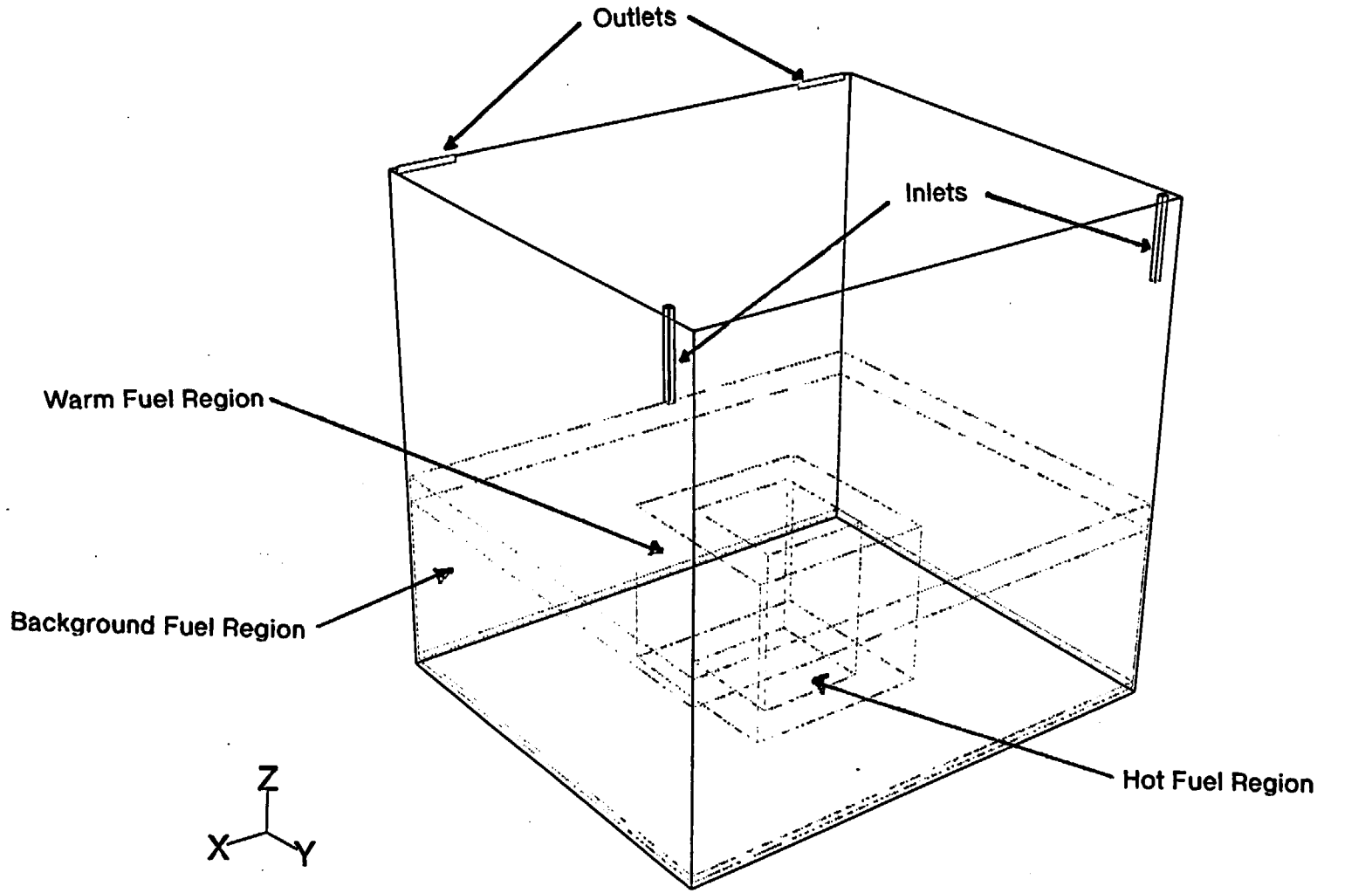

FIGURE 5.6.1: Three-Dimensional Local Temperature CFD Model Grid Region Boundaries

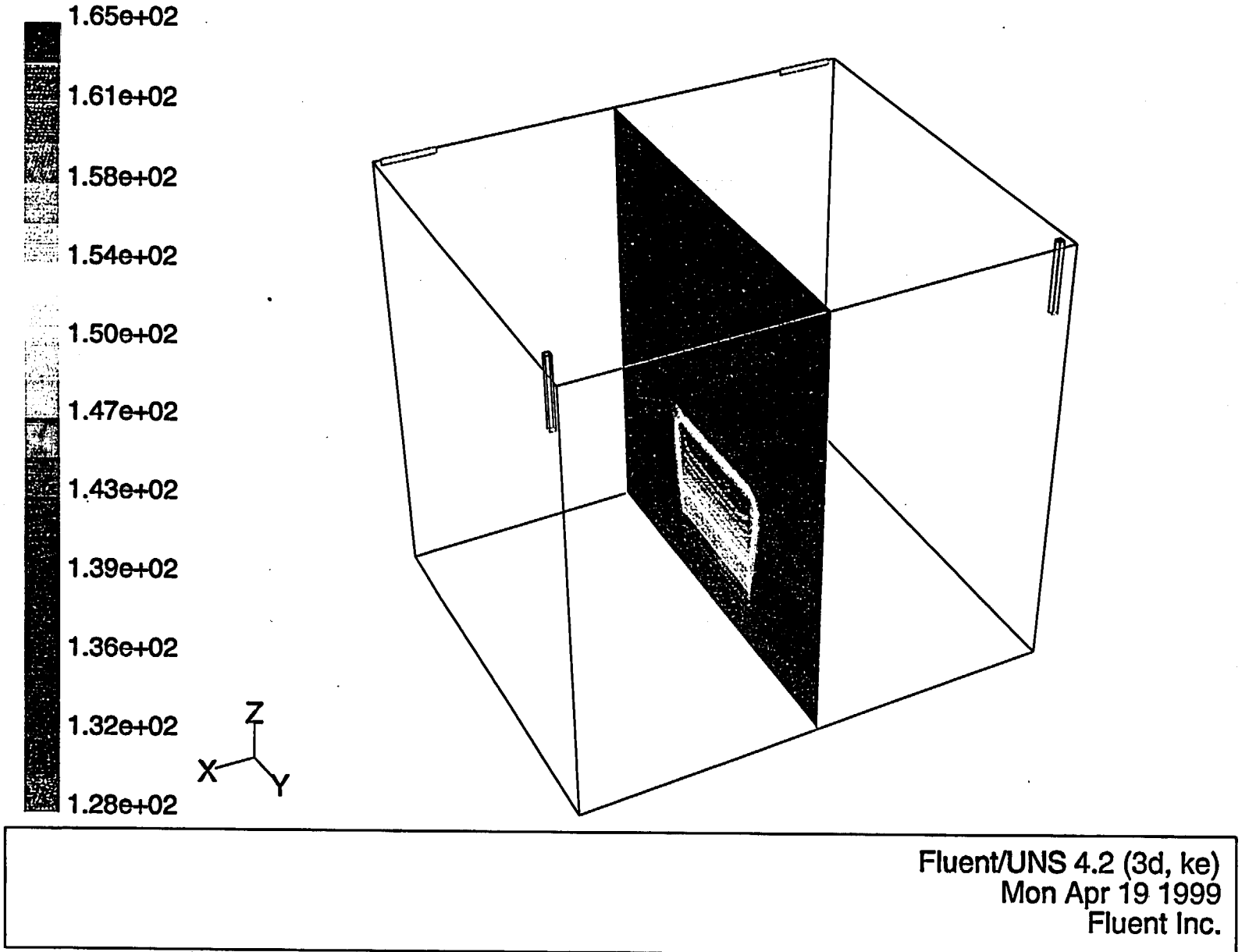

FIGURE 5.6.2: Converged Temperature Contours in Vertical Slice through Hot Region

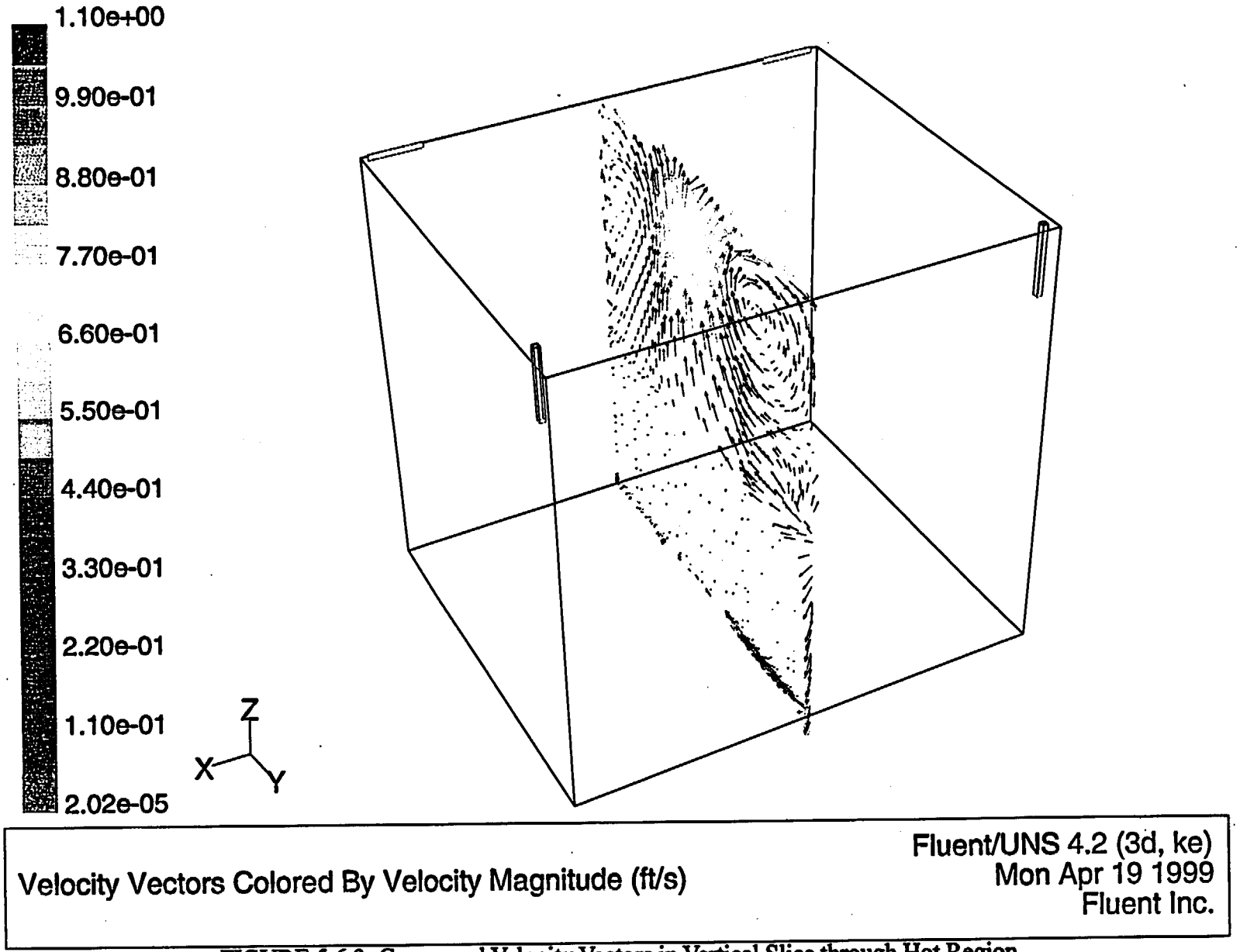

FIGURE 5.6.3: Converged Velocity Vectors in Vertical Slice through Hot Region

6.0 STRUCTURAL/SEISMIC CONSIDERATIONS

6.1 Introduction

This section considers the structural adequacy of the new high density spent fuel racks under all loadings postulated for normal, seismic, and accident conditions at Fermi 2. The proposed final pool layout is shown in Figure 1.2.3.

As discussed in Chapter 1, the reracking of Fermi 2 involves three phases, often termed campaigns. The first phase of the rerack involves the addition of three new high density rack modules in the pool, plus an additional module "A" to be installed in the Cask Area to accommodate the full core offload, only if necessary. Campaign II of the rerack will consist of removal of existing hardware (sparger piping, control rod blade rack, low density racks, channel storage rack, etc.) and existing modules E11 and E15 followed by the addition of five new high density racks. In the final phase (campaign III) of the rerack, all remaining existing racks are to be removed and fourteen new high density racks will be installed for a total of twenty three new high density racks in the pool.

At the time of the original rack installation, the state-of-the-art limited the seismic evaluation to single rack 3-D simulations. As we discuss in this chapter, it is now possible to model the entire assemblage of rack modules in one comprehensive simulation known as the 3-D Whole-Pool-Multi-Rack (WPMR) analysis. In order to maintain continuity with previous analytical methods, both single rack and WPMR analyses have been performed to establish the structural margins of safety in the Fermi II racks.

The analyses undertaken to confirm the structural integrity of the racks are performed in compliance with the USNRC Standard Review Plan [6.1.1] and the OT Position Paper [6.1.2]. For each of the analyses, an abstract of the methodology, modeling assumptions, key results, and summary of parametric evaluations are presented. Delineation of the relevant criteria are discussed in the text associated with each analysis.

6.2 Overview of Rack Structural Analysis Methodology

The response of a free-standing rack module to seismic inputs is highly nonlinear and involves a complex combination of motions (sliding, rocking, twisting, and turning), resulting in impacts and friction effects. Some of the unique attributes of the rack dynamic behavior include a large fraction of the total structural mass in a confined rattling motion, friction support of rack pedestals against lateral motion, and large fluid coupling effects due to deep submergence and motion of closely spaced adjacent structures.

Linear methods, such as modal analysis and response spectrum techniques, cannot accurately simulate the structural response of such a highly nonlinear structure to seismic excitation. An accurate simulation is obtained only by direct integration of the nonlinear equations of motion with the three pool slab acceleration time-histories applied as the forcing functions acting simultaneously.

Both Whole Pool Multi-Rack (WPMR) and Single Rack analysis are used in this project to simulate the dynamic behavior and interaction of the complex storage rack structures. The following sections provide the basis for this selection and discussion on the development of the methodology.

6.2.1 Background of Analysis Methodology

Reliable assessment of the stress field and kinematic behavior of the rack modules calls for a conservative dynamic model incorporating all *key attributes* of the actual structure. This means that the model must feature the ability to execute the concurrent motion forms compatible with the free-standing installation of the modules.

The model must possess the capability to effect momentum transfers which occur due to rattling of fuel assemblies inside storage cells and the capability to simulate lift-off and subsequent impact of support pedestals with the pool liner (or bearing pad). The contribution of the water mass in the interstitial spaces around and between the rack modules and around fuel assemblies must be

included in the model. This fluid mass significantly alters the dynamic behavior of fuel and rack masses during a seismic event. Therefore, the additional fluid mass must be modeled in an accurate manner, since erring in quantification of fluid coupling on either side of the actual value is no guarantee of conservatism.

The Coulomb friction coefficient at the pedestal-to-pool liner (or bearing pad) interface may lie in a rather wide range and a conservative value of friction cannot be prescribed *a priori*. In fact, a perusal of results of rack dynamic analyses in numerous dockets (Table 6.2.1) indicates that an upper bound value of the coefficient of friction often maximizes the computed rack displacements as well as the equivalent elastostatic stresses.

In short, there are a large number of parameters with potential influence on the rack kinematics. The comprehensive structural evaluation must deal with all of these without sacrificing conservatism.

The three-dimensional single rack dynamic model introduced in the Enrico Fermi Unit 2 rack project (ca. 1980) and used in some 50 rerack projects since that time (Table 6.2.1) addresses most of the above mentioned array of parameters. The details of this methodology are also published in the permanent literature [6.2.1]. Despite the versatility of the 3-D seismic model, the accuracy of the single rack simulations has been suspect due to one key element; namely, hydrodynamic participation of water around the racks. During dynamic rack motion, hydraulic energy is either drawn from or added to the moving rack, modifying its submerged motion in a significant manner. Therefore, the dynamics of one rack affects the motion of all others in the pool.

However, Single Rack analysis is still a valuable tool to examine the behavior of a rack under different load conditions. It is used here as a first step in evaluating the racks. WPMR analysis builds upon the Single Rack model. The worst case loads and stresses that result from either of these two models are used to determine the structural adequacy of the racks.

The 3-D rack model dynamic simulation, involving one or more spent fuel racks, handles the array of variables as follows:

Interface Coefficient of Friction: Parametric runs are made with upper bound and lower bound values of the coefficient of friction. The limiting values are based on experimental data, which have been found to be bounded by the values 0.2 and 0.8. Simulations are also performed with the array of pedestals having randomly chosen coefficients of friction in a Gaussian distribution with a mean of 0.5 and lower and upper limits of 0.2 and 0.8, respectively. In the fuel rack simulations, the Coulomb friction interface between rack support pedestal and liner is simulated by piecewise linear (friction) elements. These elements function only when the pedestal is physically in contact with the pool liner.

Rack Beam Behavior: Rack elasticity, relative to the rack base, is included in the model by introducing linear springs to represent the elastic bending action, twisting, and extensions.

Impact Phenomena: Compression-only gap elements are used to provide for opening and closing of interfaces such as the pedestal-to-bearing pad interface, and the fuel assembly-to-cell wall interface. These interface gaps are modeled using nonlinear spring elements. The term "nonlinear spring" is a generic term used to denote the mathematical representation of the condition where a restoring force is not linearly proportional to displacement.

Fuel Loading Scenarios: The fuel assemblies are conservatively assumed to rattle in unison which obviously exaggerates the contribution of impact against the cell wall.

Fluid Coupling: Holtec International extended Fritz's classical two-body fluid coupling model to multiple bodies and utilized it to perform the first two-dimensional multi-rack analysis (Diablo Canyon, ca. 1987). Subsequently, laboratory experiments were conducted to validate the multi-rack fluid coupling theory. This technology was incorporated into the computer code DYNARACK [6.2.4] which handles simultaneous simulation of all racks in the pool as a Whole Pool Multi-Rack 3-D analysis. This development was first utilized in Chinshan, Oyster Creek, and Shearon Harris plants [6.2.1, 6.2.3] and, subsequently, in numerous other rerack projects. The WPMR analyses have corroborated the accuracy of the single rack 3-D solutions in predicting the maximum structural stresses, and also serve to improve predictions of rack kinematics.

For closely spaced racks, demonstration of kinematic compliance is verified by including all modules in one comprehensive simulation using a WPMR model. In WPMR analysis, all rack modules are modeled simultaneously and the coupling effect due to this multi-body motion is included in the analysis. Due to the superiority of this technique in predicting the dynamic behavior of closely spaced submerged storage racks, the Whole Pool Multi-Rack analysis methodology is used for this project.

6.3 Description of Racks

The design features of the new high-density racks proposed for Fermi 2 are described in Chapter 3 of this report. The rack material properties are provided in Table 6.3.1.

6.3.1 Fuel Weights

For the dynamic rack simulations, the dry fuel bundle weight is conservatively taken to be 690 lbs.

6.3.2 Holtec Overhead Platform

The spent fuel racks B and G as identified in Figure 6.8.2 are also qualified for an additional storage function, i.e., the racks are designed to accommodate a Holtec Overhead Platform (HOP), which has a capacity of storing 5 tons (dry). The 1,460-lb platform for rack B and a smaller 1,100-lb platform for rack G are movable, and can be installed on top of the rack by inserting its four support legs into empty storage cells. The surface of the platform for rack B is elevated 16 inches above the top of the rack and measures 57 inches square, which covers a ten by ten area of cells. The surface of the platform for rack G is also elevated 16 inches above the top of the rack but measures a smaller surface area of 37 inches square, which covers a seven by seven area of cells. Multiple items can be stored on these platforms as long as (i) the total dry weight is less than 10,000 lb and (ii) each item completely rests on the storage surface (i.e., 57 and 37 inch square area for rack B platform and rack G platform, respectively). The stored objects are protected from falling off of the platform by 14-inch high sidewalls. The dynamic simulation of racks considers the effect of the Holtec Overhead Platform (HOP) on the subject racks during the occurrence of a seismic event.

6.4 Synthetic Time-Histories

The synthetic time-histories in three orthogonal directions (N-S, E-W, and vertical) are generated in accordance with the provisions of SRP 3.7.1 [6.4.1]. In order to prepare an acceptable set of acceleration time-histories, Holtec International's proprietary code GENEQ [6.4.2] is utilized.

A preferred criterion for the synthetic time-histories in SRP 3.7.1 calls for both the response spectrum and the power spectral density corresponding to the generated acceleration time-history to envelope their target (design basis) counterparts with only finite enveloping infractions. The time-histories for the pools have been generated to satisfy this preferred (and more rigorous) criterion. The seismic files also satisfy the requirements of statistical independence mandated by SRP 3.7.1.

Figures 6.4.1 through 6.4.3 and 6.4.4 through 6.4.6 provide plots of the time-history accelerograms which were generated for a 20 second duration of OBE and SSE events, respectively. These artificial time-histories are used in all non-linear dynamic simulations of the racks.

Results of the correlation function of the three time-histories are given in Table 6.4.1. Absolute values of the correlation coefficients are shown to be less than 0.15, indicating that the desired statistical independence of the three data sets has been met.

6.5 22-DOF Nonlinear Rack Model for Dynamic Analysis

6.5.1 General Remarks

The single rack 3-D model of the Fermi 2 racks has been prepared with due consideration of the following characteristics, which are typical of high-density modules designed by Holtec International.

i. As a continuous structure, the rack possesses an infinite number of degrees-of-freedom, of which the cantilever beam type modes are most pronounced under seismic excitation if the rack is of the honeycomb construction genre. (The Fermi 2 racks, like all prior Holtec designs, are of the honeycomb type.)

ii. The fuel assemblies are "nimble" structures with a relatively low beam mode fundamental frequency.

iii. The interstitial gap between the storage cells and the stored fuel assemblies leads to a rattling condition in the storage cells during a seismic event.

iv. The lateral motion of the rack due to seismic input is resisted by the pedestal-to-pool slab interfacial friction and is abetted or retarded by the fluid coupling forces produced by the proximity of the rack to other structures. (The fluid coupling forces are distinct from the nonconservative forces such as fluid "drag" which are excluded from the analysis in accordance with NRC regulations). The construction of a 3-D single rack dynamic model consists of modeling the rack as a multi-degree-of-freedom structure such a manner that the selected DOFs capture all macro-motion modes of the rack, such as twisting, overturning, lift-off, sliding, flexing, and combinations thereof. Particular attention must be paid to incorporating the potential for the friction-resisted sliding of the rack on the liner, lift-off and subsequent impact of the pedestals on the slab, collision of the rack with adjacent structures, and most important, rattling of the fuel in the storage cells. The dynamic model must also provide for the ability to simulate the scenarios of partially loaded racks with arbitrary loading patterns.

As the name implies, the single rack dynamic model is a 3-D structural model for *one* rack in the pool. The rack selected for the SR analysis in this project is the one with the most non-square cross section (i.e., highest aspect ratio). The dynamic model of this rack, i.e., its structural stiffness characteristics, rattling effect of the stored fuel, etc., can be prepared with extreme diligence in the manner described in the following, resulting in an excellent articulation of the rack structure. Even the fluid coupling effects between the fuel assemblies and the storage cell can be modeled with acceptable accuracy [6.5.2]. If the rack is adjacent to a wall, the fluid coupling effects between the rack and the wall can also be set down deterministically because the wall is a fixed structure. Such a definitive situation does not exist, however, when the neighboring structure to the subject rack is another free-standing rack. During a seismic event, the subject rack and the neighboring rack will both undergo dynamic motions which will be governed by the interaction among the inertia, fluid, friction, and rattling forces for each rack. The fluid coupling forces between two racks, however, depend on their *relative* motions. Because the motion of the neighboring rack is undefined, it is not possible to characterize the hydrodynamic forces arising from the fluid coupling between the

neighboring rack and the subject rack. This inability to accurately model the inter-rack fluid coupling effects is a central limitation in the single rack analysis.

To overcome this limitation intrinsic to the single rack solutions, an artificial boundary condition, referred to as the "out-of-phase" assumption, has been historically made to bound the problem.

In the opposed (out-of-phase) motion assumption, it is assumed that *all* racks adjacent to the subject rack are vibrating 180^0 out-of-phase, resulting in a plane of symmetry between the subject rack and the neighboring rack across which water will not flow. Thus, the subject rack is essentially surrounded by a fictitious rigid box with walls that are placed an offset dimension from the subject rack periphery. The offset dimension is assumed to be one-half of the nominal initial distance to the adjacent racks. Impact with the adjacent rack is assumed to have occurred if the subject rack contacts the "box wall".

In summary, the analyst makes the assumption that the subject rack is moving at 180^0 out-of-phase from the adjacent racks at all times during the seismic event. This is an artificial technical construct, albeit one that is known to conservatively predict rack-to-rack impact.

Therefore, to maintain consistency with past analyses, an array of single rack 3-D simulations were carried out, principally to compare the results (viz., rack-to-rack impact, maximum primary stress levels, pedestal loads, etc.) with the more definitive WPMR analysis. The description below provides the essentials of the 22 DOF model for a single rack. This model is used in both 3-D single rack simulations and as the building block for the more complicated WPMR analyses, described later in this chapter.

The dynamic modeling of the rack structure is prepared with special consideration of all nonlinearities and parametric variations. Particulars of modeling details and assumptions for the rack analysis are given in the following

a. The fuel rack structure motion is captured by modeling the rack as a 12 degree-of-freedom structure. Movement of the rack cross-section at any height is described by six degrees-of-freedom of the rack base and six degrees-of-freedom at the rack top. In this manner, the response of the module, relative to the baseplate, is captured in the dynamic analyses once suitable springs are introduced to couple the rack degrees-of-freedom and simulate rack stiffness.

b. Rattling fuel assemblies within the rack are modeled by five lumped masses located at H, .75H, .5H, .25H, and at the rack base (H is the rack height measured above the baseplate). Each lumped fuel mass has two horizontal displacement degrees-of-freedom. Vertical motion of the fuel assembly mass is assumed equal to rack vertical motion at the baseplate level. The centroid of each fuel assembly mass can be located off-center, relative to the rack structure centroid at that level, to simulate a partially loaded rack.

c. Seismic motion of a fuel rack is characterized by random rattling of fuel assemblies in their individual storage locations. All fuel assemblies are assumed to move in-phase within a rack. This exaggerates computed dynamic loading on the rack structure and, therefore, yields conservative results.

d. Fluid coupling between rack and fuel assemblies, and between rack and wall, is simulated by appropriate inertial coupling in the system kinetic energy. Inclusion of these effects uses the methods of [6.5.2, 6.5.3] for rack/assembly coupling and for rack-to-rack coupling.

e. Fluid damping and form drag are conservatively neglected.

f. Sloshing is found to be negligible at the top of the rack and is, therefore, neglected in the analysis of the rack.

g. Potential impacts between the cell walls of the new racks and the contained fuel assemblies are accounted for by appropriate compression-only gap elements between masses involved. The possible incidence of rack-to-wall or rack-to-rack impact is simulated by gap elements at the top and bottom of the rack in two horizontal directions. Bottom gap elements are located at the baseplate elevation. The initial gaps reflect the presence of baseplate extensions, and the rack stiffnesses are chosen to simulate local structural detail.

h. Pedestals are modeled by gap elements in the vertical direction and as "rigid links" for transferring horizontal stress. Each pedestal support is linked to the pool liner (or bearing pad) by two friction springs. The spring rate for the friction springs includes any lateral elasticity of the stub pedestals. Local pedestal vertical spring stiffness accounts for floor elasticity and for local rack elasticity just above the pedestal.

i. Rattling of fuel assemblies inside the storage locations causes the gap between fuel assemblies and cell wall to change from a maximum of twice the nominal gap to a theoretical zero gap. Fluid coupling coefficients are based on the nominal gap in order to provide a conservative measure of fluid resistance to gap closure.

j. The model for the rack is considered supported, at the base level, on four pedestals modeled as non-linear compression only gap spring elements and eight piecewise linear friction spring elements; these elements are properly located with respect to the centerline of the rack beam, and allow for arbitrary rocking and sliding motions.

6.5.2 Element Details

Figure 6.5.1 shows a schematic of the dynamic model of a single rack. The schematic depicts many of the characteristics of the model including all of the degrees-of-freedom and some of the spring restraint elements.

Table 6.5.1 provides a complete listing of each of the 22 degrees-of-freedom for a rack model. Six transitional and six rotational degrees-of-freedom (three of each type on each end) describe the motion of the rack structure. Rattling fuel mass motions (shown at nodes 1^*, 2^*, 3^*, 4^*, and 5^* in Figure 6.5.1) are described by ten horizontal transitional degrees-of-freedom (two at each of the five fuel masses). The vertical fuel mass motion is assumed (and modeled) to be the same as that of the rack baseplate.

Figure 6.5.2 depicts the fuel to rack impact springs (used to develop potential impact loads between the fuel assembly mass and rack cell inner walls) in a schematic isometric. Only one of the five fuel masses is shown in this figure. Four compression only springs, acting in the horizontal direction, are provided at each fuel mass.

Figure 6.5.3 provides a 2-D schematic elevation of the storage rack model, discussed in more detail in Section 6.5.3. This view shows the vertical location of the five storage masses and some of the support pedestal spring members.

Figure 6.5.4 shows the modeling technique and degrees-of-freedom associated with rack elasticity. In each bending plane a shear and bending spring simulate elastic effects [6.5.4]. Linear elastic springs coupling rack vertical and torsional degrees-of-freedom are also included in the model.

Figure 6.5.5 depicts the inter-rack impact springs (used to develop potential impact loads between racks or between rack and wall).

6.5.3 Fluid Coupling Effect

In its simplest form, the so-called "fluid coupling effect" [6.5.2, 6.5.3] can be explained by considering the proximate motion of two bodies under water. If one body (mass m_1) vibrates adjacent to a second body (mass m_2), and both bodies are submerged in frictionless fluid, then Newton's equations of motion for the two bodies are:

$$(m_1 + M_{11})\, X_1 + M_{12}\, X_2 = \text{applied forces on mass } m_1 + O(X_1^2)$$
$$M_{21}\, X_1 + (m_2 + M_{22})\, X_2 = \text{applied forces on mass } m_2 + O(X_2^2)$$

X_1 and X_2 denote absolute accelerations of masses m_1 and m_2, respectively, and the notation $O(X^2)$ denotes nonlinear terms.

M_{11}, M_{12}, M_{21}, and M_{22} are fluid coupling coefficients which depend on body shape, relative disposition, etc. Fritz [6.5.3] gives data for M_{ij} for various body shapes and arrangements. The fluid adds mass to the body (M_{11} to mass m_1), and an inertial force proportional to acceleration of the adjacent body (mass m_2). Thus, acceleration of one body affects the force field on another. This force field is a function of inter-body gap, reaching large values for small gaps. Lateral motion of a fuel assembly inside a storage location encounters this effect. For example, fluid coupling behavior will be experienced between nodes 2 and 2* in Figure 6.5.1. The rack analysis also contains inertial fluid coupling terms which model the effect of fluid in the gaps between adjacent racks.

Terms modeling the effects of fluid flowing between adjacent racks in a single rack analysis suffer from the inaccuracies described earlier. These terms are computed assuming that all racks adjacent to the rack being analyzed are vibrating 180° out of phase. The WPMR analyses do not require any assumptions with regard to phase.

6.5.4 Stiffness Element Details

Table 6.5.2 lists all spring elements used in the model prepared to simulate campaign 3. Single rack models and those prepared for campaigns 1 and 2 are similar. In the table, the following coordinate system applies:

x = Horizontal axis along plant North

y = Horizontal axis along plant West

z = Vertical axis upward from the rack base

If the simulation model is restricted to two dimensions (one horizontal motion plus one vertical motion, for example), for the purposes of model clarification only, then Figure 6.5.3 describes the configuration. This simpler model is used to elaborate on the modeling for various stiffness elements.

Type 3 gap elements modeling impacts between fuel assemblies and racks have local stiffness K_i in Figure 6.5.3. In Table 6.5.2, for example, type 3 gap elements 5 through 8 act on the rattling fuel mass at the rack top. Support pedestal spring rates K_S are modeled by type 3 gap elements 1 through 4, as listed in Table 6.5.2. Local compliance of the concrete floor is included in K_S. The type 2 friction elements listed in Table 6.5.2 are shown in Figure 6.5.3 as K_f. The spring elements depicted in Figure 6.5.4 represent type 1 linear stiffness elements.

Friction at support/liner interface is modeled by the piecewise linear friction springs with suitably large stiffness K_f up to the limiting lateral load μN, where N is the current compression load at the interface between support and liner. At every time-step during transient analysis, the current value of N (either zero if the pedestal has lifted off the liner, or a compressive finite value) is computed.

The gap element K_S, modeling the effective compression stiffness of the structure in the vicinity of the support, includes stiffness of the pedestal, local stiffness of the underlying pool slab, and local stiffness of the rack cellular structure above the pedestal.

The previous discussion is limited to a 2-D model solely for simplicity. Actual analyses incorporate 3-D motions and include all stiffness elements listed in Table 6.5.2.

6.6 Whole Pool Multi-Rack Methodology

6.6.1 General Remarks

The single rack 3-D (22-DOF) models for the new racks outlined in the preceding subsection are used as a first step to evaluate the structural integrity and physical stability of the rack modules. However, prescribing the motion of the racks adjacent to the module being analyzed is an assumption in the single rack simulations which cannot be defended on the grounds of conservatism. For closely spaced racks, demonstration of the kinematic compliance is further verified by including all modules in one comprehensive simulation using a Whole Pool Multi-Rack (WPMR) model. The WPMR analysis builds on the Single Rack model by simultaneously modeling all racks; a coupling effect results due to the multi-body motion.

Recognizing that the analysis work effort must deal with both stress and displacement criteria, the sequence of model development and analysis steps that are undertaken are summarized in the following:

a. Prepare 3-D dynamic models suitable for a time-history analysis of the new high density racks. These models include the assemblage of all new rack modules in the pool. Include all fluid coupling interactions and mechanical coupling appropriate to performing an accurate non-linear simulation. This 3-D simulation is referred to as a Whole Pool Multi-Rack model.

b. Perform 3-D dynamic analyses on various physical conditions (such as coefficient of friction and extent of cells containing fuel assemblies). Archive appropriate displacement and load outputs from the dynamic model for post-processing.

c. Perform stress analysis of high stress areas for the limiting case of all the rack dynamic analyses. Demonstrate compliance with ASME Code Section III, Subsection NF limits on stress and displacement.

6.6.2 Multi-Body Fluid Coupling

During the seismic event, all racks in the pool are subject to the input excitation simultaneously. The motion of each free-standing module would be autonomous and independent of others as long as they do not impact each other and no water is present in the pool. While the scenario of inter-rack impact is not a common occurrence and depends on rack spacing, the effect of water - the so-called fluid coupling effect - is a universal factor. As noted in Ref. [6.5.2, 6.5.3], the fluid forces can reach rather large values in closely spaced rack geometries. It is, therefore, essential that the contribution of the fluid forces be included in a comprehensive manner. This is possible only if all racks in the pool are *allowed* to execute 3-D motion in the mathematical model. For this reason, single rack or even multi-rack models involving only a portion of the racks in the pool, are inherently inaccurate. The Whole Pool Multi-Rack model removes this intrinsic limitation of the rack dynamic models by simulating the 3-D motion of all modules simultaneously. The fluid coupling effect, therefore, encompasses interaction between *every* set of racks in the pool, i.e., the motion of one rack produces fluid forces on all other racks and on the pool walls. Stated more formally, both near-field and far-field fluid coupling effects are included in the analysis.

The derivation of the fluid coupling matrix [6.6.2] relies on the classical inviscid fluid mechanics principles, namely the principle of continuity and Kelvin's recirculation theorem. While the derivation of the fluid coupling matrix is based on no artificial construct, it has been nevertheless verified by an extensive set of shake table experiments [6.6.2].

6.6.3 Coefficients of Friction

To eliminate the last significant element of uncertainty in rack dynamic analyses, multiple simulations are performed to adjust the friction coefficient ascribed to the support pedestal/pool bearing pad interface. These friction coefficients are chosen consistent with the two bounding extremes from Rabinowicz's data [6.5.1]. Simulations are also performed by imposing intermediate value friction coefficients developed by a random number generator with Gaussian normal distribution characteristics. The assigned values are then held constant during the entire simulation

in order to obtain reproducible results.† Thus, in this manner, the WPMR analysis results are brought closer to the realistic structural conditions.

The coefficient of friction (μ) between the pedestal supports and the pool floor is indeterminate. According to Rabinowicz [6.5.1], results of 199 tests performed on austenitic stainless steel plates submerged in water show a mean value of μ to be 0.503 with standard deviation of 0.125. Upper and lower bounds (based on twice standard deviation) are 0.753 and 0.253, respectively. Analyses are therefore performed for coefficient of friction values of 0.2 (lower limit), 0.8 (upper limit), and for random friction values clustered about a mean of 0.5. The bounding values of $\mu = 0.2$ and 0.8 have been found to envelope the upper limit of module response in previous rerack projects.

6.6.4 Governing Equations of Motion

Using the structural model discussed in the foregoing, equations of motion corresponding to each degree-of-freedom are obtained using Lagrange's Formulation [6.6.1]. The system kinetic energy includes contributions from solid structures and from trapped and surrounding fluid. The final system of equations obtained have the matrix form:

$$[M]\left[\frac{d^2q}{dt^2}\right] = [Q] + [G]$$

where:

[M] - total mass matrix (including structural and fluid mass contributions). The size of this matrix will be 22n x22n for a WPMR analysis (n = number of racks in the model).

† It is noted that DYNARACK has the capability to change the coefficient of friction at any pedestal at each instant of contact based on a random reading of the computer clock cycle. However, exercising this option would yield results that could not be reproduced. Therefore, the random choice of coefficients is made only once per run.

q - the nodal displacement vector relative to the pool slab displacement (the term with q indicates the second derivative with respect to time, i.e., acceleration)

[G] - a vector dependent on the given ground acceleration

[Q] - a vector dependent on the spring forces (linear and nonlinear) and the coupling between degrees-of-freedom

The above column vectors have length 22n. The equations can be rewritten as follows:

$$\left[\frac{d^2q}{dt^2}\right] = [M]^{-1}[Q] + [M]^{-1}[G]$$

This equation set is mass uncoupled, displacement coupled at each instant in time. The numerical solution uses a central difference scheme built into the proprietary computer program DYNARACK [6.2.4].

6.7 Structural Evaluation of Spent Fuel Rack

6.7.1 Kinematic and Stress Acceptance

There are two sets of criteria to be satisfied by the rack modules:

a. Kinematic Criteria

An isolated fuel rack situated in the middle of the storage cavity is most vulnerable to overturning because such a rack would be hydrodynamically uncoupled from any adjacent structures. Therefore, to assess the margin against overturning, a single rack module is evaluated. According to the O.T. Position paper (USNRC, ca 1978), the minimum required safety margins under the OBE and SSE events is 1.5 and 1.1, respectively. The maximum rotation of the rack (about its two principal axes) is obtained from a post processing of the rack time history response output. The ratio of the rotation required to produce incipient tipping in either principal plane to the actual maximum rotation in that plane from the time history solution is the margin of safety. All ratios available for the OBE and SSE events should be greater than 1.5 and 1.1, respectively to satisfy the regulatory acceptance criteria.

b. Stress Limit Criteria

Stress limits must not be exceeded under the postulated load combinations provided herein.

6.7.2 Stress Limit Evaluations

The stress limits presented below apply to the rack structure and are derived from the ASME Code, Section III, Subsection NF [6.7.1]. Parameters and terminology are in accordance with the ASME Code. Material properties are obtained from the ASME Code Appendices [6.7.2], and are listed in Table 6.3.1.

(i) Normal and Upset Conditions (Level A or Level B)

a. Allowable stress in tension on a net section is:

$$F_t = 0.6\ S_y$$

Where, S_y = yield stress at temperature, and F_t is equivalent to primary membrane stress.

b. Allowable stress in shear on a net section is:

$F_v = .4\ S_y$

c. Allowable stress in compression on a net section

$$F_a = S_y\left(.47 - \frac{k\lambda}{444r}\right)$$

$k\lambda/r$ for the main rack body is based on the full height and cross section of the honeycomb region and does not exceed 120 for all sections.

λ = unsupported length of component

k = length coefficient which gives influence of boundary conditions. The following values are appropriate for the described end conditions:

= 1 (simple support both ends)

= 2 (cantilever beam)

= 1/2 (clamped at both ends)

r = radius of gyration of component

d. Maximum allowable bending stress at the outermost fiber of a net section, due to flexure about one plane of symmetry is:

$F_b = 0.60\ S_y$ (equivalent to primary bending)

e. Combined bending and compression on a net section satisfies:

$$\frac{f_a}{F_a} + \frac{C_{mx}\ f_{bx}}{D_x\ F_{bx}} + \frac{C_{my}\ f_{by}}{D_y\ F_{by}} < 1$$

where:

f_a = Direct compressive stress in the section

f_{bx} = Maximum bending stress along x-axis

f_{by} = Maximum bending stress along y-axis

C_{mx} = 0.85

C_{my} = 0.85

$D_x = 1 - (f_a/F'_{ex})$

$D_y = 1 - (f_a/F'_{ey})$

$F'_{ex,ey} = (\pi^2 E)/(2.15\ (kl/r)^2_{x,y})$

E = Young's Modulus

and subscripts x,y reflect the particular bending plane.

f. Combined flexure and compression (or tension) on a net section:

$$\frac{f_a}{0.6 S_y} + \frac{f_{bx}}{F_{bx}} + \frac{f_{by}}{F_{by}} < 1.0$$

The above requirements are to be met for both direct tension or compression.

g. Welds

Allowable maximum shear stress on the net section of a weld is given by:

$$F_w = 0.3\ S_u$$

where S_u is the weld material ultimate strength at temperature. For fillet weld legs in contact with base metal, the shear stress on the gross section is limited to $0.4S_y$, where S_y is the base material yield strength at temperature.

(ii) Level D Service Limits

Section F-1334 (ASME Section III, Appendix F) [6.7.2], states that the limits for the Level D condition are the minimum of 1.2 (S_y/F_t) or ($0.7S_u/F_t$) times the corresponding limits for the Level A condition. S_u is ultimate tensile stress at the specified rack design temperature. Examination of material properties for 304L stainless demonstrates that 1.2 times the yield strength is less than the 0.7 times the ultimate strength.

Exceptions to the above general multiplier are the following:

a) Stresses in shear shall not exceed the lesser of $0.72S_y$ or $0.42S_u$. In the case of the Austenitic Stainless material used here, $0.72S_y$ governs.

b) Axial Compression Loads shall be limited to 2/3 of the calculated buckling load.

c) Combined Axial Compression and Bending - The equations for Level A conditions shall apply except that:

F_a = 0.667 x Buckling Load/ Gross Section Area,

and the terms F'_{ex} and F'_{ey} may be increased by the factor 1.65.

d) For welds, the Level D allowable maximum weld stress is not specified in Appendix F of the ASME Code. An appropriate limit for weld throat stress is conservatively set here as:

$F_w = (0.3\ S_u)$ x factor

where:

factor = (Level D shear stress limit)/(Level A shear stress limit)

6.7.3 Dimensionless Stress Factors

For convenience, the stress results are presented in dimensionless form. Dimensionless stress factors are defined as the ratio of the actual developed stress to the specified limiting value. The limiting value of each stress factor is 1.0, based on the allowable strengths for each level, for Levels A, B, and D (where $1.2S_y < .7S_u$). Stress factors reported are:

R_1 = Ratio of direct tensile or compressive stress on a net section to its allowable value (note pedestals only resist compression)

R_2 = Ratio of gross shear on a net section in the x-direction to its allowable value

R_3 = Ratio of maximum x-axis bending stress to its allowable value for the section

R_4 = Ratio of maximum y-axis bending stress to its allowable value for the section

R_5 = Combined flexure and compressive factor (as defined in the foregoing)

R_6 = Combined flexure and tension (or compression) factor (as defined in the foregoing)

R_7 = Ratio of gross shear on a net section in the y-direction to its allowable value

6.7.4 Loads and Loading Combinations for Spent Fuel Racks

The applicable loads and their combinations which must be considered in the seismic analysis of rack modules is excerpted from Refs. [6.1.2] and [6.6.3]. The load combinations considered are identified below:

Loading Combination	Service Level
$D+L$ $D+L+T_o$ $D+L+T_o+E$	Level A
$D+L+T_a+E$ $D+L+T_o+P_f$	Level B
$D+L+T_a+E'$ $D+L+T_o+F_d$	Level D The functional capability of the fuel racks must be demonstrated.

Where:

D = Dead weight-induced loads (including fuel assembly weight)

L = Live Load (not applicable for the fuel rack, since there are no moving objects in the rack load path)

P_f = Upward force on the racks caused by postulated stuck fuel assembly

F_d = Impact force from accidental drop of the heaviest load from the maximum possible height.

E = Operating Basis Earthquake (OBE)

E' = Safe Shutdown Earthquake (SSE)

T_o = Differential temperature induced loads (normal operating or shutdown condition based on the most critical transient or steady state condition)

T_a = Differential temperature induced loads (the highest temperature associated with the postulated abnormal design conditions)

T_a and T_o produce local thermal stresses. The worst thermal stress field in a fuel rack is obtained when an isolated storage location has a fuel assembly generating heat at maximum postulated rate and surrounding storage locations contain no fuel. Heated water makes unobstructed contact with the inside of the storage walls, thereby producing maximum possible temperature difference between adjacent cells. Secondary stresses produced are limited to the body of the rack; that is, support pedestals do not experience secondary (thermal) stresses.

6.8 Seismic Analysis

6.8.1 Acceptance Criteria

In lieu of performing load case combinations for both OBE and SSE seismic conditions, the SSE case will be performed and compared against stress allowables associated with the OBE conditions. The maximum stress factor limit for OBE events is one half of the stress factor limit for SSE events. Therefore, if the stress factors obtained from the SSE cases are less than 0.5 then they also meet the OBE stress factor limits and hence no OBE runs are required.

6.8.2 Parametric Simulations

Consideration of the parameters described earlier results in a number of scenarios for both the WPMR and the single rack analyses. Although the criterion presented in 6.8.1 applies in that the maximum stress factor observed in the WPMR SSE runs was less than 0.5 (in fact less than 0.25), multi-rack simulations were also performed for OBE scenarios to ensure meeting the acceptance criteria. The single rack analyses consider only SSE simulations, since the results from these simulations meet the above acceptance criteria.

The table below presents a complete listing of the simulations discussed herein. WPMR analyses are performed considering 18, 22, or 23 racks for Campaigns I, II, and III, respectively. The module identification scheme identifying the racks for whole-pool-multi-rack (WPMR) simulations is shown in Figures 6.8.1, 6.8.2 and 6.8.3, for Campaigns I, II, and III, respectively. Single rack analyses are performed to investigate the structural adequacy of the rack when subjected to an array

of different fuel loading patterns (e.g., fully and partially loaded) along with various interface coefficient of frictions. Single rack simulations are also used to confirm the WPMR results, investigate the effect of the HOP (see section 6.3.2) and to determine the potential for rack overturning.

LIST OF RACK SIMULATIONS

Run	Model	Load Case	COF	Event
1	WPMR	Camp I Racks Fully Loaded	0.2	SSE
2	WPMR	Camp I Racks Fully Loaded	0.8	SSE
3	WPMR	Camp I Racks Fully Loaded	Random	SSE
4	WPMR	Camp II Racks Fully Loaded	0.2	SSE
5	WPMR	Camp II Racks Fully Loaded	0.8	SSE
6	WPMR	Camp II Racks Fully Loaded	Random	SSE
7	WPMR	Camp III Racks Fully Loaded	0.2	SSE
8	WPMR	Camp III Racks Fully Loaded	0.8	SSE
9	WPMR	Camp III Racks Fully Loaded	Random	SSE
10	WPMR	Camp I Racks Fully Loaded	0.2	OBE
11	WPMR	Camp I Racks Fully Loaded	0.8	OBE
12	WPMR	Camp I Racks Fully Loaded	Random	OBE
13	WPMR	Camp II Racks Fully Loaded	0.2	OBE
14	WPMR	Camp II Racks Fully Loaded	0.8	OBE
15	WPMR	Camp II Racks Fully Loaded	Random	OBE
16	WPMR	Camp III Racks Fully Loaded	0.2	OBE
17	WPMR	Camp III Racks Fully Loaded	0.8	OBE
18	WPMR	Camp III Racks Fully Loaded	Random	OBE

LIST OF RACK SIMULATIONS				
Run	**Model**	**Load Case**	**COF**	**Event**
19	Single Rack	Module A Fully Loaded	0.2	SSE
20	Single Rack	Module A Fully Loaded	0.8	SSE
21	Single Rack	Module A Fully Loaded	Random	SSE
22	Single Rack	Module A Half Loaded	0.2	SSE
23	Single Rack	Module A Half Loaded	0.8	SSE
24	Single Rack	Module A Half Loaded	Random	SSE
25	Single Rack	Module A Nearly Empty	0.2	SSE
26	Single Rack	Module A Nearly Empty	0.8	SSE
27	Single Rack	Module A Nearly Empty	Random	SSE
28	Single Rack	Module B (full)	0.8	SSE
29	Single Rack	Module B (full) with HOP	0.8	SSE
30	Single Rack	Module G (full)	0.8	SSE
31	Single Rack	Module G (full) with HOP	0.8	SSE
32	Single Rack Overturn Check	Full Rack Module D	0.8	SSE

Where:

Random = Gaussian distribution with a mean of 0.5 coefficient of friction (upper and lower limits of 0.2 and 0.8)

6.9 Time History Simulation Results

The results from the DYNARACK runs may be seen in the raw data output files. However, due to the huge quantity of output data, a post-processor is used to scan for worst case conditions and develop the stress factors. Further reduction in this bulk of information is provided in this section by extracting the worst case values from the parameters of interest, namely displacements, support pedestal forces, impact loads, and stress factors. This section also summarizes other analyses performed to develop and evaluate structural member stresses, which are not determined by the post processor. For each table, the COF column refers to the interface coefficient of friction discussed in subsection 6.2.1. The "Module" column denotes racks by letter (applicable to the pool layout drawing).

6.9.1 Rack Displacements

A summary of the maximum displacement for each simulation is provided in Table 6.9.1. Note that all of the maximum displacements occurred at the tops of the storage racks, as expected from swaying, bending, and tipping behavior. The table shows that the maximum rack displacement is 0.83 inches, which occurs during run 3. This small displacement indicates that rack overturning is not a concern.

6.9.2 Pedestal Vertical Forces

The maximum vertical pedestal loads for each simulation are provided in Table 6.9.2. As may be seen, the highest pedestal load of 166000 lbs. occurs in run 5 of the WPMR model. The effect of this load is evaluated in the bearing pad analysis.

6.9.3 Pedestal Friction Forces

The maximum (x or y direction) friction loads bounding all pedestals in each simulation are obtained by inspection of the complete tabular data. The maximum friction loads are given in Table 6.9.3. The largest pedestal load of 56,900 lbs occurs in run 2 of the WPMR model. The effect of this load is evaluated in the liner fatigue analysis.

6.9.4 Rack Impact Loads

A freestanding rack, by definition, is a structure subject to potential impacts during a seismic event. Impacts arise from rattling of the fuel assemblies in the storage rack locations and, in some instances, from localized impacts between the racks, or between a peripheral rack and the pool wall. The following sections discuss the bounding values of these impact loads.

6.9.4.1 Rack to Rack Impacts

There is no rack to rack impact at rack top or baseplate between any two racks during any of the seismic events.

6.9.4.2 Rack to Wall Impacts

Racks did not impact the pool walls under any simulation.

6.9.4.3 Fuel to Cell Wall Impact Loads

A review of all simulations performed allows determination of the maximum instantaneous impact load between fuel assembly and fuel cell wall at any modeled impact site. The maximum fuel/cell wall impact load values are reported in Table 6.9.4. The maximum Fuel-to-Cell Wall Impact is recorded to be 449 lbs. during run no. 3. The structural integrity of the cell wall under the impact of this load must be evaluated. The discussion of this evaluation is provided in Section 6.10.3.

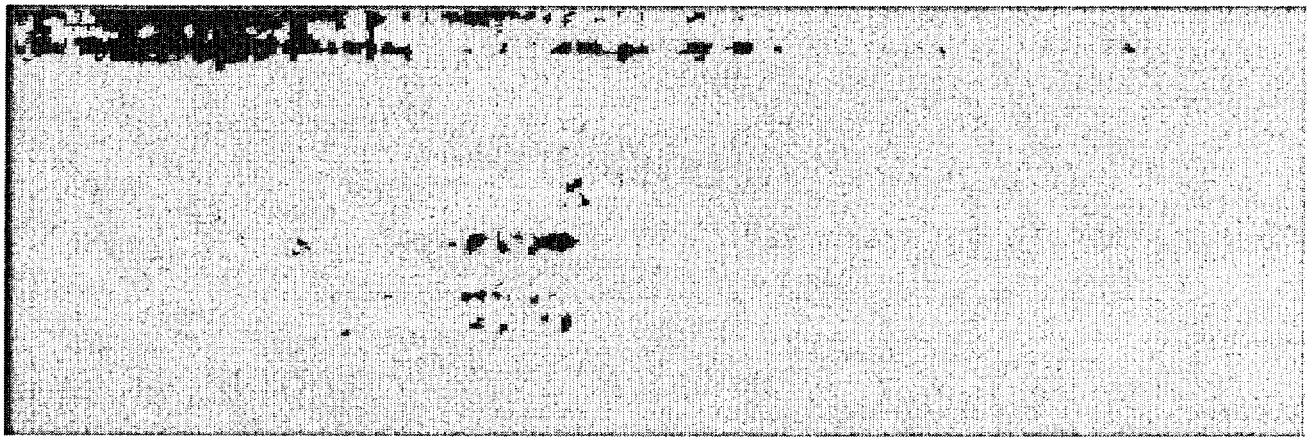

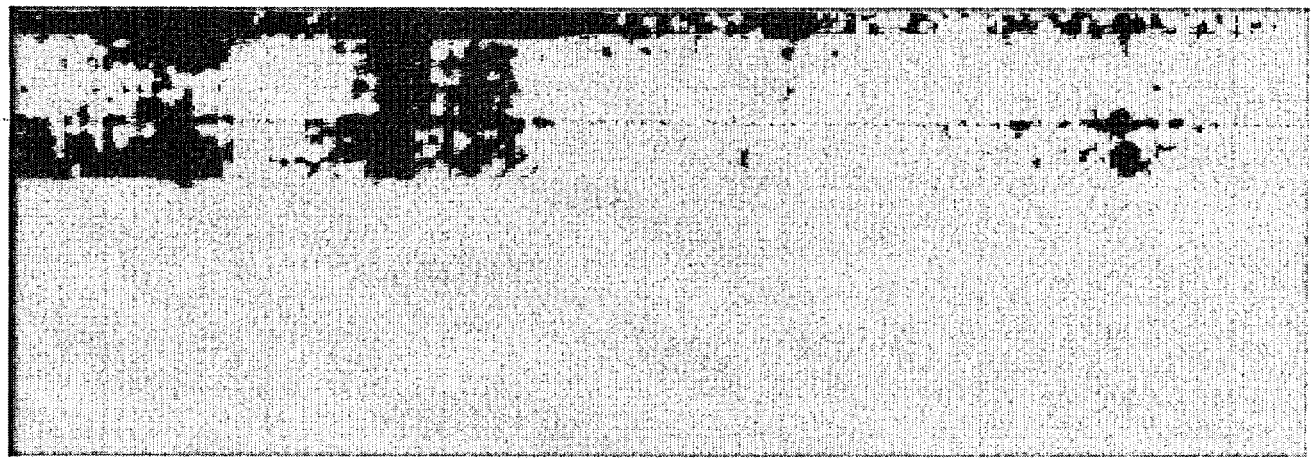

6.10 Rack Structural Evaluation

6.10.1 Rack Stress Factors

With time history results available for pedestal normal and lateral interface forces, the maximum values for the previously defined stress factors can be determined for every pedestal in the array of racks. With this information available, the structural integrity of the pedestal can be assessed and reported. The net section maximum (in time) bending moments and shear forces can also be determined at the bottom casting-rack cellular structure interface for each spent fuel rack in the pool. With this information in hand, the maximum stress in the limiting rack cell (box) can be evaluated. From all of the simulations, the bounding stress factors for each run, in either cellular or the pedestal region, are summarized in Table 6.9.5.

The maximum stress factor in either pedestal or cellular region for SSE and OBE are 0.225 and 0.257, respectively. An evaluation of the stress factors for all of the simulations performed, leads to the conclusion that all stress factors are less than the mandated limit of 1.0 for the load cases examined. The stress allowables are indeed satisfied for the load levels considered for every limiting location in every rack in the array.

6.10.2 Pedestal Thread Shear Stress

The complete post-processor results give thread stresses under faulted conditions for every pedestal with threads for every rack in the pool. The average shear stress in the engagement region is given in Table 6.9.6 for the limiting pedestal in each simulation.

Pedestals for existing racks are one-piece, non-adjustable, not involving thread shear. For pedestals for the new high density racks, the ultimate strength of the female part of the pedestal is 66,200 psi. The yield stress for this material is 21,300 psi. The allowable shear stress for Level B (OBE) conditions is 0.4 times the yield stress which gives 8,520 psi and the allowable shear stress for level D (SSE) is 0.72 times the yield stress which gives 15,336 psi. The maximum calculated shear stress value for the OBE is 8,089 psi and 11,234 psi for the SSE, which are less than their respective allowable values. Therefore, thread shear stresses are acceptable under all conditions.

6.10.3 Local Stresses Due to Impacts

Impact loads at the pedestal base (discussed in subsection 6.9.2) produce stresses in the pedestal for which explicit stress limits are prescribed in the Code. However, impact loads on the cellular region of the racks, as discussed in subsection 6.9.4.3 above, produce stresses, which attenuate rapidly away from the loaded region. This behavior is characteristic of secondary stresses.

Even though limits on secondary stresses are not prescribed in the Code for class 3 NF structures, evaluations must be made to ensure that the localized impacts do not lead to plastic deformations in the storage cells which affect the subcriticality of the stored fuel array.

a. Impact Loading Between Fuel Assembly and Cell Wall

Local cell wall integrity is conservatively estimated from peak impact loads. Plastic analysis is used to obtain the limiting impact load which would lead to gross permanent deformation. Table 6.9.7 indicates that the limiting impact load (of 2,151 lbf, including a safety factor of 2.0) is much greater than the highest calculated impact load value (of 449

lbf, see subsection 6.9.4.3) obtained from any of the rack analyses. Therefore, fuel impacts do not represent a significant concern with respect to fuel rack cell deformation.

b. Impacts Between Adjacent Racks

Impact between the racks is shown not to occur.

6.10.4 Assessment of Rack Fatigue Margin

Deeply submerged high-density spent fuel storage racks arrayed in close proximity to each other in a free-standing configuration behave primarily as a nonlinear cantilevered structure when subjected to 3-D seismic excitations. In addition to the pulsations in the vertical load at each pedestal, lateral friction forces at the pedestal/bearing pad-liner interface, which help prevent or mitigate lateral sliding of the rack, also exert a time-varying moment in the baseplate region of the rack. The friction-induced lateral forces act simultaneously in the x and y directions with the requirement that their vectorial sum does not exceed μN, where μ is the limiting interface coefficient of friction and N is the concomitant vertical thrust on the liner (at the *given* time instant). N is a time-varying function of τ. As N at a pedestal location changes, so does the maximum friction force, F, that the interface can exert. In other words, the lateral force at the pedestal/liner interface, F, is given by

$$F \leq \mu N(\tau)$$

F does not always equal μN; rather, μN is the maximum value it can attain at any time; the actual value, of course, is determined by the dynamic equilibrium of the rack structure. In summary, the horizontal friction force at the pedestal/liner interface is a function of time; its magnitude and direction of action varies during the earthquake event.

The time-varying lateral (horizontal) and vertical forces on the extremities of the support pedestals produce stresses at the root of the pedestals in the manner of an end-loaded cantilever. The stress field in the cellular region of the rack is quite complex, with its maximum values located in the region closest to the pedestal. The maximum magnitude of the stresses depends on the severity of the pedestal end loads and on the geometry of the pedestal/rack baseplate region.

Alternating stresses in metals produce metal fatigue if the amplitude of the stress cycles is sufficiently large. In racks designed for sites with moderate to high postulated seismic action, the stress intensity amplitudes frequently reach values above the material endurance limit, leading to expenditure of the fatigue "usage" reserve in the material.

Because the locations of maximum stress (viz., the pedestal/rack baseplate junction) and the close placement of racks, a post-earthquake inspection of highly stressed regions in the racks is not feasible. Therefore, the racks must be engineered to withstand multiple earthquakes without reliance on nondestructive inspections for post-earthquake integrity assessment. The fatigue life evaluation of racks is an integral aspect of a sound design.

The time-history method of analysis, employed in this report, provides the means to obtain a complete cycle history of the stress intensities in the highly stressed regions of the rack. Having determined the amplitude of the stress intensity cycles and their number, the cumulative damage factor, U, can be determined using the classical Miner's rule

$$U = \Sigma \frac{n_i}{N_i}$$

where n_i is the number of stress intensity cycles of amplitude σ_i, and N_i is the permissible number of cycles corresponding to σ_i from the ASME fatigue curve for the material of construction. U must be less than or equal to 1.0.

To evaluate the cumulative damage factor, a finite element model of a portion of the spent fuel rack in the vicinity of a support pedestal is constructed in sufficient detail to provide an accurate assessment of stress intensities. Figure 6.10.1 shows the essentials of the finite element model. The finite element solutions for unit pedestal loads in three orthogonal directions are combined to establish the maximum value of stress intensity as a function of the three unit pedestal loads. Using the archived results of the spent fuel rack dynamic analyses (pedestal load histories versus time), enables a time-history of stress intensity to be established at the most limiting location. This permits establishing a set of alternating stress intensity ranges versus cycles for SSE and OBE events. Following ASME Code guidelines for computing U, it is found that U under the combined effect of one SSE and twenty OBE events is well below the ASME Code limit of 1.0.

6.10.5 Weld Stresses

Weld locations subjected to significant seismic loading are at the bottom of the rack at the baseplate-to-cell connection, at the top of the pedestal support at the baseplate connection, and at cell-to-cell connections. Bounding values of resultant loads are used to qualify the connections. Table 6.9.7 provides the comparison of calculated stress vs. allowable stress.

a. Baseplate-to-Rack Cell Welds

The highest predicted weld stress for SSE is calculated from the set of forces Fx, Fy and Fz at the Cell Baseplate interface when R6 (defined above in 6.10.1) is maximum. This is for module E5 of run #5 with a stress factor of 0.213. The weld between the cell and the baseplate is checked to determine the maximum weld stress under SSE event. The Ratio 2.07 is developed from the differences in material thickness and length versus weld throat dimension and length:

***RATIO*= (0.075 * 6.11) / (0.0625 * 0.7071 * 5)**

R6(sse) * [(1.2) Fy] * *RATIO* = 0.213 [1.2* 25000] * 2.07 = 13227 psi

This calculated stress value is well below the SSE allowable of 35,748 psi. Therefore, weld stresses between the baseplate and cell wall base are acceptable.

b. Baseplate-to-Pedestal Welds

The weld between baseplate and support pedestal is checked to determine that the maximum stress under the SSE and the OBE event are 8,314 psi and 4,107 psi respectively. These calculated stress values are well below the SSE and OBE allowable of 35,748 psi and 19,860 psi, respectively.

c. Cell-to-Cell Welds

Cell-to-cell connections are formed by a series of connecting welds along the cell height. Stresses in storage cell to cell welds develop due to fuel assembly impacts with the cell wall. These weld stresses are conservatively calculated by assuming that fuel assemblies in adjacent cells are moving out of phase with one another so that impact loads in two adjacent cells are in opposite directions; this tends to separate the two cells from each other at the weld. Table 6.9.7 gives results for the maximum allowable load that can be transferred by these welds based on the available weld area. An upper bound on the load required to be transferred is also given in Table 6.9.7 and is much lower than the allowable load. This upper bound value is very conservatively obtained by applying the bounding rack-to-fuel impact load from any simulation in two orthogonal directions simultaneously, and multiplying the result by 2 to account for the simultaneous impact of two assemblies. An equilibrium analysis at the connection then yields the upper bound load to be transferred. It is seen from the results in Table 6.9.7 that the calculated load is well below the allowable load.

6.11 Level A Evaluation

The Level A condition is not a governing condition for spent fuel racks since the general level of loading is far less than Level B loading. To illustrate this, the heaviest spent fuel rack is considered under the dead weight load. It is shown below that the maximum pedestal load is low and that further stress evaluations are unnecessary.

LEVEL A MAXIMUM PEDESTAL LOAD

Dry Weight of Largest Holtec Rack	=	37,905 lbf
Dry Weight of 361 Fuel Assemblies	=	249,090 lbf
Total Dry Weight	=	286,995 lbf
Total Buoyant Weight (0.87 x Total Dry Weight)	=	249,686 lbf
Load per Pedestal	=	62,422 lbf

The stress allowables for the normal condition is the same as for the upset condition, which resulted in a maximum pedestal load of 166,000 lbs. Since this load (and the corresponding stress throughout the rack members) is much greater than the 62,422 lb load calculated above, the seismic condition controls over normal (Gravity) condition. Therefore, no further evaluation is performed.

6.12 Hydrodynamic Loads on Pool Walls

The maximum hydrodynamic pressures (in psi) that develop between the fuel racks and the spent fuel pool walls develops for the case of the rack that exhibits the largest displacement. This has been done for both the SSE and OBE cases. The results for these worst case conditions, which would occur during campaign III are shown in the table below.

Case	Maximum Pressure (psi)
SSE	7.33
OBE	4.25

These hydrodynamic pressures were considered in the evaluation of the Spent Fuel Pool structure.

6.13 Conclusion

Thirty-two discrete freestanding dynamic simulations of three campaigns involving new high density and existing high density spent fuel storage racks have been performed to establish the structural margins of safety. Of the thirty-two parametric analyses, eighteen simulations consisted of modeling all fuel racks in the pool for a given campaign in one comprehensive Whole Pool Multi Rack (WPMR) model. The remaining fourteen runs were carried out with the classical single rack 3-D model. The parameters varied in the different runs consisted of the rack/pool liner interface coefficient of friction, extent of storage locations occupied by spent nuclear fuel (ranging from nearly empty to full), the presence of the Holtec Overhead Platform and the type of seismic input (SSE or OBE). Maximum (maximum in time and space) values of pedestal vertical, shear forces, displacements and stress factors (normalized stresses for NF class 3 linear type structures) have been post-processed from the array of runs and summarized in tables in this chapter. The results show that:

(i) All stresses are well below their corresponding "NF" limits.

(ii) There is no rack-to-rack or rack-to-wall impact.

(iii) The rack overturning is not a concern.

An evaluation of the fatigue expenditure in the most stressed location in the most heavily loaded rack module under combined effect of one SSE and twenty OBE events shows that the Cumulative Damage Factor (using Miner's rule) is below the permissible value of 1.0.

In conclusion, all evaluations of structural safety, mandated by the OT Position Paper [6.1.2] and the contemporary fuel rack structural analysis practice have been carried out. They demonstrate consistently large margins of safety in all new storage modules.

6.14 References for Chapter 6

[6.1.1] USNRC NUREG-0800, Standard Review Plan, June 1987.

[6.1.2] (USNRC Office of Technology) "OT Position for Review and Acceptance of Spent Fuel Storage and Handling Applications", dated April 14, 1978, and January 18, 1979 amendment thereto.

[6.2.1] Soler, A.I. and Singh, K.P., "Seismic Responses of Free Standing Fuel Rack Constructions to 3-D Motions", Nuclear Engineering and Design, Vol. 80, pp. 315-329 (1984).

[6.2.2] Soler, A.I. and Singh, K.P., "Some Results from Simultaneous Seismic Simulations of All Racks in a Fuel Pool", INNM Spent Fuel Management Seminar X, January, 1993.

[6.2.3] Singh, K.P. and Soler, A.I., "Seismic Qualification of Free Standing Nuclear Fuel Storage Racks - the Chin Shan Experience, Nuclear Engineering International, UK (March 1991).

[6.2.4] Holtec Proprietary Report HI-961465 - WPMR Analysis User Manual for Pre&Post Processors & Solver, August, 1997.

[6.4.1] USNRC Standard Review Plan, NUREG-0800 (Section 3.7.1, Rev. 2, 1989).

[6.4.2] Holtec Proprietary Report HI-89364 - Verification and User's Manual for Computer Code GENEQ, January, 1990.

[6.5.1] Rabinowicz, E., "Friction Coefficients of Water Lubricated Stainless Steels for a Spent Fuel Rack Facility," MIT, a report for Boston Edison Company, 1976.

[6.5.2] Singh, K.P. and Soler, A.I., "Dynamic Coupling in a Closely Spaced Two-Body System Vibrating in Liquid Medium: The Case of Fuel Racks," 3rd International Conference on Nuclear Power Safety, Keswick, England, May 1982.

[6.5.3] Fritz, R.J., "The Effects of Liquids on the Dynamic Motions of Immersed Solids," Journal of Engineering for Industry, Trans. of the ASME, February 1972, pp 167-172.

[6.6.1] Levy, S. and Wilkinson, J.P.D., "The Component Element Method in Dynamics with Application to Earthquake and Vehicle Engineering," McGraw Hill, 1976.

[6.6.2] Paul, B., "Fluid Coupling in Fuel Racks: Correlation of Theory and Experiment", (Proprietary), NUSCO/Holtec Report HI-88243.

[6.7.1] ASME Boiler & Pressure Vessel Code, Section III, Subsection NF, 1995 Edition.

[6.7.2] ASME Boiler & Pressure Vessel Code, Section III, Appendices, 1995 Edition.

[6.7.3] USNRC Standard Review Plan, NUREG-0800 (Section 3.8.4, Rev. 2, 1989).

[6.10.1] Chun, R., Witte, M. and Schwartz, M., "Dynamic Impact Effects on Spent Fuel Assemblies," UCID-21246, Lawrence Livermore National Laboratory, October 1987.

Table 6.2.1

PARTIAL LISTING OF FUEL RACK APPLICATIONS USING DYNARACK

PLANT	DOCKET NUMBER(s)	YEAR
Enrico Fermi Unit 2	USNRC 50-341	1980
Quad Cities 1 & 2	USNRC 50-254, 50-265	1981
Rancho Seco	USNRC 50-312	1982
Grand Gulf Unit 1	USNRC 50-416	1984
Oyster Creek	USNRC 50-219	1984
Pilgrim	USNRC 50-293	1985
V.C. Summer	USNRC 50-395	1984
Diablo Canyon Units 1 & 2	USNRC 50-275, 50-323	1986
Byron Units 1 & 2	USNRC 50-454, 50-455	1987
Braidwood Units 1 & 2	USNRC 50-456, 50-457	1987
Vogtle Unit 2	USNRC 50-425	1988
St. Lucie Unit 1	USNRC 50-335	1987
Millstone Point Unit 1	USNRC 50-245	1989
Chinshan	Taiwan Power	1988
D.C. Cook Units 1 & 2	USNRC 50-315, 50-316	1992
Indian Point Unit 2	USNRC 50-247	1990
Three Mile Island Unit 1	USNRC 50-289	1991
James A. FitzPatrick	USNRC 50-333	1990
Shearon Harris Unit 2	USNRC 50-401	1991
Hope Creek	USNRC 50-354	1990
Kuosheng Units 1 & 2	Taiwan Power Company	1990
Ulchin Unit 2	Korea Electric Power Co.	1990
Laguna Verde Units 1 & 2	Comision Federal de Electricidad	1991
Zion Station Units 1 & 2	USNRC 50-295, 50-304	1992

Table 6.2.1

PARTIAL LISTING OF FUEL RACK APPLICATIONS USING DYNARACK

Sequoyah	USNRC 50-327, 50-328	1992
LaSalle Unit 1	USNRC 50-373	1992
Duane Arnold Energy Center	USNRC 50-331	1992
Fort Calhoun	USNRC 50-285	1992
Nine Mile Point Unit 1	USNRC 50-220	1993
Beaver Valley Unit 1	USNRC 50-334	1992
Salem Units 1 & 2	USNRC 50-272, 50-311	1993
Limerick	USNRC 50-352, 50-353	1994
Ulchin Unit 1	KINS	1995
Yonggwang Units 1 & 2	KINS	1996
Kori-4	KINS	1996
Connecticut Yankee	USNRC 50-213	1996
Angra Unit 1	Brazil	1996
Sizewell B	United Kingdom	1996
Waterford 3	USNRC 50-382	1996
Vogtle	USNRC 50-424	1997
J. A. Fitzpatrick	USNRC 50-333	1997
Vermont Yankee	USNRC 50-271	1998
Callaway	USNRC 50-483	1998
Wolf Creek	USNRC 50-482	1998
Nine Mile	USNRC 50-220	1998
Harris	USNRC 50-400	1998

Table 6.3.1 RACK MATERIAL DATA (200°F) (ASME - Section II, Part D)			
Material	**Young's Modulus E (psi)**	**Yield Strength S_y (psi)**	**Ultimate Strength S_u (psi)**
SA240; 304L S.S.	27.6×10^6	21,300	66,200
SUPPORT MATERIAL DATA (200°F)			
SA240, Type 304L (upper part of support feet)	27.6×10^6	21,300	66,200
SA-564-630 (lower part of support feet; age hardened at 1100F)	27.6×10^6	106,300	140,000

Table 6.4.1 TIME-HISTORY STATISTICAL CORRELATION RESULTS	
OBE	
Data1 to Data2	0.023
Data1 to Data3	0.023
Data2 to Data3	0.022
SSE	
Data1 to Data2	0.003
Data1 to Data3	-0.00001
Data2 to Data3	0.016

Data1 corresponds to the time-history acceleration values along the **X axis (North)**

Data2 corresponds to the time-history acceleration values along the **Y axis (East)**

Data3 corresponds to the time-history acceleration values along the **Z axis (Vertical)**

Table 6.5.1

Degrees-of-freedom

LOCATION (Node)	DISPLACEMENT			ROTATION		
	U_x	U_y	U_z	θ_x	θ_y	θ_z
1	p_1	p_2	p_3	q_4	q_5	q_6
2	p_7	p_8	p_9	q_{10}	q_{11}	q_{12}

Node 1 is assumed to be attached to the rack at the bottom most point.
Node 2 is assumed to be attached to the rack at the top most point.
Refer to Figure 6.5.1 for node identification.

2*	p_{13}	p_{14}
3*	p_{15}	p_{16}
4*	p_{17}	p_{18}
5*	p_{19}	p_{20}
1*	p_{21}	p_{22}

where the relative displacement variables q_i are defined as:

$p_i = q_i(t) + U_x(t)$ $\quad i = 1,7,13,15,17,19,21$

$= q_i(t) + U_y(t)$ $\quad i = 2,8,14,16,18,20,22$

$= q_i(t) + U_z(t)$ $\quad i = 3,9$

$= q_i(t)$ $\quad i = 4,5,6,10,11,12$

p_i denotes absolute displacement (or rotation) with respect to inertial space

q_i denotes relative displacement (or rotation) with respect to the floor slab

* denotes fuel mass nodes

U(t) are the three known earthquake displacements

Table 6.5.2

(DYNARACK) NUMBERING SYSTEM FOR GAP ELEMENTS AND FRICTION ELEMENTS

I. Nonlinear Springs (Type 3 Gap Elements - 776 Total)

Number	Node Location	Description
Rack Number 1		
1	Support S1	Z compression-only element
2	Support S2	Z compression-only element
3	Support S3	Z compression-only element
4	Support S4	Z compression-only element
5	2,2*	+X rack/fuel assembly impact element between nodes 2 and 2*
6	2,2*	-X rack/fuel assembly impact element between nodes 2 and 2*
7	2,2*	+Y rack/fuel assembly impact element between nodes 2 and 2*
8	2,2*	-Y rack/fuel assembly impact element between nodes 2 and 2*
9-24	Impact elements corresponding to the rattling fuel masses at nodes 1*, 3*, 4* and 5* (similar to elements 5 thru 8)	
Rack numbers 2 through 23		
25-552	Impact elements corresponding to the pedestal supports and rattling fuel masses at nodes 1*, 2*,3*, 4* and 5* (similar to elements 1 through 24)	
All racks		
553-776	Rack-to-rack and rack-to-wall impact elements modeled at the rack top and bottom corners (i.e., top and bottom of each rack)	

Table 6.5.2

(DYNARACK) NUMBERING SYSTEM FOR GAP ELEMENTS AND FRICTION ELEMENTS

II. Linear Springs (Type 1 Elements - 138 Total)

Number	Rack No.	Description
1	1	Rack beam bending element (x-z plane)
2	1	Rack shear deformation element (x-z plane)
3	1	Rack beam bending element (y-z plane)
4	1	Rack shear deformation element (y-z plane)
5	1	Rack beam axial deformation element
6	1	Rack beam torsional deformation element
7-138	2-23	Similar to elements 1 thru 6

III. Piece-wise Linear Friction Springs (Type 2 Elements - 184 Total)

Number	Rack No.	Description
1	1	Pedestal 1, X direction
2	1	Pedestal 1, Y direction
3	1	Pedestal 2, X direction
4	1	Pedestal 2, Y direction
5	1	Pedestal 3, X direction
6	1	Pedestal 3, Y direction
7	1	Pedestal 4, X direction
8	1	Pedestal 4, Y direction
9-184	2-23	Similar to elements 1 thru 8

TABLE 6.9.1

RACK DISPLACEMENT RESULTS

Run	Model	Excitation	COF	Max. Displacement (inches)	Module
1	WPMR – Campaign I	SSE	0.2	0.6035	C2
2	WPMR – Campaign I	SSE	0.8	0.7502	E11
3	WPMR – Campaign I	SSE	Random	0.8295	E15
4	WPMR – Campaign II	SSE	0.2	0.6604	F
5	WPMR – Campaign II	SSE	0.8	0.5801	C1
6	WPMR – Campaign II	SSE	Random	0.6205	E6
7	WPMR – Campaign III	SSE	0.2	0.6540	E
8	WPMR – Campaign III	SSE	0.8	0.5563	E
9	WPMR – Campaign III	SSE	Random	0.7281	E
10	WPMR – Campaign I	OBE	0.2	0.1990	C1
11	WPMR – Campaign I	OBE	0.8	0.1940	E7
12	WPMR – Campaign I	OBE	Random	0.2331	E15
13	WPMR – Campaign II	OBE	0.2	0.2690	G
14	WPMR – Campaign II	OBE	0.8	0.2620	G
15	WPMR – Campaign II	OBE	Random	0.2710	G
16	WPMR – Campaign III	OBE	0.2	0.2034	F
17	WPMR – Campaign III	OBE	0.8	0.1989	E
18	WPMR – Campaign III	OBE	Random	0.1934	E
19	Single Rack (Full)	SSE	0.2	0.1240	A
20	Single Rack (Full)	SSE	0.8	0.1340	A
21	Single Rack (Full)	SSE	Random	0.1541	A
22	Single Rack (Half Full)	SSE	0.2	0.0880	A
23	Single Rack (Half Full)	SSE	0.8	0.0860	A
24	Single Rack (Half Full)	SSE	Random	0.0926	A

TABLE 6.9.1

RACK DISPLACEMENT RESULTS

Run	Model	Excitation	COF	Max. Displacement (inches)	Module
25	Single Rack (Nearly Empty)	SSE	0.2	0.0223	A
26	Single Rack (Nearly Empty)	SSE	0.8	0.0225	A
27	Single Rack (Nearly Empty)	SSE	Random	0.0225	A
28	Single Rack (Full)	SSE	0.8	0.1370	B
29	Single Rack (Full with HOP)	SSE	0.8	0.1350	B
30	Single Rack (Full)	SSE	0.8	0.2420	G
31	Single Rack (Full with HOP)	SSE	0.8	0.3030	G
32	Single Rack (Full) Overturn Check	SSE	0.8	0.2290	D

TABLE 6.9.2

MAXIMUM VERTICAL LOADS

Run	Model	Excitation	COF	Maximum Vertical Load (lbs)	Module
1	WPMR – Campaign I	SSE	0.2	143000	E2,E6
2	WPMR – Campaign I	SSE	0.8	150000	B
3	WPMR – Campaign I	SSE	Random	152000	E7
4	WPMR – Campaign II	SSE	0.2	149000	E6
5	WPMR – Campaign II	SSE	0.8	166000	E5
6	WPMR – Campaign II	SSE	Random	151000	E6
7	WPMR – Campaign III	SSE	0.2	118000	B
8	WPMR – Campaign III	SSE	0.8	121000	B
9	WPMR – Campaign III	SSE	Random	123000	B
10	WPMR – Campaign I	OBE	0.2	111000	E1
11	WPMR – Campaign I	OBE	0.8	106000	B
12	WPMR – Campaign I	OBE	Random	106000	B
13	WPMR – Campaign II	OBE	0.2	112000	E6
14	WPMR – Campaign II	OBE	0.8	111000	E6
15	WPMR – Campaign II	OBE	Random	116000	E6
16	WPMR – Campaign III	OBE	0.2	100000	Cask Pit
17	WPMR – Campaign III	OBE	0.8	103000	Cask Pit
18	WPMR – Campaign III	OBE	Random	104000	Cask Pit
19	Single Rack (Full)	SSE	0.2	82000	A
20	Single Rack (Full)	SSE	0.8	82300	A
21	Single Rack (Full)	SSE	Random	83000	A
22	Single Rack (Half Full)	SSE	0.2	47100	A
23	Single Rack (Half Full)	SSE	0.8	47800	A

TABLE 6.9.2

MAXIMUM VERTICAL LOADS

Run	Model	Excitation	COF	Maximum Vertical Load (lbs)	Module
24	Single Rack (Half Full)	SSE	Random	48400	A
25	Single Rack (Nearly Empty)	SSE	0.2	11300	A
26	Single Rack (Nearly Empty)	SSE	0.8	11800	A
27	Single Rack (Nearly Empty)	SSE	Random	11800	A
28	Single Rack (Full)	SSE	0.8	139000	B
29	Single Rack (Full with HOP)	SSE	0.8	133000	B
30	Single Rack (Full)	SSE	0.8	72600	G
31	Single Rack (Full with HOP)	SSE	0.8	82100	G
32	Single Rack (Full) Overturn Check	SSE	0.8	72000	D

TABLE 6.9.3

MAXIMUM HORIZONTAL LOADS

Run	Model	Excitation	COF	Maximum Horizontal Load(lbs)	Module
1	WPMR – Campaign I	SSE	0.2	25800	E7
2	WPMR – Campaign I	SSE	0.8	56900	E1
3	WPMR – Campaign I	SSE	Random	37600	E4
4	WPMR – Campaign II	SSE	0.2	26200	E3
5	WPMR – Campaign II	SSE	0.8	54700	E6
6	WPMR – Campaign II	SSE	Random	39300	E5
7	WPMR – Campaign III	SSE	0.2	23600	B
8	WPMR – Campaign III	SSE	0.8	36100	A
9	WPMR – Campaign III	SSE	Random	35300	B
10	WPMR – Campaign I	OBE	0.2	17800	E2
11	WPMR – Campaign I	OBE	0.8	25300	E2
12	WPMR – Campaign I	OBE	Random	19600	E2
13	WPMR – Campaign II	OBE	0.2	17200	E6
14	WPMR – Campaign II	OBE	0.8	31500	E6
15	WPMR – Campaign II	OBE	Random	24800	E6
16	WPMR – Campaign III	OBE	0.2	18600	Cask Pit
17	WPMR – Campaign III	OBE	0.8	17100	Cask Pit
18	WPMR – Campaign III	OBE	Random	17500	Cask Pit
19	Single Rack (Full)	SSE	0.2	15300	A
20	Single Rack (Full)	SSE	0.8	23400	A
21	Single Rack (Full)	SSE	Random	20500	A
22	Single Rack (Half Full)	SSE	0.2	8550	A
23	Single Rack (Half Full)	SSE	0.8	16500	A

TABLE 6.9.3

MAXIMUM HORIZONTAL LOADS

Run	Model	Excitation	COF	Maximum Horizontal Load(lbs)	Module
24	Single Rack (Half Full)	SSE	Random	15100	A
25	Single Rack (Nearly Empty)	SSE	0.2	2080	A
26	Single Rack (Nearly Empty)	SSE	0.8	4180	A
27	Single Rack (Nearly Empty)	SSE	Random	4410	A
28	Single Rack (Full)	SSE	0.8	31900	B
29	Single Rack (Full with HOP)	SSE	0.8	26800	B
30	Single Rack (Full)	SSE	0.8	19100	G
31	Single Rack (Full with HOP)	SSE	0.8	20600	G
32	Single Rack (Full) Overturn Check	SSE	0.8	22700	D

TABLE 6.9.4

FUEL-TO-CELL WALL IMPACT

Run	Model	Excitation	COF	Max. Impact Load (lbs)	Module
1	WPMR – Campaign I	SSE	0.2	385	E1
2	WPMR – Campaign I	SSE	0.8	334	E6
3	WPMR – Campaign I	SSE	Random	449	E11
4	WPMR – Campaign II	SSE	0.2	370	E6
5	WPMR – Campaign II	SSE	0.8	337	F
6	WPMR – Campaign II	SSE	Random	365	E5
7	WPMR – Campaign III	SSE	0.2	327	M3
8	WPMR – Campaign III	SSE	0.8	322	P
9	WPMR – Campaign III	SSE	Random	342	F
10	WPMR – Campaign I	OBE	0.2	208	C1
11	WPMR – Campaign I	OBE	0.8	244	E11
12	WPMR – Campaign I	OBE	Random	214	E11
13	WPMR – Campaign II	OBE	0.2	224	E10
14	WPMR – Campaign II	OBE	0.8	280	E1
15	WPMR – Campaign II	OBE	Random	247	D
16	WPMR – Campaign III	OBE	0.2	211	J1
17	WPMR – Campaign III	OBE	0.8	207	R
18	WPMR – Campaign III	OBE	Random	222	Q
19	Single Rack (Full)	SSE	0.2	225	A
20	Single Rack (Full)	SSE	0.8	225	A
21	Single Rack (Full)	SSE	Random	225	A
22	Single Rack (Half Full)	SSE	0.2	134	A
23	Single Rack (Half Full)	SSE	0.8	133	A
24	Single Rack (Half Full)	SSE	Random	152	A

TABLE 6.9.4

FUEL-TO-CELL WALL IMPACT

Run	Model	Excitation	COF	Max. Impact Load (lbs)	Module
25	Single Rack (Nearly Empty)	SSE	0.2	2	A
26	Single Rack (Nearly Empty)	SSE	0.8	3	A
27	Single Rack (Nearly Empty)	SSE	Random	2	A
28	Single Rack (Full)	SSE	0.8	307	B
29	Single Rack (Full with HOP)	SSE	0.8	265	B
30	Single Rack (Full)	SSE	0.8	282	G
31	Single Rack (Full with HOP)	SSE	0.8	294	G
32	Single Rack (Full) Overturn Check	SSE	0.8	212	D

TABLE 6.9.5

MAXIMUM STRESS FACTORS

Run	Model	COF	Event	Stress Factor Cell (CRB)	Stress Factor Type/Module
1	WPMR – Campaign I	0.2	SSE	0.162	R5/E6
2	WPMR – Campaign I	0.8	SSE	0.190	R6/E8
3	WPMR – Campaign I	Random	SSE	0.195	R5/E12
4	WPMR – Campaign II	0.2	SSE	0.166	R5/E6
5	WPMR – Campaign II	0.8	SSE	0.225	R5/E5
6	WPMR – Campaign II	Random	SSE	0.194	R5/E6
7	WPMR – Campaign III	0.2	SSE	0.146	R5,R6/C2
8	WPMR – Campaign III	0.8	SSE	0.139	R5/C2
9	WPMR – Campaign III	Random	SSE	0.147	R6/C2
10	WPMR – Campaign I	0.2	OBE	0.245	R5/C2
11	WPMR – Campaign I	0.8	OBE	0.245	R5/C2
12	WPMR – Campaign I	Random	OBE	0.245	R5/C2
13	WPMR – Campaign II	0.2	OBE	0.240	R5/E6
14	WPMR – Campaign II	0.8	OBE	0.233	R5/E6
15	WPMR – Campaign II	Random	OBE	0.257	R5/E6
16	WPMR – Campaign III	0.2	OBE	0.216	R5/C1
17	WPMR – Campaign III	0.8	OBE	0.216	R5/C1
18	WPMR – Campaign III	Random	OBE	0.216	R5/C1
19	Single Rack (Full)	0.2	SSE	0.111	R5/A
20	Single Rack (Full)	0.8	SSE	0.112	R5/A
21	Single Rack (Full)	Random	SSE	0.112	R5/A
22	Single Rack (Half Full)	0.2	SSE	0.065	R5,R6/A
23	Single Rack (Half Full)	0.8	SSE	0.066	R5,R6/A
24	Single Rack (Half Full)	Random	SSE	0.066	R5,R6/A

TABLE 6.9.5

MAXIMUM STRESS FACTORS

Run	Model	COF	Event	Stress Factor Cell (CRB)	Stress Factor Type/Module
25	Single Rack (Nearly Empty)	0.2	SSE	0.016	R5,R6/A
26	Single Rack (Nearly Empty)	0.8	SSE	0.016	R5,R6/A
27	Single Rack (Nearly Empty)	Random	SSE	0.016	R5,R6/A
28	Single Rack (Full)	0.8	SSE	0.098	R5/B
29	Single Rack (Full with HOP)	0.8	SSE	0.095	R5/B
30	Single Rack (Full)	0.8	SSE	0.134	R5/G
31	Single Rack (Full with HOP)	0.8	SSE	0.154	R5,R6/G
32	Single Rack (Full) Overturn Check	0.8	SSE	0.121	R5/D

TABLE 6.9.6

THREAD SHEAR STRESS

Run	Model	COF	Excitation	Stress (psi)	Module
1	WPMR – Campaign I	0.2	SSE	10485	B
2	WPMR – Campaign I	0.8	SSE	11234	B
3	WPMR – Campaign I	Random	SSE	10410	B
4	WPMR – Campaign II	0.2	SSE	9587	B
5	WPMR – Campaign II	0.8	SSE	10336	B
6	WPMR – Campaign II	Random	SSE	10635	B
7	WPMR – Campaign III	0.2	SSE	8838	B
8	WPMR – Campaign III	0.8	SSE	8688	B
9	WPMR – Campaign III	Random	SSE	9736	B
10	WPMR – Campaign I	0.2	OBE	7939	B
11	WPMR – Campaign I	0.8	OBE	7939	B
12	WPMR – Campaign I	Random	OBE	7939	B
13	WPMR – Campaign II	0.2	OBE	8089	B
14	WPMR – Campaign II	0.8	OBE	8089	B
15	WPMR – Campaign II	Random	OBE	8089	B
16	WPMR – Campaign III	0.2	OBE	7490	Cask Pit
17	WPMR – Campaign III	0.8	OBE	7714	Cask Pit
18	WPMR – Campaign III	Random	OBE	7789	Cask Pit
19	Single Rack (Full)	0.2	SSE	6141	A
20	Single Rack (Full)	0.8	SSE	6164	A
21	Single Rack (Full)	Random	SSE	6216	A
22	Single Rack (Half Full)	0.2	SSE	3528	A
23	Single Rack (Half Full)	0.8	SSE	3580	A
24	Single Rack (Half Full)	Random	SSE	3625	A

TABLE 6.9.6

THREAD SHEAR STRESS

Run	Model	COF	Excitation	Stress (psi)	Module
25	Single Rack (Nearly Empty)	0.2	SSE	846	A
26	Single Rack (Nearly Empty)	0.8	SSE	884	A
27	Single Rack (Nearly Empty)	Random	SSE	884	A
28	Single Rack (Full)	0.8	SSE	10410	B
29	Single Rack (Full with HOP)	0.8	SSE	9961	B
30	Single Rack (Full)	0.8	SSE	5437	G
31	Single Rack (Full with HOP)	0.8	SSE	6149	G
32	Single Rack (Full) Overturn Check	0.8	SSE	5392	D

Table 6.9.7

COMPARISON OF BOUNDING CALCULATED LOADS/STRESSES VS/ CODE ALLOWABLES AT IMPACT LOCATIONS AND WELDS

Item/Location	Calculated	Allowable
Fuel assembly/cell wall impact, lbf.	449	2,151†
Rack Cell to baseplate weld, psi	13,227 (SSE)	35,748 (SSE)
Female pedestal to baseplate weld, psi	8,314 (SSE) 4,107 (OBE)	35,748 (SSE) 19,860 (OBE)
Cell to cell welds, psi.	4,324††	8,520

† Based on the limit load for a cell wall. The allowable load on the fuel assembly itself may be less than this value but is greater than 449 lbs

†† Based on the fuel assembly to cell wall impact load simultaneously applied in two orthogonal directions.

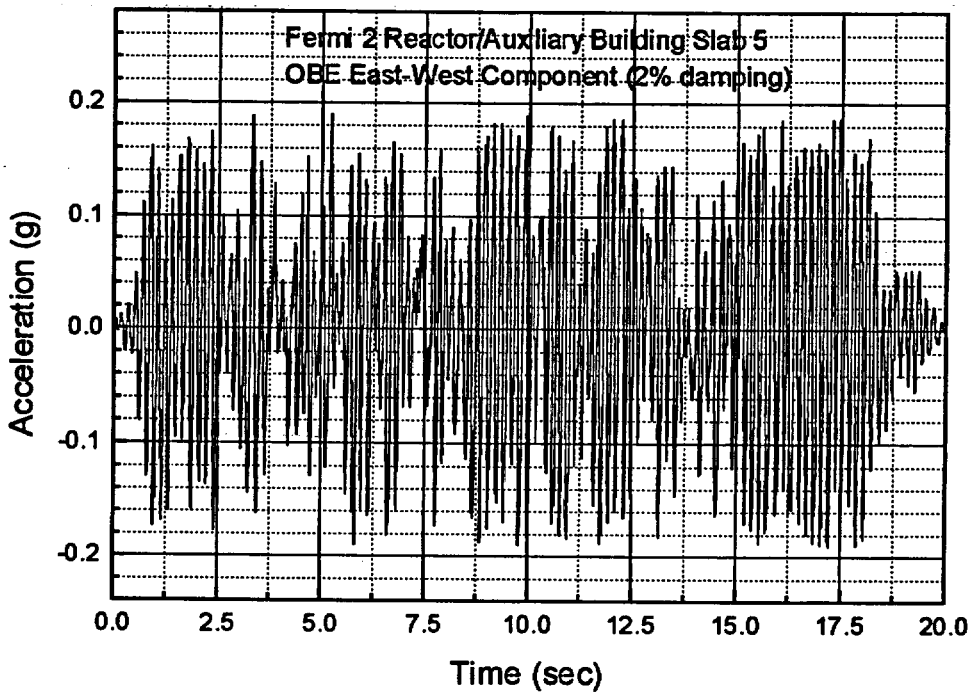

Figure 6.4.1; OBE acceleration time history in the x-direction (East-West)

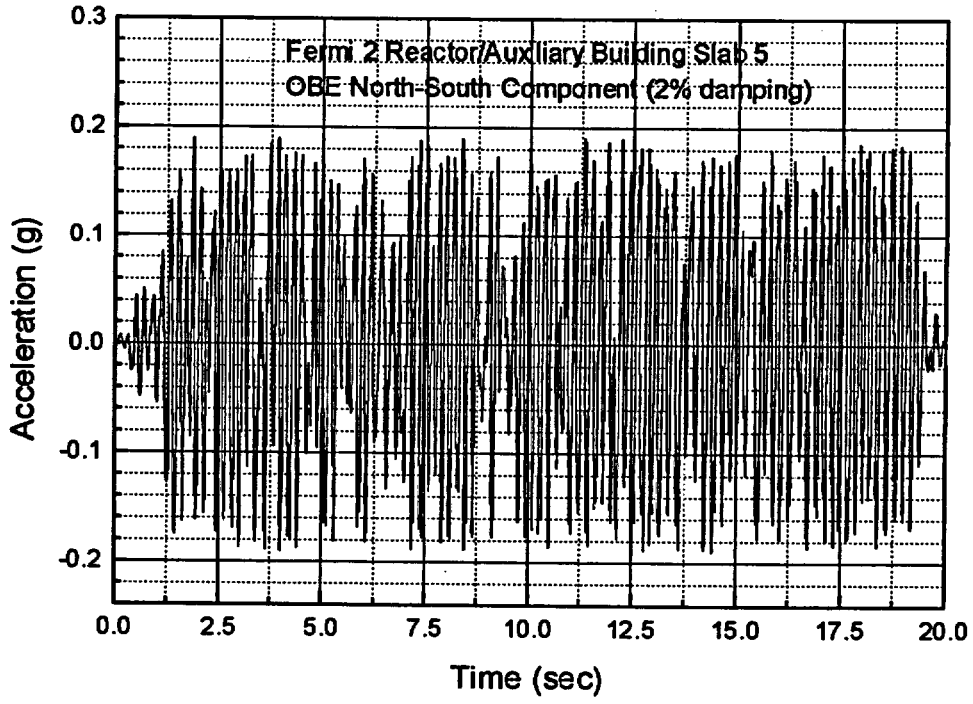

Figure 6.4.2; OBE acceleration time history in the y-direction (North-South)

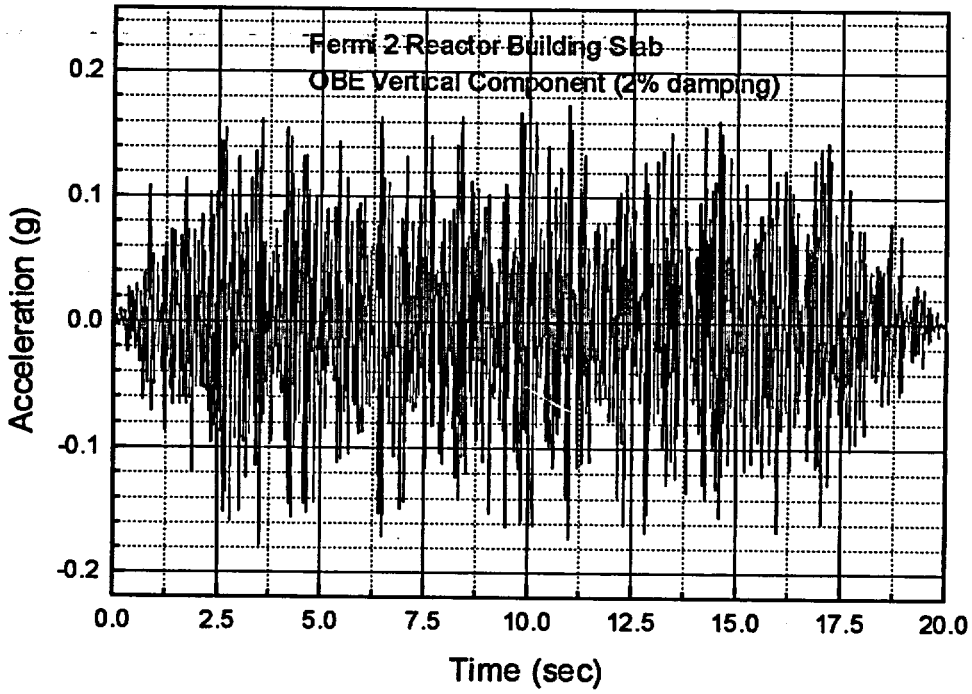

Figure 6.4.3; OBE acceleration time history in the z-direction (Vertical)

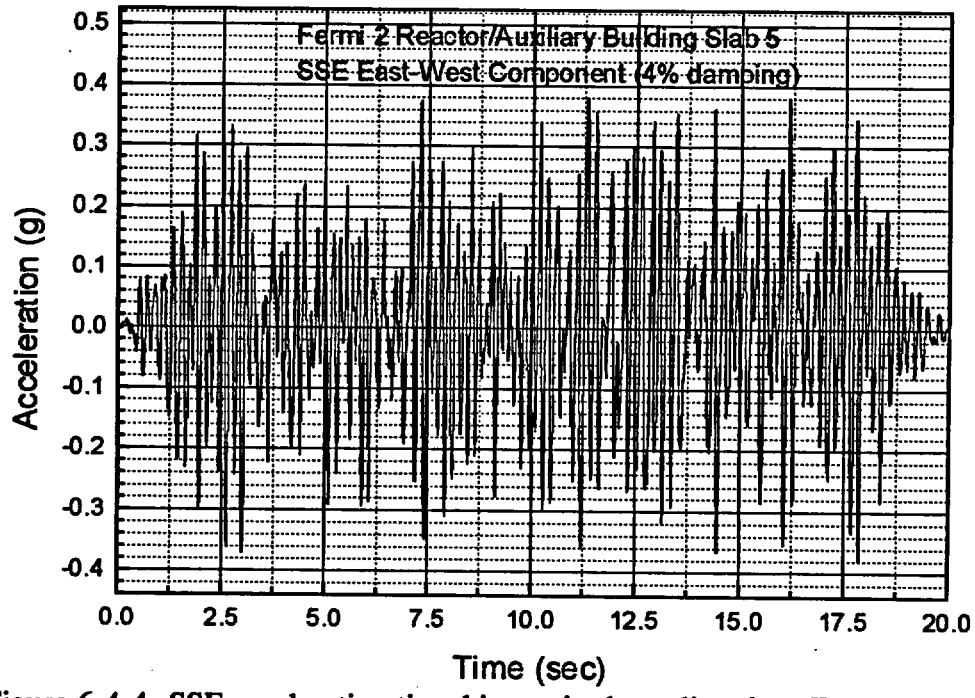

Figure 6.4.4; SSE acceleration time history in the x-direction (East-West)

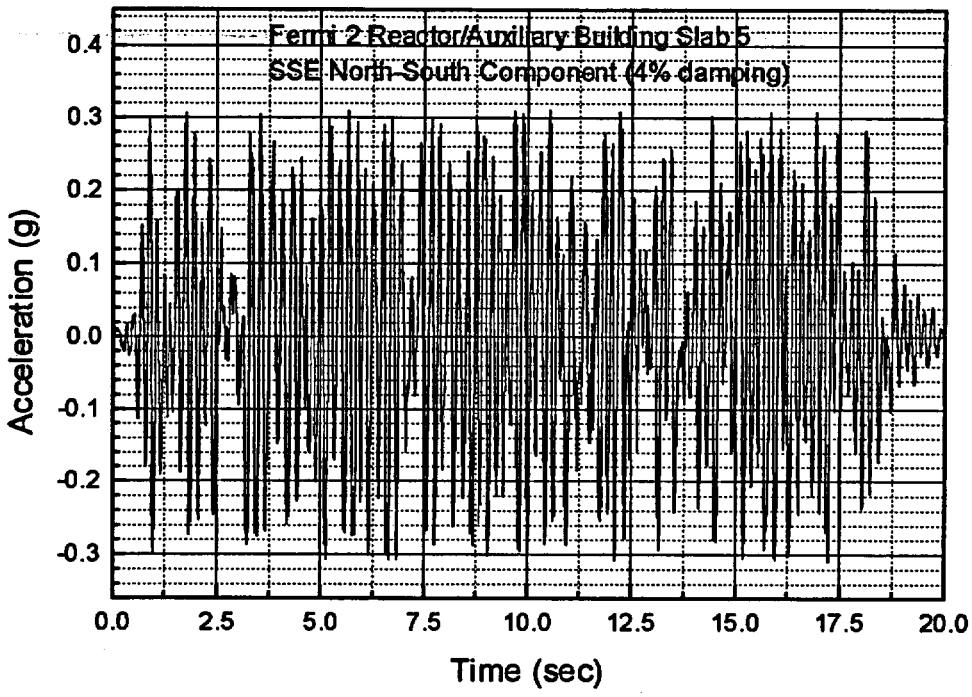

Figure 6.4.5; SSE acceleration time history in the y-direction (North-South)

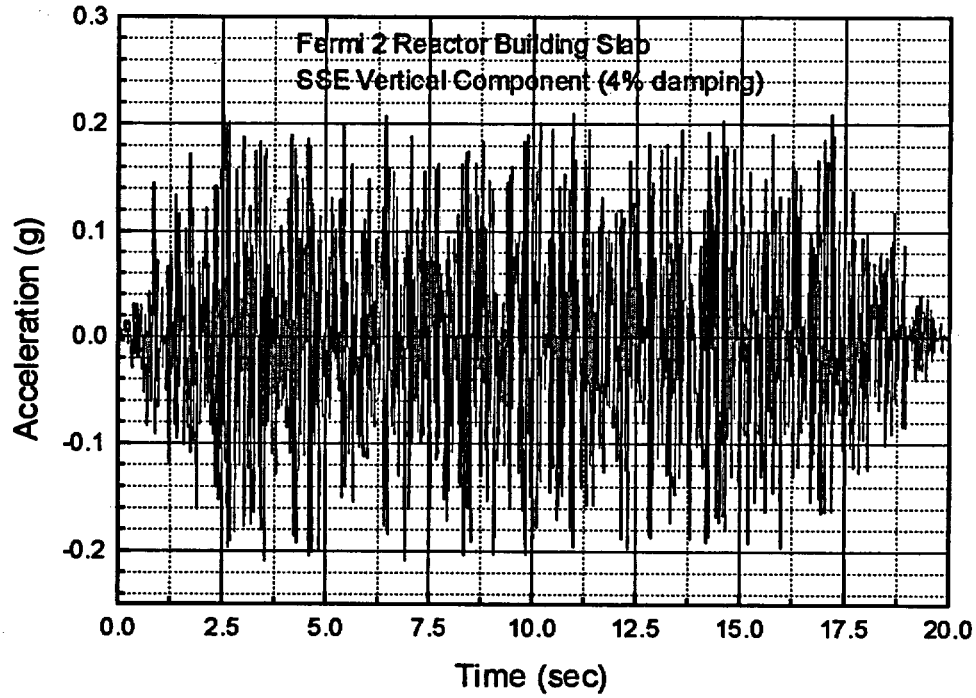

Figure 6.4.6; SSE acceleration time history in the z-direction (Vertical)

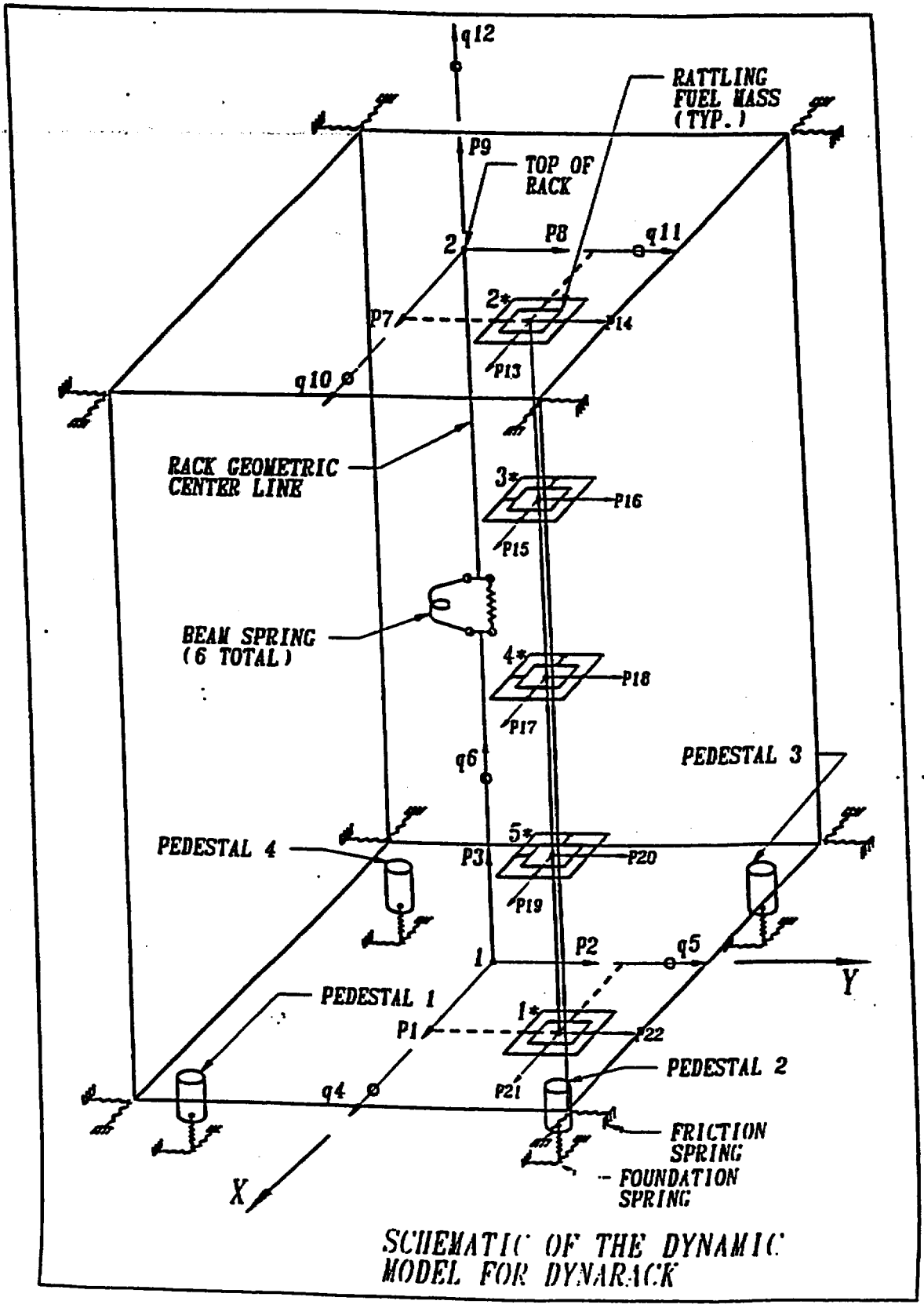
q12
RATTLING FUEL MASS (TYP.)
P9
TOP OF RACK
2
P8
q11
2*
P7
P14
P13
q10
RACK GEOMETRIC CENTER LINE
3*
P16
P15
BEAM SPRING (6 TOTAL)
4*
P18
P17
q6
PEDESTAL 3
PEDESTAL 4
5*
P3
P20
P19
1
P2
q5
Y
PEDESTAL 1
1*
P1
P22
PEDESTAL 2
q4
P21
FRICTION SPRING
FOUNDATION SPRING
X
SCHEMATIC OF THE DYNAMIC MODEL FOR DYNARACK

Figure 6.5.1

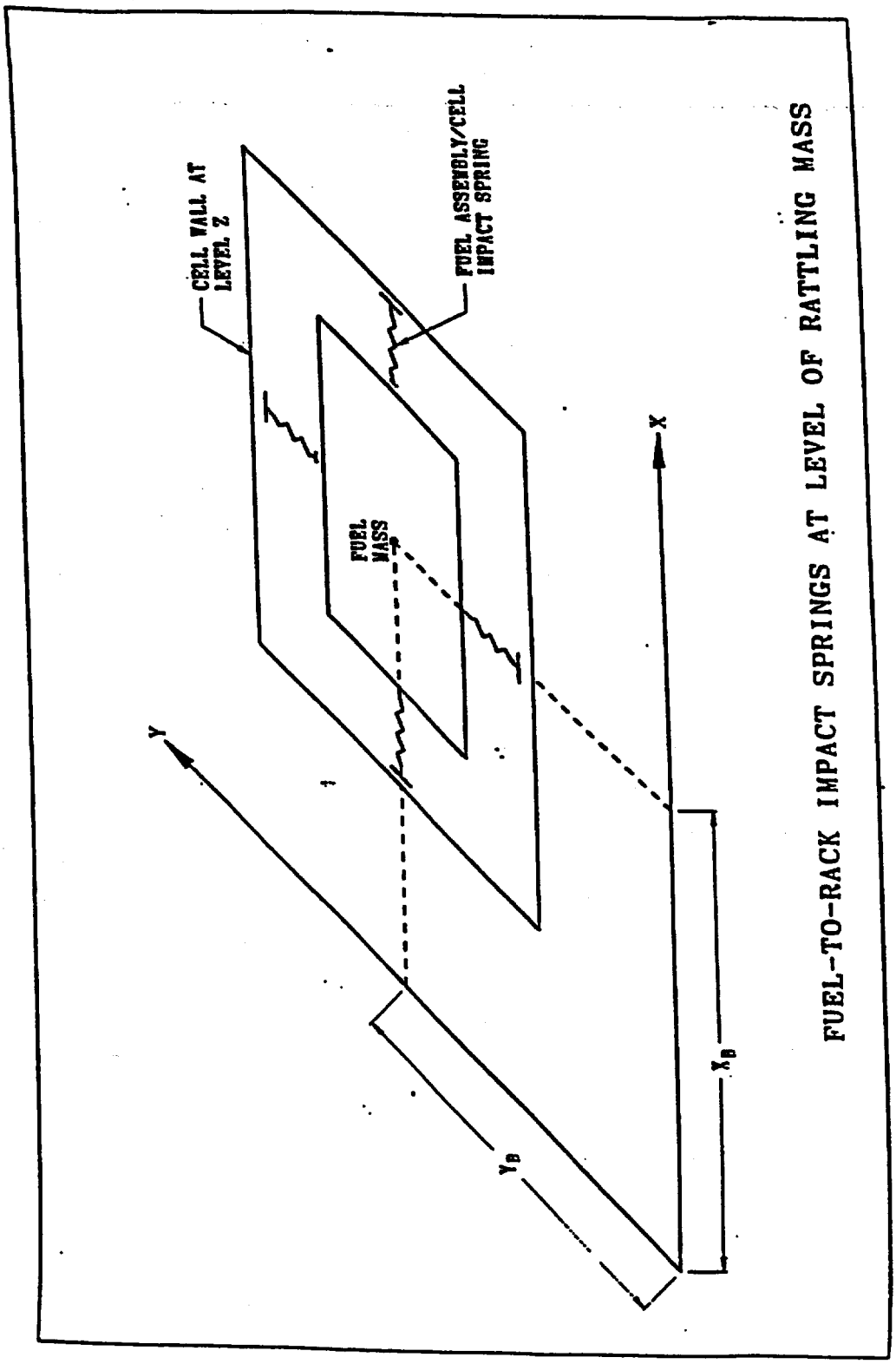
FUEL-TO-RACK IMPACT SPRINGS AT LEVEL OF RATTLING MASS
CELL WALL AT LEVEL Z
FUEL ASSEMBLY/CELL IMPACT SPRING
FUEL MASS
X
Y
X_B
Y_B

Figure 6.5.2

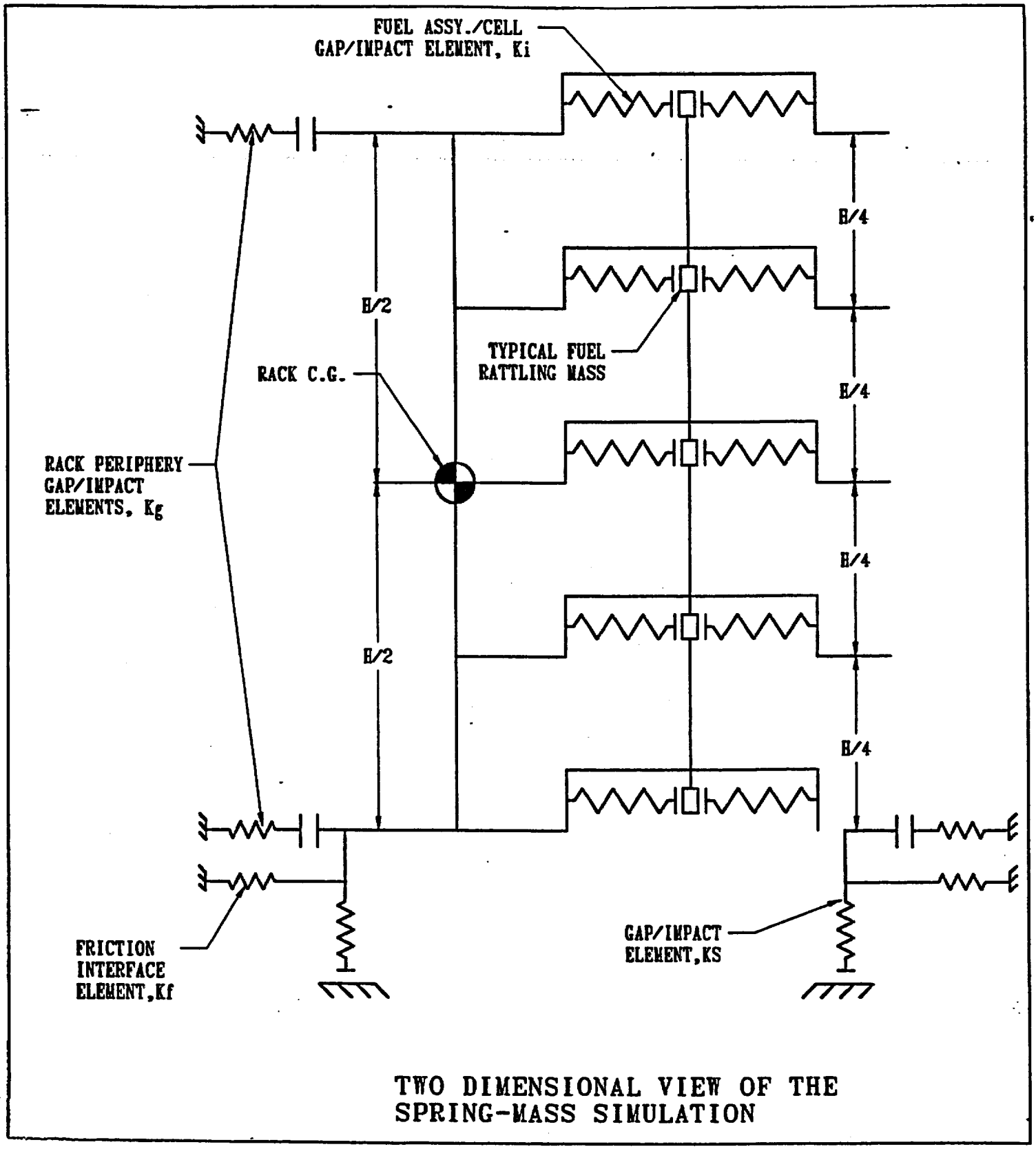
FUEL ASSY./CELL
GAP/IMPACT ELEMENT, Ki
H/4
H/2
TYPICAL FUEL
RATTLING MASS
RACK C.G.
H/4
RACK PERIPHERY
GAP/IMPACT
ELEMENTS, Kg
H/4
H/2
H/4
FRICTION
INTERFACE
ELEMENT,Kf
GAP/IMPACT
ELEMENT,KS
TWO DIMENSIONAL VIEW OF THE
SPRING-MASS SIMULATION

Figure 6.5.3

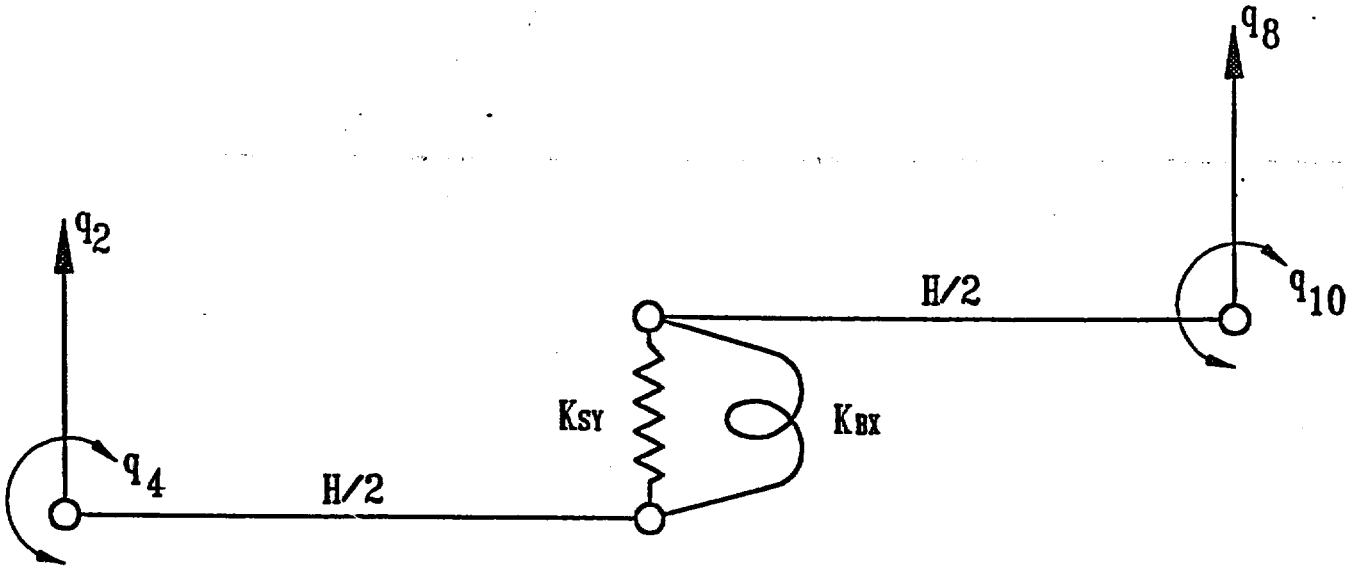

RACK DEGREES-OF-FREEDOM FOR Y-Z PLANE BENDING WITH SHEAR AND BENDING SPRING

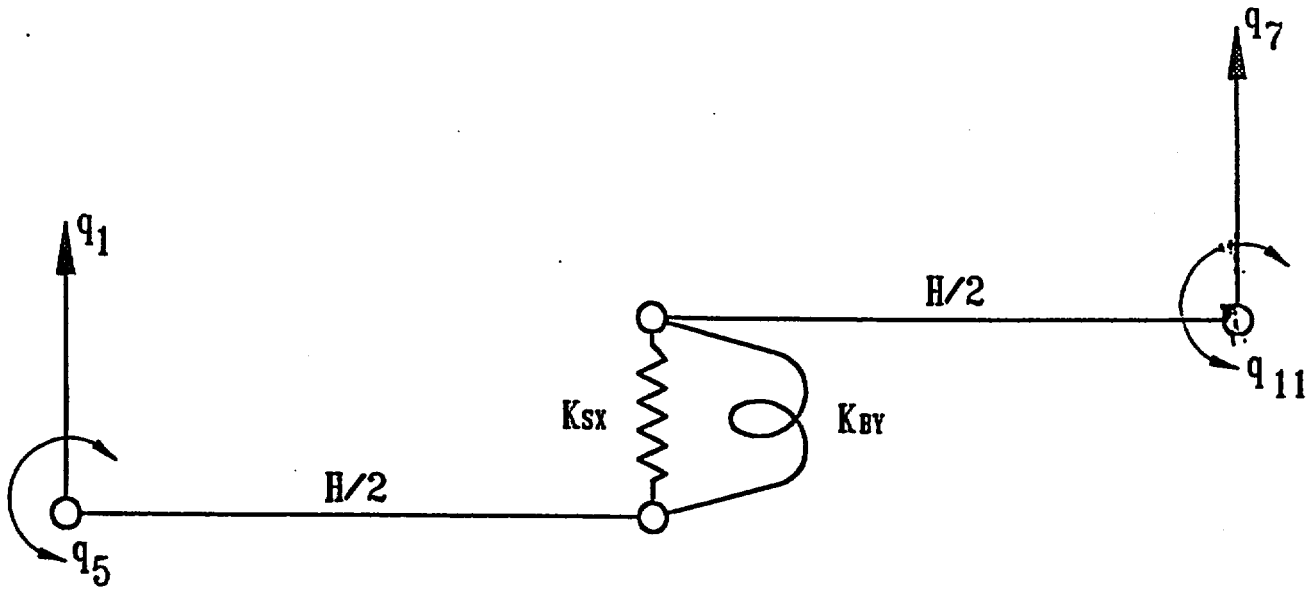

RACK DEGREES-OF-FREEDOM FOR X-Z PLANE BENDING WITH SHEAR AND BENDING SPRING

Figure 6.5.4

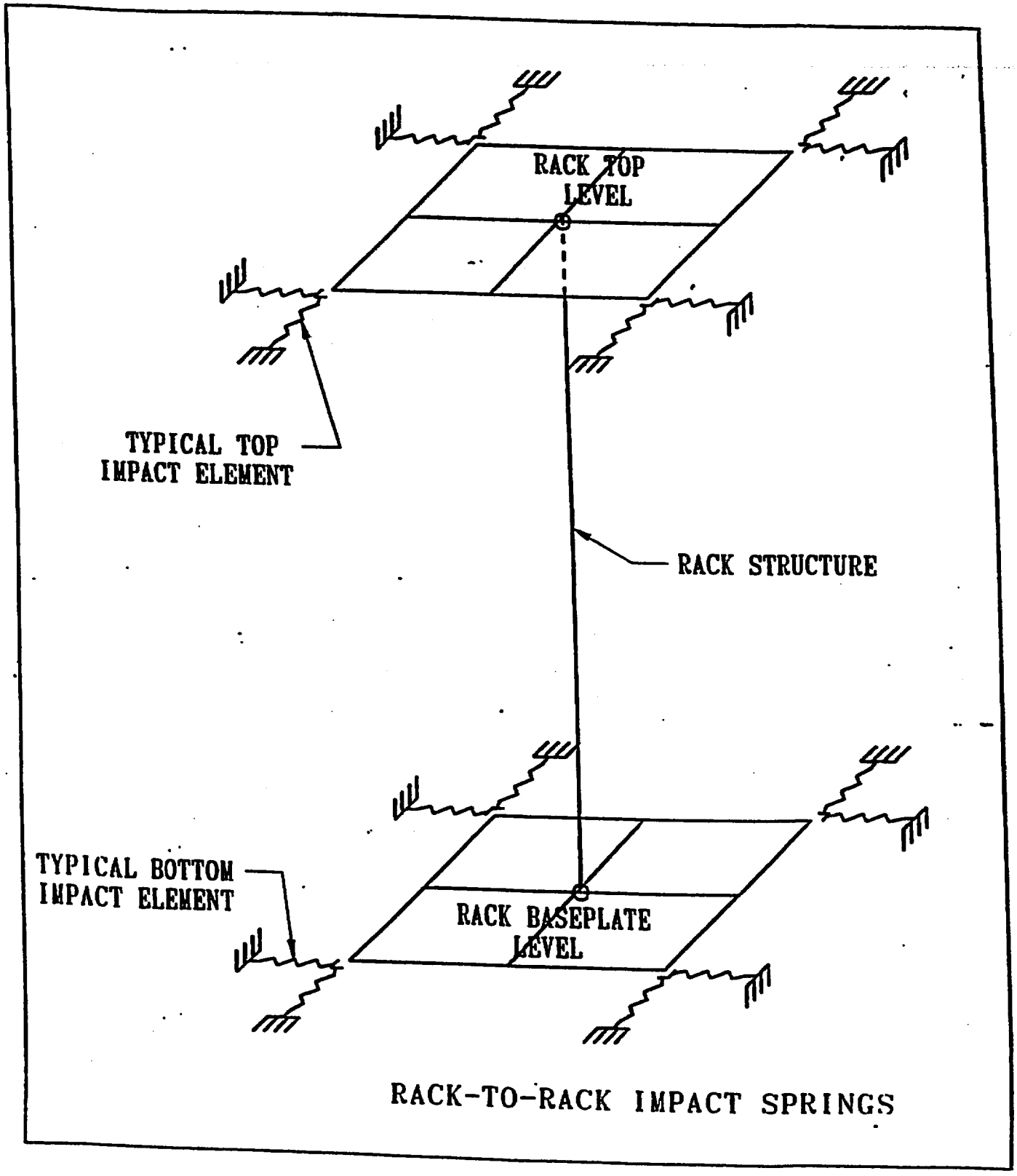
RACK TOP
LEVEL
TYPICAL TOP
IMPACT ELEMENT
RACK STRUCTURE
TYPICAL BOTTOM
IMPACT ELEMENT
RACK BASEPLATE
LEVEL
RACK-TO-RACK IMPACT SPRINGS

Figure 6.5.5

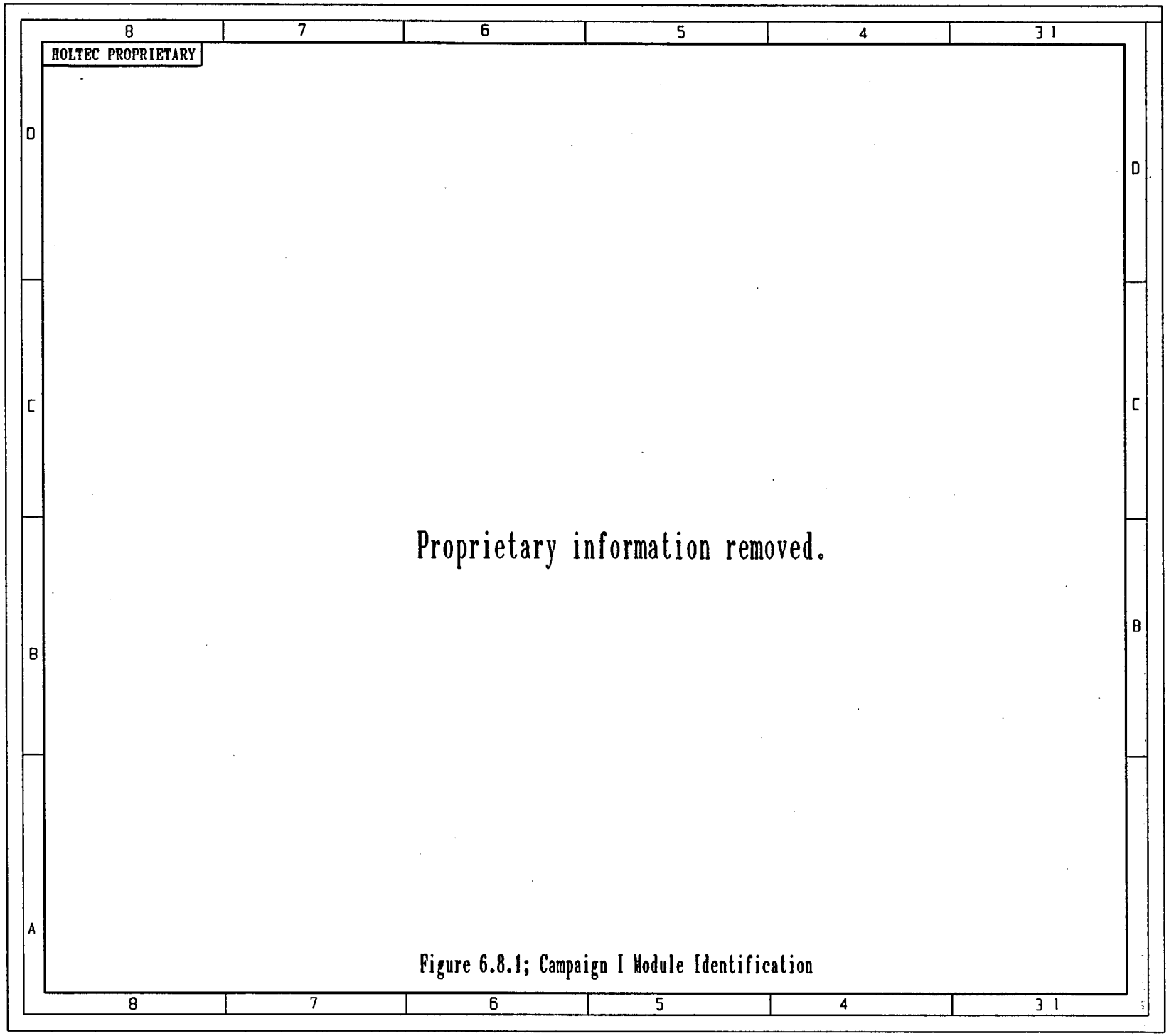

Figure 6.8.1; Campaign I Module Identification

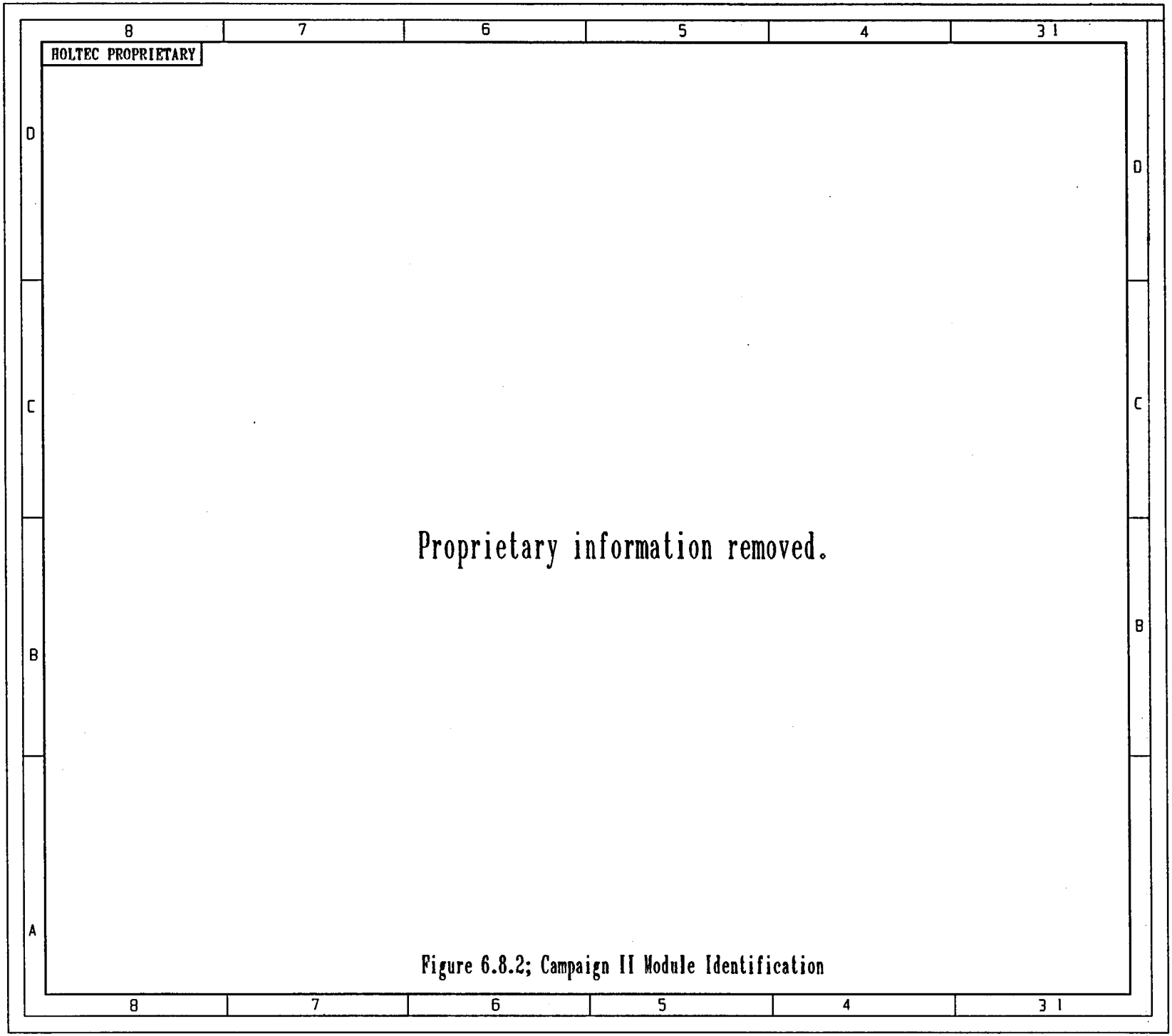

Figure 6.8.2; Campaign II Module Identification

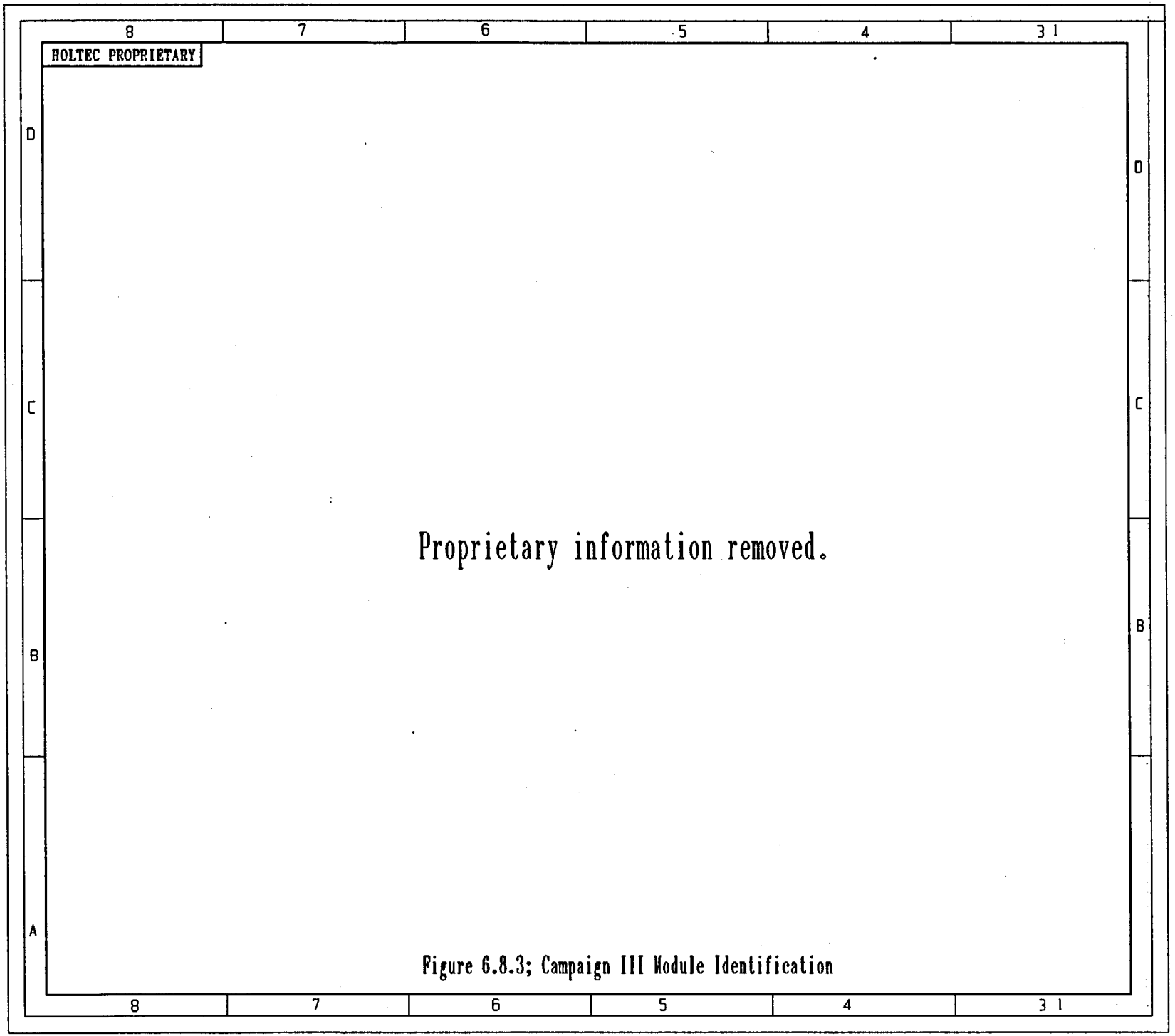

Figure 6.8.3; Campaign III Module Identification

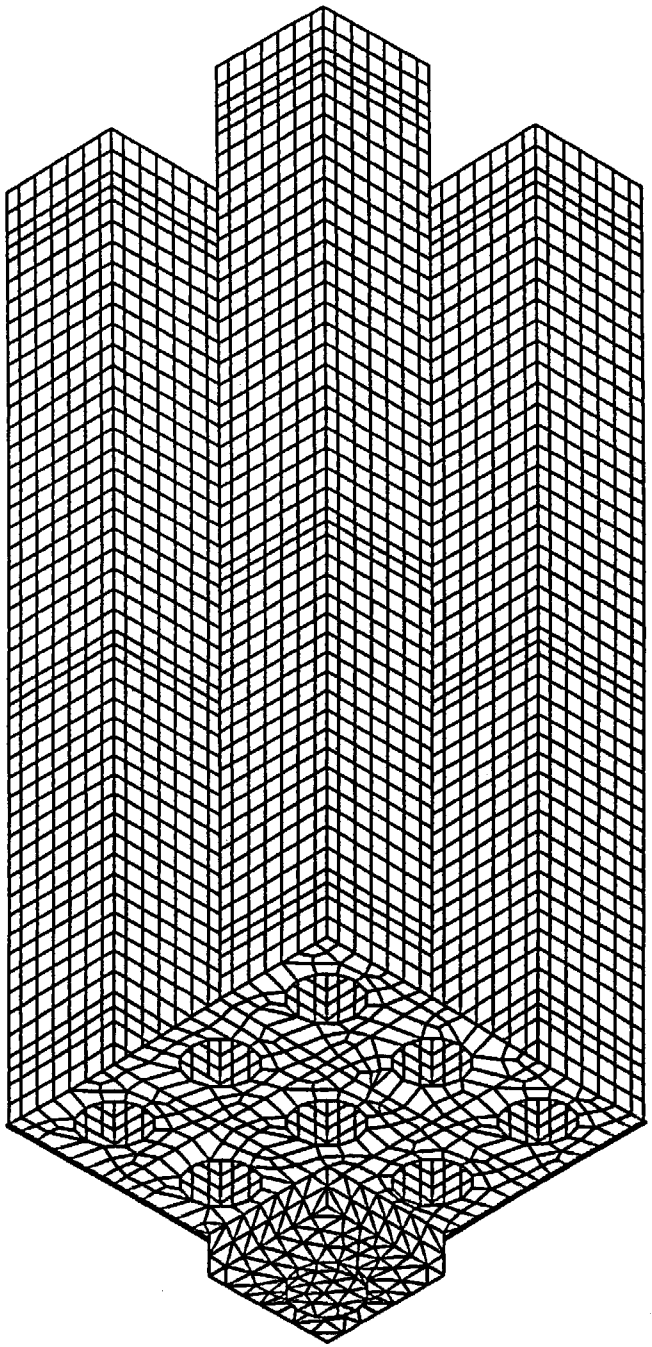

Figure 6.10.1; Rack Fatigue Model

7.0 MECHANICAL ACCIDENTS

7.1 Introduction

The USNRC OT position paper [7.1.1] specifies that the design of the rack must ensure the functional integrity of the spent fuel racks under all credible fuel assembly drop events.

This chapter contains synopses of the analyses carried out to demonstrate the regulatory compliance of the proposed racks under postulated accidental drop events germane to the fuel pools; namely, that of a fuel assembly, a fuel rack and a gate.

7.2 Description of Mechanical Accidents

Several categories of accidental drop events are considered. Fuel drop evaluations are performed to evaluate the racks subsequent to a fuel assembly impact. The pool structure is evaluated for the drop of a fuel rack during construction. A pool gate drop is also evaluated to assess damage to the pool structure and the stored fuel assemblies in a fuel rack. The drop of an overhead platform during installation onto the top of a rack is also evaluated. Additional evaluations were also performed to consider the ability of the rack to withstand the uplift force from a stuck fuel assembly.

In the so-called "shallow" drop event, a fuel assembly, along with the portion of handling tool, which is severable in the case of a single element failure, is assumed to drop vertically and hit the top of the rack. Inasmuch as the new racks are of honeycomb construction, the deformation produced by the impact is expected to be confined to the region of collision. However, the "depth" of damage to the affected cell walls must be demonstrated to remain limited to the portion of the cell above the top of the "active fuel region", which is essentially the elevation of the top of the Boral neutron absorber. Stated in qualitative terms, this criterion implies that the plastic deformation of the rack cell walls should not extend more than 19 inches (downwards) from the top. In order to utilize an upper bound of kinetic energy at impact, the impactor is assumed to weigh 1,600 lbs and the free-fall height is assumed to be 40 inches.

It is readily apparent from the description of the rack modules in Section 3 that the impact resistance of a rack at its periphery is considerably less than its interior. Accordingly, the limiting shallow drop scenario, which would produce maximum cell wall deformation, consists of the case where the fuel assembly impacts the peripheral cell wall, as shown in Figure 7.2.1.

The second class of fuel drop event postulates that the impactor falls through an empty storage cell impacting the fuel assembly support surface (i.e., rack baseplate). This so-called "deep" drop event threatens the structural integrity of the baseplate. If the baseplate is pierced, and fuel assembly impacts the pool liner, then an abnormal condition of the enriched zone of fuel assembly outside the "poisoned" space of the fuel rack may develop. To preclude damage to the pool liner and to avoid the potential of an abnormal fuel storage configuration in the aftermath of a deep drop event, it is required that the baseplate remain unpierced and that the maximum lowering of the baseplate is shown to be acceptable by the criticality evaluations.

The deep drop event can be classified into two scenarios, namely, drop in an interior cell away from the support pedestal, as shown in Figure 7.2.2, and drop through cell located above a support leg, as shown in Figure 7.2.3. In deep drop scenario 1, the fuel assembly impacts the baseplate away from the support pedestal, where it is more flexible. Severing or large deflection of the baseplate leading to a secondary impact with the pool liner are unacceptable results. In deep drop scenario 2, the baseplate is buttressed by the support pedestal and presents a hardened impact surface, resulting in a high load. The principal design objective is to ensure that the support pedestal does not tear the liner that overlays the reinforced concrete pool slab.

In the third type of drop event, a rack is assumed to drop from the top water level in the pool and hits the liner plate, as shown in Figure 7.2.4. The heaviest rack in the pool, Module B with 19×19 cells, is used for the rack drop analysis. The structural integrity of the concrete floor must be demonstrated to be maintained in the rack drop event and the effect on the liner plate is also evaluated. The acceptance criterion is that catastrophic pool structure damage, such that there is rapid loss of pool water inventory, is not allowed.

A gate is assumed to drop from 17.75 feet above the pool floor in the fourth type of drop accident. The heaviest gate, Gate A (4.3 tons), is conservatively considered in the analysis as it has considerably greater kinetic energy than the other gate (Gate B weighed 2.5 tons). Two gate drop scenarios are identified. In gate drop scenario 1, as shown in Figure 7.2.5, the gate is postulated to fall all the way to the pool floor and impact the liner plate and the concrete slab. Local puncture of the liner plate and local crushing of the concrete slab are allowed in this postulated accident. However, the impact should not lead to primary damage to the pool slab. In gate drop scenario 2, the gate is assumed to be dropped over a rack containing stored fuel assemblies. To conservatively estimate the damage of fuel rods, the gate is assumed to directly hit fuel assemblies by neglecting the cell wall supports that are shown in Figure 7.2.6. In this case, the damaged fuel rods must not occur in more than two fuel assemblies. The drop of the heaviest (1460 pounds) overhead platform onto the top of a storage rack during installation is also considered. However, a comparison of the kinetic energy developed by the 9479 pounds gate dropping onto a rack bounds the kinetic energy of the heaviest overhead platform. Therefore, the results of the gate drop evaluation bound the overhead platform

Finally, for the uplift force evaluation, a vertical force of 1200 lbf and a horizontal force of 1100 lbf are applied, individually and simultaneously, to the top of the cell wall, to ensure that the rack cell wall is able to withstand this load without deforming the rack cell such that it no longer satisfies dimensional requirements and adversely affects the subcriticality of stored fuel array. The acceptance criterion for this evaluation is that local cell wall stress shall remain below the yield point.

7.3 Incident Impact Velocity

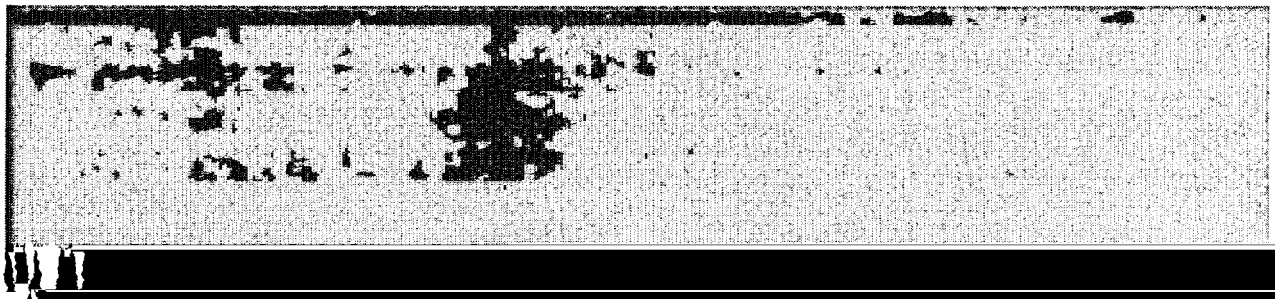

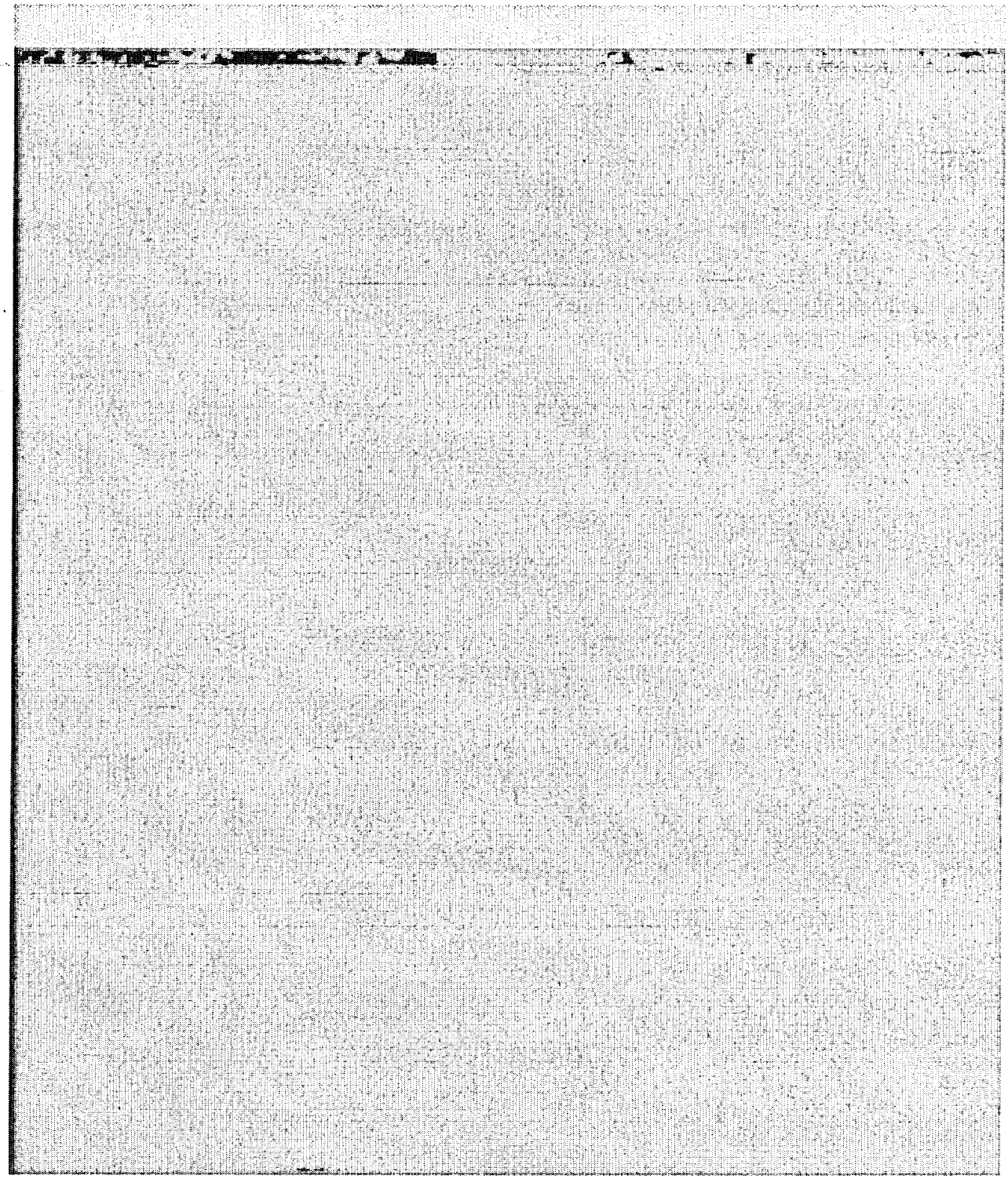

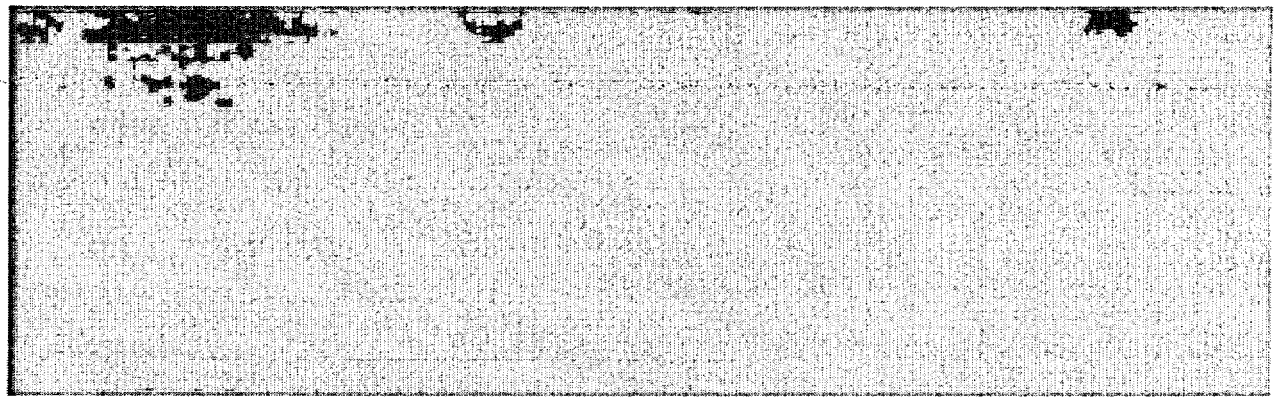

7.4 Mathematical Model

In the first step of the solution process, the velocity of the dropped object (impactor) is computed for the condition of underwater free fall in the manner of the formulation presented in the above section. Table 7.4.1 contains the computed velocities for the various drop events.

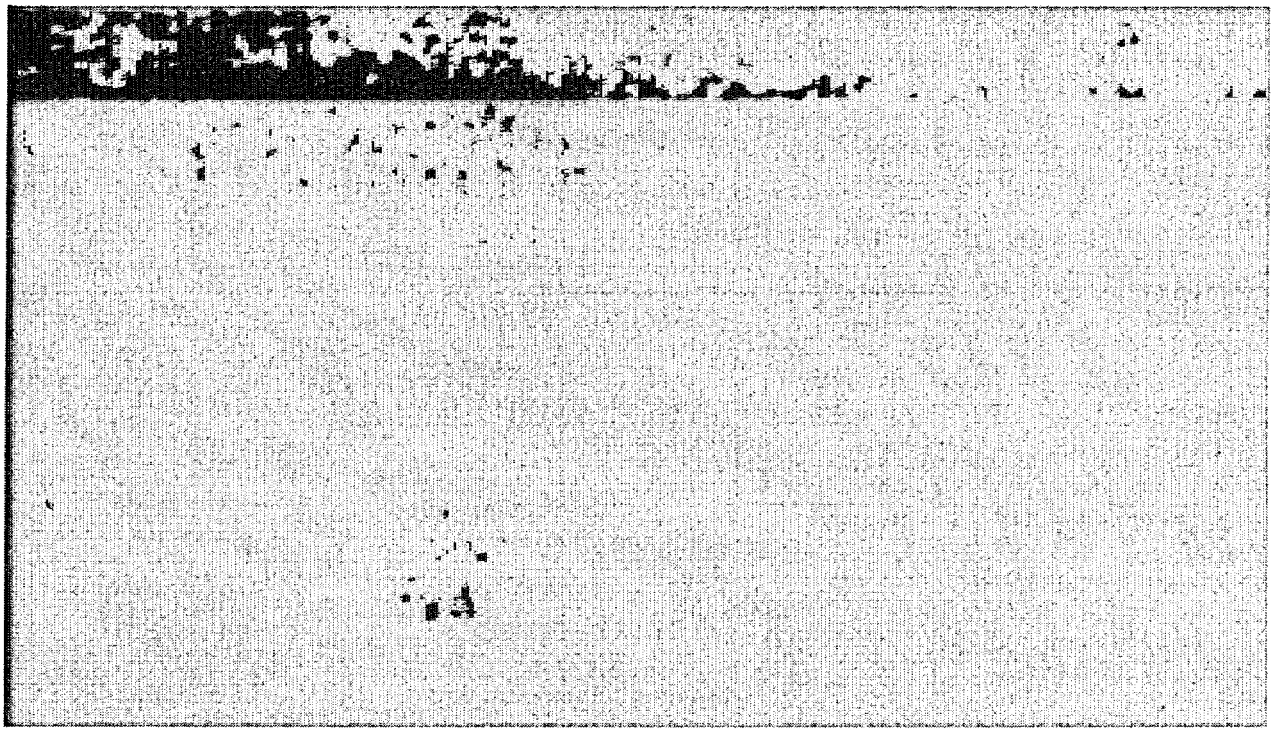

7.5 Results

7.5.1 Shallow Drop Event

For the shallow drop event, the dynamic analysis shows that the top of the impacted region undergoes localized plastic deformation. Figure 7.5.1 shows an isometric view of the post-impact geometry of the rack. The maximum depth of plastic deformation is limited to 14 inches, which is below the design limit of 19 inches.

7.5.2 Deep Drop Events

The deep drop through an exterior cell does produce some deformation of the baseplate and localized severing of the baseplate/cell wall welds. Figure 7.5.2 shows the deformed baseplate configuration. However, the fuel assembly support surface is lowered by a maximum of 1.37 inches, which is much less than the distance of 5.5 inches from the baseplate to the liner. Therefore, the pool liner will not be contacted by the deformed baseplate. The deformation of the baseplate has been determined to be acceptable with respect to lowering the fuel seating position and the resulting criticality consequences, as discussed in Chapter 4.0.

The deep drop event wherein the impact region is located above the support pedestal is found to produce a maximum stress of 25 ksi, which is less than the failure limit stress of 71 ksi for the liner, as shown in Figure 7.5.3. However, the maximum compressive stress of 8.3 ksi in the concrete slab is larger than the concrete compressive strength of 5.9 ksi, as shown in Figure 7.5.4. The concrete is locally crushed, but substantial damage to the pool slab is not indicated. Therefore, there will be no abrupt loss of water from the fuel pool.

7.5.3 Rack Drop Event

The liner plate experiences a maximum stress of 46,764 psi in the heaviest rack drop accident, as shown in Figure 7.5.5, indicating that the liner will yield, but not fail. Moreover, the maximum compressive stress in the concrete slab is shown to be 36,758 psi in Figure 7.5.6, which is higher than the concrete compressive strength of 5,900 psi. However, the stress contour plot shows that

the rack drop accident would crush the concrete only locally. Analyses on the integrity of the pool slab indicate that a primary failure in the spent fuel pool structure will not occur.

7.5.4 Gate Drop Events

Figure 7.5.7 shows the deformed shape of the pool liner plate after the gate drops onto the pool floor. The liner plate is ruptured locally at the location of the impact. Figure 7.5.8 provides the contour plot of the compressive stress in the concrete slab. The maximum stress in the concrete is higher than the concrete compressive strength. However, the damage is limited to the vicinity of the leak chase boundaries.

For the second scenario of postulated gate drop, the gate may impact up to twelve stored fuel assemblies based on the gate's width and the rack cell size. Therefore, a series of simulations involving different number of stored fuel assemblies in the accident has been performed. The result of this analysis indicates that the fuel rod rupture from the gate impact is limited to no more than 81 fuel rods, which is less than the structural consequences from the previously analyzed design basis accident resulting in 140 ruptured rods. It should be noted that the obtained result is conservative because the rack cell walls are not modeled in the analysis, which otherwise could provide additional supports to the impacted fuel assemblies.

The radiological consequences of this drop scenario has been shown to be enveloped by the existing Fermi 2 UFSAR, Fuel Handling Accidents Analysis. The damaged fuel assemblies are not a criticality concern since the crushing of fuel rods as a result of this drop will reduce the water-to-fuel ratio and reduce reactivity. The potential local boiling of the cell resulting from this drop has been shown not to occur, as discussed in Chapter 5.0.

7.5.5 Uplift Force Evaluation

The uplift force evaluation shows that the rack is able to withstand the vertical uplift force of 1200 pounds and the horizontal force of 1100 pounds. The evaluation determines that the damaged region caused by these forces extends no greater than 1.30 inches down the cell wall,

which is well above the top edge of the neutron absorber material (active fuel region). For the load applied vertically anywhere along a cell wall, the resultant stress is only 2,653 psi, which is well below the yield stress of the material.

7.6 Conclusion

The drop accident events postulated for the Fermi 2 fuel pools were analyzed and found to produce localized damage well within the design limits for the racks. The shallow drop event is found to produce some localized plastic deformation in the top of the storage cell, but the region of permanent strain is limited to the portion of the rack structure situated above the top of the active fuel region. The analysis of the deep drop event at cell locations selected to maximize baseplate deformation indicates that the downward displacement of the baseplate is limited to 1.37 inches, which ensures that a secondary impact of the fuel assembly with the pool liner would not occur. The deep drop case analyzed for the scenario to produce maximum pedestal force indicates that the pedestal axial load is sufficiently small to preclude liner damage. Rack drop analysis (in a construction accident scenario) shows that the concrete slab can maintain its structural integrity under the postulated impact of the heaviest rack in the pool. Only local concrete crushing is observed. Finally, the analysis of the gate drop events indicates that the drop of the heaviest gate onto the pool liner may locally rupture the liner but no primary damage to the pool slab will occur. For the gate drop onto the top of fuel assemblies, the fuel rod damage is bounded by the existing Fermi 2 UFSAR, Fuel Handling Analysis. The rack uplift force evaluation shows that configuration of the fuel and poison (Boral) is not compromised from the configurations analyzed in the criticality evaluations discussed in Section 4.0. It is therefore concluded that the new Holtec high-density spent fuel racks for the Fermi 2 pool possess acceptable margins of safety under the postulated mechanical accidents.

7.7 References for Chapter 7

[7.1.1] "OT Position for Review and Acceptance of Spent Fuel Storage and Handling Applications," dated April 14, 1978, and addendum dated 1979.

[7.1.2] Design Specification No. 3071-548, Detroit Edison Company, Revision 0.

[7.4.1] NUREG/CR-6608, "Summary and Evaluation of Low-Velocity Impact Tests of Solid Steel Billet Onto Concrete Pads", dated February 1998.

Table 7.4.1

IMPACT EVENT DATA

Case	Impactor Weight (lb)	Impactor Type	Drop Height (in)	Impact Velocity (in/sec)
1. Shallow drop event	1,600	Fuel assembly assemblage	40	159.8
2. Deep drop event scenario 1 (away from pedestal)	1,600	Fuel assembly assemblage	215	333.9
3. Deep drop event scenario 2 (above pedestal)	1,600	Fuel assembly assemblage	215	296.4
4. Rack drop event	37,905	Rack B	480	228.4
5. Gate drop event scenario 1 (to pool floor)	9,480	Gate A	213	335.6
6. Gate drop event scenario 2 (above rack)	9,480	Gate A	30	133.3

Table 7.4.2

MATERIAL DEFINITION

Material Name	Material Type	Density (pcf)	Elastic Modulus (psi)	Stress		Strain	
				First Yield (psi)	Failure (psi)	Elastic	Failure
Stainless Steel Rack Walls and Female Pedestal	SA240-304L	490	2.760e+07	2.130e+04	6.620e+04	7.717e-04	3.800e-01
Stainless Steel Liner	SA240-304	490	2.760e+07	2.500e+04	7.100e+04	7.717e-04	3.800e-01
Zircaloy Fuel Cladding	--	404	1.040e+07	8.05e+04	8.05e+04	1.000e-02	1.500e-02
Stainless Steel Male Pedestal	SA564-630	490	2.760e+07	1.063e+05	1.400e+05	3.851e-02	3.800e-01
Concrete †	f'_c=5,900 psi	150	3.605e+06	--	5.900e+03	--	--

† The concrete is modeled as recommended in NUREG /CR-6608 [7.4.1].

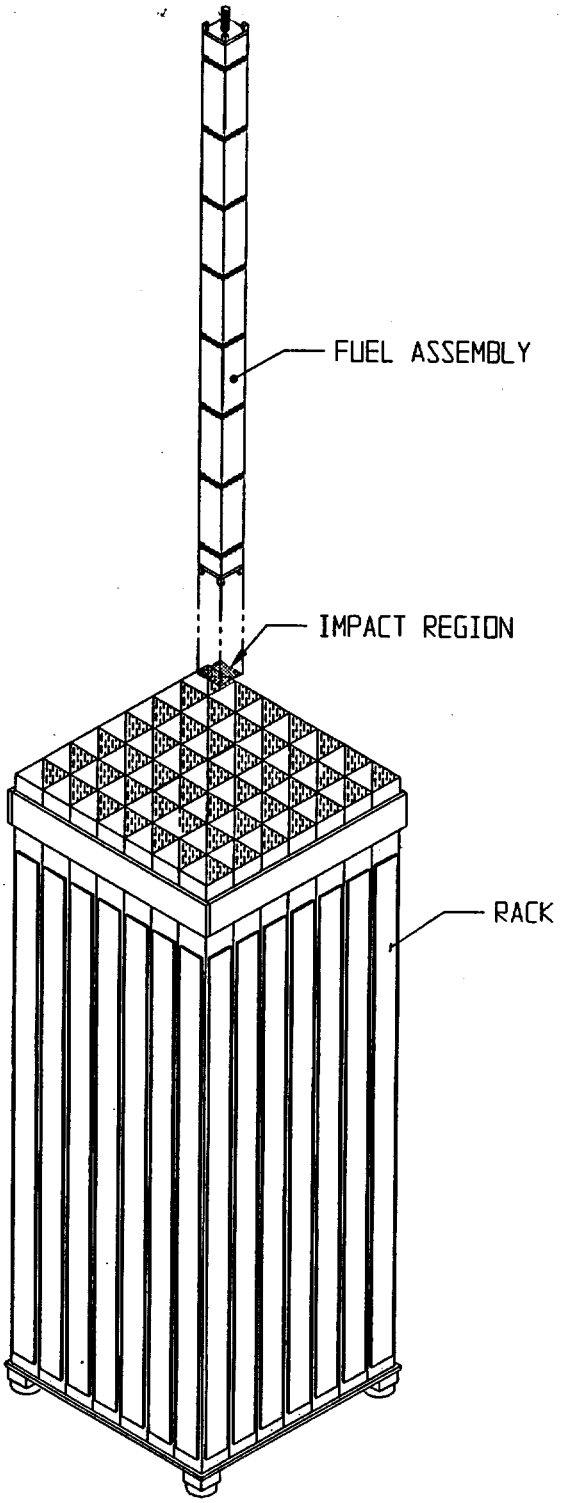

Figure 7.2.1 "Shallow" Drop on a Peripheral Cell

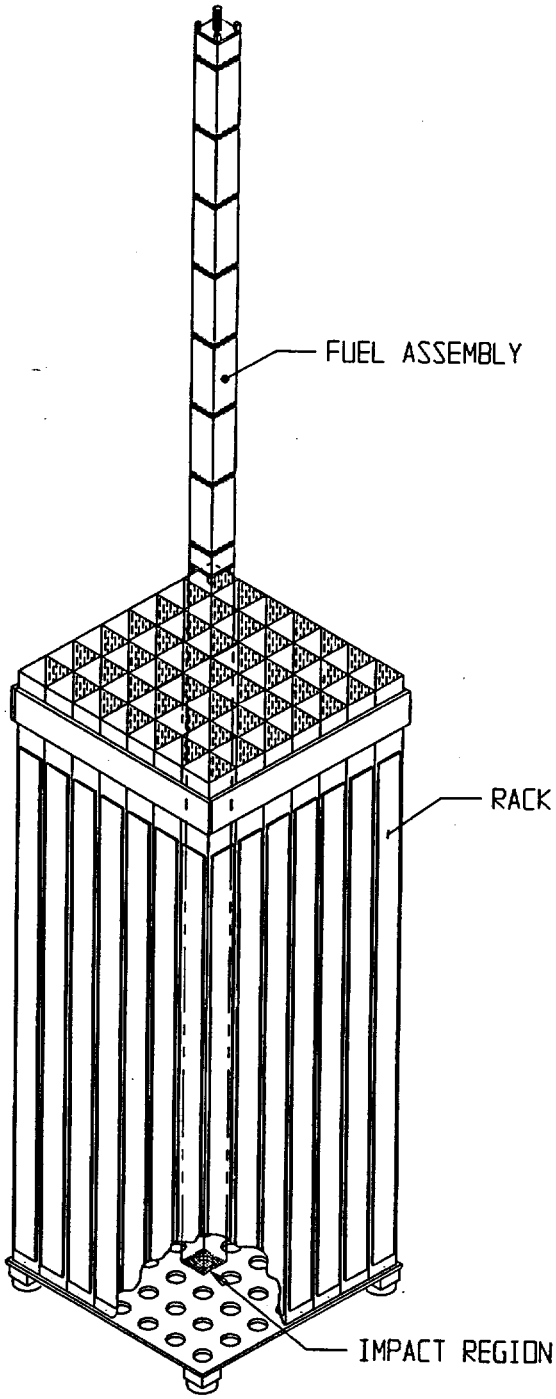

Figure 7.2.2 "Deep" Drop (Scenario 1) on a Center Cell Location

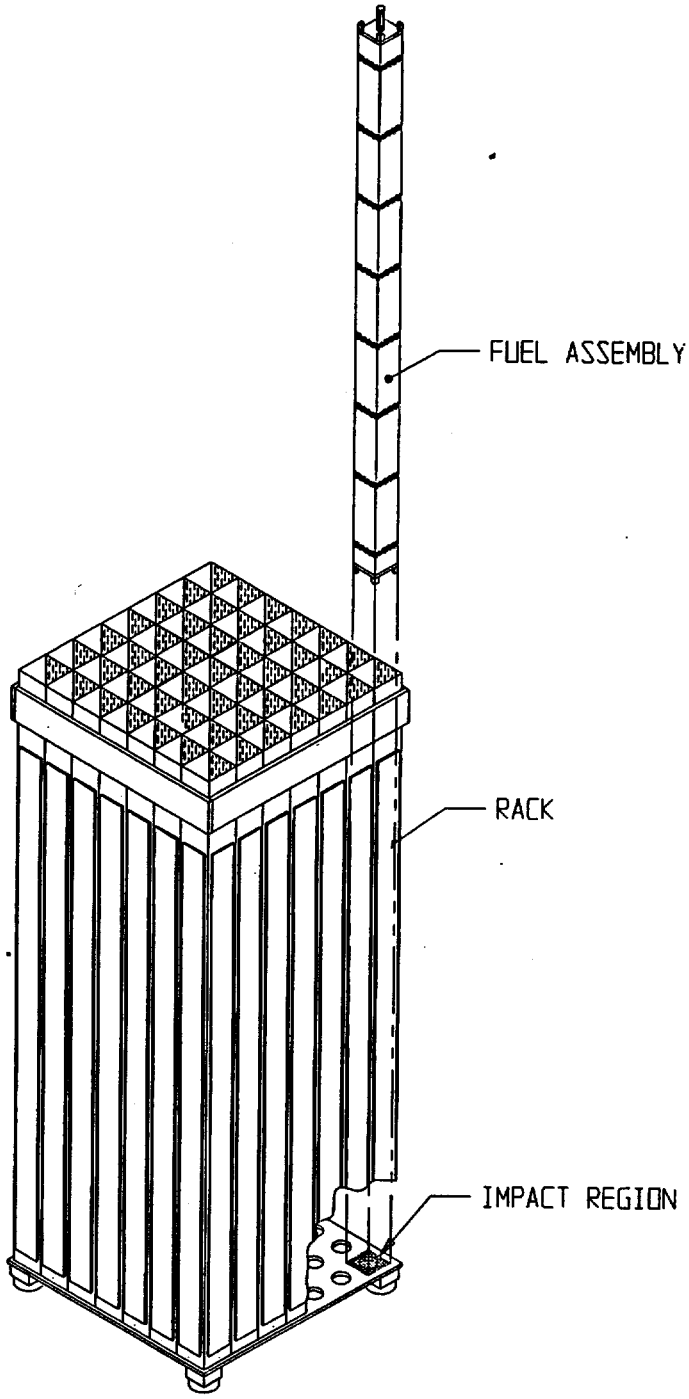

Figure 7.2.3 "Deep" Drop (Scenario 2) on a Support Leg Location

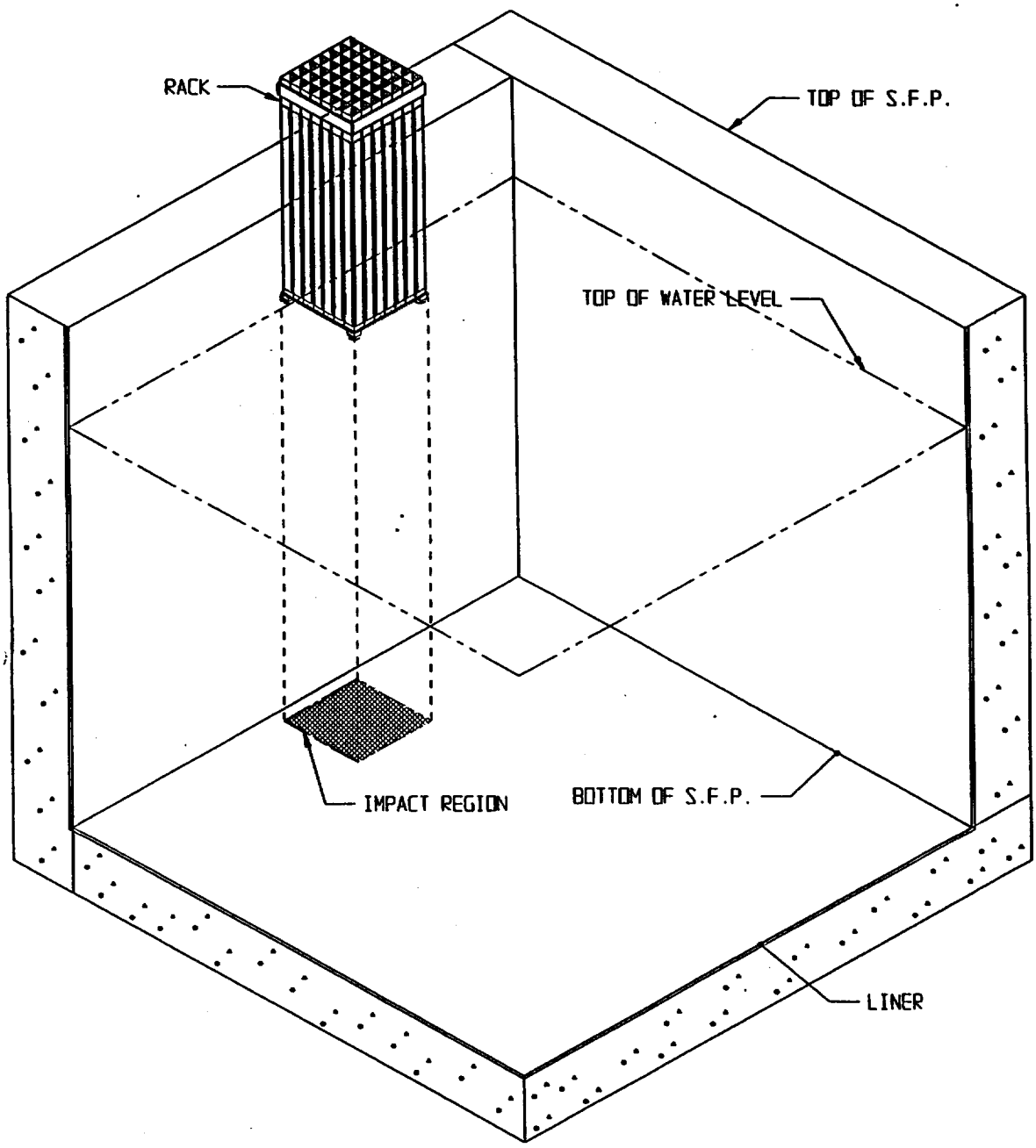

Figure 7.2.4 Rack Drop on the Pool Floor

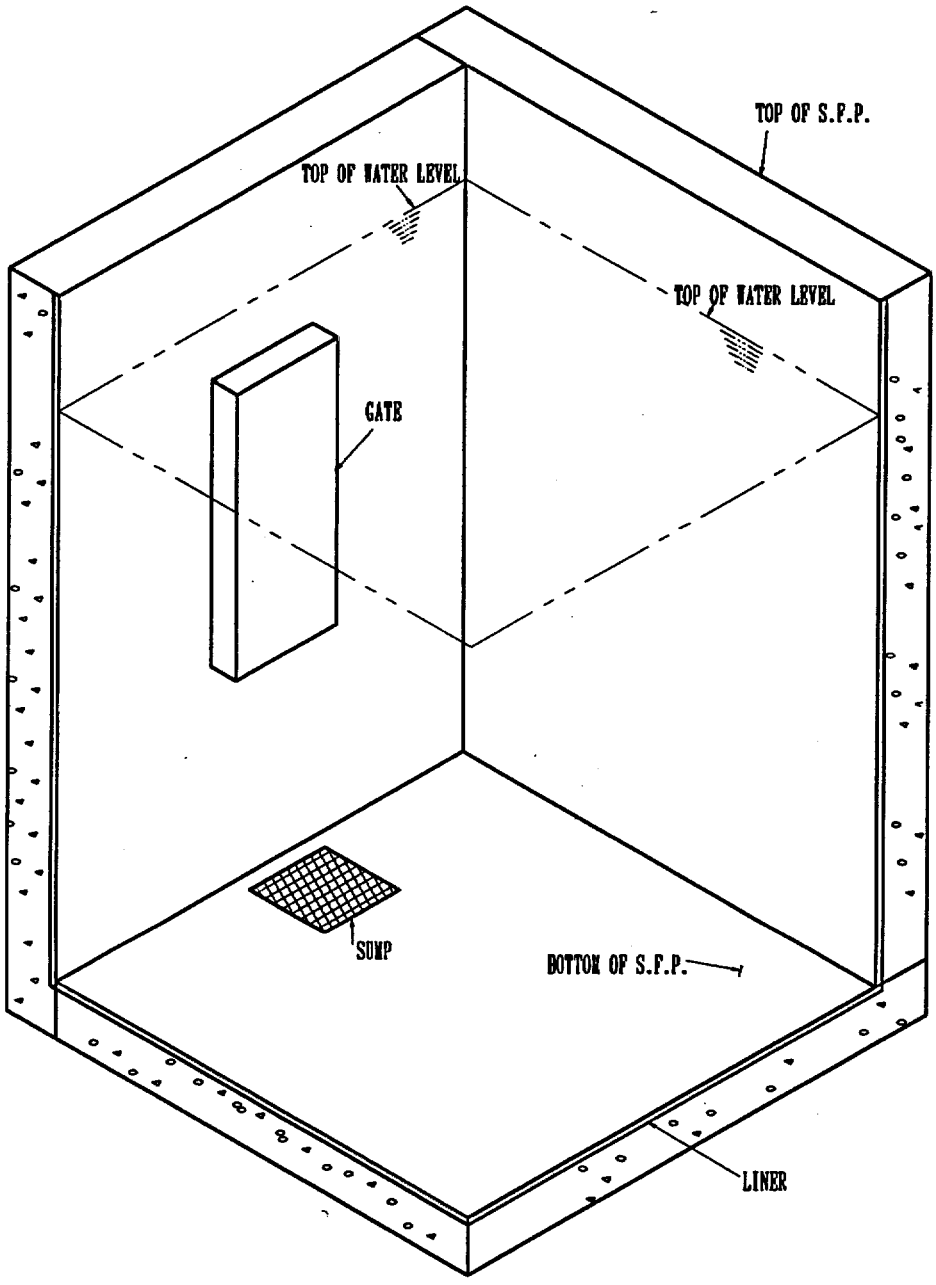

Figure 7.2.5 Gate Drop (Scenario 1) on the Pool Floor

Proprietary information removed.

Figure 7.2.6 Gate Drop Scenrio 2: BWR Fuel Assembly Schematics

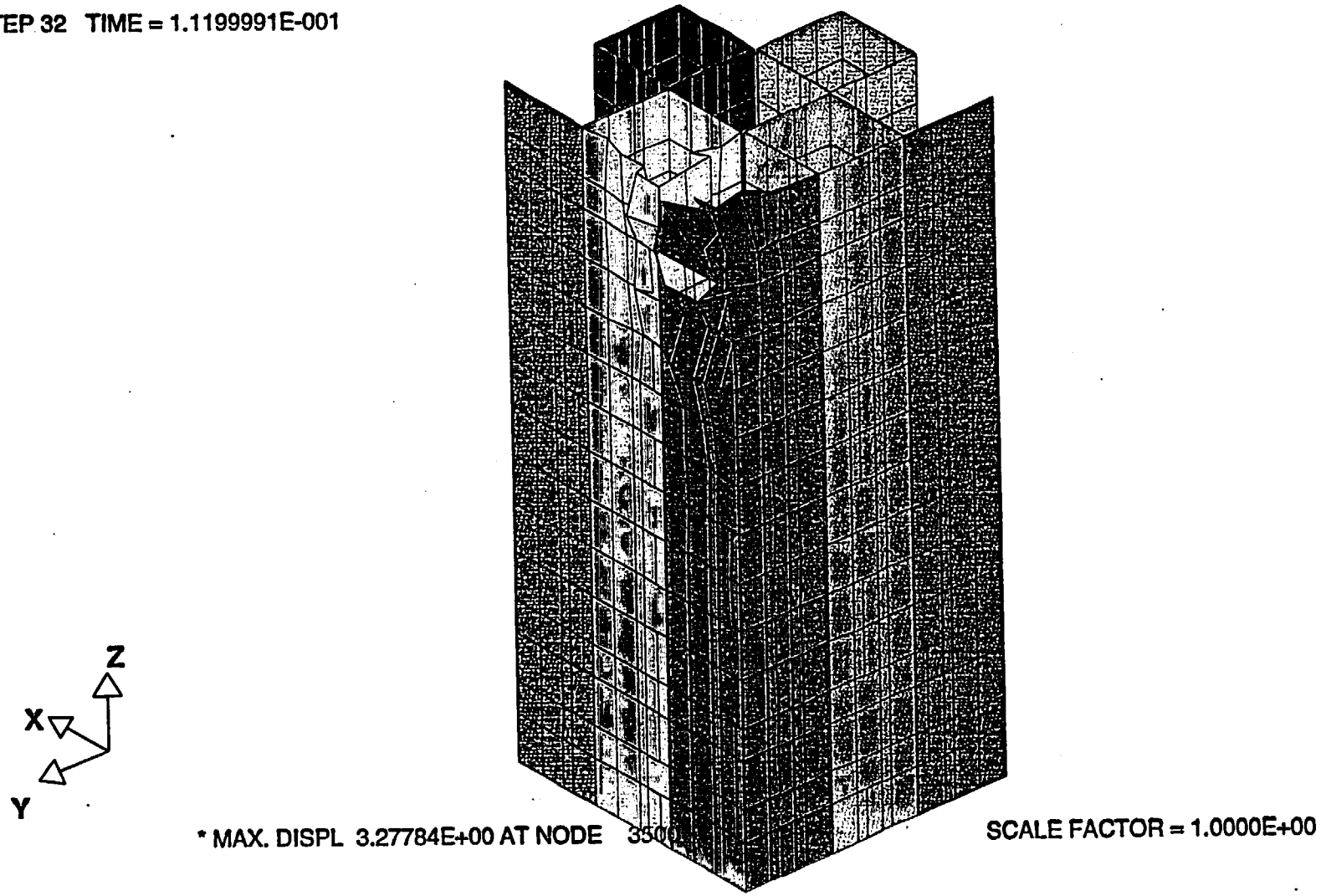

Figure 7.5.1 Maximum Cell Deformation for the "Shallow" Drop

STEP 24 TIME = 1.1999984E-002

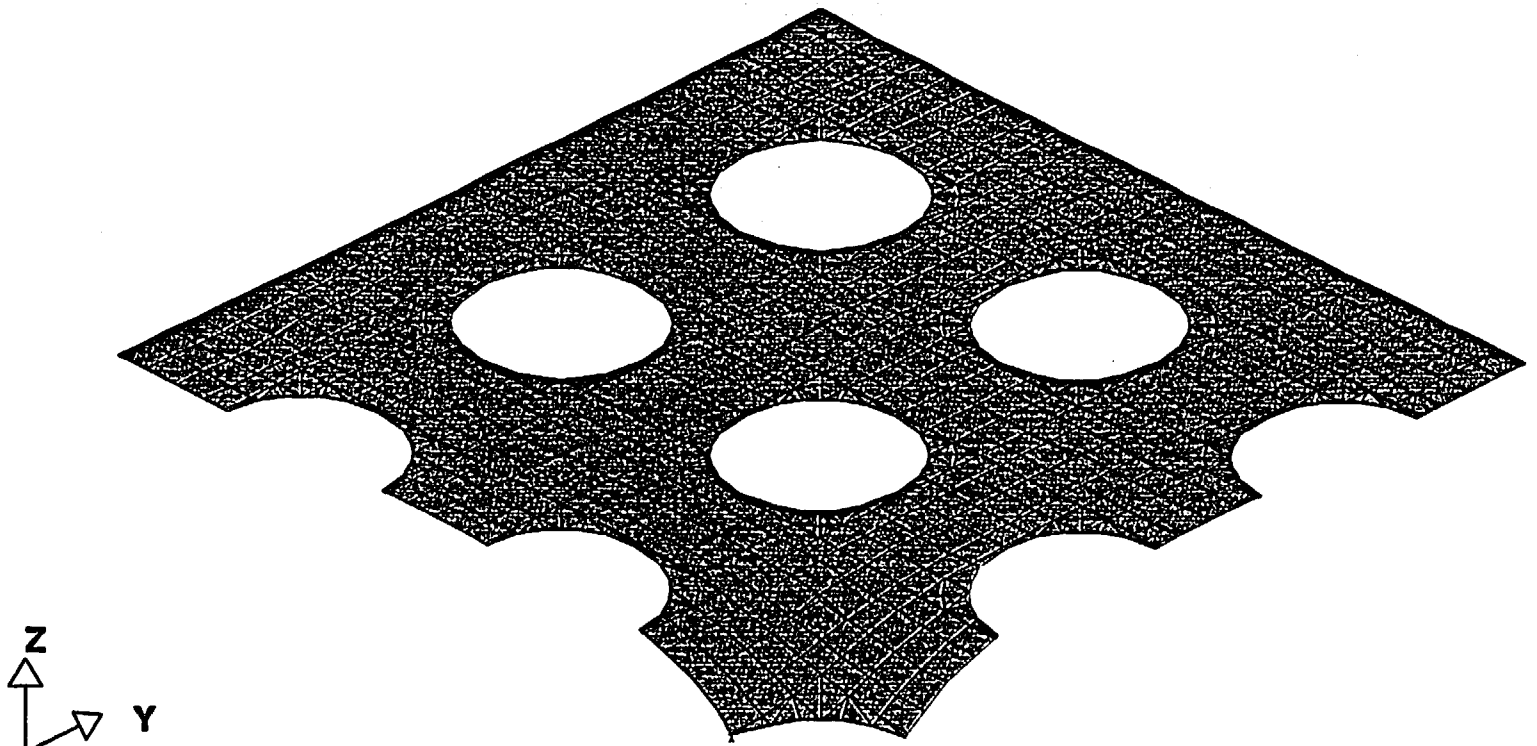

* MAX. DISPL 1.36651E+00 AT NODE 4627

SCALE FACTOR = 1.0000E+00

Figure 7.5.2 Maximum Deformation of the Base Plate for "Deep" Drop Scenario 1

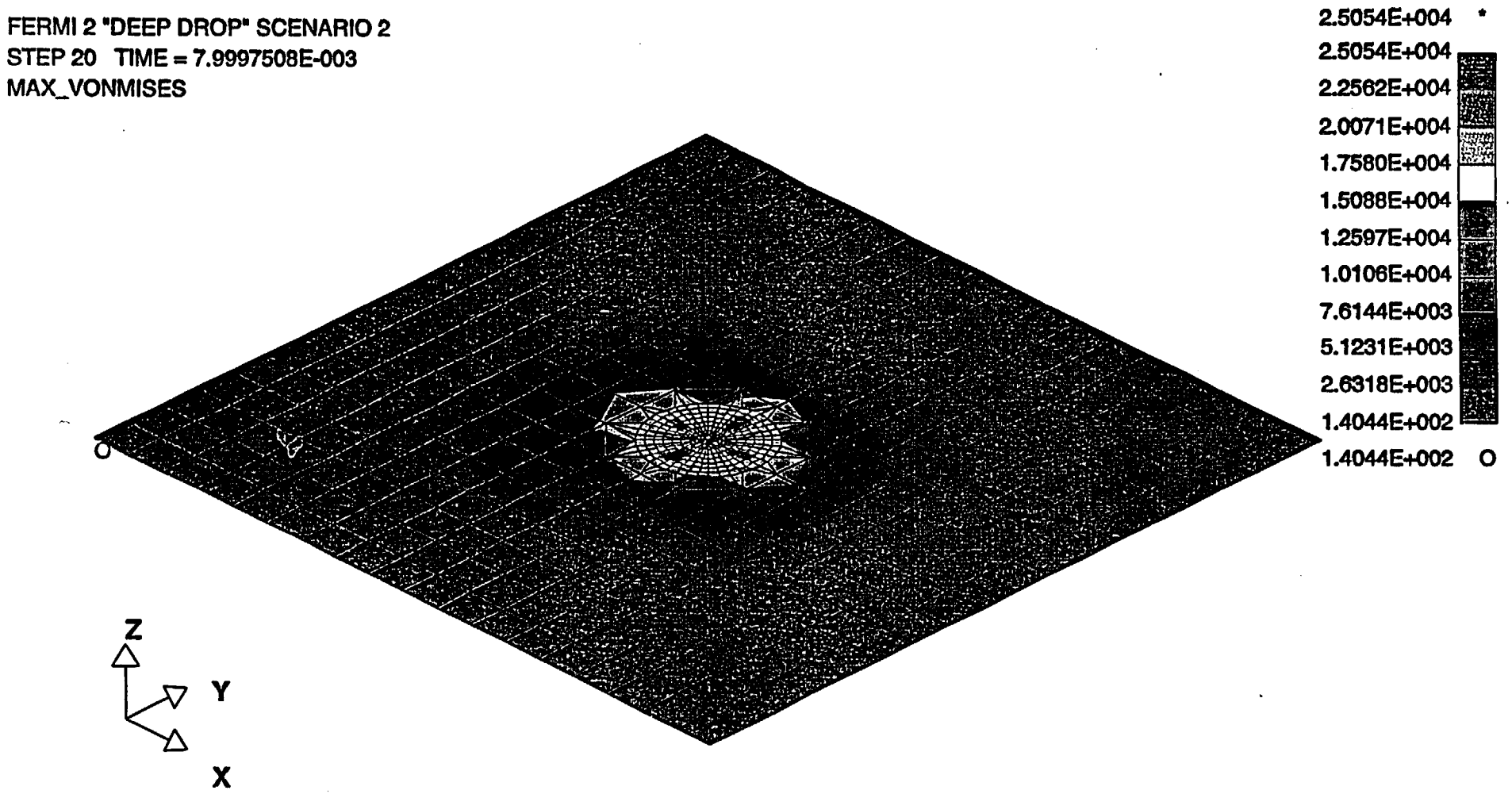

Figure 7.5.3 Maximum Von Mises Stress of the Liner for "Deep" Drop Scenario 2

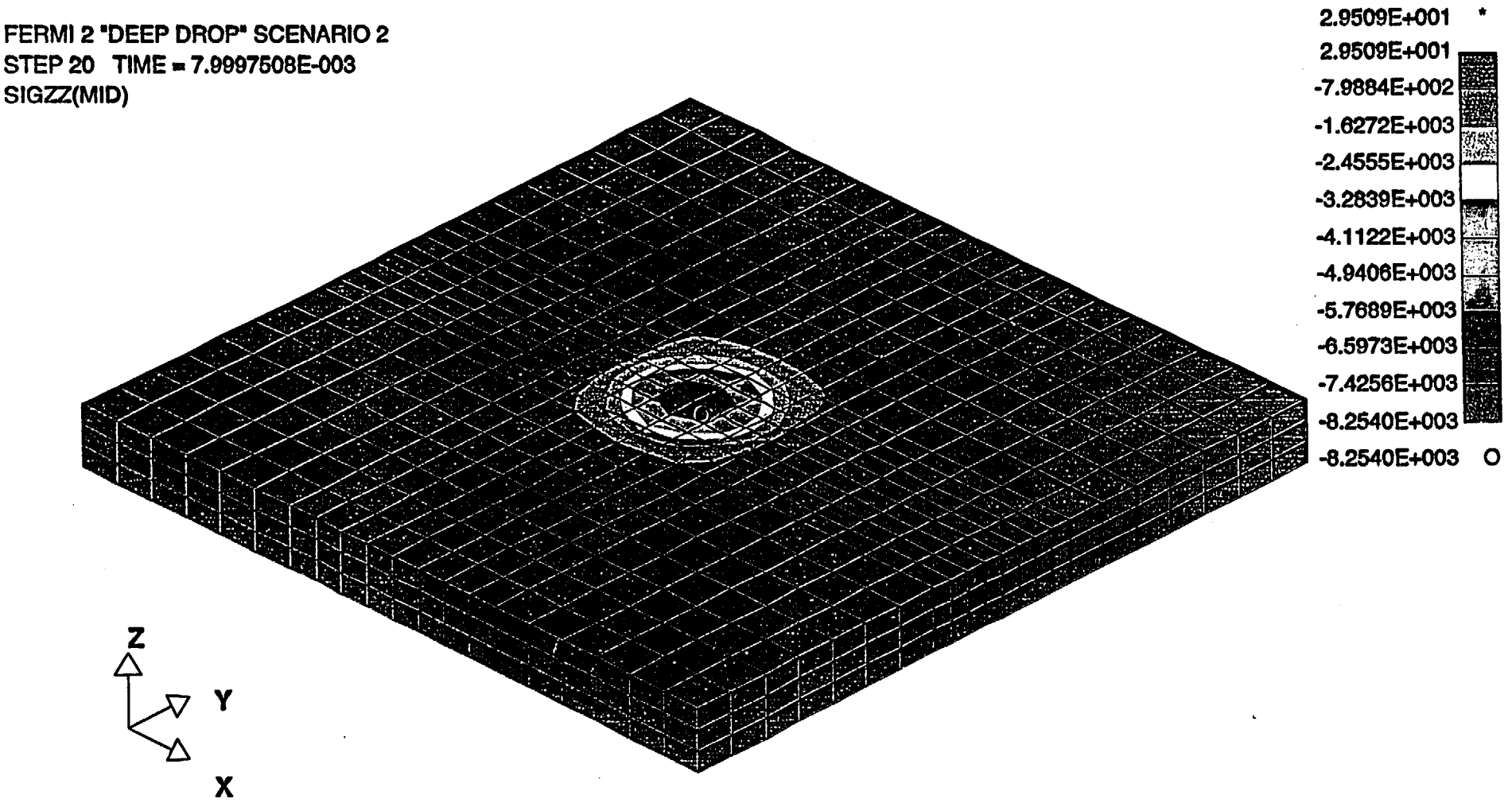

Figure 7.5.4 Maximum Normal Stress of the Concrete Slab for "Deep" Drop Scenario 2

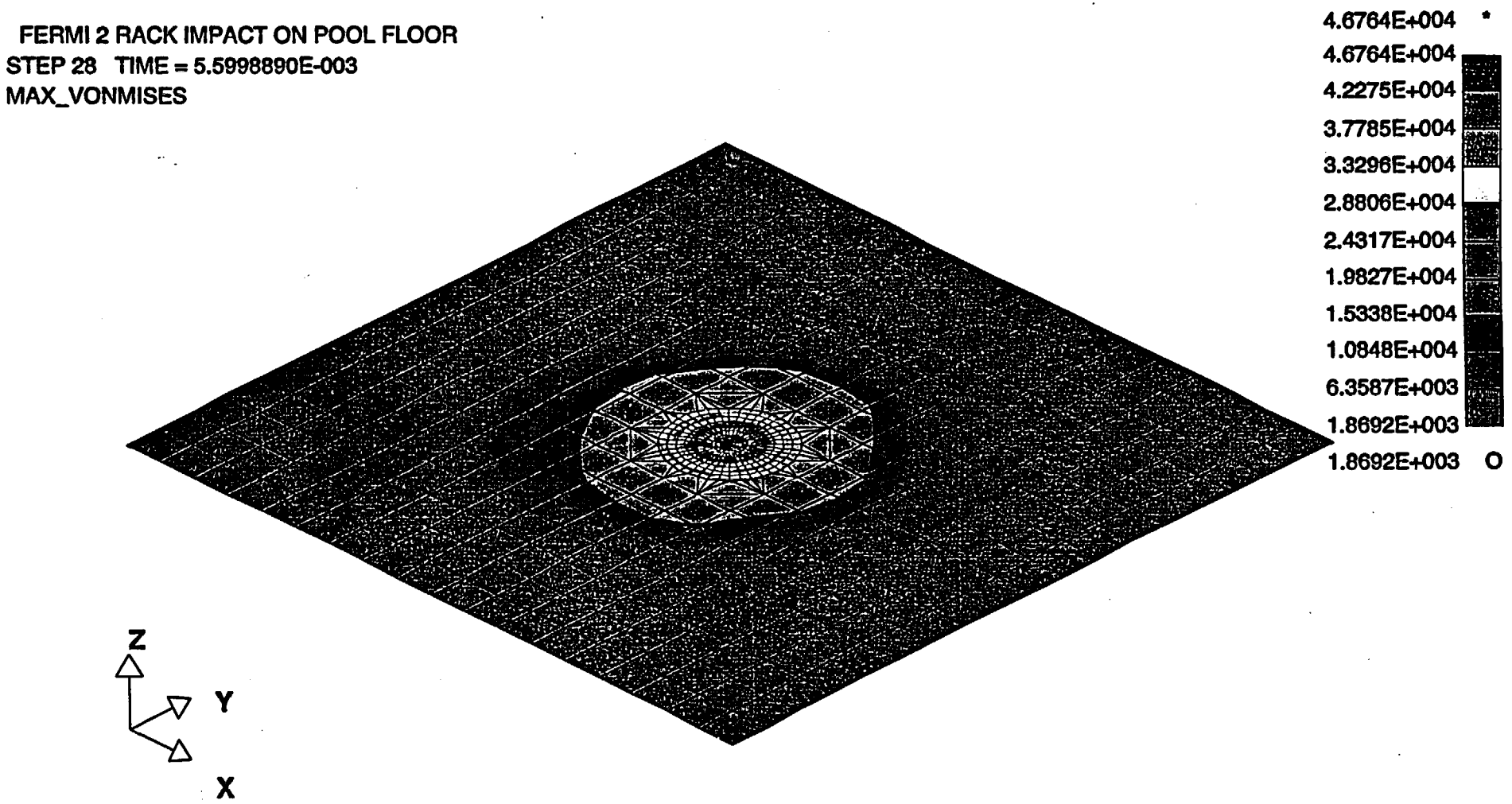

Figure 7.5.5 Maximum Von Mises Stress of the Liner for the Heaviest Rack Drop

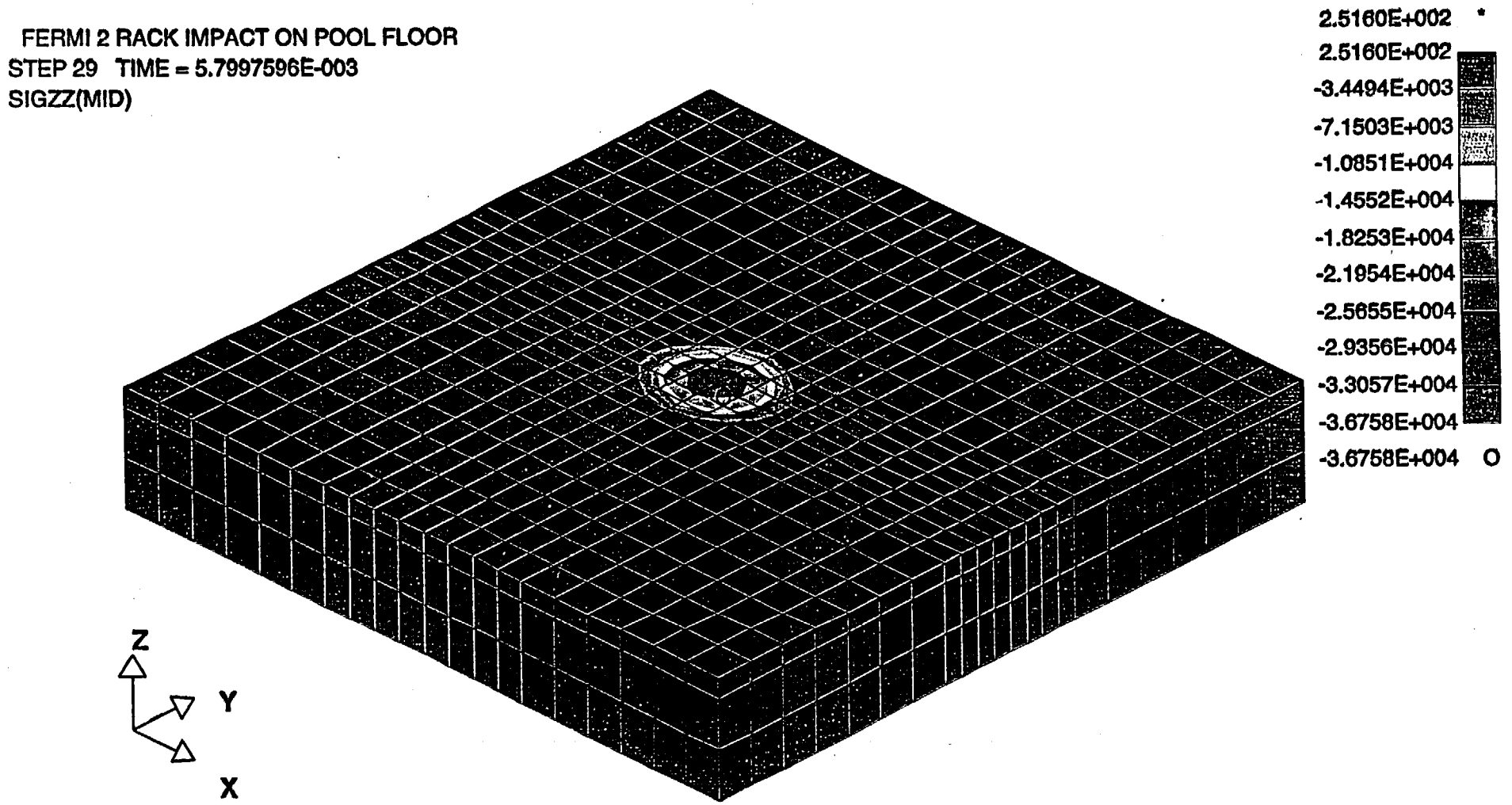

Figure 7.5.6 Maximum Normal Stress of the Concrete Slab for the Heaviest Rack Drop

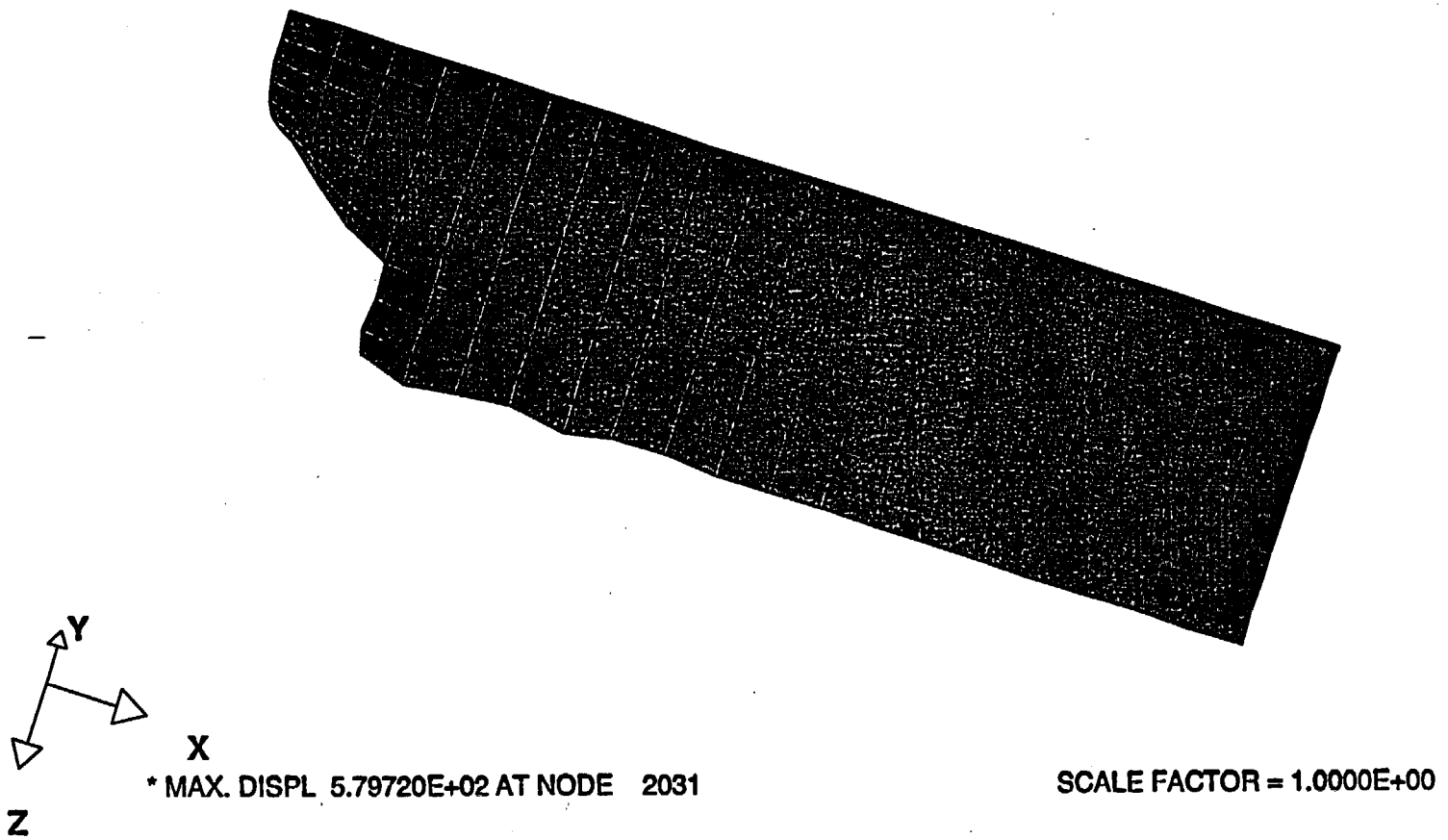

Figure 7.5.7 Punctured Liner in Gate Drop Scenario 1

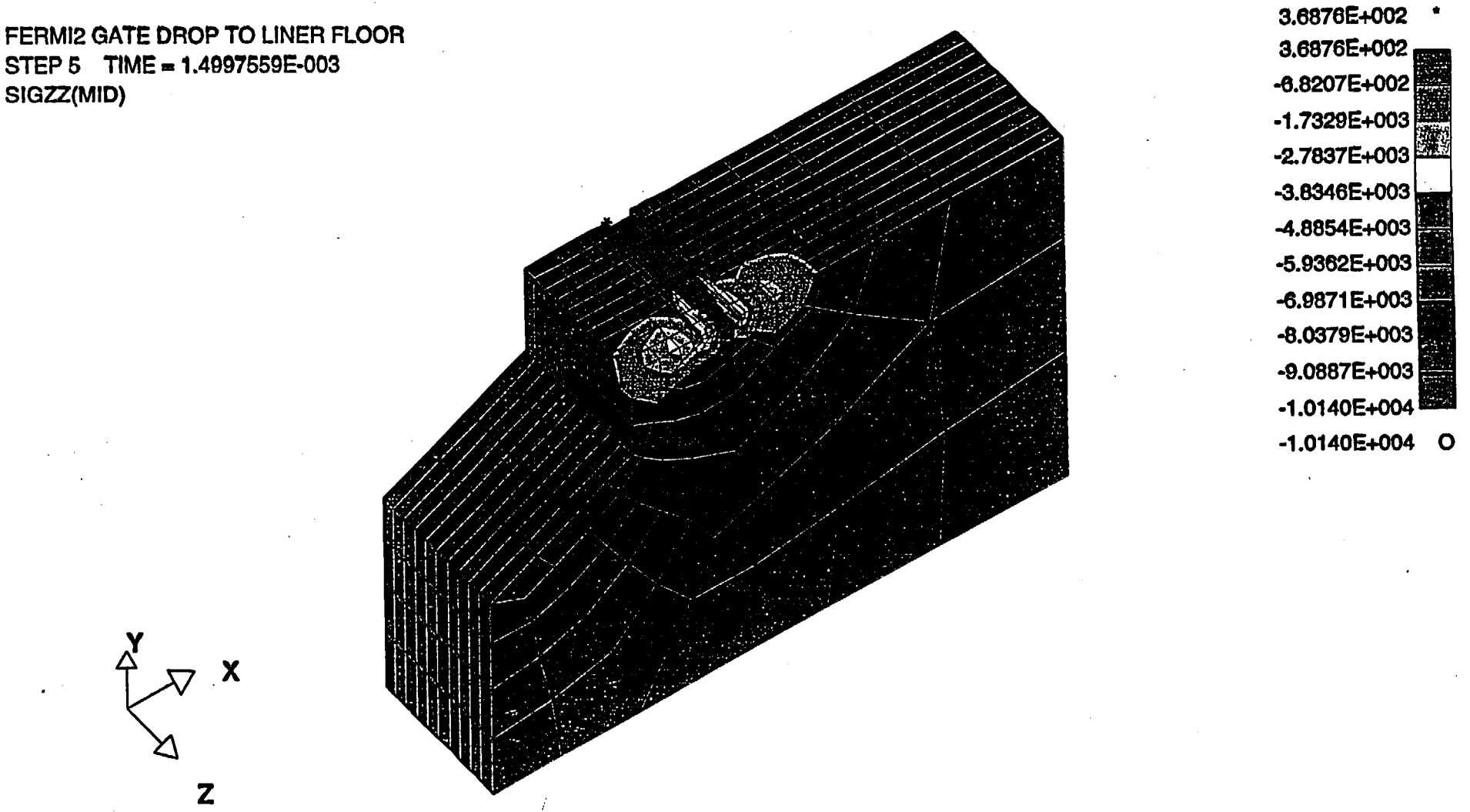

Figure 7.5.8 Maximum Normal Stress of the Concrete Slab for Gate Drop Scenario 1

8.0 FUEL POOL STRUCTURE INTEGRITY CONSIDERATIONS

8.1 Introduction

The Spent Fuel Pool (SFP) at Fermi 2 is a safety related, seismic category I, reinforced concrete structure. In this section, the analysis performed to demonstrate structural adequacy of the pool structure is summarized.

The pool region is analyzed using the finite element method. Results for individual load components are combined using factored load combinations mandated by SRP 3.8.4 [8.1.1] based on the "ultimate strength" design method. It is demonstrated that for the critical bounding factored load combinations, structural integrity is maintained when the pool is assumed to be fully loaded with spent fuel racks with all storage locations occupied by fuel assemblies.

The regions examined in the SFP are the floor slab, and the highly loaded wall sections adjoining and supporting the slab. Moment and shear capabilities are checked for concrete structural integrity. Local punching and bearing integrity of the slab in the vicinity of a rack module support pedestal pad is evaluated. All structural capacity calculations are made using design formulas meeting the requirements of the American Concrete Institute (ACI) [8.1.2].

8.2 Description of Pool Structure

The Spent Fuel Pool (SFP) is located at the fifth floor of the Fermi 2 Reactor Building, north of the reactor drywell. The nominal inner dimensions of the pool are: 34' in the North-South direction, 40' in the East-West direction, and 38'-9" deep. The top of the 6' thick reinforced concrete slab is at elev. 645'-2", and the top of the steel liner reaches elev. 645'-9" (the liner and the top reinforcement are separated by concrete fill). The normal level of the water in the pool is at elev. 683'-6". Figure 8.1 shows a 3-D sketch of the Fermi spent fuel pool and the surrounding areas. Table 8.1 summarizes the key geometric data for the spent fuel pool structure.

The south wall that separates the spent fuel pool from the reactor drywell is an integral part of the reactor's reinforced concrete containment. The pool slab and the side walls extend to the north, beyond the confines of the pool, and transfer a portion of the vertical load from the spent fuel pool to the reactor building outer wall. The room between the pool north wall and the outer wall serves for equipment storage. At elev. 659'-6", two 3.5' thick reinforced concrete floor slabs also provide external bracing to the pool in East-West direction. Below elev. 659'-6", the thickness of the pool walls increases from 72" to 76" (side walls) and from 48" to 72" (north wall).

The SFP slab, side and north walls are reinforced with #11 and #10 reinforcing steel. The reinforcement is uniformly spaced at 6". Table 8.2 summarizes the major reinforcement in each of the member cross-sections. In addition to the reinforcement presented in the table, additional reinforcement is placed in the SFP side walls as follows:

- 85 #18 re-bars within the top 72" of the east wall,
- 80 #18 re-bars within the top 72" of the west wall,
- 24 #18 re-bars within the bottom 12" of the east and west walls.

The design input concrete compressive strength and reinforcement yield strength is as follows:

$f_c = 5{,}900$ psi

$\sigma_y = 60{,}000$ psi

8.3 Definition of Loads

The results from the structural/seismic analysis of the racks showed that Campaign III provides bounding values for the relevant loads for all of the proposed re-racking phases. Pool structural loading involves the following discrete components (Capital letters in parentheses represent load type identifiers used later to define the relevant load combinations):

8.3.1 Static Loading (Dead Loads and Live Loads)

- Dead weight of reinforced concrete structure and steel liner (D).

- Maximum dead weight of rack modules and fuel assemblies stored in the modules (D). The buoyant weight of the racks in Campaign III fully loaded with spent fuel was uniformly distributed on the total wet area of the spent fuel pool slab.

- Hydrostatic pressure on walls and slab (F).

8.3.2 Live Loads (L)

- Load from the mechanical equipment stored in the room north of SFP uniformly distributed on the extension slab.

8.3.3 Seismic Induced Loads

- Vertical loads are transmitted by the rack support pedestals to the slab during a Safe Shutdown Earthquake (SSE (E')) or an Operating Basis Earthquake (OBE (E)). Using the results from the Whole Pool Multi-Rack (WPMR) analyses associated with Campaign III, the total load from all rack pedestals less the dead weight load can be computed as a function of time. Identifying the instantaneous peak load and dividing by the wetted area of the slab defines the slab pressure that represents the seismically induced "pressure adders" from the rack dynamic motion.

- Hydrodynamic inertia loads due to the contained water mass and sloshing loads (considered in accordance with [8.3.1]) which arise during a seismic event (E or E'). Based on the results of the WPMR analyses, equivalent uniform pressures were used in the finite element analysis to account for the action of impulsive and convective water pressures above the top of the racks.

- Hydrodynamic pressures between racks and pool walls are caused by rack motion in the pool during a seismic event (E or E'). Using results from the Campaign III WPMR analyses, lateral pressures were applied on the pool walls below the top of the spent fuel racks to simulate these effects.

- Seismic inertia forces develop in the walls and slab during a seismic event (E or E'). The seismic loads were imposed as static loads using appropriate seismic coefficients from the response spectra for each earthquake direction. The results from a finite element modal analysis establish the frequencies used for selection of seismic coefficients.

Table 8.3 summarizes the static and quasi-static pressure loads applied to the slab and walls.

8.3.3 Thermal Loading

Thermal loading is defined by the temperature existing at the faces of the pool concrete walls and slabs. Two thermal loading conditions are evaluated: The normal operating temperature and the accident temperature. The following pool water and airside temperatures are used to establish normal and accident through-wall temperature gradients:

Normal – 150 degrees F
Pool Boiling – 212 degrees F
Ambient Air Side – 70 degrees F

The thermal stress analysis does not consider the thermal loads due to Gamma (γ) heating that increases the average temperatures in the reinforced concrete members and decreases the linear temperature gradients. This is a conservative assumption because these thermal loads increase the in-plane compression in the reinforced concrete cross-sections and reduce the thermal bending moments, thus resulting in higher safety margins.

8.4 Analysis Procedures

8.4.1 Finite Element Analysis Model

The finite element model encompasses the spent fuel pool slab, the east and west walls adjacent to the slab from the reactor shield wall out to the north wall of the reactor building, and the north wall of the spent fuel pool. Imposing appropriate boundary conditions simulates the interaction with the portion of the building structure that is not included in the finite-element model. The ANSYS Finite Element (FE) computer code [8.4.1] was used for the structural analysis of the spent fuel pool. Three types of FE analysis were performed: mechanical, thermal, and modal. Mechanical FE analysis provided the internal forces and moments in the reinforced concrete members from postulated static and seismic quasi-static loads. The thermal analysis provided internal forces and moments due to the imposed temperature gradients. The modal analysis was used to obtain lowest modal frequencies in each direction that were used to select appropriate seismic coefficients and compute the pool structure inertia forces.

The FE model of the Fermi 2 Spent Fuel Pool contained 1326 nodes, 1246 shell elements, and 79 beam elements. The shell elements, having 4 nodes each with 6 degrees of freedom, modeled the SFP reinforced concrete slab and walls. The 3-D elastic beam elements simulated the stiffness provided by the additional reinforcement placed at the top and bottom ends of the pool East-West walls.

The analysis conservatively neglected the stiffness of the pool steel liner and accounted for liner mass increasing the specified unit weight of the concrete by 10%. A linear elastic and isotropic constitutive behavior was assumed both for the reinforced concrete and the additional reinforcement. The mechanical and modal analyses assumed elastic isotropy and used un-cracked stiffness characteristics of the reinforced concrete members that are independent of the contained reinforcement. In accordance with the ACI Standard [8.1.2], the thermal simulations assumed cracked stiffness properties of the reinforced concrete members that are represented by material elastic modulii reduced to simulate the variation and the degree of the crack patterns. The degree

of reduction of the elastic modulus is calculated based on the average of the cracked moments of inertia of the particular structural element's reinforced concrete cross-sections.

Figure 8.2 depicts the geometry of the Finite Element Model and its global coordinate system. The positive directions of the X and Y global coordinates are oriented towards North and East respectively, and the positive Z-axis is directed upward.

The boundary conditions, at the connections to portions of the building not included in the finite element model, were chosen to simulate fixed or clamped support, depending on the adjacent structure. Lateral displacements of walls were restrained at locations where support was provided by intermediate floor slabs exterior to the pool. Structural support provided by walls below the pool slab is conservatively excluded from the model.

8.4.2 Analysis Methodology

Finite element analyses are performed for the mechanical and thermal load cases defined previously. Results for individual load cases are combined using the factored load combinations discussed below. The combined force and moment resultants are compared with the ultimate moments and shear capacities of all structural elements pertinent to the Spent Fuel Pool, which are calculated in accordance with the ACI 349-85 [8.1.2] to develop the safety factors.

8.4.3 Load Combinations

The various individual load cases are combined in accordance with the NUREG-0800 Standard Review Plan [8.1.1] requirements with the intent to obtain the most critical force and moment fields for the investigated reinforced concrete structural elements.

In accordance with the governing standards [8.1.1] and [8.1.2], the analysis of the pool structural integrity identified and considered the following most critical load combinations:

$1.4\,(D + F) + 1.7\,L + 1.9\,E$

$1.05\,(D + F +) + 1.425\,E + 1.275\,(L + T_0)$

$D + F + L + T_0 + E'$

$D + F + L + T_a + 1.25\,E$

where:

D = dead loads;

F = hydrostatic loads;

L = live loads;

T_0 = thermal load during normal operation;

T_a = thermal load under accident condition;

E = OBE earthquake induced loads;

E' = SSE earthquake induced loads.

8.5 Results of Analysis

The bending moments, axial forces, and shear forces were evaluated for each of the critical load combination. The comparison of these internal forces against the factored ultimate capacities of the reinforced concrete cross sections furnished safety factors for bending moments and shear forces for each of the SFP components modeled (the slab, and the east, west, and north walls). Appropriate interactions between force and moment were included in the safety factor evaluation. Safety factors are defined as Maximum Capacity of the Section/Calculated Bending Moment or Shear Force. Table 8.4 and Table 8.5 list the minimum safety factors for bending and shear moment capacity that serve as indicators of the SFP structural integrity.

The calculated safety factors in Tables 8.4 and 8.5 are all greater than 1.0 and demonstrate that the structural integrity of the Spent Fuel Pool is maintained under the increased loads and governing load combinations.

8.6 Pool Liner

The spent fuel pool liner is subject to in-plate strains due to movement of the rack support feet during the seismic event. Analyses were performed to establish that the liner would not tear or rupture under limiting loading conditions in the pool, and that there was no fatigue problem under the condition of 1 SSE event plus 20 OBE events (i.e. cumulative damage factor (CDF) <1.0). The liner analyses were based on loading imparted from the most highly loaded pedestal in the pool conservatively assumed positioned in the most unfavorable location. Bearing strength requirements were demonstrated to be satisfied by conservatively analyzing the most highly loaded pedestal located in the worst configuration with respect to underlying leak chases. An analysis of the pool liner under the combined effects of maximum thermal load (pool boiling) and hydrostatic pressure was performed. It was demonstrated that the liner must be subject to more than 5000 boiling cycles before any fatigue failure is possible. The liner welds were shown to have a safety factor (based on stress) greater than 1.0 as required.

8.7 Bearing Pad

To protect the pool slab from high localized dynamic loadings, bearing pads are placed between the pedestal base and the slab. Fuel rack pedestals impact on these bearing pads during a seismic event and pedestal loading is transferred to the liner. Bearing pad dimensions are set to ensure that the average pressure on the slab surface due to a static load plus a dynamic impact load does not exceed the American Concrete Institute, ACI-349 [8.1.2] limit on bearing pressures. Section 10 of the code gives the design bearing strength as

$$f_b = \Phi\,(.85\,f_c')\varepsilon$$

where $\Phi = .7$ and f_c' is the specified concrete strength for the spent fuel pool. $\varepsilon = 1$ except when the supporting surface is wider on all sides than the loaded area. In that case, $\varepsilon = (A_2/A_1)^{.5}$, but not more than 2. A_1 is the actual loaded area, and A_2 is an area greater than A_1 and is defined in [8.1.2]. Using a value of $\varepsilon > 1$ includes credit for the confining effect of the surrounding concrete. It is noted that this criterion is in conformance with the ultimate strength primary

design methodology of the American Concrete Institute in use since 1971.

The bearing pad size selected is 1" thick, austenitic stainless steel plate stock for the cask area rack and 2" thick, austenitic stainless steel plate stock for the remaining racks in the pool. All rack pedestals are located away from leak chases. Both sizes of the bearing pads are analyzed using a finite element code (ANSYS) for its structural adequacy to diffuse the seismic load imparted by the racks.

An ANSYS finite element simulation of a representative bearing pad model is presented in Figure 8.7.1. The model permits the bearing pad to deform and lose contact with the liner, if the conditions of elastostatics so dictate. The slab is modeled as an elastic foundation which supports the liner. A bounding vertical pedestal load, which is calculated from the ACI-349 factored load combinations for SSE and OBE, is applied to the model.

The average pressure at the pad to liner interface is computed and compared against the stress limit. Analysis result shows that the average pressure computed at the slab/liner interface is below the ACI allowable limit.

The stress distribution in the bearing pads of both sizes is also evaluated. The maximum bending stress in the bearing pad under the peak vertical load is calculated to be below the material yield strength limit.

Therefore, the bearing pad design devised for Fermi 2 racks is deemed appropriate for the prescribed loadings.

8.8 Conclusions

Regions affected by loading the fuel pool completely with new high-density racks were examined for structural integrity under bending and shearing action. It was determined that adequate safety margins exist conservatively assuming that all racks are fully loaded with fuel. It

was also shown that local loading on the liner does not compromise liner integrity under a postulated fatigue condition and that concrete bearing strength limits were not exceeded.

8.9 References

[8.1.1] NUREG-0800, SRP-3.8.4, Rev. 1., July 1981.

[8.1.2] ACI 349-85, Code Requirements for Nuclear Safety Related Concrete Structures, American Concrete Institute, Detroit Michigan, 1985.

[8.3.1] "Nuclear Reactors and Earthquakes, U.S. Department of Commerce, National Bureau of Standards, National Technical Information Service, Springfield, Virginia (TID 7024).

[8.4.1] ANSYS, Version 5.4, ANSYS, Inc., 1998.

TABLE 8.1

KEY GEOMETRIC DATA FOR THE SPENT FUEL POOL

ITEM	VALUE
Pool Depth	38.75'
Pool N-S Length	34.0'
Pool E-W Length	40.0'
Top Water Elevation	683'-6"
Pool Bottom Elevation	645'-9"
Top Racks Elevation	661'-1/8"
Top Reinforced Concrete Slab Elevation	645'-2"
Slab Thickness	72.0"
East and West Wall Thickness	76" (72") †
North Wall Thickness (opposite to reactor)	72" (48") †

TABLE 8.2

SPENT FUEL POOL REINFORCEMENT

RC-MEMBER	DIRECTION	OUTER SIDE	INNER SIDE
Pool Slab	Both ways	#11@6" and #10@6"	#11@12"
Side (E-W) Walls	Vertical	#11@6" and #10@6"	#11@12"
	Horizontal	2 X #11@6"	#11@12"
North Wall	Vertical	#11@6" and #10@6"	#11@12"
	Horizontal	2 X #11@6"	#11@12"

† Walls have increased thickness below elev. 659'-6"

TABLE 8.3

PRESSURE LOADS APPLIED TO FINITE ELEMENT MODEL

ITEM	LOCATION	PRESSURE (psi)
Dead weight of racks plus fuel	Pool Slab	16.27
Hydrostatic pressure	Gradient on walls from zero to maximum value on slab	16.31
Live Load	Extension Slab	1.4
Rack pedestal seismic loads	Slab pressure – OBE Slab pressure - SSE	5.43 6.69
Hydrodynamic loads from contained water and sloshing during a seismic event	Walls (above the top of racks) N-S OBE/SSE E-W OBE/SSE	 1.45/2.40 1.73/2.90
Hydrodynamic loads from rack horizontal motion during a seismic event	Walls (below the top of racks) North Wall OBE/SSE East Wall OBE/SSE West Wall OBE/SSE	 4.5/6.0 5.0/5.0 -5.0/-7.5 †

† The negative values represent a suction effect that reduces the hydrostatic pressure on the wall.

TABLE 8.4

SAFETY FACTORS - BENDING

R.C. Member	Cross Section	Load Combinations			
		LC 1	LC 2	LC 3	LC 4
Pool Slab †	N-S	1.25 (1.70)	1.95	2.27	1.81
	E-W	1.38 (2.44)	2.40	3.15	2.00
East Wall (lower portion)	Horizontal	6.03	4.50	5.70	3.28
	Vertical	1.50	4.62	5.61	3.58
West Wall (lower portion)	Horizontal	4.81	4.67	5.80	3.39
	Vertical	1.35	4.49	5.44	3.43
North Wall (lower portion)	Horizontal	1.10	4.78	3.40	3.87
	Vertical	1.11	4.99	1.25	3.71
East Wall (upper portion)	Horizontal	1.26	4.39	5.30	3.17
	Vertical	6.39	4.34	5.29	3.36
West Wall (upper portion)	Horizontal	5.07	4.42	5.69	3.00
	Vertical	5.40	4.14	5.01	3.22
North Wall (upper portion)	Horizontal	1.73	2.75	3.39	2.00
	Vertical	12.20	3.51	4.44	2.62

† The values in parentheses indicate slab positive bending moment (outer reinforcement in tension) capacity.

TABLE 8.5

SAFETY FACTORS - SHEAR

R.C. Member	Cross Section	Load Combinations			
		LC 1	LC 2	LC 3	LC 4
Pool Slab	N-S	1.12	1.34	1.57	1.26
	E-W	1.14	2.14	2.33	2.69
East Wall (lower portion)	horizontal	6.65	4.76	6.35	3.09
	vertical	1.51	4.45	5.11	3.62
West Wall (lower portion)	horizontal	3.24	5.07	5.87	4.51
	vertical	1.53	4.62	4.79	4.17
North Wall (lower portion)	horizontal	2.16	2.17	1.55	2.53
	vertical	1.59	1.90	2.14	2.22
East Wall (upper portion)	horizontal	3.55	1.69	2.09	1.28
	vertical	4.03	3.21	3.55	2.77
West Wall (upper portion)	horizontal	4.97	1.67	2.20	1.22
	vertical	4.65	4.17	5.47	3.07
North Wall (upper portion)	horizontal	2.13	1.52	1.89	1.48
	vertical	3.94	2.11	2.67	1.18

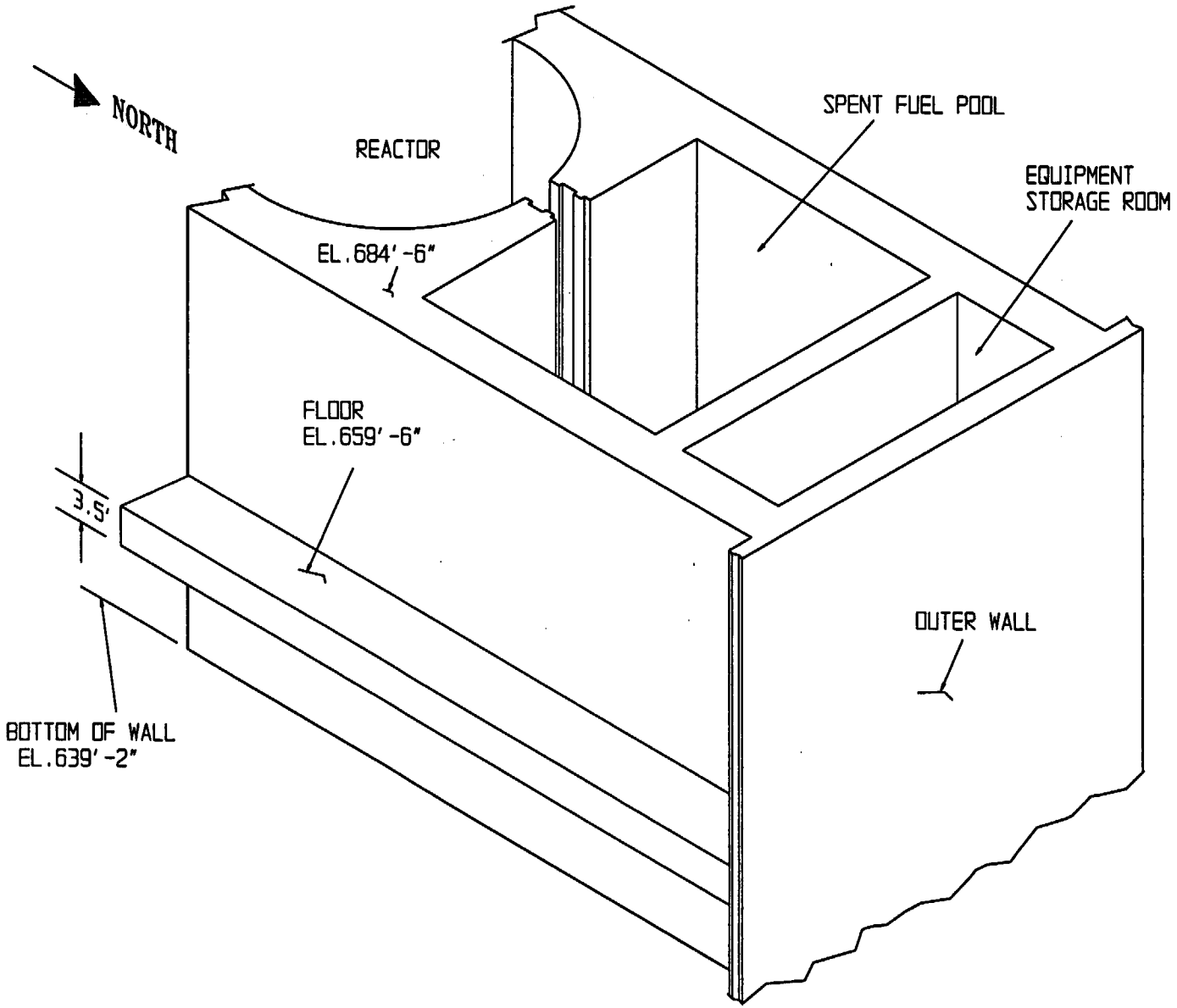

FIGURE 8.1; FERMI UNIT 2 SPENT FUEL POOL

HI992154

\PROJECTS\980964\HI992154\8_1

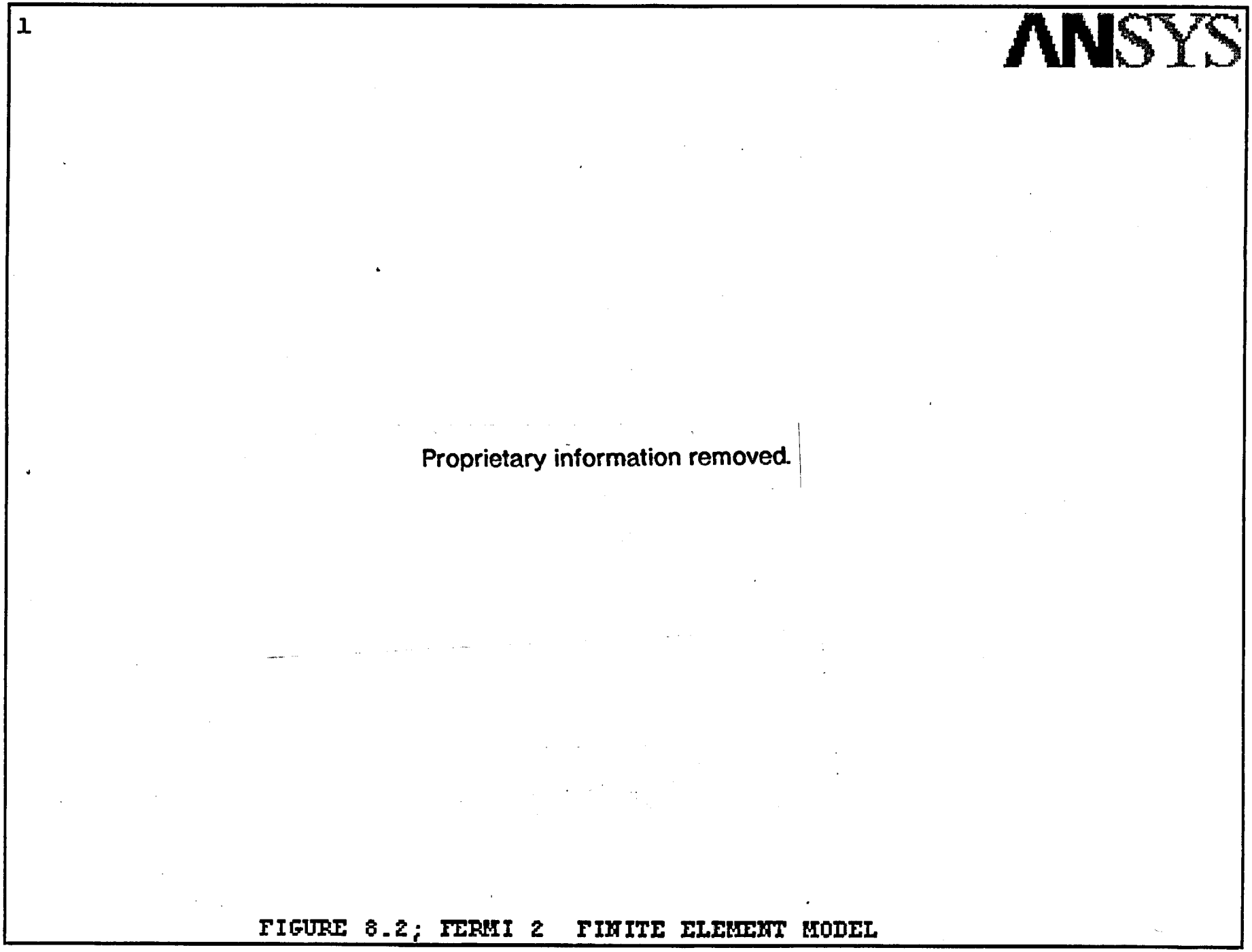

FIGURE 8.2; FERMI 2 FINITE ELEMENT MODEL

HOLTEC PROPRIETARY

Proprietary information removed.

Figure 8.7.1

9.0 RADIOLOGICAL EVALUATION

9.1 Fuel Handling Accident

The potential radiological consequences at the Fermi 2 exclusion area boundary (EAB) of a fuel handling accident in the spent fuel pool have been determined.

9.1.1 Assumptions and Source Term Calculations

Evaluations of the accident were based on fuel of 5.0 wt% initial enrichment burned to 50,000 Mwd/mtU. The reactor was assumed to have been operating at 3499 Mw thermal power with 764 fuel assemblies in the core prior to shutdown. The fuel handling accident was assumed to result in the release of the gaseous fission products contained in the fuel/cladding gaps of all the fuel rods in a peak-power, 8x8 fuel assembly. Gap inventories of fission products available for release were estimated using the release fractions identified in Regulatory Guide 1.25 [9.1.1] except for Iodine-131, for which the release fraction is increased 20% in accordance with NUREG/CR-5009 [9.1.2]. Cooling time for the failed fuel prior to the accident was 60 hours.

The gaseous fission products that have the greatest impacts on the off-site doses following short fuel-cooling periods are the short-lived nuclides of iodine and xenon, which reach saturation inventories during in-core operation. These inventories depend primarily on the fuel specific power over the few months immediately preceding reactor shutdown. In the highest power assemblies, the specific power and hence the inventory of iodine and xenon will be proportional to the peaking factor (taken as 1.50, per Reg Guide 1.25).

At the cooling time of 60 hours used in the Fermi 2 calculations, approximately 90 percent of the thyroid dose comes from Iodine-131, while over 80 percent of the whole-body dose comes from Xenon-133. Though these iodine and xenon isotopes are the major contributors to off-site doses, the contributions from other radionuclides are calculated and included in the overall dose values.

The present evaluation uses values for atmospheric diffusion factor (χ/Q) and for filter efficiencies that have been specified previously. Core specific inventories (Curies per metric ton of uranium) of fission products were estimated with the ORIGEN code [9.1.3] based upon parameters stated earlier (Initial enrichment of 5.0 wt% U, burnup of 50,000 Mwd/mtU, and a cooling time of 60 hours), along with a specific power of 25.63 kw/kgU. Data and assumptions used in the dose calculations are given in Table 9.1.1.

The equation given on the following page was taken from Reg Guide 1.25 and was used to calculate the thyroid dose (D, in rads) from the inhalation of radioiodine.

$$Dose = \frac{\sum}{i} \frac{F_g I_i FPBR_i(\chi / Q)}{DF_p\, DF_f}, where$$

F_g = fraction of fuel rod iodine inventory in gap space

I_i = core iodine radionuclide inventory at time of the accident (curies)

F = fraction of core damaged so as to release iodine in the rod gap

P = core peaking factor

B = breathing rate (cubic meters per second)

R_i = dose conversion factor (rads per curie)

χ/Q = atmospheric diffusion factor (sec per cubic meter)

DF_p = effective iodine decon. factor for pool water

DF_f = effective iodine decon. factor for filters

The equation given below was used to calculate the external whole-body dose from gamma radiation in the cloud of radionuclides released in the fuel-handling accident. The equation contains several of the terms defined above.

$$Dose_y = \sum_i 0.25(\chi/Q)FPG_iE_{y-i}$$

In this expression, G_i is the gap inventory of the gaseous radionuclides of krypton and xenon, while the E_{y-i} term is the average energy per disintegration of each radionuclide (in Mev per disintegration. The equation assumes the noble gas decontamination factors in water and the charcoal filters are 1.0. The gap inventories of radioiodine make negligible contributions to the whole body dose, D_y, because of the large decontamination factors applicable to the iodines.

9.1.2 Results

The doses at the Fermi 2 EAB from the postulated fuel handling accident are well within the exposure guideline values of 10 CFR Part 100, paragraph 11. As defined in Standard Review Plan 15.7.4, *Radiological Consequences of Fuel Handling Accidents*, "well within" means 25 percent or less of the 10CFR100 guidelines, or values of 75 rad for thyroid doses and 6 rem for whole-body doses. The potential doses at Fermi 2 Plant from the conservative scenario presented here meet the criteria for "well within."

9.2 Solid Radwaste

No significant increase in the volume of solid radioactive wastes is expected from operating with the expanded storage capacity. The necessity for pool filtration resin replacement is determined primarily by the requirement for water clarity, and the resin is normally changed about once a year. New types of resin and operational procedures are decreasing these volumes and future volumes are expected to be generated at half the current rate. Accordingly, the proposed increase

in storage capacity of the Fermi 2 pool will have a negligible impact on the amount of resin waste that will be generated.

Vacuuming operations may be performed for general pool maintenance prior to the rack installation, or to reduce local dose rates in areas required for dive operations, if necessary. Vacuuming will occur in areas in which the diver may have to enter, provided the dose rates in the area warrant vacuuming.

9.3 Gaseous Releases

Normally, the contribution from the fuel storage area is negligible compared to the other releases and no significant increases are expected as a result of the expanded storage capacity. Release of radioactive gases by Fermi 2 will remain a small fraction of the limits of 10 CFR 20.1301 and the design objectives of Appendix I to 10 CFR 50 following the implementation of the proposed modification to increase the capacity of Fermi 2 spent fuel storage. This conclusion is based on the following supporting statements:

a) The half lives of short lived nuclides such as I-131 are short in comparison to fuel cycle length, therefore, short-lived nuclides are present only in freshly offloaded fuel. The quantity of freshly offloaded fuel placed into the SFP each refueling outage is not affected by the number of spent fuel assemblies being stored in the SFP. Therefore, the inventory of I-131 in the SFP will not be affected by the increased SFP capacity.

b) Inventories of long-lived fission products (e.g. Kr-85, I-129, and ternary tritium) in spent fuel assemblies will decrease slowly within individual fuel assemblies over years in storage. Therefore, an increase in the number of spent fuel assemblies stored in the SFP would increase the total SFP inventory of these radionuclides. However, these radionuclides are not released in significant amounts from the stored fuel to the SFP water, even for failed fuel since the fuel pellet temperature of stored fuel is not high enough to create sufficient gas pressure in the gap to overcome the static pressure of the SFP water.

c) The radioactivity in the SFP water is independent of the number of assemblies in the pool. This activity originates in the reactor coolant system (RCS) and is introduced into the SFP when the SFP and RCS are connected during refueling outages.

d) The increased number of spent fuel assemblies in storage will raise the heat load on the SFP and could result in an increase in the evaporation rate. Other than a small amount of tritiated water released by evaporation, SFP radionuclides are non-volatile and consequently are not released from the pool water. The increased evaporation rate of tritiated water would result in an increase in gaseous tritium released in Fermi 2 effluents. However, the discharge of gaseous radioactive effluents will continue to be a small fraction of the limits of 10 CFR 20.1301 and the design objectives of Appendix I to 10 CFR 50.

9.4 Liquid Releases

The number of spent fuel assemblies in storage does not affect the release of radioactive liquids from the plant. The contribution of radioactive materials in the spent fuel pool water from the stored assemblies is insignificant relative to other sources of activity, such as the reactor coolant system. The volume of spent fuel pool water processed for discharge is independent of the number of fuel assemblies stored in the spent fuel pool.

9.5 Personnel Doses

During normal operations, personnel working in the fuel storage area are exposed to radiation from the spent fuel pool. Operating experience has shown that area radiation dose rates originate primarily from radionuclides in the pool water. Therefore, during refueling and other fuel-movement operations, pool water concentrations are expected to increase slightly due to crud deposits spalling from spent fuel assemblies and due to activities carried into the pool from the primary system. With respect to the rack installation, fuel movements may be required in support of this project in order to facilitate safe load paths. During any necessary fuel shuffle

activities, dose rates above and around the pool perimeter may increase marginally. However, for normal storage conditions the dose fields will still approximate conditions experienced during the normal operating/storage conditions that existed prior to the proposed change. The radiation dose rates in accessible areas adjacent to spent fuel storage will continue to be monitored per current Radiation Protection procedures. No changes to the zone designations identified in the Fermi 2 UFSAR are anticipated. Fuel storage in the new storage modules will be provided with the same water coverage to act as shielding.

Operating experience has also shown that there have been negligible concentrations of airborne radioactivity in the Spent Fuel Pool area. Therefore, no increase in airborne radioactivity above the SFP area or at the site boundary is expected as a result of the expanded storage capacity.

9.6 Anticipated Dose During Rack Installation

All of the operations involved in the rack installation will utilize detailed procedures prepared with full consideration of ALARA principles. Similar operations have been performed in a number of facilities in the past, and there is every reason to believe that rack installation can be safely and efficiently accomplished at Fermi 2, with low radiation exposure to personnel. This project will be carried out in three distinct campaigns.

The total dose for the three rack installation campaigns is estimated to be between 6 and 12 person-rem. This exposure estimate is based on previous rack installation projects at other facilities as shown in Table 9.6.1 and considers the following parameters:

- The dose rates in and around the pool area
- Approximate manhours and associated dose for various activities on previous similar projects.
- Contingency for the possibility of use of divers

While individual task efforts and doses may differ from those stated above, the total is believed to be a reasonable estimate for planning purposes. Though divers will be used only if necessary, the estimated person-rem burden for rack installation takes their possible dose into consideration.

The existing radiation protection program at Fermi 2 is adequate for the rack installation operations. Where there is a potential for significant airborne activity, continuous air monitors will be in operation. Personnel will wear protective clothing as required and, if necessary, respiratory protective equipment. Activities will be governed by a Radiation Work Permit, and personnel monitoring equipment will be issued to each individual. As a minimum, this will include thermoluminescent dosimeters (TLDs) and self-reading dosimeters. Additional personnel monitoring equipment (i.e., extremity TLDs or multiple TLDs) may be utilized as required.

Work, personnel traffic, and the movement of equipment will be monitored and controlled to minimize contamination and to assure that dose is maintained ALARA.

After the rack installations, the lifting device will be cleaned and wrapped for contamination controls. The lift rig will then be stored at Fermi 2.

9.7 References for Section 9

[9.1.1] Regulatory Guide 1.25 (AEC Safety Guide 25), "Assumptions Used For Evaluating The Potential Radiological Consequences Of A Fuel Handling Accident In The Fuel Handling And Storage Facility For Boiling And Pressurized Water Reactors", March 23, 1972.

[9.1.2] C. E. Beyer, et al., "Assessment of the Use of Extended Burnup Fuel in Light Water Power Reactors", NUREG/CR-5009, Pacific Northwest Laboratory, February, 1988.

[9.1.3] SAS2H-ORIGEN-S/ARP, in "Scale 4.3-Modular Code System for Performing Standardized Computer Analyses for Licensing Evaluation", NUREG-CR-0200, Rev. 5, September 1995.

Table 9.1.1

DATA AND ASSUMPTIONS FOR THE EVALUATION

OF THE FUEL HANDLING ACCIDENT

Core power level, Mw(t)	3499
Fuel enrichment, wt% U	5.0
Fuel burnup, Mwd/mt U	50,000
Specific power, kw/kg U	25.63
Fuel cooling time, hrs	60
Power peaking factor	1.50
No. of failed fuel rods	All in 1 assembly
Core inventory released to gap, %	
Iodine-131	12
Other iodines	10
Krypton-85	30
Xenon-133	10
Other xenons	10
Iodine composition, %	
Elemental	99.75
Organic	0.25
Pool decontamination factors	
Elemental iodine	133
Organic iodine	1
Noble gases	1
Filter decontamination factors	
Elemental iodine	99
Organic iodine	99
Noble gases	1
Atmospheric diffusion factor χ/Q),sec/m^3	1.23×10^{-4}
Breathing rate, m^3/sec	3.47×10^{-4}

Table 9.6.1

PRELIMINARY ESTIMATE OF

PERSON-REM DOSE DURING RE-RACKING

Step	Number of Personnel	Estimated Person-Rem Dose
Remove empty racks	5	0.5 to 1.0
Wash racks	3	0.08 to 0.2
Clean and vacuum pool	3	0.3 to 0.6
Remove underwater appurtenances	4	0.4 to 0.8
Partial installation of new rack modules	5	0.25 to 0.5
Move fuel to new racks	2	0.8 to 1.5
Remove remaining racks	5	1.5 to 3.0
Install remaining new rack modules	5	0.4 to 0.8
Decon and prepare old racks for shipment	4	1.0 to 2.0†
Total Dose, person-rem		6 to 12

† Maximum expected dose, although details of preparation and packaging of old racks for shipment have not yet been determined.

10.0 INSTALLATION

10.1 Introduction

To realize the proposed in-pool capacity expansions in the Fermi 2 spent fuel pool, Holtec International and DECo will have to carry out installation activities at the Fermi 2 site which involve rigging and handling of heavy loads, contamination control, and radiation protection considerations. In this chapter, a synopsis is provided of the heavy load considerations and the site operation procedures to carry out the proposed plant modification with utmost safety and minimum dose to the plant personnel.

10.2 Heavy Load Considerations for the Proposed Reracking Operation

The 117-ton single failure-proof cask handling crane will be utilized for lifting the racks from the first floor of the Reactor Building and placing them into the spent fuel pool. Final placement of the racks within the spent fuel pool will be performed using a combination of the cask handling crane and the 5-ton auxiliary crane. An additional temporary hoist with sufficient capacity shall also be used to prevent submergence of the cask handling and auxiliary crane hooks.

A remotely engageable lift rig, which meets NUREG-0612 stress criteria, will be used to lift the new modules. It consists of independently loaded lift rods that engage at the underside of the solid baseplate in the rack. This ensures that failure of one lift rod will not result in uncontrolled lowering of the load, compliant with Section 5.1.6(1) of NUREG-0612. The remotely engageable lift rig also has the following attributes:

a. The stresses in the lift rods are self-limiting inasmuch as an increase in the magnitude of the load reduces the eccentricity between the upward force and downward reaction (moment arm).

b. It is impossible for a lift rod to lose engagement with the lifted rack because the downward load secures each rod in its locking slot. Moreover, the locked configuration can be directly verified from above the pool water without the aid of an underwater camera by the orientation of position locator flags atop each lift rod.

c. A stress analysis of the rig has been performed, and the stress limits postulated in ANSI 14.6 (1978) are shown to be met.

d. The rig is load tested with 300% of the maximum weight to be lifted. The test weight is maintained in the air for one hour. All critical weld joints are liquid penetrant examined, after the load test, to establish the soundness of all critical joints.

Pursuant to the defense-in-depth approach of NUREG-0612, the following additional measures of safety will be undertaken for the reracking operation:

a. The cranes and lifting devices used in the project will be given a preventive maintenance checkup and inspection per Fermi 2 plant procedures.

b. Safe load paths will be developed for moving the new racks in the Reactor Building. The new racks will not be carried over any region of the pool containing fuel.

c. Rack upending will be carried out in an area away from the spent fuel pool. Additionally, this area will not overlap any safety-related component.

d. All crew members involved in the rack installation will be given training in the use of the lifting, upending equipment, and all other aspects of rack installation.

e. Crane stop blocks will be temporarily installed to prevent movement over fuel.

The fuel shuffle scheme developed for the spent fuel pool is predicated on the following criteria:

a. No heavy load (rack or rig) with a potential to drop on a rack shall be carried over or near active fuel. This shall be accomplished by shuffling fuel into racks that are not in the area of the safe load path.

b. All heavy loads are lifted in such a manner that the C.G. of the lift point is aligned with the C.G. of the load being lifted.

c. Turnbuckles are utilized to "fine tune" the verticality of the rack being lifted.

All phases of the rack installation will be conducted in accordance with written procedures, which will be reviewed and approved by DECo.

The guidelines contained in NUREG-0612, Section 5 will be followed throughout the rack installation. The guidelines of NUREG-0612 call for measures to "provide an adequate defense-in-depth for handling of heavy loads near spent fuel..." and cite four major causes of load handling accidents, namely:

i. Operator errors
ii. Rigging failure
iii. Lack of adequate inspection
iv. Inadequate procedures

The Fermi 2 rack expansion program mitigates the potential for load drop accidents by implementing measures that increase overall quality and safety in the four aforementioned areas. A summary of the measures specifically planned to deal with the major causes is provided below.

Operator errors: As mentioned above, DECo plans to provide comprehensive training to the installation crew.

Rigging failure: The lifting device designed for handling and installation of the racks in the fuel pool has redundancies in the lift legs, and lift eyes such that there are four independent load members. Failure of any one load bearing member would not lead to uncontrolled lowering of the load. The rig complies with all provisions of ANSI 14.6 - 1978, including compliance with the primary stress criteria, load testing at 300% of maximum lift load, and dye penetrant examination of critical welds.

The Fermi 2 lift rig design is similar to the lift rigs used to rerack numerous other plants, such as Sequoyah, J. A. Fitzpatrick, Duane Arnold, Three Mile Island Unit 1, D.C. Cook, Connecticut Yankee, Callaway, Wolf Creek, Waterford 3, and Byron Units 1 and 2. .

Lack of adequate inspection: The designer of the racks will develop a set of inspection points which have proven to eliminate any incidence of re-work or erroneous installation in numerous prior rerack projects. Inspection of lifting equipment will be performed per NUREG-0612.

Inadequate procedures: DECo plans to implement a multitude of procedures to cover the entire rack installation, such as mobilization, rack handling, upending, lifting, installation, verticality, alignment, dummy gage testing, site safety, and ALARA compliance.

The operating procedures planned for the Fermi 2 rack installation are the successors of procedures that were implemented successfully for other projects.

In addition to the above, a complete inspection and preventive maintenance program of all the cranes and lifting equipment used in the project are planned prior to the start of rack installation. Safe load paths will be developed as required by NUREG-0612.

Table 10.2.1 provides a synopsis of the requirements delineated in NUREG-0612 and our intended compliance.

In summary, the measures implemented in the Fermi 2 rack installations are similar to those utilized in all recent rerack projects in the U.S.

10.3 Site Operation Procedures

Holtec International and DECo are developing a complete set of operating procedures which cover the entire gamut of operations pertaining to the rack installation effort. Similar procedures have been utilized and successfully implemented by Holtec International during numerous previous rack installation projects. These procedures assure that ALARA practices are followed and provide detailed requirements to ensure equipment, personnel, and plant safety. The following is a list of procedures that will be used to implement the rack installation phase of the project.

a. Receipt Inspection Procedure:

   This procedure delineates the steps necessary to perform a thorough receipt inspection of the new racks after their arrival on site. The receipt inspection includes dimensional measurements, cleanliness inspection, and visual examination.

b. Cleaning Procedure:

   This procedure provides for the cleaning of the new racks, if it is required, in order to meet the requirements of ANSI N45.2.1, Level B. Permissible cleaning agents, methods and limitations on materials to be employed are provided.

c. Fuel Rack Storage Procedure:

This procedure establishes the requirements for safely storing the new racks on site, in the event that long-term site storage is necessary. This procedure provides environmental restrictions, temperature limits, cleanliness requirements, and packaging requirements.

d. Pre-Installation Drag Test Procedure:

This procedure stipulates the requirements for performing a functional test on the new racks prior to installation into the spent fuel pool. The procedure provides direction for inserting and withdrawing a "dummy" fuel assembly into designated cell locations, and establishes an acceptance criterion in terms of maximum kinetic drag force during withdrawal.

e. Installation/Handling/Removal Procedure:

This procedure provides direction for the handling/installation of the new high-density racks and the removal of the existing racks. The procedure delineates the steps necessary to receive new high-density racks on site, to unload and upright the racks, to stage the racks prior to installation, and to install the racks. The procedure also provides for the installation of new rack bearing pads, adjustment of the new rack pedestals and performance of the as-built field survey. Any pool modifications that may be necessary, such as protrusion truncation, are also described in the procedure. Finally, this procedure also outlines the rack removal activities.

f. Post-Installation Drag Test Procedure:

This procedure stipulates the requirements for performing a functional test on new racks following installation into the spent fuel pool. The procedure will provide direction for inserting and withdrawing a "dummy" fuel assembly into designated cell locations, and establishes an acceptance criterion in terms of maximum kinetic drag force.

g. Underwater Diving Procedure:

It is DECo's intention to perform the rack installation without using divers. However, should underwater diving operations become necessary to support the new rack installation, diving activities will be strictly controlled by DECo and

Holtec procedures. These procedures describe the method for introducing a diver into the spent fuel pool, provide for radiological monitoring during the operation, and define the egress of the diver from the fuel pool following work completion. Furthermore, these procedures require strict compliance with OSHA Standard 29CFR-1910, Subpart T, and establish contingencies in the event of an emergency.

In addition to the procedural controls, underwater cameras will also be used to monitor the movements of the diver.

h. ALARA Procedure:

Consistent with both Holtec International and Fermi 2 plant ALARA Programs, this procedure provides details to minimize the total person-rem received during the rack installation project. Additionally, pre-job briefings are performed in order to mitigate the potential for overexposure.

i. Liner Inspection Procedure:

In the event that a visual inspection of any submerged portion of the spent fuel pool liner is deemed necessary, this procedure describes the method to perform such an inspection, and describes the requirements for documenting any observations.

j. Leak Detection Procedure:

This procedure describes the method to test the spent fuel pool liner for potential leakage using a vacuum box. This procedure may be applied to any suspect area of the pool liner.

k. Underwater Welding Procedure:

In the event of a positive leak test result, an underwater welding procedure may be implemented which provides for the placement of a stainless steel repair patch over the area in question. The procedure contains appropriate qualification records documenting relevant variables, parameters, and limiting conditions. The weld procedure is qualified in accordance with AWS D3.6-93, Specification for Underwater Welding or may be qualified to an alternate code acceptable to DECo and Holtec International.

10.4 Pool Survey and Inspection

A pool inspection shall be performed to determine if any items attached to the liner wall or floor will interfere with the placement of the new racks or prevent usage of any cell locations subsequent to installation.

In the event that protrusions are found which would pose any interference to the installation process, appropriate actions will be taken to ensure safe rack installation.

10.5 Pool Cooling and Purification

10.5.1 Pool Cooling

The Fuel Pool Cooling and Cleanup system shall be operated in order to maintain the pool water temperature at an acceptable level. It is anticipated that specific activities, such as bearing pad elevation measurements, may require the temporary shutdown of the Spent Fuel Pool cooling system. At no time, however, will pool cooling be terminated in a manner or for a duration that would create a violation of the Fermi 2 procedures.

10.5.2 Purification

The existing spent fuel pool filtration system shall be operational in order to maintain pool clarity. Additionally, an underwater vacuum system will be used, as racks are removed, to supplement fuel pool purification. The vacuum system may be employed to remove extraneous debris, reduce general contamination levels prior to diving operations, and to assist in the restoration of pool clarity following any pressure washing operations.

10.6 Fuel Shuffling

As new high-density racks are installed into the pool, it is anticipated that fuel shuffles will be performed in independent phases in order to transfer irradiated assemblies from existing racks

into Holtec racks. During the transition phase when both the existing racks and Holtec racks are in the spent fuel pool, fuel shall be shuffled in accordance with the Technical Specification requirements.

Fuel shuffle operations shall be conducted in accordance with Fermi 2 procedures and in a manner consistent with the rack installation sequence. Fuel shuffle operations shall not be conducted concurrently with the new rack installation.

10.7 Installation of New Racks

The new high-density racks, which are supplied by Holtec International, will be delivered in the horizontal position. Each new rack will be removed from the shipping trailer using a suitably rated crane, while maintaining the horizontal configuration, and placed upon an upender and secured. Using two independent overhead hooks, or a single overhead hook and a spreader beam, the module will be uprighted into the vertical position.

The new rack lifting device will be installed into the rack and each lift rod successively engaged. Thereafter, the rack will be transported to a pre-leveled surface where the appropriate quality control receipt inspection will be performed.

As indicated in Section 10.6 above, a procedure shall be developed to shuffle spent fuel, as required, in accordance with Technical Specification requirements.

In preparing the spent fuel pool for the rack installation, the pool floor will be inspected and any debris which may inhibit the installation of bearing pads will be removed. After the bearing pads are positioned on the pool floor, elevation measurements will then be taken at each pad location. The rack pedestals will be adjusted in accordance with the bearing pad elevation measurements in order to achieve levelness when the racks are installed.

The new racks will be lifted using the reactor building crane. A temporary hoist with a suitably rated capacity may be attached to the overhead crane for installation activities in order to avoid

submerging the main hook and causing contamination. For rack movements along the pool floor, the height of the rack above the liner shall not exceed six inches, except where floor projections obstruct the path. Once the rack has reached its final position it will be carefully lowered onto its bearing pad.

Elevation readings will be taken to confirm that the module is level and as-built rack-to-rack and rack-to-wall offsets will be recorded. The lifting device will be disengaged and removed from the fuel pool under Radiation Protection direction. A post-installation drag test may be performed using an inspection gage to ensure that no cell location poses excessive resistance to the insertion or withdrawal of a bundle.

An intensive surveillance and inspection program shall be maintained throughout the rack installation phase of the project. A set of inspection points which have been proven, in numerous previous rack installation campaigns, to eliminate any incidence of rework or erroneous installation will be implemented.

10.8 Safety, Radiation Protection, and ALARA Considerations

10.8.1 Safety

During the rack installation phase of the project, personnel safety is of paramount importance, outweighing all other concerns. All work shall be carried out in strict compliance with approved procedures.

10.8.2 Radiation Protection

Radiation Protection personnel shall provide necessary coverage in order to provide radiological protection and monitor dose rates. The Radiation Protection department shall prepare Radiation Work Permits (RWPs) that will instruct project personnel in the areas of protective clothing, general dose rates, contamination levels, and dosimetry requirements.

In addition, no activity within the radiologically restricted area shall be carried out without the knowledge and approval of Radiation Protection. Radiation Protection shall also monitor items removed from the pool, provide for the use of alarming dosimetry and supply direction for the proper storage of radioactive material.

10.8.3 ALARA

The key factors in maintaining project dose As Low As Reasonably Achievable (ALARA) are time, distance, and shielding. These factors are addressed by utilizing many mechanisms with respect to project planning and execution.

Time

Each member of the project team will be properly trained and will be provided appropriate education and understanding of critical evolutions. Additionally, daily pre-job briefings will be employed to acquaint each team member with the scope of work to be performed and the proper means of executing such tasks. Such pre-planning devices reduce worker time within the radiologically posted area and, therefore, decrease project dose.

Distance

Remote tooling such as lift fixtures, pneumatic grippers, a support leveling device and a lift rod disengagement device have been developed to execute numerous activities from the pool surface, where dose rates are relatively low. By maximizing the distance between radioactive sources and project personnel, project dose is reduced.

Shielding

During the course of the rack installation, the water in the spent fuel pool provides primary shielding. The amount of water between an individual at the surface and an irradiated fuel assembly is an essential shield that reduces dose. Additionally, other shielding, may be employed to mitigate dose when work is performed around high dose rate sources.

10.9 Radwaste Material Control

The main source of radioactive waste is the existing spent fuel racks. In Campaign I, there will be no existing rack removal. However, subsequent campaigns contemplate removal of existing racks. The disposal process for the existing racks in Campaigns II and III is briefly described below.

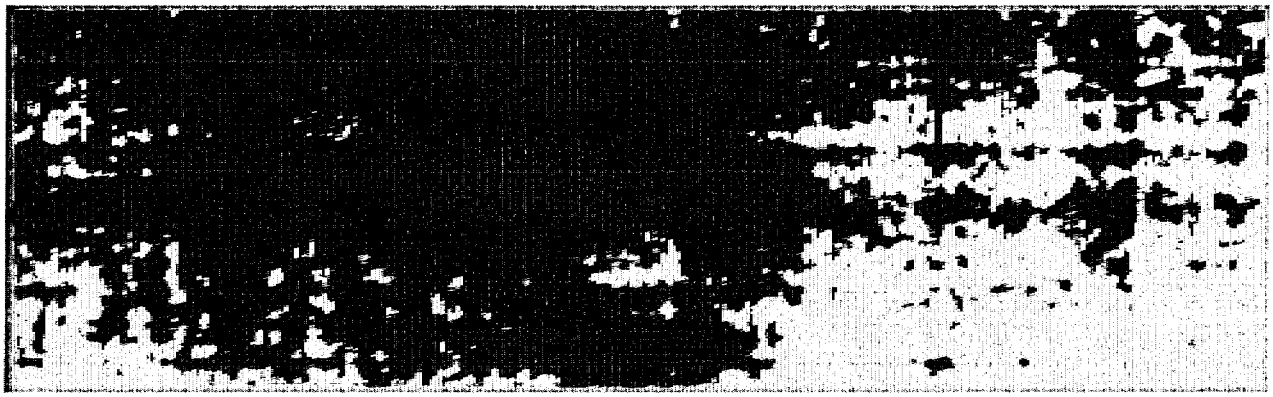

In addition to the existing spent fuel racks, radioactive waste generated from the rack installation effort may include vacuum filters, miscellaneous tooling, and protective clothing.

Vacuum filters may be removed from the pool and stored as appropriate in a suitable container in order to maintain low dose rates.

Contaminated tooling shall be properly stored per Radiation Protection direction throughout the project. At project completion, an effort will be made to decontaminate tooling to the extent practical.

10.10 Closure

The wet storage capacity expansion in the Fermi 2 spent fuel pool will be carried out using handling equipment, ancillaries, and procedures, which have a long, proven history of successful implementation.

Table 10.2.1

HEAVY LOAD HANDLING COMPLIANCE MATRIX (NUREG-0612)

	Criterion	Compliance
1.	Are safe load paths defined for the movement of heavy loads to minimize the potential of impact if dropped on irradiated fuel and safe shutdown equipment?	Yes
2.	Will procedures be developed to cover: identification of required equipment, inspection, and acceptance criteria required before movement of load, steps and proper sequence for handling the load, defining the safe load paths, and special precautions?	Yes
3.	Will crane operators be trained and qualified?	Yes
4.	Will special lifting devices meet the guidelines of ANSI 14.6-1978?	Yes
5.	Will non-customer lifting devices be installed and used in accordance with ANSI B30.9-1971?	Yes
6.	Will the cranes be inspected and tested prior to use in rerack?	Yes
7.	Does the crane meet the intent of ANSI B30.2-1976 and CMMA-70?	Yes

11.0 ENVIRONMENTAL COST/BENEFIT ASSESSMENT

11.1 Introduction

Article V of the USNRC OT Position paper [11.1.1] requires the submittal of a cost/benefit analysis in support of the chosen fuel storage capacity enhancement method. This section provides an abstract of the alternatives considered by the Detroit Edison Company and a brief summary of the costs associated with each. This section also addresses the environmental considerations pertinent to the selected wet storage capacity increase option. An assessment of the costs, viability, and availability of the various alternatives, indicates that wet storage expansion, performed in multiple campaigns, is clearly the superior approach to satisfying the future spent fuel storage needs at Fermi 2.

11.2 Imperative for Rack Replacement

The specific need to increase the existing storage capacity of the Fermi 2 spent fuel pool is based on the continually increasing inventory in the pool and a lack of viable economic alternatives with other storage technology.

11.3 Appraisal of Alternative Options

DECo has determined that spent fuel storage rack addition and replacement is by far the most viable option for the Fermi 2 plant in comparison to other alternatives. The open pool floor space, which can be created with minor in-pool construction effort, makes wet storage capacity expansion the most economical alternative.

The key considerations in evaluating the alternative options are provided below:

- Safety: minimize the number of fuel handling steps
- Economy: minimize total installed and O&M cost

- Security: protection from potential saboteurs, natural phenomena
- Non-intrusiveness: minimize required modification to existing systems
- Maturity: extent of industry experience with the technology
- ALARA: minimize cumulative dose due to handling of fuel

The following alternative options were considered in a 1994 feasibility study performed by Holtec International for the Detroit Edison Company:

i. On-Site Cask Storage

Dry cask storage is a method of storing spent nuclear fuel in a high capacity container. The cask provides radiation shielding and passive heat dissipation. Typical capacities for BWR fuel range up to 68 assemblies that have been removed from the reactor for at least five years. The casks, once loaded, are then stored outdoors on a seismically qualified concrete pad. The storage location will be required to have a high level of security that includes frequent tours, reliable lighting, intruder detection, and continuous visual monitoring.

The casks, as presently licensed, are limited to 20-year storage service life. Once the twenty years has expired, the cask manufacturer or the utility must recertify the cask or the utility must remove the spent fuel from the container. Recently, the U.S. DOE has embraced the concept of multi-purpose canister (MPC), obsolescing all existing licensed cask designs.

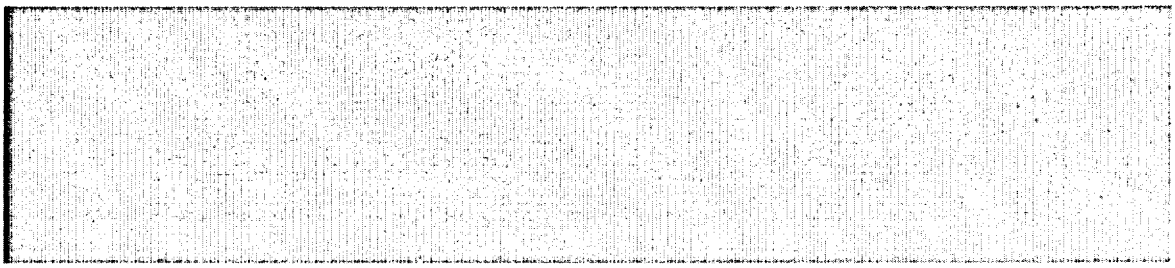

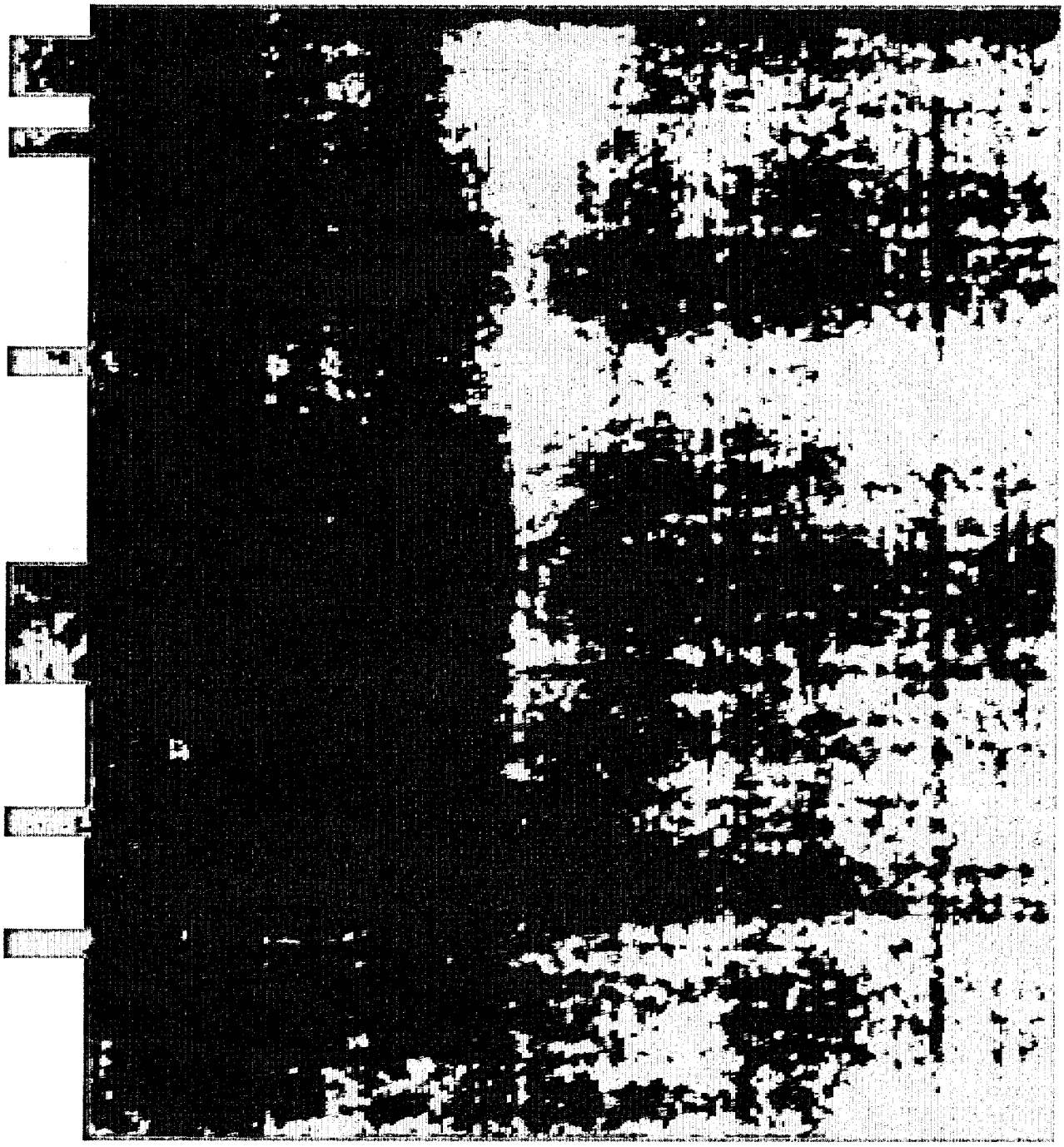

It is clear from the foregoing that there are several plant modifications required to support cask use. Tap-ins must be made to the gaseous waste system and chilled water to support vacuum drying of the spent fuel and piping must be installed to return cask water back to the spent fuel

pool/cask pit. A seismic concrete pad must be made to store the loaded casks. This pad must have a security fence, surveillance protection, emergency power, and video surveillance.

Finally, facilities must be provided to vacuum dry the cask, back fill it with helium, perform leak checks, remachine the gasket surfaces if leaks persist, and assemble the cask on-site.

The on-site dry storage is the only available alternative to plants that have no further potential for wet storage expansion in their pools. Fortunately, such is not the case for Fermi 2.

ii. Modular Vault Dry Storage

Vault storage consists of storing spent fuel in shielded stainless steel cylinders in a horizontal configuration in a reinforced concrete vault. The concrete vault provides radiation shielding and missile protection. It must be designed to withstand the postulated seismic loadings for the site.

A transfer cask is needed to deliver the storage canisters from the fuel pool. The plant must provide for a decontamination bay to decontaminate the transfer cask and connection to its gaseous waste system and chilled water systems. A collection and delivery system must be installed to return the pool water entrained in the canisters back to the fuel pool. Provisions for canister drying, helium injection, handling and automatic welding are also necessary.

The storage area must be designed to have a high level of security. Due to the required space, the vault secured area must be located outside the secured perimeter. Consideration of safety and security requires it to have its own video surveillance system, intrusion detection, and an autonomous power source.

Some other concerns relating to the vault storage system are: the inevitable "repackaging" for shipment to the DOE repository, the responsibility to eventually decommission the new facility, the large "footprint" (land consumption), the potential fuel handling accidents, the potential fuel/clad rupture due to high temperatures, and the high cost.

At the present time, no MPC technology based vault system has been licensed for fuel transport. The high cost and uncertainty make this option less prudent.

iii. Horizontal Silo Storage

A variation of the horizontal vault storage technology is more aptly referred to as "horizontal silo" storage. This technology suffers from the same drawbacks that other dry cask technologies have, namely:

a. No fuel with cladding defects can be placed in the silo.

b. Concern regarding long term integrity of the fuel at elevated temperature.

c. Potential for eventual repackaging at the site.

d. Potential for fuel handling accidents.

e. Relatively high cumulative dose to personnel in effecting fuel transfer (compared to reracking).

f. Compatibility of reactor/fuel building crane with fuel transfer hardware.

g. Potential incompatibility with DOE shipment for eventual off-site shipment.

h. Potential for sabotage.

Dry storage technology is not intended as a total replacement for spent fuel storage pools at operating plants and, therefore, no dry storage system was considered technically or economically viable.

iv. New Fuel Pool

Constructing and licensing a new fuel pool is not a practical alternative for either plant since such an effort may take up to ten years. Moreover, the cost of this option is prohibitively high.

11.4 Cost Estimate

An estimate of relative costs in 1999 dollars for the aforementioned options is provided in the following:

Rack addition (Campaigns I & II):	$9 million
Horizontal Silo (NUHOMS):	$15 to 20 million
HI-STAR 100 (dual-purpose MPC technology metal cask):	$22 million
HI-STORM 100 (MPC technology storage cask):	$16 million
Modular vault:	$35 million
New fuel pool:	$150 million

DECo's estimate of comparative costs of various options is consistent with other published industry data [11.3.1,11.3.2].

To summarize, there is no other viable alternative to adding spent fuel storage racks at Fermi 2. First, there are no commercial independent spent fuel storage facilities operating in the U.S. Second, the adoption of the Nuclear Waste Policy Act (NWPA) created a de facto throw-away nuclear fuel cycle. Since the cost of spent fuel reprocessing is not offset by the salvage value of the residual uranium, reprocessing represents an added cost for the nuclear fuel cycle which already includes the NWPA Nuclear Waste Fund fees. In any event, there are no domestic reprocessing facilities.

11.5 Resource Commitment

The cumulative resource utilization of primary resources from all three campaigns is estimated as follows:

Stainless steel:	200 tons
Boral neutron absorber:	15 tons (12 tons Boron Carbide, 3 tons aluminum)

The requirements for stainless steel and aluminum represent a small fraction of total world output of these metals (less than 0.001%). Although the fraction of world production of Boron Carbide required for the fabrication is somewhat higher than that of stainless steel or aluminum, it is unlikely that the commitment of Boron Carbide to this project will affect other related activities. Experience has shown that the production of Boron Carbide is highly variable and depends upon need and can easily be expanded to accommodate worldwide needs.

11.6 Environmental Considerations

In addition to the increase in the number of fuel assemblies stored in the SFP, this amendment report requests a revision of the maximum normal SFP bulk temperature from 125°F to 150°F. The increase in the allowable bulk temperature is performed to allow the storage of an increased number of fuel assemblies without having to increase cooling water requirements. An evaluation of the Reactor Building ventilation system has demonstrated that the heat and vapor emission to the building environment, at the higher SFP bulk temperature, does not cause the current design basis Reactor Building exit air conditions to exceed the currently licensed value of 104°F. As the Reactor Building air is exhausted to the environment, the heat and water vapor emission to the environment is therefore unchanged from the current Fermi 2 design basis. No other environmental consequence from the increased spent fuel storage capacity and allowable bulk temperature has been identified.

11.7 References for Section 11

[11.1.1] USNRC Letter to All Power Reactor Licensees transmitting the "OT Position for Review and Acceptance of Spent Fuel Storage and Handling Applications," April 14, 1978, and Addendum dated January 18, 1979.

[11.3.1] Electric Power Research Institute, Report No. NF-3580, May 1984.

[11.3.2] "Spent Fuel Storage Options: A Critical Appraisal," by K.P. Singh and M. Bale, Power Generation Technology, Sterling Publishers, pp. 137-140, U.K. (November 1990).